MIT - 2344 - 11
MITNE - 84

MASSACHUSETTS INSTITUTE OF TECHNOLOGY

DEPARTMENT OF NUCLEAR ENGINEERING

Cambridge , Massachusetts 02139

USE OF A MOMENTS METHOD FOR THE ANALYSIS OF FLUX DISTRIBUTIONS IN SUBCRITICAL ASSEMBLIES

by

H. S. Cheng, I. Kaplan, T. J. Thompson,
M. J. Driscoll

February, 1968

AEC Research and Development Report
UC-34 Physics
(TID-4500, 47th Edition)

Contract AT (30-1) 2344

U.S. Atomic Energy Commission

MASSACHUSETTS INSTITUTE OF TECHNOLOGY
DEPARTMENT OF NUCLEAR ENGINEERING
Cambridge, Massachusetts

USE OF A MOMENTS METHOD FOR THE ANALYSIS OF FLUX DISTRIBUTIONS IN SUBCRITICAL ASSEMBLIES

by

H. S. Cheng, I. Kaplan, T. J. Thompson,
M. J. Driscoll

February, 1968

MIT - 2344 - 11
MITNE - 84
AEC Research and Development Report
UC - 34 Physics
(TID - 4500, 47th Edition)

Contract AT(30-1) 2344
U.S. Atomic Energy Commission

DISTRIBUTION

MIT-2344-11 MITNE-84

AEC Research and Development Report

UC-34 Physics

(TID-4500, 47th Edition)

1. USAEC, New York Operations Office, Library
2-4. USAEC, Reactor Physics Branch, Division of Reactor Development and Technology
5. USAEC, New York Patents Office, Brookhaven National Laboratories
6. USAEC, Cambridge Branch, New York Operations Office, Research Contracts Division
7. USAEC, Division of Reactor Development and Technology
8. USAEC, HWOCR Branch
9. USAEC, Water Projects Branch
10. USAEC, Core Design Branch
11. USAEC, Division of Naval Reactors
12. Advisory Committee on Reactor Physics (E. R. Cohen)
13. ACRP (G. Dessauer)
14. ACRP (R. Fluharty)
15. ACRP (E. Gaerttner)
16. ACRP (R. Ehrlich)
17. ACRP (F. C. Maienschein)
18. ACRP (J. Chernick)
19. ACRP (R. Avery)
20. ACRP (M. Nelkin)
21. ACRP (F. Dawson)
22. ACRP (G. Hansen)
23. ACRP (W. B. Loewenstein)
24. ACRP (L. W. Nordheim)
25. ACRP (T. M. Snyder)
26. ACRP (R. Bayard)
27-29. D. T. I. E., Oak Ridge, for Standard Distribution
30-100. Internal Distribution
101. Combustion Engineering (S. Visner)
102. Brookhaven National Laboratories (H. Kouts)

ABSTRACT

A moments method has been developed for the analysis of flux distributions in subcritical neutron-multiplying assemblies. The method determines values of the asymptotic axial and radial buckling, and of the extrapolated height and radius, from foil activation data, in terms of flux moments defined in the usual sense. Analytic expressions are derived for the axial and radial buckling and extrapolated dimensions in terms of the flux moments. These expressions have clear physical meaning and are suitable for the interpretation of conventional buckling measurements. The method treats the moment index as a variable parameter and allows freedom in the choice of the locations of the first and last data points used in the analysis. These degrees of freedom make it possible to reduce the effects of source neutrons, flux transients, and higher harmonics. As a result, the moments method can be applied successfully to very small lattices ("miniature lattices") as well as to large exponential assemblies.

The moments method has been tested, in comparison with the conventional least-squares curve-fitting method, by applying the two methods to the analysis of measurements made in several uranium-heavy water, and uranium oxide-heavy water lattices investigated at the M. I. T. Lattice Project. In the case of large exponential assemblies, the moments method yielded more consistent results than the curve-fitting method. In the case of miniature lattices, the moments method made it possible for the first time to determine values of axial and radial buckling and extrapolated dimensions.

ACKNOWLEDGMENTS

The success of this work and the M. I. T. Heavy Water Lattice Project, as a whole, has been due to the support of the U. S. Atomic Energy Commission and to the contributions of a number of individuals. The results of this report are due primarily to the work of the principal author, Hsiang-Shou Cheng, who has submitted substantially this same report in partial fulfillment of the requirements for the Ph. D. degree at M. I. T.

Overall direction of the Lattice Project during the period of this research was shared by Professors I. Kaplan, T. J. Thompson, and M. J. Driscoll. The author wishes to acknowledge the assistance and guidance of his thesis supervisors, Professors I. Kaplan and Professor M. J. Driscoll. The helpful suggestions and criticisms of Professor Driscoll were very important in guiding the work of the present report. The assistance of Professor Kaplan in putting the manuscript into a clear and concise form is very much appreciated. Thanks are also due to Professor K. F. Hansen for some helpful suggestions.

Mr. Albert Supple and Miss Barbara Kelley have cooperated in arranging the use of computer time. Mrs. Mary Bosco has ably typed the final manuscript. All computer calculations were done at the M. I. T. Computation Center.

The encouragement and support of the author's wife have been instrumental to the completion of this work; his wife assisted in typing the early versions of the report.

TABLE OF CONTENTS

LIST OF FIGURES

LIST OF TABLES

Chapter I

INTRODUCTION

1.1 THE M.I.T. HEAVY WATER LATTICE PROJECT

The Nuclear Engineering Department at M.I.T., under the sponsorship of the United States Atomic Energy Commission, has undertaken a research program, the Heavy Water Lattice Project. The primary purpose of this project is to carry out experimental and theoretical studies of the physics of D_2O-moderated lattices of slightly enriched uranium rods.

The results of the program have been summarized in annual progress reports (H1, H2, H3, H4, H5, H6) and in individual reports.

1.2 THE PROBLEMS IN THE ANALYSIS OF BUCKLING MEASUREMENTS BY THE CONVENTIONAL CURVE-FITTING METHOD

Two types of assemblies (or "experiments") have been used in the experimental determination of the material buckling – one of the reactor parameters of prime interest to the reactor designer: the critical experiment (G1, K1) and the exponential experiment (P1, P3, K9). The latter, because of its economy and safety, has been used extensively in the investigation of the physics of new reactor types, and has been especially valuable in the development of thermal power reactors. Three different methods have been used to obtain values of the material buckling from exponential experiments: the flux shape method (K1), the variable loading method (H7, K1) and the

substitution method (P4, P7, L3); of these, the flux shape method has been used most often. When the assembly is cylindrical, as is usually the case when the moderator is a liquid, this method requires the accurate determination of the axial and radial bucklings. (In the exponential experiments at the M. I. T. Lattice Project, cylindrical tanks three and four feet in diameter, respectively, have been used.)

The flux shape method involves the analysis of axial and radial foil activation data by means of a curve-fitting method based on the least-squares principle (R1, P1). The curve-fitting method has worked reasonably well in large exponential assemblies owing to the availability of a sufficiently large asymptotic region where the fundamental mode of the flux distribution predominates. Some questions arise, however, in connection with the determination of the axial buckling and the extrapolated height (P1). To see how this comes about, we recall that the axial flux distribution is given, within the framework of asymptotic neutron transport theory, by the expression (K4)

$$\phi(Z) = A \sinh \gamma(\tilde{H} - Z) , \tag{1.1}$$

where A is a normalization constant, γ^2 is the axial buckling, and $\tilde{H}$ is the extrapolated height. The essence of the curve-fitting method is to fit the experimental axial activation data to the theoretical axial flux distribution given by Eq. (1.1). The fitting process is accomplished by linearizing the axial flux distribution with respect to the three independent parameters A, γ, and $\tilde{H}$ through a Taylor series expansion:

$$\phi(z,A,\gamma,\tilde{H}) \approx \phi(z,A_o,\gamma_o,\tilde{H}_o) + (A-A_o)\frac{\partial}{\partial A}\phi(z,A,\gamma,\tilde{H})\Big|_o + (\gamma-\gamma_o)\frac{\partial}{\partial \gamma}\phi(z,A,\gamma,\tilde{H})\Big|_o + (\tilde{H}-\tilde{H}_o)\frac{\partial}{\partial \tilde{H}}\phi(z,A,\gamma,\tilde{H})\Big|_o , \tag{1.2}$$

where A_o, γ_o, and $\tilde{H}_o$ are the initially guessed values of the three parameters with which the iteration is begun. The corrected values of A, γ, and $\tilde{H}$ are determined by minimizing the flux residual with respect to A, γ, and $\tilde{H}$. The flux residual is defined as

$$(\Delta\phi)^2 = \sum_{i=1}^{N} w_i \left(\phi_i^{exp} - \phi_i^{th}\right)^2 , \tag{1.3}$$

where the ϕ_i^{exp} are the experimental activation data, the ϕ_i^{th} are the corresponding theoretical flux values given by Eq. (1.2), and the w_i are a set of appropriate weighting factors usually chosen to be the inverse square fluxes. The minimization is done by setting

$$\frac{\partial(\Delta\phi)^2}{\partial A} = \frac{\partial(\Delta\phi)^2}{\partial\gamma} = \frac{\partial(\Delta\phi)^2}{\partial\tilde{H}} = 0 . \tag{1.4}$$

These conditions give rise to the defining equations for the new values of A, γ, and $\tilde{H}$ which must be solved simultaneously. Since the method described depends on the use of only the first order terms of the Taylor series, it is necessary to repeat the calculation with the new values of A, γ, and $\tilde{H}$ substituted for the intial values of A_o, γ_o, and $\tilde{H}_o$. The procedure is repeated until the following convergence criteria are satisfied:

$$\left|\frac{A_j - A_{j-1}}{A_{j-1}}\right| < \epsilon_1 , \quad \left|\frac{\gamma_j - \gamma_{j-1}}{\gamma_{j-1}}\right| < \epsilon_2 , \quad \left|\frac{\tilde{H}_j - \tilde{H}_{j-1}}{\tilde{H}_{j-1}}\right| < \epsilon_3 , \tag{1.5}$$

where ϵ_1, ϵ_2 and ϵ_3 are some small arbitrarily chosen numbers.

This formal least-squares technique is widely used to analyze experimental data. It is indeed a powerful method but only for extracting those parameters that are linear, such as the normalization

constant A in the present case. This is due to the fact that the least-squares technique is a linearized process; the linearization is necessary because otherwise the defining equations for the parameters of interest can be solved in practice only with great difficulty. This limitation has caused trouble in the determination of material buckling: experience has shown that it is difficult to determine the extrapolated height $\tilde{H}$ consistently (R1, P1). A similar difficulty arises in curve-fitting the experimental radial flux data when there is a reflector effect (S2).

The usual way of circumventing the difficulty with the extrapolated height $\tilde{H}$ has been to assume a value for it and to do the least-squares fitting with regard to the two parameters, A and γ only. Since the value of the axial buckling obtained in this way increases with the assumed value of $\tilde{H}$, the following procedure has been adopted to determine the best values of γ and $\tilde{H}$ (P1):

(i) First, calculate the axial buckling γ^2 from a series of assumed $\tilde{H}$ values with the use of a set of experimental data points, and then plot the curve of γ^2 vs. $\tilde{H}$.

(ii) Second, repeat step (i) for modified sets of data points obtained by dropping points from the ends of the first set. Plot the results on the same figure.

(iii) The best values of γ^2 and $\tilde{H}$ are then taken as the intersection of the curves as shown in Figure 1.1.

In practice, a unique intersection seldom occurs. In most cases the three γ^2 vs. $\tilde{H}$ curves form a triangle as indicated in Figure 1.2. In this case the geometric center of the triangle is assumed to give the best values of γ^2 and $\tilde{H}$. Occasionally, the three

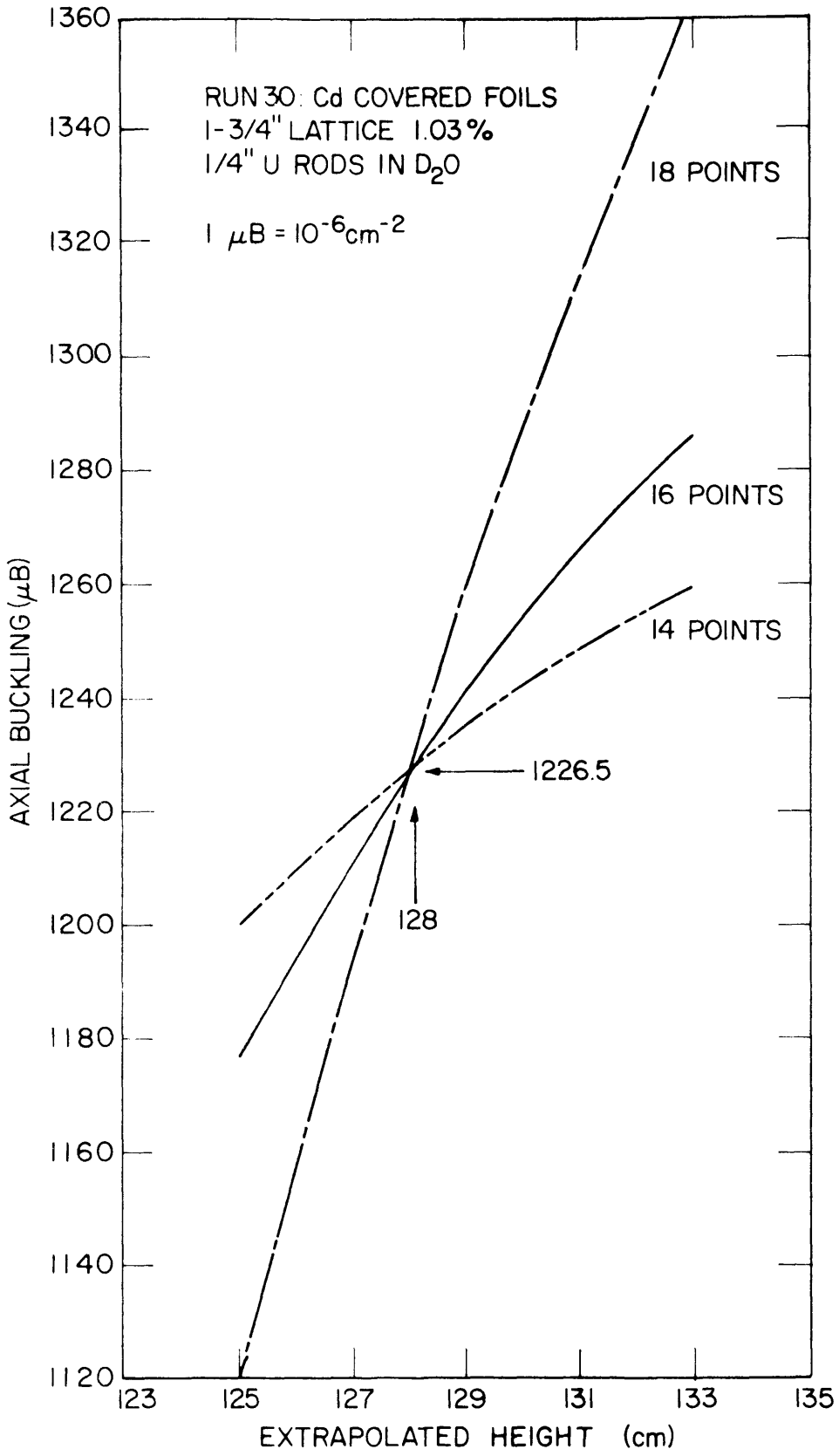

FIG. I.I AXIAL BUCKLING VS. EXTRAPOLATED HEIGHT BY CURVE-FITTING METHOD.

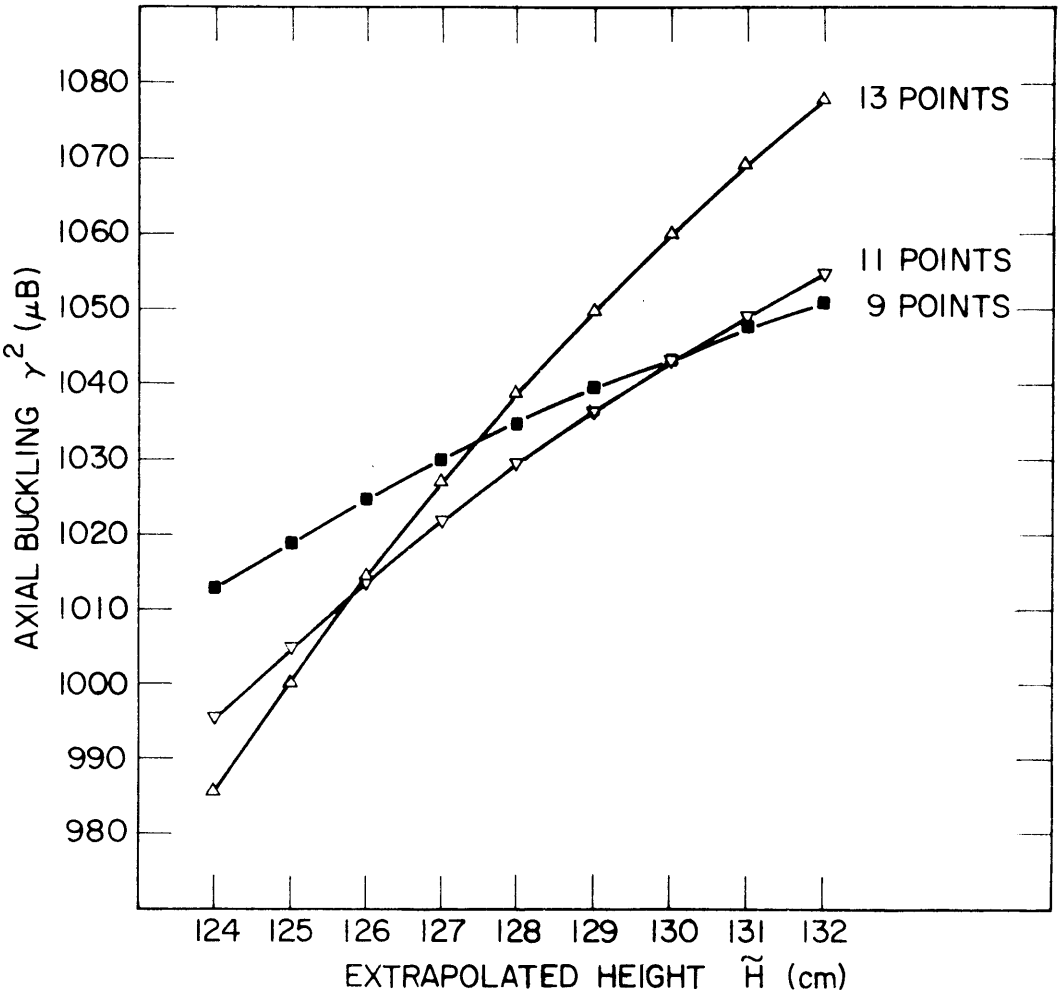

FIG. I.2 CURVES OF THE AXIAL BUCKLING VS. THE EXTRAPOLATED HEIGHT OBTAINED BY MEANS OF THE CURVE-FITTING METHOD FOR THE RUN C2: Cd-COVERED FOILS, 1.75"-LATTICE, 1.43% U^{235}, 0.25"-U RODS.

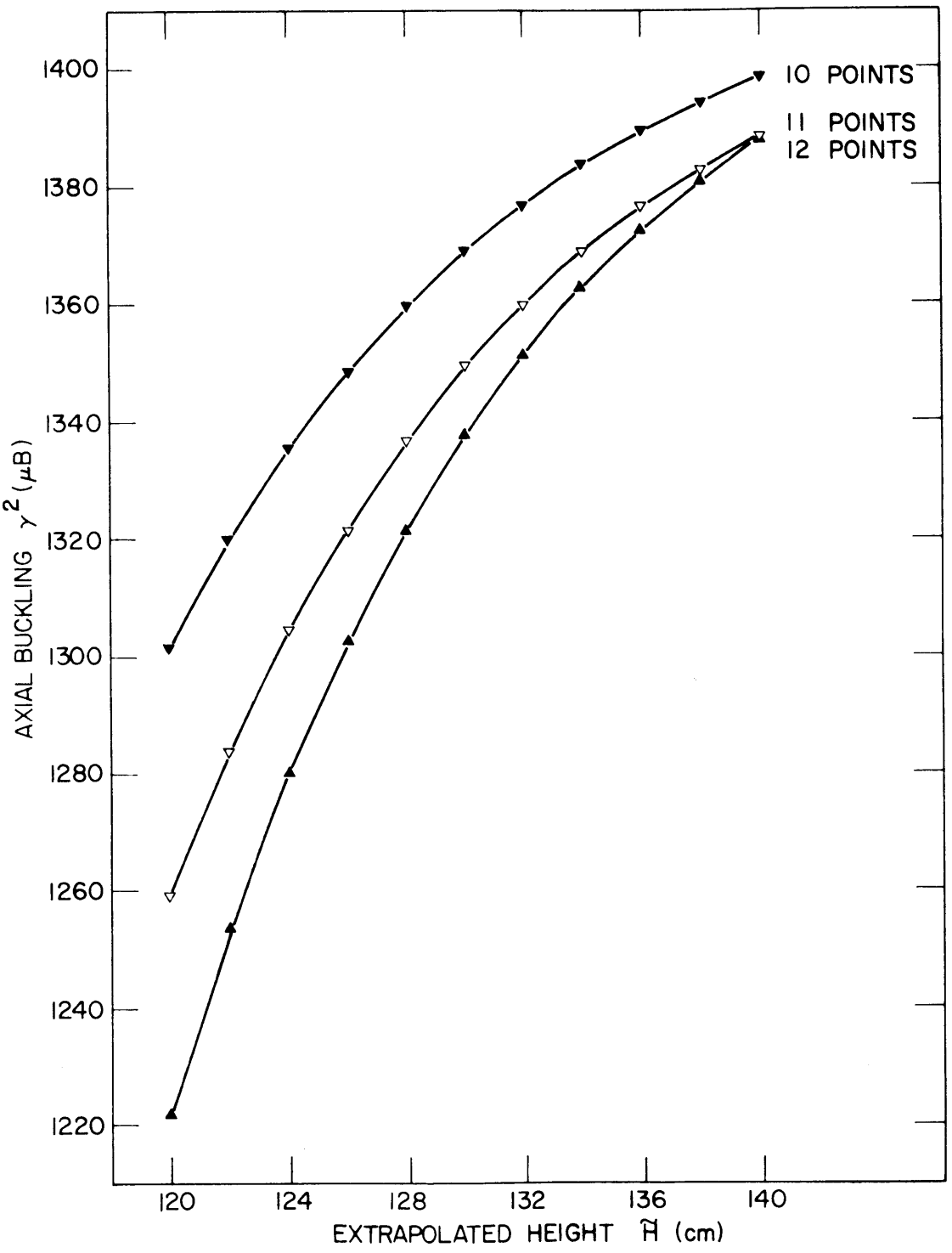

FIG. 1.3 CURVES OF THE AXIAL BUCKLING VS. THE EXTRAPOLATED HEIGHT OBTAINED BY MEANS OF THE CURVE-FITTING METHOD FOR THE RUN P5: 1.5" LATTICE, 0.947 % U^{235}, 0.387" U RODS.

curves never cross each other, as in Figure 1.3; the experimental data are then discarded. For the reasons outlined, the consistency in the determination of axial buckling and extrapolated height is not as good as is desired. Inconsistencies are indicated, as will be shown in Chapter III, by the relatively large values of the standard deviations of γ^2 and $\tilde{H}$. It seems likely that the method of data analysis is responsible (at least in part) for these inconsistencies, and a new method of data analysis will be applied and examined in this report.

The experimental determination of the extrapolation distance has been a matter of controversy for some time. In addition to the difficulty of providing proper conditions for measuring the extrapolation distance, the lack of a consistent scheme for data reduction has also contributed to the inconsistency of the results that have been obtained. The importance of experiments with pulsed neutron sources in reactor physics emphasizes the need for an improved method for obtaining the extrapolation distance or extrapolated size. In these experiments, it is essential to understand just what is meant by "geometric buckling" in an energy-dependent system and the geometric buckling is highly sensitive to the extrapolation distance.

The basic problems involved in the conventional measurements of the material buckling arise from the presence of a source neutron contribution and from possible transport and energy effects on the axial and radial flux distributions. All of these effects can lead to systematic errors in the measured values of the material buckling. The usual way of avoiding the difficulties is to use a sufficiently large assembly so that there will be a region within it where the

perturbing effects are negligible. But it is sometimes desirable, for convenience and economy, to use small assemblies in which these effects may not be negligible. For example, the use of miniature lattices for measurements of reactor physics parameters instead of large exponential assemblies is attractive, if feasible (K10, W5). Peak (P2) and Sefchovich (S1) have demonstrated the feasibility of miniature lattices for the measurement of the following parameters: the ratio ρ_{28} of epicadmium to subcadmium capture rates in U-238, the ratio δ_{25} of epicadmium to subcadmium fission rates in U-235, the ratio δ_{28} of fast fissions in U-238 to the total number of fissions in U-235, and the ratio C^* of the total capture rate in U-238 to the total fission rate in U-235. However, it has so far not been possible to determine the material buckling in the miniature lattices because of the transport and energy effects and the relatively large contribution of the source neutrons. This shortcoming could be a serious obstacle in the way of the increased use of miniature lattices.

One of the purposes of the research to be described in this report has been to try to derive values of the material buckling from activation data obtained in miniature lattices. Preliminary work indicated that the failure to obtain any consistent values of the axial buckling and extrapolated height in a small assembly such as a miniature lattice might be due to the inadequacy of the curve-fitting method. The reason for the inadequacy is not difficult to understand: it is the inherent numerical difficulty in convergence associated with the least-squares technique when three or more independent parameters have to be fitted by the linearized least-squares process (S2).

In addition, when the assembly under study is small, the neutron flux cannot be described by means of a simple two-parameter function. Hence, the development of a theoretical method for buckling analysis seems necessary: first, to obtain values of the material buckling of miniature lattices; second, to improve the consistency (i.e., standard deviation) in the buckling values and extrapolated sizes.

1.3 OBJECTIVES OF THE PRESENT WORK

The main objective of the present work is, then, to develop a new scheme for extracting buckling values and the extrapolated sizes from measured activity distributions, a scheme that might be applied to small assemblies as well as to large exponential assemblies.

The second objective is to study transport and energy effects on the determination of buckling and to seek criteria for the existence and location of an asymptotic region in an assembly.

The final objective is to investigate the possibility of the use of the concept of buckling in small assemblies, and hence to determine if miniature lattices can be used for the measurement of the material buckling.

1.4 CONTENTS OF THE REPORT

Chapter II presents arguments that justify the measurement of the material buckling in small assemblies. Chapter III describes the new data reduction scheme, the Moments Method, for the analysis of the axial buckling and extrapolated height. The corresponding moments analysis for the radial buckling and the extrapolated radius

is given in Chapter IV. Chapter V treats the application of the moments method to miniature lattices. Chapter VI discusses the transport effect on the determination of the buckling. Conclusions and recommendations for future work are given in Chapter VII. The appendices consist, in order, of a description of the computer codes used, Simpson's rule for unequal intervals, the application of the moments method to a parallelepiped assembly, a finite difference method for the calculation of geometric bucklings, an error analysis for the case with reflector effect, a least-squares technique for the estimate of the coefficient corresponding to the reflector effect, a measure of the fit of theoretical curves predicted by the moments method to experimental data points, and bibliography.

Chapter II

THE JUSTIFICATION OF BUCKLING MEASUREMENTS IN MINIATURE LATTICES

Attempts to measure the material buckling in small subcritical assemblies such as miniature lattices have so far not been successful (P2, S1). In this chapter, the theory of small assemblies will be investigated further to see if conditions exist under which the material buckling can be derived from flux measurements in such assemblies.

2.1 FUNDAMENTAL ASSUMPTIONS OF THE CONVENTIONAL BUCKLING MEASUREMENT

The concept of buckling is well defined within the region of validity of the First and Second Fundamental Theorems of Homogeneous Reactor Theory expressed by Weinberg and Wigner (W1), or of the asymptotic reactor theory developed by Ferziger and Zweifel (F1). These treatments supply a theoretical basis for buckling measurements and set conditions for the validity of such measurements.

The basic assumptions that must be made for the measurement of material buckling by means of subcritical assemblies have been discussed by Palmedo (P1) and others (K3, K1). It will suffice here to review the conditions imposed on the conventional buckling experiment:

(a) The transport effect on buckling should not be so severe as to break down the diffusion approximation — the asymptotic condition.

(b) The medium of interest is isotropic and homogeneous so that the nuclear parameters – cross sections and diffusion coefficients – are independent of position. This condition is listed for the sake of mathematical rigor. In practice, it is not necessary: even for a heterogeneous assembly, we can map the flux at points of symmetry in the moderator region and can describe the envelope of the flux shape by means of the fundamental mode solution of the neutron diffusion equation. Thus, as far as the measurement of material buckling by means of the flux shape method is concerned, the assumption is satisfied to a good approximation in a heterogeneous system.

Under the two conditions stated above, the behavior of a single group of neutrons far from an external source is governed by the Helmholtz equation

$$\nabla^2\Phi(\vec{r}) + B_m^2\Phi(\vec{r}) = 0 \,, \tag{2.1}$$

where B_m^2 is the material buckling and

$$\Phi(\vec{r}) = \Phi(\vec{r}, z, \theta)$$

for a cylindrical system. We shall use cylindrical coordinates throughout the analysis because the miniature lattice experiments were made in a cylindrical tank. There are an infinite number of different solutions of an equation of the type of Eq. (2.1). However, in a limited set of coordinate systems, called separable coordinate systems for the equation in question, one can find a set of Φ's with nodal surfaces which all coincide with the three families of coordinate surfaces. We may then write

$$\Phi(\vec{r}) = \phi(r)\,\phi(z)\,\Theta(\theta)\ . \tag{2.2}$$

The conditions for separable coordinate systems are discussed by Morse and Feshbach (M2). The separability of Eq. (2.2) has been verified experimentally, even in miniature lattices (S1). An immediate consequence of Eq. (2.2) is the fact that the material buckling can be expressed in terms of the separation constants corresponding to the fundamental modes; namely,

$$B_m^2 = \alpha^2 - \gamma^2 + B_\theta^2\ , \tag{2.3}$$

where

$$\alpha^2 = \frac{d^2\phi(r)/dr^2}{\phi(r)} = \text{radial buckling,} \tag{2.4}$$

$$\gamma^2 = \frac{d^2\phi(z)/dz^2}{\phi(z)} = \text{axial buckling,} \tag{2.5}$$

$$B_\theta^2 = -\frac{d^2\Theta(\theta)/d\theta^2}{\Theta(\theta)} = \text{azimuthal buckling.} \tag{2.6}$$

The conventional way of measuring the material buckling is based on the expression (2.3) with the additional assumption that the neutron flux is azimuthally symmetric so that B_θ^2 vanishes. This assumption is, of course, made merely for convenience; one could actually determine B_θ^2 by measuring many radial traverses. It usually suffices to measure B_θ^2 in a typical lattice experiment to see how much it may contribute to the material buckling B_m^2; its contribution is usually negligible.

(c) The energy transients are insignificant, so that the neutron flux is separable in space and energy in a sufficiently large region inside the system of interest — spectral equilibrium.

(d) The contribution of the external neutron source must be nullified: either experimentally, so that the neutron flux becomes characteristic of the lattice under investigation; or it must be subtracted, in accord with an appropriate theoretical analysis.

2.2 JUSTIFICATION OF THE DIFFUSION APPROXIMATION

Inönü (I1), Dresner (D1), and Yip and Zweifel (Y1) have investigated the validity of the Second Fundamental Theorem of Reactor Theory. Their results indicate that asymptotic reactor theory is applicable, in the one-speed case, even to systems whose linear dimensions are of the order of a neutron mean free path. Generally speaking, the use of asymptotic reactor theory is satisfactory so long as the asymptotic flux from an external source is a reasonable approximation to the actual flux. This condition should be achieved, in principle, for systems larger than a few mean free paths, and asymptotic reactor theory should therefore be applicable even to relatively small systems (Y1, F1).

The assembly for miniature lattice experiments at the M.I.T. Lattice Project is a thin-walled aluminum tank in the shape of a right cylinder, 21 inches high and 20 inches in diameter, as shown in Figure 2.1. Though small in terms of neutron migration length in heavy water, it is still enough to justify the use of asymptotic reactor theory according to the results obtained by Yip and others (Y1, I1, D1).

In particular, we shall investigate the gross leakage of neutrons in the miniature lattices, since neutron leakage is of decisive importance to small systems in general. We shall establish the

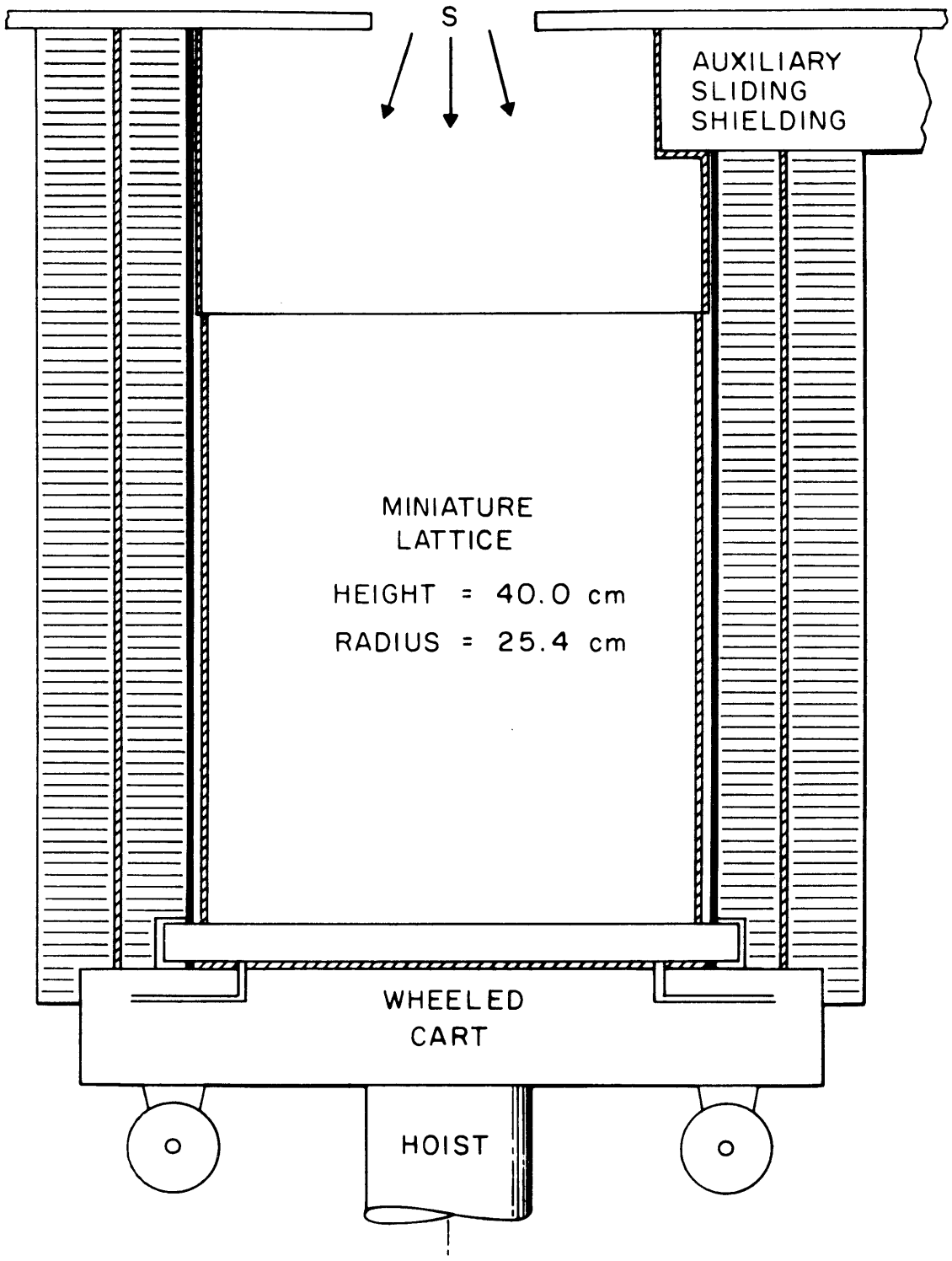

FIG. 2.1 EXPERIMENTAL SETUP DURING IRRADIATION FOR THE MINIATURE LATTICE EXPERIMENTS.

relationship between the diffusion-theory leakage cross section and that of asymptotic transport theory. The leakage cross section in diffusion theory is given by

$$\Sigma_L^{DIF} = DB^2 = \Sigma_{tr}\left[\frac{1}{3}\left(\frac{B}{\Sigma_{tr}}\right)^2\right], \tag{2.7}$$

where B^2 is the geometric buckling and Σ_{tr} is the transport cross section. In asymptotic transport theory, the leakage cross section is (O1)

$$\Sigma_L^{TR} = \Sigma_{tr}\left\{\frac{\left(\frac{B}{\Sigma_{tr}}\right)}{\tan^{-1}\left(\frac{B}{\Sigma_{tr}}\right)} - 1\right\}. \tag{2.8}$$

We seek the condition under which Eq. (2.8) reduces to Eq. (2.7): we use the formula

$$\tan^{-1} x = x - \frac{1}{3}x^3 + \frac{1}{5}x^5 - \frac{1}{7}x^7 + \ldots, \quad x^2 < 1 . \tag{2.9}$$

Suppose that B/Σ_{tr} is sufficiently small so that

$$\tan^{-1}\left(\frac{B}{\Sigma_{tr}}\right) \approx \frac{B}{\Sigma_{tr}}\left[1 - \frac{1}{3}\left(\frac{B}{\Sigma_{tr}}\right)^2\right] .$$

Then we may write

$$\Sigma_L^{TR} \approx \Sigma_{tr}\left\{\frac{1}{\left[1 - \frac{1}{3}\left(\frac{B}{\Sigma_{tr}}\right)^2\right]} - 1\right\}$$

$$\approx \Sigma_{tr}\left\{\left[1 + \frac{1}{3}\left(\frac{B}{\Sigma_{tr}}\right)^2\right] - 1\right\} = \Sigma_L^{DIF} . \tag{2.10}$$

In the case of the miniature lattices investigated at the M.I.T. Lattice Project,

$$B \approx 0.08 \text{ cm}^{-1}, \qquad \Sigma_{tr} \approx 0.40 \text{ cm}^{-1}$$

so that

$$\left(\frac{B}{\Sigma_{tr}}\right) \approx 0.20, \quad \text{and} \quad \left(\frac{B}{\Sigma_{tr}}\right)^2 \approx 0.04 \ll 1 .$$

The condition (2.10) holds, and the diffusion approximation is justified for the leakage cross section.

A sensitive parameter for testing the existence of an asymptotic region is the geometric buckling defined in terms of the parameters α^2 and γ^2 of Eqs. (2.4) and (2.5). The geometric buckling is, in general, space-dependent but becomes independent of position in an asymptotic region where only the fundamental flux mode persists. To show this, let us consider a cylindrical system where the fundamental mode of the radial flux distribution is given by $CJ_o(\alpha r)$ and that of the axial flux distribution is given by A sinh $\gamma(\tilde{H}-z)$. It can be readily verified by inserting these functions into Eqs. (2.4) and (2.5) that the radial and axial geometric bucklings do indeed become α^2 and γ^2, respectively, which are certainly independent of position. However, in the neighborhood of boundaries, the neutron flux is contaminated by spatial and/or energy transients, and the geometric buckling varies with position.

A one-group P_3 calculation of the axial geometric buckling of the miniature lattice ML3 has been made to examine the transport effect on buckling (see Chapter VI for details). The result is shown in Figure 2.2. It is evident that there is indeed an asymptotic region of about 15 cm where the axial buckling is very nearly constant. Furthermore, the moments method, which will be described in

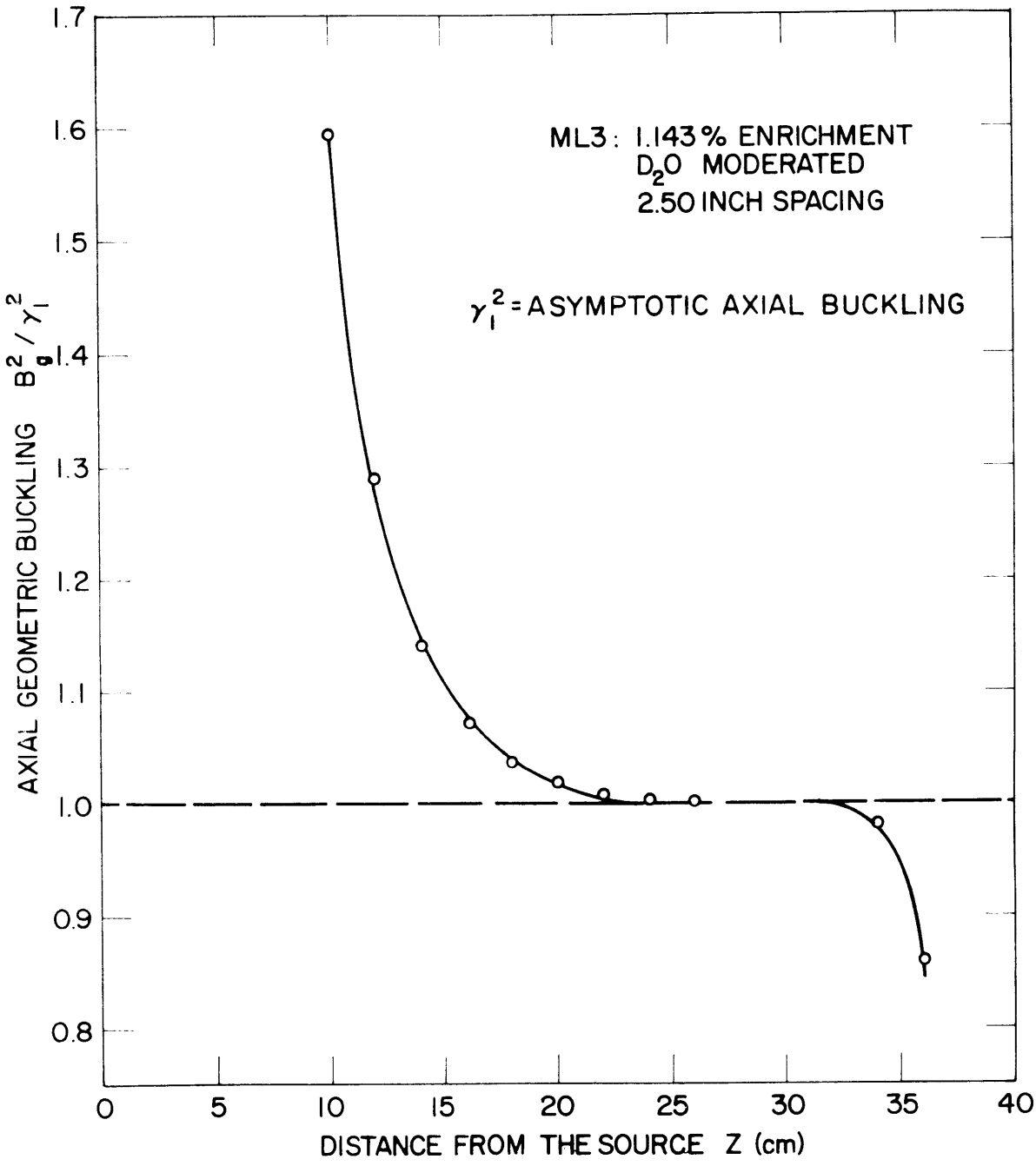

FIG. 2.2 DISTRIBUTION OF THE AXIAL GEOMETRIC BUCKLING AS A FUNCTION OF THE DISTANCE FROM THE SOURCE OF THE MINIATURE LATTICE ML3 IN A ONE-GROUP P3 APPROXIMATION.

Chapter III, has been used to obtain the axial buckling as a function of the distance from the source to the first data point (of the same miniature lattice ML3) from the experimental activation data. The result plotted in Figure 2.3 indicates that the axial buckling does level off in this lattice, starting at about 13 cm from the source. Figure 2.3 also shows that for each miniature lattice there is some region in which the axial buckling is constant or nearly constant.

2.3 JUSTIFICATION OF SPECTRAL EQUILIBRIUM

By definition, the neutron energy spectrum reaches its equilibrium state if and only if the neutron flux becomes separable in space and energy. This is, in fact, the essence of the First Fundamental Theorem of Reactor Theory. The condition is exactly true in a homogeneous infinite medium, but it could be met in a bare uniform reactor over a certain region far from boundaries (W1). The question of separability requires investigation, however, in finite heterogeneous systems. Experiments have been performed by Inönü (I2) at Oak Ridge to test the space-energy separability. He measured the subcadmium and epicadmium fluxes and showed that only if data near the boundary (within about 3 to 3.5 inches) of a large critical aqueous U^{235} solution were rejected, is the extrapolation distance independent of energy. The commonly used experimental criterion for space-energy separability is the constancy of the cadmium ratio as a function of position (P1, H8, H9). But this criterion may not really provide a valid condition for the separability of the flux in space and energy; it will be discussed in section 2.4.

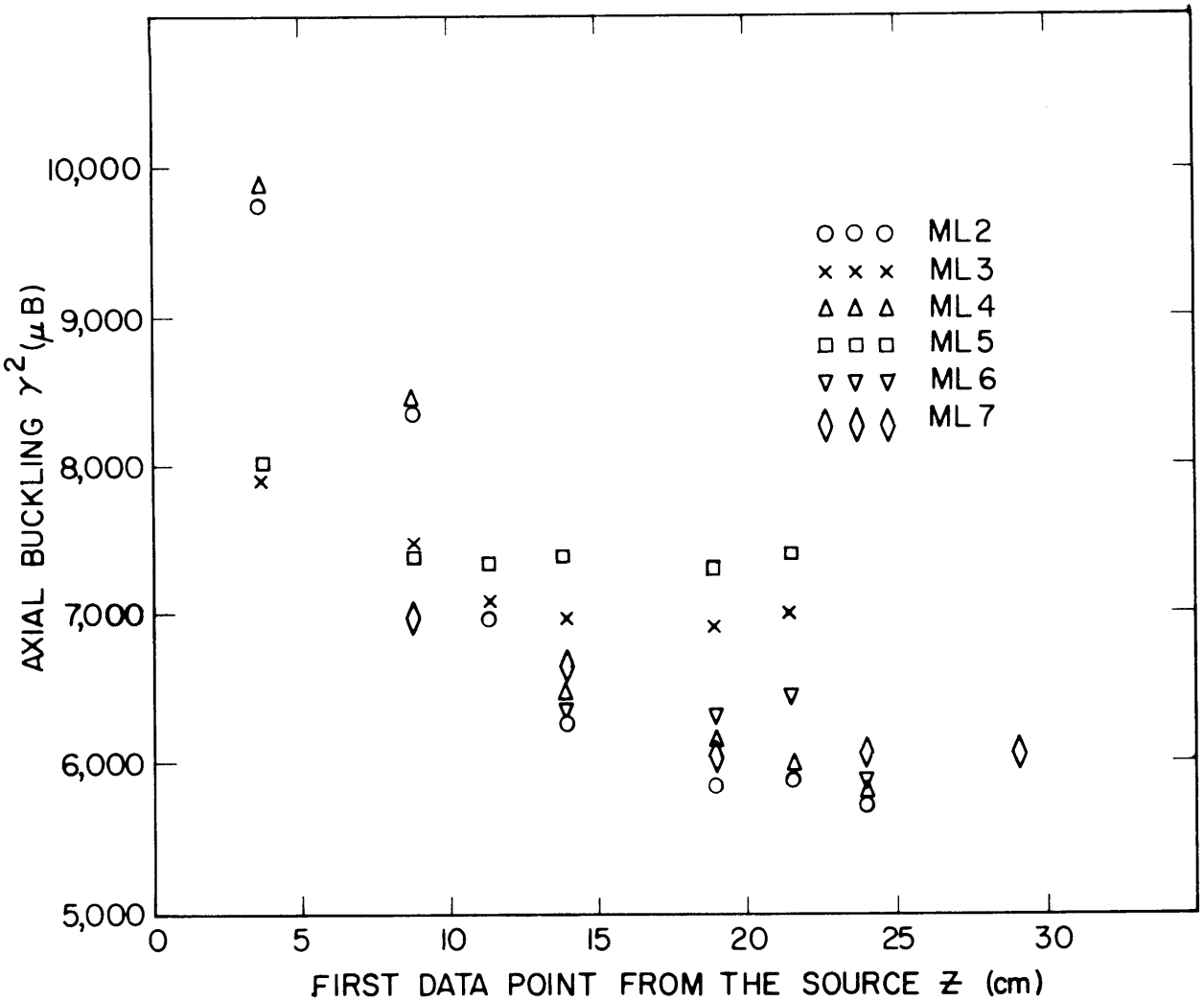

FIG. 2.3 VARIATION OF THE AXIAL BUCKLING FOR THE ACTIVATION DATA OF BARE GOLD FOILS WITH THE FIRST DATA POINT FROM THE SOURCE OF THE MINIATURE LATTICES.

We now try to estimate the distance in a finite system from boundaries at which spectral equilibrium may be attained. We start with the rigorous neutron transport equation under the assumption that all neutron cross sections are functions of neutron energy only:

$$\vec{\Omega} \cdot \vec{\nabla}\Phi(\vec{r}, E, \vec{\Omega}) + \Sigma_t(E)\Phi(\vec{r}, E, \vec{\Omega})$$

$$= \int_{\vec{\Omega}} d\vec{\Omega}' \int_0^\infty dE' \, \Sigma_s(E) f(E' \to E ; \vec{\Omega}' \to \vec{\Omega}) \Phi(\vec{r}, E', \vec{\Omega}')$$

$$+ \int_{\vec{\Omega}} d\vec{\Omega}' \int_0^\infty dE' \, \nu\Sigma_f(E') \chi(E' \to E ; \vec{\Omega}' \to \vec{\Omega}) \Phi(\vec{r}, E', \vec{\Omega}')$$

$$+ S(\vec{r}, E, \vec{\Omega}) \, , \qquad (2.11)$$

where

$S(\vec{r}, E, \vec{\Omega})$ is the external neutron source,

$f(E' \to E ; \vec{\Omega}' \to \vec{\Omega})$ is the probability that a neutron with initial energy E' and direction $\vec{\Omega}'$ emerges from a scattering collision with an energy E in dE and a direction $\vec{\Omega}$ in $d\vec{\Omega}$,

$\chi(E' \to E ; \vec{\Omega}' \to \vec{\Omega})$ is the probability that a neutron with energy E in dE and direction $\vec{\Omega}$ in $d\vec{\Omega}$ is emitted in a fission process induced by a neutron with initial energy E' and direction $\vec{\Omega}'$.

To cast Eq. (2.11) into a simpler form, we define the collision kernel

$$\Sigma_c(E) \, g(E' \to E ; \vec{\Omega}' \to \vec{\Omega})$$

$$\equiv \Sigma_s(E) f(E' \to E ; \vec{\Omega}' \to \vec{\Omega}) + \nu\Sigma_f(E) \chi(E' \to E ; \vec{\Omega}' \to \vec{\Omega}) \qquad (2.12)$$

by combining the scattering and fission processes. Since the external source is located at z=0, Eq. (2.11) reduces to

$$\vec{\Omega}\cdot\vec{\nabla}\Phi(\vec{r},E,\vec{\Omega}) + \Sigma_t(E)\,\Phi(\vec{r},E,\vec{\Omega})$$

$$= \int_{\vec{\Omega}} d\vec{\Omega}' \int_0^\infty dE'\,\Sigma_c(E')\; g(E'\to E\,;\,\vec{\Omega}'\to\vec{\Omega})\,\Phi(\vec{r},E',\vec{\Omega}')\ ,$$

$$\text{for}\quad z > 0\,. \qquad (2.13)$$

In the case of a finite cylinder (as in the miniature lattice experiments) with symmetry about the axis of the cylinder, the leakage term can be written (D2)

$$\vec{\Omega}\cdot\vec{\nabla}\Phi(\vec{r},E,\vec{\Omega}) = \Omega_r\left[\cos(\theta'-\theta)\,\frac{\partial}{\partial r} + \frac{\sin(\theta'-\theta)}{r}\,\frac{\partial}{\partial\theta}\right]\Phi(\vec{r},E,\vec{\Omega})$$

$$+\,\Omega_z\,\frac{\partial}{\partial z}\,\Phi(\vec{r},E,\vec{\Omega})\ , \qquad (2.14)$$

where θ' is the azimuthal angle corresponding to the direction $\vec{\Omega}'$.

Suppose that the neutron flux is separable in the spatial coordinates in the following manner:

$$\Phi(\vec{r},E,\vec{\Omega}) = \phi(z,E,\vec{\Omega})\;\phi(r,E,\vec{\Omega})\;\Theta(\theta,E,\vec{\Omega})\ . \qquad (2.15)$$

Substituting Eqs. (2.14) and (2.15) in Eq. (2.13), and then dividing throughout the equation by Eq. (2.15), we obtain

$$\Omega_r\cos(\theta'-\theta)\,\frac{\frac{\partial}{\partial r}\,\phi(r,E,\vec{\Omega})}{\phi(r,E,\vec{\Omega})} + \Omega_r\,\frac{\sin(\theta'-\theta)}{r}\,\frac{\frac{\partial}{\partial\theta}\,\Theta(\theta,E,\vec{\Omega})}{\Theta(\theta,E,\vec{\Omega})} + \Omega_z\,\frac{\frac{\partial}{\partial z}\,\phi(z,E,\vec{\Omega})}{\phi(z,E,\vec{\Omega})} + \Sigma_t(E)$$

$$= \int_{\vec{\Omega}} d\vec{\Omega}' \int_0^\infty dE'\,\Sigma_c(E')\,g(E'\to E\,;\vec{\Omega}'\to\vec{\Omega})\cdot\frac{\phi(r,E',\vec{\Omega}')}{\phi(r,E,\vec{\Omega})}\cdot\frac{\Theta(\theta,E',\vec{\Omega}')}{\Theta(\theta,E,\vec{\Omega})}$$

$$\cdot\,\frac{\phi(z,E',\vec{\Omega}')}{\phi(z,E,\vec{\Omega})}\ ,\quad \text{for}\quad z > 0\ . \qquad (2.16)$$

If we assume that the flux is azimuthally symmetric,

$$\frac{\partial}{\partial\theta}\,\Theta(\theta,E,\vec{\Omega}) = 0\ ,$$

$$\text{and}\qquad \frac{\Theta(\theta,E',\vec{\Omega}')}{\Theta(\theta,E,\vec{\Omega})} = 1\ . \qquad (2.17)$$

Even with the above assumption, Eq. (2.16) is still two-dimensional, and the mathematical treatment is extremely difficult. But it is possible to break the problem up into two one-dimensional problems in the following way. First, arrange the experiment in such a way that the axial flux distribution is measured along the axis of the cylinder at or near the center r=0 where asymptotic reactor theory is valid; then

$$\frac{\phi(r=0, E', \vec{\Omega}')}{\phi(r=0, E, \vec{\Omega})} \approx 1 \ . \tag{2.18}$$

Call the radial leakage

$$\Sigma_{Lr}(E) \equiv \Omega_r \cos(\theta'-\theta) \frac{\frac{\partial}{\partial r} \phi(r, E, \vec{\Omega})}{\phi(r, E, \vec{\Omega})} \ , \tag{2.19}$$

which may be calculated either by means of Eq. (2.8), the asymptotic transport theory result, or by Eq. (2.7), the diffusion theory result. With the help of Eqs. (2.17), (2.18), and (2.19), Eq. (2.16) then gives the neutron balance equation for the axial flux distribution

$$\mu \frac{\partial}{\partial z} \phi(z, E, \mu) + [\Sigma_t(E) + \Sigma_{Lr}(E)] \phi(z, E, \mu)$$
$$= \int_{-1}^{1} d\mu' \int_{0}^{\infty} dE' \, \Sigma_c(E') \, g(E' \to E \, ; \mu' \to \mu) \, \phi(z, E', \mu'),$$
$$\text{for } z > 0 \ , \tag{2.20}$$

where $\mu \equiv \Omega_z$.

Second, to obtain the corresponding equation for the radial flux distribution, we arrange the foil detectors on the plane $z=z_o$ where the axial flux has become asymptotic so that

$$\frac{\phi(z=z_o, E', \vec{\Omega}')}{\phi(z=z_o, E, \vec{\Omega})} \approx 1 \ . \tag{2.21}$$

We call the axial leakage

$$-\Sigma_{Lz}(E) \equiv \Omega_z \frac{\frac{\partial}{\partial z}\phi(z, E, \vec{\Omega})}{\phi(z, E, \vec{\Omega})} . \tag{2.22}$$

The negative sign comes from the fact that an external neutron source is feeding the system in the axial direction, with the result that we have a net in-leakage of neutrons as far as the radial flux is concerned. Thus, Eq. (2.16) leads to the following balance equation for the radial flux:

$$\Omega_r \cos(\theta'-\theta) \frac{\partial}{\partial r}\phi(r, E, \Omega_r) + [\Sigma_t(E)-\Sigma_{Lz}(E)]\phi(r, E, \Omega_r)$$

$$= \int_{\Omega_r} d\Omega'_r \int_0^\infty dE' \, \Sigma_c(E') \, g(E' \to E ; \Omega'_r \to \Omega_r) \, \phi(r, E', \Omega'_r) . \tag{2.23}$$

We first explore the equilibrium condition in the axial flux distribution. Define

$$\Sigma_t^*(E) \equiv \Sigma_t(E) + \Sigma_{Lr}(E) ; \tag{2.24}$$

Equation (2.20) becomes

$$\mu \frac{\partial}{\partial z}\phi(z, E, \mu) + \Sigma_t^*(E) \, \phi(z, E, \mu)$$

$$= \int_{-1}^{1} d\mu' \int_0^\infty dE' \, \Sigma_c(E') \, g(E' \to E ; \mu' \to \mu) \, \phi(z, E', \mu') ,$$

$$\text{for } z > 0 . \tag{2.25}$$

The external source is located at z=0 and will enter as a boundary condition. To treat the external source effect properly, we separate the neutron flux into two parts (D2):

$$\phi(z, E, \mu) = \phi^{uc}(z, E, \mu) + \phi^{c}(z, E, \mu) , \tag{2.26}$$

where $\phi^{uc}(z, E, \mu)$ represents the uncollided flux, while $\phi^{c}(z, E, \mu)$ denotes the collided flux. The uncollided flux satisfies Eq. (2.25) exactly without the integral term:

$$\mu \frac{\partial}{\partial z} \phi^{uc}(z, E, \mu) + \Sigma_t^*(E)\, \phi^{uc}(z, E, \mu) = 0 \ . \tag{2.27}$$

The solution is

$$\phi^{uc}(z, E, \mu) = A\, e^{-\Sigma_t^*(E) z/\mu} \ . \tag{2.28}$$

The constant A is determined by the boundary condition at $z=0$,

$$A = \phi^{uc}(0, E, \mu) = Q_o q(E)\, \delta(\mu - 1) \ . \tag{2.29}$$

Here we have assumed a <u>unidirectional</u> source with a source spectrum q(E) because this is very nearly the case for the miniature lattice experiments. Thus, the uncollided flux is given by

$$\phi^{uc}(z, E, \mu) = Q_o q(E)\ \delta(\mu - 1)\ e^{-\Sigma_t^*(E) z/\mu} \ , \tag{2.30}$$

where Q_o is the source intensity. By substituting Eq. (2.26) in Eq. (2.25), we obtain the neutron balance equation for the collided flux

$$\begin{aligned} &\mu \frac{\partial}{\partial z} \phi^{c}(z, E, \mu) + \Sigma_t^*(E)\, \phi^{c}(z, E, \mu) \\ &\quad = \int_{-1}^{1} d\mu \int_{0}^{\infty} dE'\, \Sigma_c(E')\, g(E' \to E\, ; \mu' \to \mu)\, \phi^{c}(z, E', \mu') \\ &\qquad + Q_o \int_{0}^{\infty} dE'\, \Sigma_c(E')\, g(E' \to E\, ; \mu' \to \mu)\ q(E')\ e^{-\Sigma_t(E') z} \ . \end{aligned} \tag{2.31}$$

We see that the collided flux satisfies the same neutron transport equation as does the total flux with an additional distributed source term due to the uncollided flux.

Suppose that the total cross section $\Sigma_t^*(E)$ is a slowly varying function of neutron energy so that the last term in Eq. (2.31) may be written

$$Q_o e^{-\bar{\Sigma}_t z} \int_0^\infty dE' \, \Sigma_c(E') \, g(E' \to E \, ; \, 1 \to \mu) \, q(E') = Q_o e^{-\bar{\Sigma}_t z} \, S(E) \, , \qquad (2.32)$$

where

$$S(E) \equiv \int_0^\infty dE' \, \Sigma_c(E') \, g(E' \to E \, ; \, 1 \to \mu) \, q(E') \, , \qquad (2.33)$$

and $\bar{\Sigma}_t$ is the properly averaged total cross section. Then Eq. (2.31) becomes

$$\mu \frac{\partial}{\partial z} \phi^c(z, E, \mu) + \Sigma_t^*(E) \, \phi^c(z, E, \mu)$$

$$= \int_{-1}^{1} d\mu' \int_0^\infty dE' \, \Sigma_c(E') \, g(E' \to E \, ; \, \mu' \to \mu) \, \phi^c(z, E', \mu') + Q_o S(E) \, e^{-\bar{\Sigma}_t z} \, . \qquad (2.34)$$

It is evident from this equation that the neutron flux characteristic of the assembly would be the collided flux, which must be separable in space and energy to achieve spectral equilibrium.

From the study of the Milne problem by means of asymptotic transport theory (K4), it has been found that the neutron flux far from the boundary has an asymptotic hyperbolic sine shape, and that this flux extrapolates to zero a short distance from the physical boundary of the system. So the desired asymptotic solution of Eq. (2.34) to establish spectral equilibrium is given by

$$\phi^c_{asy}(z, E, \mu) = \sinh \gamma(\tilde{H} - z) \, \psi(E, \mu) \, , \qquad (2.35)$$

where $\psi(E, \mu)$ is the angular neutron spectrum, γ^2 is the axial buckling

(γ^{-1} being the relaxation length), and $\tilde{H}$ is the extrapolated height. Insertion of Eq. (2.35) into Eq. (2.34) yields

$$\psi(E,\mu) = \frac{\frac{1}{\mu\gamma}\tanh\gamma(\tilde{H}-z)}{\left[\frac{\Sigma_t^*(E)}{\mu\gamma}\tanh\gamma(\tilde{H}-z) - 1\right]} \int_{-1}^{1} d\mu' \int_{0}^{\infty} dE'\, \Sigma_c(E')\, g(E'\to E\,;\mu'\to\mu)\, \psi(E',\mu')$$

$$+ \frac{\frac{Q_o}{\mu\gamma}\left[\frac{e^{-\bar{\Sigma}_t z}}{\cosh\gamma(\tilde{H}-z)}\right]}{\left[\frac{\Sigma_t^*(E)}{\mu\gamma}\tanh\gamma(\tilde{H}-z) - 1\right]} \cdot S(E)\ . \qquad (2.36)$$

We can infer from Eq. (2.36) some information concerning spectral equilibrium. First, since the neutron flux must be positive and nonzero, it is necessary that

$$\left[\frac{\Sigma_t^*(E)}{\mu\gamma}\tanh\gamma(\tilde{H}-z) - 1\right] > 0\ . \qquad (2.37)$$

Second, for the neutron spectrum to be characteristic of the lattice under consideration, the source neutron contribution, that is, the second term of the right-hand side of Eq. (2.36), must vanish:

$$Q_o S(E)\left\{\frac{e^{-\bar{\Sigma}_t z}}{\cosh\gamma(\tilde{H}-z)}\right\} = 0\ . \qquad (2.38)$$

Strictly speaking, this condition requires an infinitely large distance z; but we can meet the condition in a practical sense if

$$\left\{\frac{e^{-\bar{\Sigma}_t z}}{\cosh\gamma(\tilde{H}-z)}\right\} \approx 0\ . \qquad (2.39)$$

It is also evident from Eq. (2.36) that, regardless of the spectrum of the neutron source, the neutron spectrum inside the system should be always nonseparable when the neutron source contribution is significant. This is an inherent disadvantage of exponential experiments. It is therefore necessary to have a system that fulfills the condition given by Eq. (2.39) if the exponential experiments to be performed in that system are to be meaningful. Finally, even if we have satisfied the condition of Eq. (2.39), the neutron spectrum is still not separable owing to the boundary effect unless we satisfy the condition

$$\tanh \gamma(\tilde{H}-z) = 1 \, . \qquad (2.40)$$

The fact that the hyperbolic tangent is a well-behaved function and approaches its asymptotic value of 1 rapidly (A2) assures us that the last condition can be satisfied, in practice, without difficulty in the case of relatively large assemblies. (See Figure 2.4.)

The condition of Eq. (2.40) can, however, be very serious for the miniature lattices. To see this, we note that the condition is very nearly met if $\gamma(\tilde{H}-z) \geqslant 2.0$, since

$$\tanh \gamma(\tilde{H}-z) \approx 1 - 2\,e^{-2\gamma(\tilde{H}-z)} = 1.0 - 0.0366 \, ,$$

and the deviation amounts to only about 4%. For the miniature lattices, $\gamma \approx 0.08 \text{ cm}^{-1}$, $\tilde{H} = 46$ cm,

$$(\tilde{H}-z) \geqslant \frac{2.0}{0.08} = 25 \text{ cm} \, ,$$

or $$z \leqslant (\tilde{H} - 25) = 21 \text{ cm} \, .$$

This is certainly serious when the total axial length available is only 40 cm. In the full-size M.I.T. lattices, the axial buckling is about

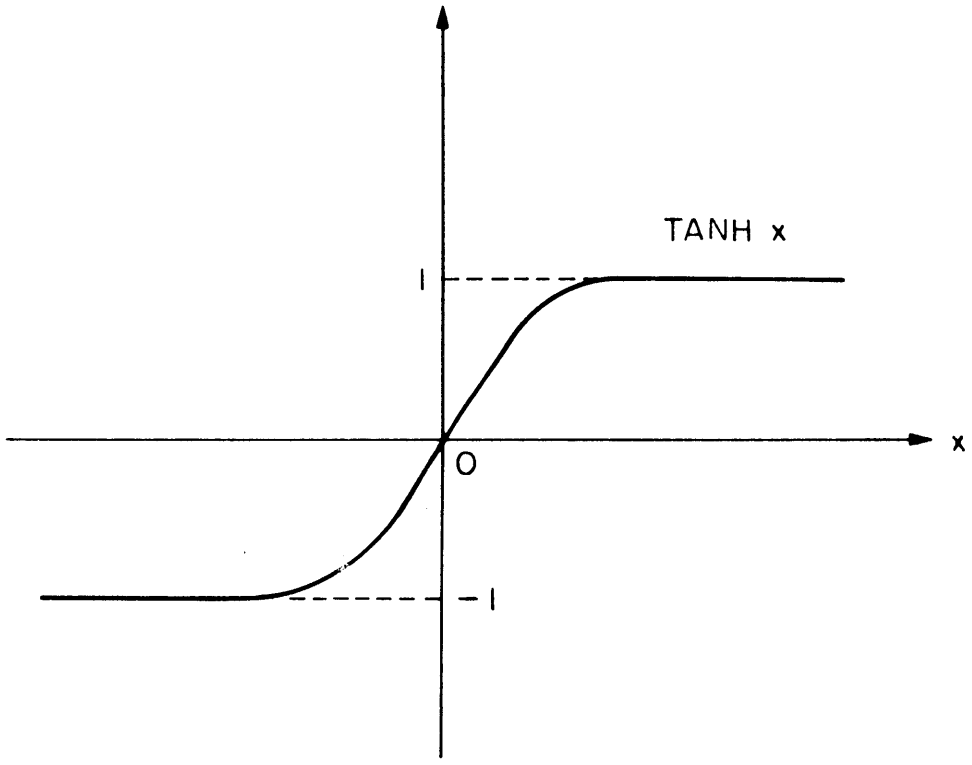

FIG. 2.4 ASYMPTOTIC BEHAVIOR OF THE HYPERBOLIC TANGENT.

1500 μB, which leads to

$$(\tilde{H}-z) \geq 40 \text{ cm},$$

or $$z \leq (128-40) = 88 \text{ cm}.$$

In this case, there is no problem since the total axial length available is about 122 cm.

The condition of Eq. (2.40) is, however, unnecessarily stringent because space-energy separability is also achieved if

$$\frac{\Sigma_t^*(E)}{\mu\gamma} \tanh \gamma(\tilde{H}-z) \gg 1 , \tag{2.41}$$

when the function $\tanh \gamma(\tilde{H}-z)$ cancels in Eq. (2.36). The condition of Eq. (2.41) is better satisfied by a larger assembly whose γ is smaller, as it should be. For the miniature lattices,

$$\left[\frac{\Sigma_t^*(E)}{\mu\gamma}\right]_{min} \approx \frac{0.44}{0.08} = 5.5 .$$

If $\tanh \gamma(\tilde{H}-z) \geq 0.728$,

$$\left[\frac{\Sigma_t^*(E)}{\mu\gamma}\right]_{min} \tanh \gamma(\tilde{H}-z) \gtrapprox 4.0 > 1 .$$

The neglect of 1 in the denominator in the first term on the right side of Eq. (2.36) leads to a deviation of 25%. This is, of course, an overestimate because $\tanh \gamma(\tilde{H}-z)$ is already approaching a constant value around 0.73. In this case, we have

$$(\tilde{H}-z) \geq \frac{0.93}{0.08} = 11.63 \text{ cm},$$

or $$z \leq (\tilde{H} - 11.63) = 46 - 11.63 = 34.37 \text{ cm}$$

to achieve spectral equilibrium.

Table 2.1 gives the values of the axial position where the neutron flux is nearly free of the boundary effect (and spectral equilibrium should be attained) for the six miniature lattices investigated at the M.I.T. Lattice Project. It is seen that about within 4 or 5 cm from the physical boundary the axial flux can be nonseparable in space and energy.

With Eq. (2.40), the condition (2.37) becomes

$$\mathrm{Re}[\gamma] < [\Sigma_t^*(E)]_{min} , \tag{2.42}$$

where $[\Sigma_t^*(E)]_{min}$ is the minimum value of the total macroscopic cross section corresponding to $|\mu| = 1$, and Re denotes the real part of γ which may, in general, be a complex number. The condition of Eq. (2.42) assures the existence of a physically realizable solution of Eq. (2.36) and hence of the axial buckling. The condition (2.42) is satisfied for the miniature lattices, since $\bar{\Sigma}_t \approx 0.44\ \mathrm{cm}^{-1}$ which well exceeds the value of γ (see Table 2.1). This result warrants the existence of the axial buckling. A formal mathematical proof of the existence of a relaxation length has been given by S. Kaplan (K5). It seems clear that the basic problem associated with the miniature lattices is not the question of the existence of the fundamental eigenvalue, but it is rather that of whether the neutron flux has become separable in space and energy.

We now turn to the condition (2.39). If we assume that the source neutron contribution is negligible when

$$\left\{ \frac{e^{-\bar{\Sigma}_t z}}{\cosh \gamma(\tilde{H}-z)} \right\} \geq 10^{-5}, \quad \text{(Case I)} , \tag{2.43}$$

Table 2.1 The axial position measured from the source where the nonseparability of the axial flux in space and energy due to the boundary effect is negligible for the miniature lattices.*

Lattice Designator	Lattice Specification	γ (cm^{-1})	$\tilde{H}$ (cm)	$(\tilde{H}-z)$ (cm)	Axial position near the boundary to reach spectral equilibrium z (cm)
ML2	1.143% enriched 1.25" spacing	0.0765	47.73	12.16	35.57
ML3	1.143% enriched 2.50" spacing	0.0830	46.41	11.20	35.21
ML4	1.027% enriched 1.25" spacing	0.0784	48.46	11.87	36.59
ML5	1.027% enriched 2.50" spacing	0.0885	47.84	10.50	37.34
ML6	1.027% enriched 1.75" spacing	0.0795	44.98	11.70	33.28
ML7	1.143% enriched 1.75" spacing	0.0783	44.72	11.88	32.84

* All the fuel rods of the miniature lattices have a diameter of 0.25 inch. The physical length is about 40 cm. The values of γ and $\tilde{H}$ are obtained by the moments method to be described in Chapter III, and the details of calculation will be given in Chapter V.

spectral equilibrium will be attained for most miniature lattices at about 24 cm from the source ($z \approx 24$ cm). On the other hand, if we relax the requirement so that

$$\left\{ \frac{e^{-\bar{\Sigma}_t z}}{\cosh \gamma(\tilde{H}-z)} \right\} \leq 10^{-4}, \text{ (Case II)}, \tag{2.44}$$

then $z \approx 18$ cm to reach spectral equilibrium.

Table 2.2 gives the detailed results for the six miniature lattices described in Table 2.1.

Table 2.2 The distance from the source at which spectral equilibrium is attained in the miniature lattices.

Lattice Designator	Lattice Specification	γ (cm^{-1})	Distance from the Source to Reach Spectral Equilibrium (cm)	
			Case I	Case II
ML2	1.143% enriched 1.25" spacing	0.0790	23.38	17.19
ML3	1.143% enriched 2.50" spacing	0.0835	23.10	16.90
ML4	1.027% enriched 1.25" spacing	0.0784	23.40	17.20
ML5	1.027% enriched 2.50" spacing	0.0885	22.76	16.42
ML6	1.027% enriched 1.75" spacing	0.0801	23.52	17.36
ML7	1.143% enriched 1.75" spacing	0.0785	23.63	17.50

The results listed in Table 2.2 are, in fact, highly conservative because the external source is actually not unidirectional as was assumed; there is a certain degree of isotropy in the source, and the real situation should be more favorable than the results indicate. Furthermore, the requirements expressed by Eqs. (2.43) and (2.44) may be still unnecessarily stringent in comparison with the criterion (2.41). To see this, we note that Eq. (2.39) and Eq. (2.40) reduce to the following forms for large values of the argument $\gamma(\tilde{H}-z)$:

$$2\, e^{-[\bar{\Sigma}_t z+\gamma(\tilde{H}-z)]} \approx 0 , \tag{2.45}$$

and

$$2\, e^{-2\gamma(\tilde{H}-z)} \approx 0 . \tag{2.46}$$

If $$\bar{\Sigma}_t z > \gamma(\tilde{H}-z) , \tag{2.47}$$

the first criterion, Eq. (2.45), is more conservative than the second, Eq. (2.46). Equation (2.47) leads to

$$z > \frac{\gamma\tilde{H}}{(\bar{\Sigma}_t+\gamma)} . \tag{2.48}$$

For the miniature lattices, $\bar{\Sigma}_t \approx 0.44\ \text{cm}^{-1}$, $\gamma \approx 0.08\ \text{cm}^{-1}$, and $\tilde{H} \approx 46$ cm; thus, z must be greater than 7 cm for the source effect to be less serious under the first criterion than the boundary effect would be under the second criterion. To be more specific, let us require that

$$2\, e^{-[\bar{\Sigma}_t z+\gamma(\tilde{H}-z)]} \leq 10^{-3} ;$$

then $$[\bar{\Sigma}_t z+\gamma(\tilde{H}-z)] \geq 7.7 ,$$

or $$z \geq \frac{(7.7 - \gamma\tilde{H})}{(\bar{\Sigma}_t - \gamma)} = \frac{7.7 - 3.68}{0.36} = 11.17 \text{ cm}.$$

We might then conclude that if $z > 12$ cm, the source effect is probably insignificant, and that if $z < 35$ cm, the boundary effect would be tolerable. These results mean that the region of spectral equilibrium lies approximately in the range

$$12 \text{ cm} < z < 35 \text{ cm}$$

for the miniature lattices. This conclusion should be accepted with the proviso that the neutron spectrum is very nearly, but not exactly, at equilibrium.

It is interesting to see that the above conclusion does roughly agree with the measured distributions of the cadmium ratio in the miniature lattices. A typical distribution is shown in Figure 2.5, taken from the report by Sefchovich et al. (S1).

We can study the equilibrium condition in the radial direction with the same procedure. We consider the radial equation, Eq. (2.23). We define, for brevity,

$$\Sigma_t^{**}(E) \equiv \Sigma_t(E) - \Sigma_{Lz}(E) . \tag{2.49}$$

In addition, $\cos(\theta' - \theta) = 1$ if the flux is azimuthally symmetric, as assumed. Equation (2.23) then becomes

$$\Omega_r \frac{\partial}{\partial r} \phi(r, E, \Omega_r) + \Sigma_t^{**}(E)\, \phi(r, E, \Omega_r)$$

$$= \int_{\Omega_r} d\Omega_r' \int_0^\infty dE'\, \Sigma_c(E')\, g(E' \to E ; \Omega_r' \to \Omega_r)\, \phi(r, E', \Omega_r') . \tag{2.50}$$

The asymptotic solution of this equation for spectral equilibrium is given by

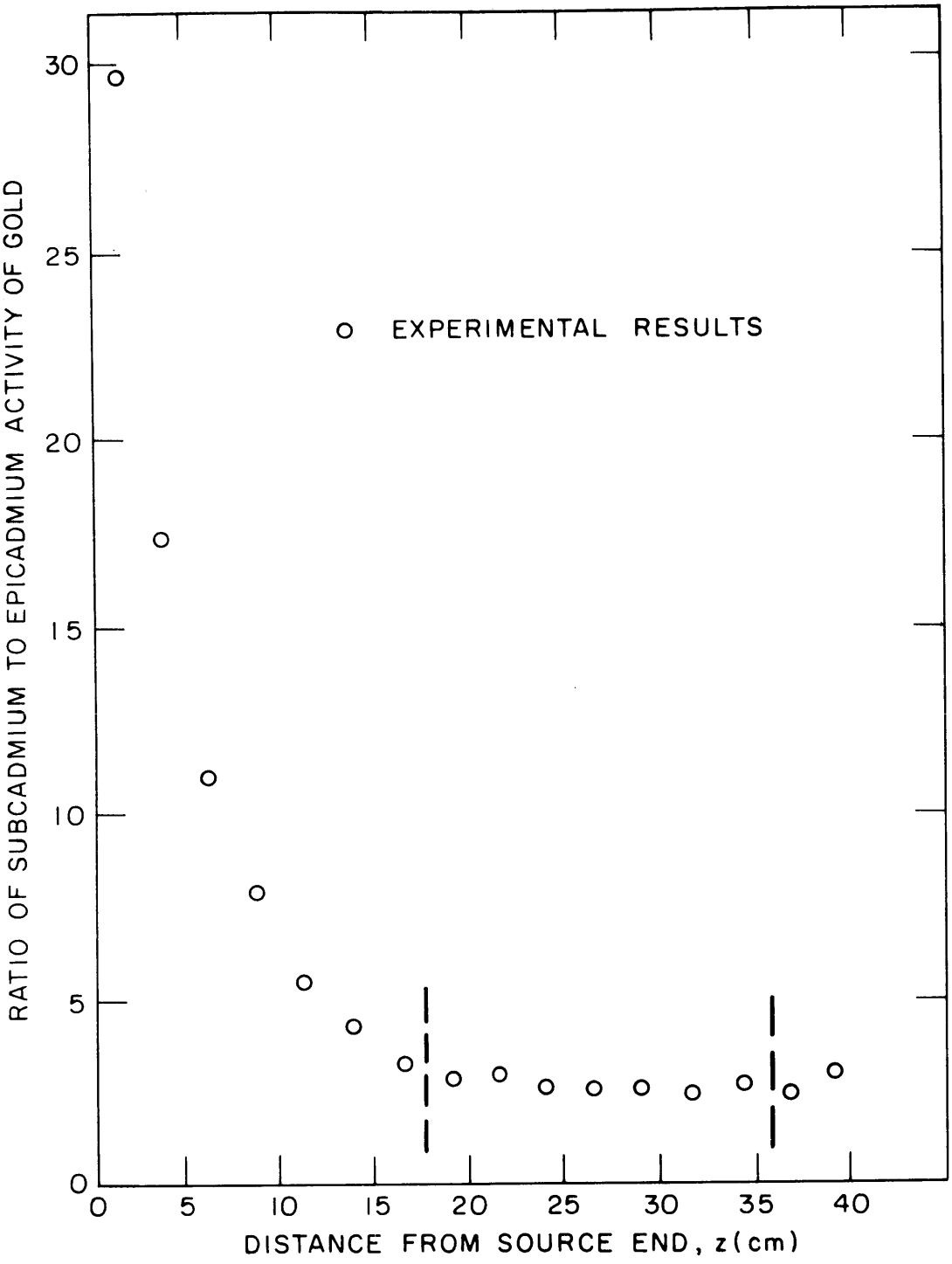

FIG. 2.5 AXIAL DISTRIBUTION OF THE CADMIUM RATIO OF GOLD IN ML2 (S1)
ML2: 1.143% ENRICHED FUEL, D_2O MODERATED, 1.25-INCH SPACING.

$$\phi_{asy}(r, E, \Omega_r) = J_o(\alpha r) \cdot \psi(E, \Omega_r) \ , \tag{2.51}$$

where $\psi(E, \Omega_r)$ is the angular neutron spectrum in the radial direction and α^2 is the radial buckling. Substitution of Eq. (2.51) in Eq. (2.50) yields

$$\psi(E, \Omega_r) = \frac{1}{\left[- \frac{J_1(\alpha r)}{J_o(\alpha r)} + \frac{\Sigma_t^{**}(E)}{\alpha \Omega_r} \right] \alpha \Omega_r} \int_{\Omega_r} d\Omega_r' \int_0^\infty dE' \, \Sigma_c(E') \, g(E' \to E \, ; \Omega_r' \to \Omega_r) \, \psi(E', \Omega_r') \ . \tag{2.52}$$

Two important conditions must be imposed if Eq. (2.52) is to be physically meaningful:

(a) Since the neutron flux must be positive and nonzero, we must have

$$\left[- \frac{J_1(\alpha r)}{J_o(\alpha r)} + \frac{\Sigma_t^{**}(E)}{\alpha |\Omega_r|} \right] > 0 \ ,$$

or

$$\frac{\Sigma_t^{**}(E)}{\alpha |\Omega_r|} > \frac{J_1(\alpha r)}{J_o(\alpha r)} \ . \tag{2.53}$$

(b) For the space-energy separability to hold, as assumed, we must have

$$\frac{J_1(\alpha r)}{J_o(\alpha r)} = 0, \text{ or nearly independent of } r. \tag{2.54}$$

We see immediately that only at the center, r=0, does the condition (2.54) hold exactly. A similar conclusion was reached by Hellens

(H7, K8) as a result of calculations made in connection with experiments on reflected, water-moderated lattices at Brookhaven. He calculated the radial distribution of the flux in a multigroup scheme and found that deviations from asymptotic behavior persisted all the way to the center. Hence, the best radial position for measuring the axial flux distribution is the center of the cylinder (r=0). From a practical standpoint, however, if

$$\frac{J_1(\alpha r)}{J_o(\alpha r)} \ll \frac{\Sigma_t^{**}(E)}{\alpha|\Omega_r|}, \tag{2.55}$$

only slight nonseparability would be expected. It is evident that the condition (2.55) is better satisfied in a larger assembly with smaller α than in a smaller assembly.

To estimate how large the radial distance should be to satisfy the condition (2.55), let us require that

$$\frac{J_1(\alpha r)}{J_o(\alpha r)} \leq 0.1\left[\frac{\Sigma_t^{**}(E)}{\alpha\Omega_r}\right], \quad \text{(Case I)}. \tag{2.56}$$

Consider, for example, the miniature lattice ML3:

$$\Sigma_t^{**}(E_{th}) \approx \Sigma_t(E_{th}) - D\gamma^2 = 0.4322 \text{ cm}^{-1};$$

$$\left[\frac{\Sigma_t^{**}(E_{th})}{\alpha|\Omega_r|}\right]_{min} = \frac{\Sigma_t^{**}(E_{th})}{\alpha} \approx \frac{0.4322}{0.0883} = 4.90.$$

Thus, $$\frac{J_1(\alpha r)}{J_o(\alpha r)} \lesssim 0.490,$$

whence $$r \lesssim \frac{0.89}{\alpha} \approx 10 \text{ cm}.$$

[The calculation of these nuclear parameters will be described in section 6.2.3 of Chapter VI; see Table 6.1 for reference.]

For the purpose of comparison with the case of the axial distribution, let us also relax the condition (2.56) in such a way that

$$\frac{J_1(\alpha r)}{J_o(\alpha r)} \lesssim 0.25\left[\frac{\Sigma_t^{**}(E)}{\alpha \Omega_r}\right], \text{ (Case II)}. \tag{2.57}$$

We then get

$$r \leq \frac{1.225}{\alpha} \approx 14 \text{ cm}.$$

Recall that the radius of the miniature-lattice system is about 25 cm, so that, in a practical sense, only about half of it is in the equilibrium region. Table 2.3 gives the radial distances of all the miniature lattices within which the neutron spectrum is practically at equilibrium. Once again, the estimate agrees approximately with the radial distribution of the cadmium ratio, as can be seen in Figure 2.6, again taken from reference (S1).

For comparison, we investigate the corresponding full-size lattice denoted as 250 (3-foot-diameter tank):

$$\Sigma_t^{**}(E_{th}) \approx 0.444 - (0.802)(0.0025) = 0.442 \text{ cm}^{-1},$$

$$\frac{\Sigma_t^{**}(E_{th})}{\alpha} \approx \frac{0.4420}{0.050} = 8.84,$$

$$\frac{J_1(\alpha r)}{J_o(\alpha r)} \lesssim 0.884,$$

whence

$$r \lesssim \frac{1.42}{\alpha} = \frac{1.42}{0.05} = 28.4 \text{ cm}.$$

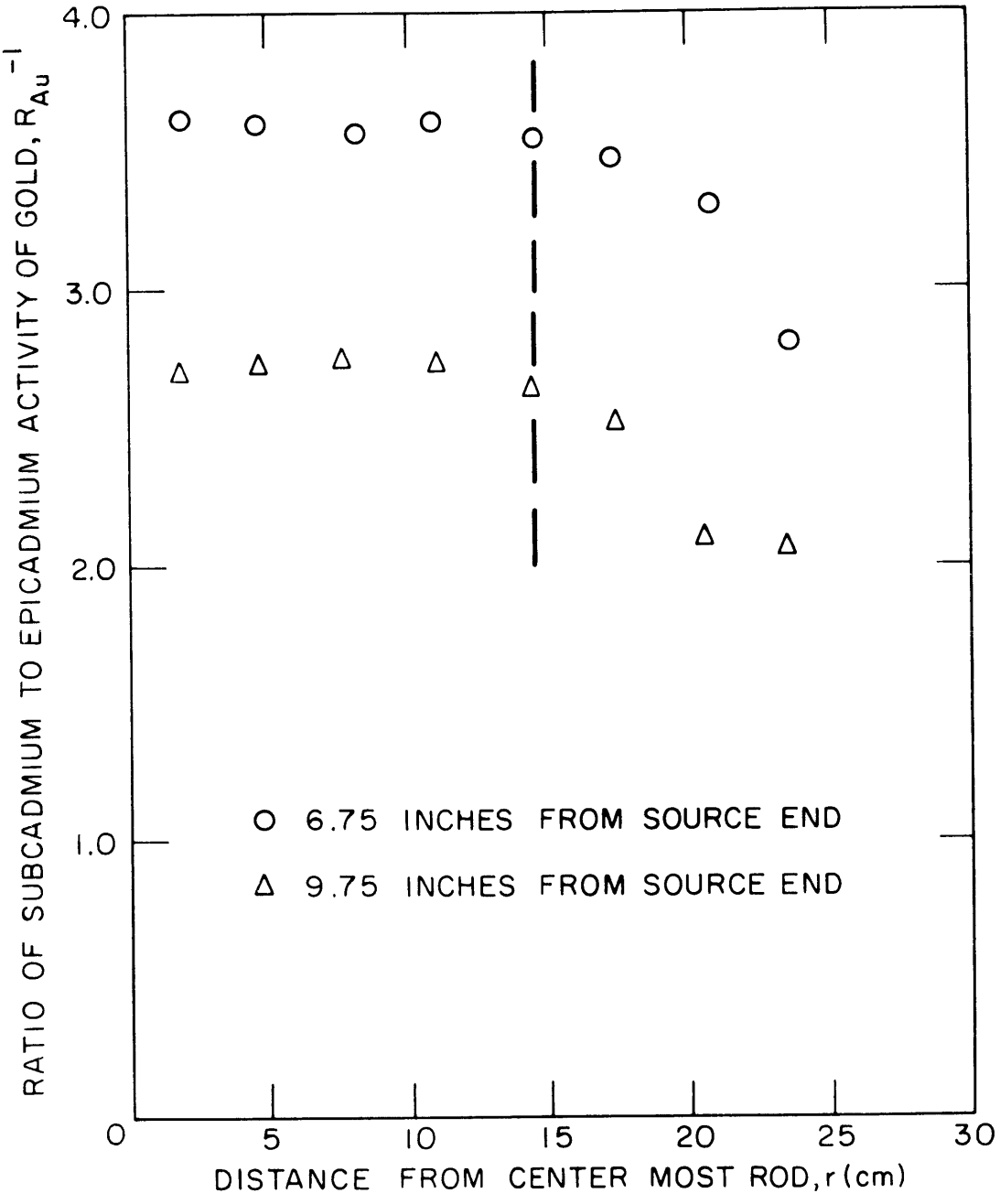

FIG. 2.6 RADIAL DISTRIBUTION OF CADMIUM RATIO OF GOLD IN ML2 (S1).
ML2: 1.143% ENRICHED FUEL, D_2O MODERATED, 1.25 - INCH SPACING.

Table 2.3. The radial distance within which the neutron spectrum is at equilibrium for the miniature lattices.

Lattice Designator	Lattice Specification	Σ_t^{**} (cm^{-1})	α^* (cm^{-1})	Radial Distance of Spectral Equilibrium (cm)	
				Case I	Case II
ML2	1.143% enriched 1.25" spacing	0.4329	0.0871	10.22	14.10
ML3	1.143% enriched 2.50" spacing	0.4322	0.0883	10.10	13.88
ML4	1.027% enriched 1.25" spacing	0.4318	0.0870	10.23	14.11
ML5	1.027% enriched 2.50" spacing	0.4315	0.0934	9.42	13.12
ML6	1.027% enriched 1.75" spacing	0.4254	0.0872	10.20	14.05
ML7	1.143% enriched 1.75" spacing	0.4264	0.0870	10.21	14.11

* The values of the α are calculated with the formula, $\alpha = 2.4048/\tilde{R}$, where $\tilde{R}$ is the extrapolated radius.

This result is again in good agreement with the radial distribution of the cadmium ratio measured by Harrington in the 3-foot tank (H9), as shown in Figure 2.7. For the 4-foot tank, $r \lesssim 38.8$ cm.

We conclude that the miniature-lattice system is really small as far as spectral equilibrium is concerned.

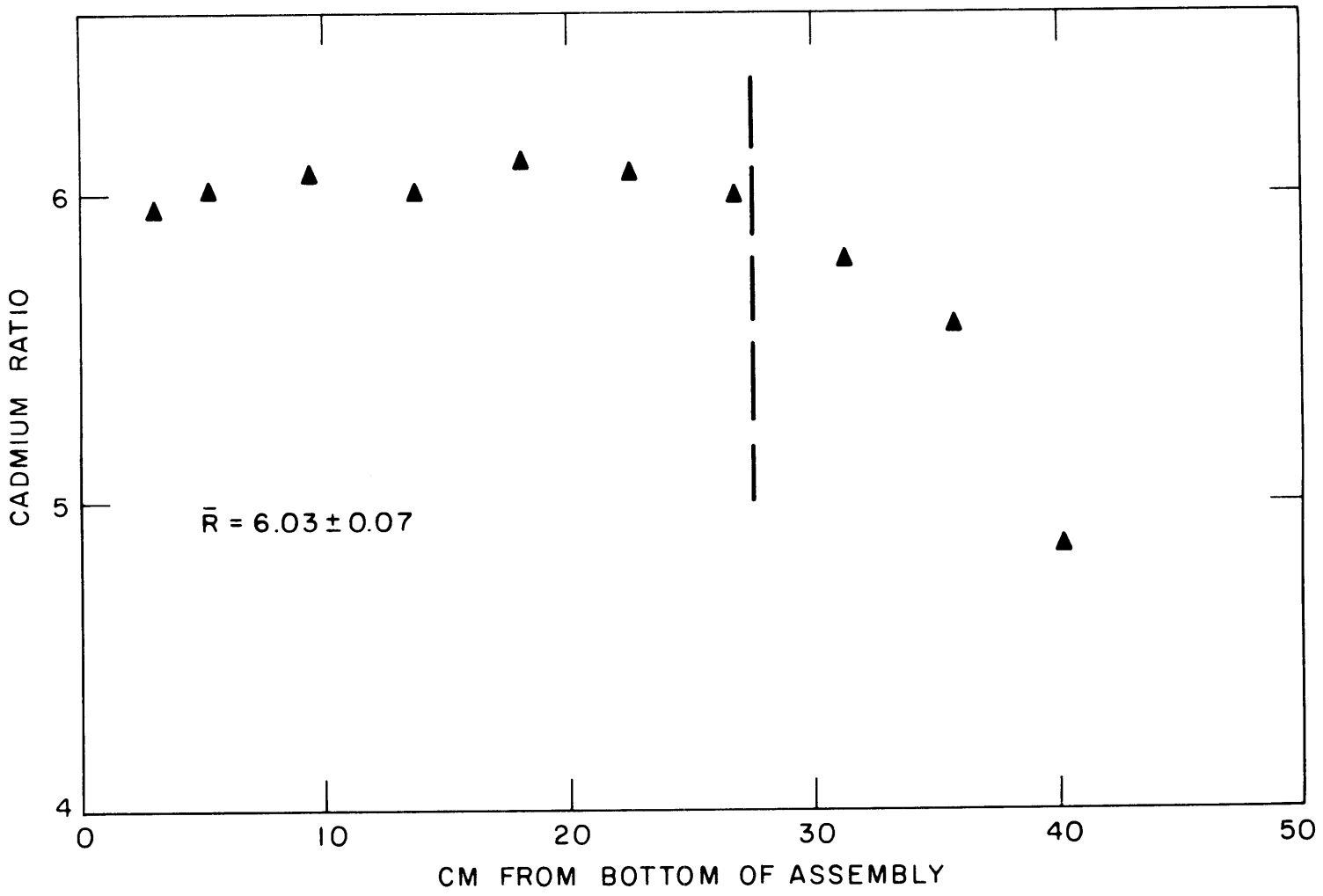

FIG. 2.7 CADMIUM RATIO IN 175AIBI ASSEMBLY AS A FUNCTION OF RADIAL POSITION (RUNS 25, 27) MEASURED IN A 3-FOOT TANK (H9).

2.4 A COMMENT ON THE CADMIUM RATIO

It has been customary to use the constancy of the cadmium ratio as a criterion for the existence of an asymptotic region in an assembly in which reactor physics experiments are to be carried out. It is open to question if this practical criterion suffices to ensure the existence of an asymptotic region within the assembly.

In this section we shall try first to answer this basic question from a mathematical point of view and then to discuss it on physical grounds. We shall also suggest another criterion. We consider the neutron flux as a function of space, energy, and direction

$$\phi = \phi(\vec{r}, E, \vec{\Omega}) .$$

The neutron flux expressed in this way may be regarded as a vector. We separate the flux into two parts, the thermal and epithermal fluxes:

$$\phi_{tot}(\vec{r}, E, \vec{\Omega}) = \phi_{th}(\vec{r}, E, \vec{\Omega}) + \phi_{epi}(\vec{r}, E, \vec{\Omega}) . \tag{2.58}$$

Since what we measure by the activation technique is an integral quantity with respect to energy and direction, we integrate Eq. (2.58) with respect to E and $\vec{\Omega}$:

$$\int_{4\pi} d\vec{\Omega} \int_0^{\infty} dE\, \phi_{tot}(\vec{r}, E, \vec{\Omega}) = \int_{4\pi} d\vec{\Omega} \int_0^{E_{th}} dE\, \phi_{th}(\vec{r}, E, \vec{\Omega}) + \int_{4\pi} d\vec{\Omega} \int_{E_{th}}^{\infty} dE\, \phi_{epi}(\vec{r}, E, \vec{\Omega}) . \tag{2.59}$$

By definition,

$$\Phi_i(\vec{r}) \equiv \int_0^{\infty} dE \int_{4\pi} d\vec{\Omega}\, \phi_i(\vec{r}, E, \vec{\Omega}) , \tag{2.60}$$

where i may denote total, thermal, or epithermal, respectively. Thus,

$$\Phi_{tot}(\vec{r}) = \Phi_{th}(\vec{r}) + \Phi_{epi}(\vec{r}) \ . \tag{2.61}$$

The cadmium ratio is defined as

$$R_{cd} \equiv \frac{\Phi_{tot}(\vec{r})}{\Phi_{epi}(\vec{r})} = \frac{\Phi_{th}(\vec{r})}{\Phi_{epi}(\vec{r})} + 1 \ . \tag{2.62}$$

The constancy of the cadmium ratio is equivalent to the constancy of the ratio

$$\frac{\Phi_{th}(\vec{r})}{\Phi_{epi}(\vec{r})} = \frac{\int_{4\pi} d\vec{\Omega} \int_0^{E_{th}} dE \ \phi_{th}(\vec{r}, E, \vec{\Omega})}{\int_{4\pi} d\vec{\Omega} \int_{E_{th}}^{\infty} dE \ \phi_{epi}(\vec{r}, E, \vec{\Omega})} \ . \tag{2.63}$$

Suppose that the neutron flux is <u>separable</u> in space and energy so that we may write

$$\phi_i(\vec{r}, E, \vec{\Omega}) = \rho_i(\vec{r}) \cdot \psi_i(E, \vec{\Omega}) \ . \tag{2.64}$$

Then we have

$$R_{cd} = \frac{\rho_{tot}(\vec{r})}{\rho_{epi}(\vec{r})} \cdot \frac{\int_{4\pi} d\vec{\Omega} \int_0^{\infty} dE \ \psi_{tot}(E, \vec{\Omega})}{\int_{4\pi} d\vec{\Omega} \int_{E_{th}}^{\infty} dE \ \psi_{epi}(E, \vec{\Omega})} \tag{2.65}$$

$$= C \cdot \frac{\rho_{tot}(\vec{r})}{\rho_{epi}(\vec{r})} \ , \tag{2.66}$$

where C is the ratio of the integrals and is a constant.

Equations (2.62) and (2.66) imply that:

(i) If the neutron flux is <u>separable</u> in space and energy, the constancy of the Cd ratio requires that the <u>spatial parts</u> of the

thermal and epithermal neutron fluxes be of the same shape, so that

$$\frac{\rho_{tot}(\vec{r})}{\rho_{epi}(\vec{r})} = \text{constant, independent of } \vec{r} \, . \tag{2.67}$$

But Eq. (2.66) shows that even if the cadmium ratio is not independent of the position $\vec{r}$, the neutron flux still can be separable in space and energy.

(ii) On the other hand, if the neutron flux is not separable in space and energy, the cadmium ratio may be still independent of position, provided that the scalar thermal and epithermal fluxes defined in Eq. (2.60) have the same shape, that is,

$$\frac{\Phi_{tot}(\vec{r})}{\Phi_{epi}(\vec{r})} = \text{constant, independent of } \vec{r} \, . \tag{2.68}$$

It is evident, therefore, that the use of the constancy of the cadmium ratio as a criterion for the existence of an asymptotic region is questionable. The cadmium ratio is certainly not a sensitive parameter, for it is just a ratio of two integral quantities which do not reveal any differential structure of the neutron flux. A certain guarantee of spectral equilibrium is that the neutron spectrum be independent of position. Of course, this is extremely difficult to determine experimentally, and most workers use the invariance of the cadmium ratio as a rough test of spectral equilibrium. It would be helpful to have a more precise criterion.

We see from the discussion in section 2.1 that the geometric bucklings defined by Eqs. (2.4) and (2.5) are spatially dependent if spatial and/or energy transients are present, but become independent

of position when only the fundamental mode of the neutron flux persists. Thus, a sensitive parameter for testing the space-energy separability would be the spatially-dependent geometric buckling. To illustrate, suppose the neutron flux is not separable in space and energy but that it can be represented by a linear combination of infinitely many separable terms:

$$\Phi(\vec{r}, E) = \sum_{i=0}^{\infty} \phi_i(\vec{r})\, \psi_i(E) \ . \tag{2.69}$$

Now define the geometric buckling, $B_g^2(\vec{r}, E)$, as

$$B_g^2(\vec{r}, E) \equiv \frac{\nabla^2 \Phi(\vec{r}, E)}{\Phi(\vec{r}, E)} \ . \tag{2.70}$$

Substitution of Eq. (2.69) in Eq. (2.70) yields

$$B_g^2(\vec{r}, E) = \frac{\sum_{i=0}^{\infty} \psi_i(E)\, \phi_i(\vec{r})\, \frac{1}{\phi_i(\vec{r})}\, \nabla^2 \phi_i(\vec{r})}{\sum_{i=0}^{\infty} \psi_i(E)\, \phi_i(\vec{r})}$$

$$= \frac{\sum_{i=0}^{\infty} \psi_i(E)\, \phi_i(\vec{r})\, B_i^2(\vec{r})}{\sum_{i=0}^{\infty} \psi_i(E)\, \phi_i(\vec{r})} \ , \tag{2.71}$$

where

$$B_i^2(r) \equiv \frac{\nabla^2 \phi_i(\vec{r})}{\phi_i(\vec{r})} \ . \tag{2.72}$$

If energy transients are negligible so that

$$\Phi(\vec{r}, E) = \psi_o(E)\, \phi_o(\vec{r}) \ , \tag{2.73}$$

then $B_g^2(\vec{r}, E) = B_o^2(\vec{r})$, independent of energy.

This geometric buckling must also be independent of $\vec{r}$ when all the spatial transients except the fundamental contained in $\phi_o(\vec{r})$ die out. This leads to the conclusion that the geometric buckling must be independent of neutron energy and position in an asymptotic region.

To correlate the theory and experiment more closely, consider the treatment of nonseparability in a two-group picture:

$$\Phi(\vec{r}, E) = \psi_o(E)\ \phi_o(\vec{r}) + \psi_1(E)\ \phi_1(\vec{r}) , \tag{2.74}$$

where the subscript o denotes the subcadmium group and the subscript 1 represents the epicadmium group. We see immediately that the neutron flux is not separable if there is a significant number of epicadmium neutrons whose flux shape is different from that of the subcadmium neutrons. This situation may arise in a small system where neutron leakage is so predominant in the neutron balance equation as to practically decouple the two different groups of neutrons. Unfortunately, this turns out to be the case for the miniature lattices; the problem will be discussed in greater detail in Chapter V.

It would be of interest to see the extent to which the nonseparability can affect the axial and radial bucklings and hence the material buckling of the miniature lattices. To do this, we insert Eq. (2.74) in Eq. (2.70) and get

$$B_g(\vec{r}, E) = B_o^2(\vec{r})\ \frac{\left[1 + \dfrac{B_1^2(\vec{r})}{B_o^2(\vec{r})}\ \dfrac{\psi_1(E)\phi_1(\vec{r})}{\psi_o(E)\phi_o(\vec{r})}\right]}{\left[1 + \dfrac{\psi_1(E)\phi_1(\vec{r})}{\psi_o(E)\phi_o(\vec{r})}\right]} . \tag{2.75}$$

Measurements in the miniature lattices indicated that

$$\frac{\psi_1(E)\phi_1(\vec{r})}{\psi_o(E)\phi_o(\vec{r})} \approx 0.1 \ ;$$

hence,

$$B_g^2(\vec{r}, E) \approx B_o^2(\vec{r}) \left\{ 1 - \left[1 - \frac{B_1^2(\vec{r})}{B_o^2(\vec{r})} \right] \frac{\psi_1(E)\phi_1(\vec{r})}{\psi_o(E)\phi_o(\vec{r})} \right\} . \qquad (2.76)$$

For the axial bucklings of the miniature lattices, we have

$$\frac{B_1^2}{B_o^2} = \frac{\gamma_{epi}^2}{\gamma_{th}^2} \approx 0.5 \ , \qquad \text{(see Chapter V)}$$

so that

$$B_g^2(z, E) \approx \gamma_{th}^2 [1 - 0.05] .$$

Thus, there may be an uncertainty of about 5 percent in the axial buckling because of the degree of nonseparability. In the case of the radial buckling, the situation is somewhat more favorable:

$$\frac{B_1^2}{B_o^2} = \frac{\alpha_{epi}^2}{\alpha_{th}^2} \approx 0.75 \ ,$$

$$B_g^2(\vec{r}, E) \approx \alpha_{th}^2 (1 - 0.025) \ ,$$

with the result that the uncertainty would be about 3 percent.

A general qualitative conclusion that can be drawn is that the effect of nonseparability is to underestimate the geometric buckling and overestimate the material buckling. This can be seen from the following argument:

$$B_m^2 = B_g^2(\vec{r}, E) - B_g^2(z, E)$$

$$= \left(\alpha_{th}^2 - \gamma_{th}^2\right) + 0.025\left(2\gamma_{th}^2 - \alpha_{th}^2\right) . \qquad (2.77)$$

But $2\gamma_{th}^2 > \alpha_{th}^2$; for example, in the miniature lattice ML2,

$$\gamma_{th}^2 \approx 5800\ \mu B,$$

$$\alpha_{th}^2 \approx 7200\ \mu B,$$

and

$$B_m^2 \approx 1400\ \mu B + 115\ \mu B = 1400\ (1 + 0.0821)\ \mu B.$$

Thus, an error of about 8 percent may be incurred owing to nonseparability.

The above discussion suggests a more reliable and convincing criterion for the existence of an asymptotic and equilibrium region, namely, that the geometric buckling be independent of energy and position. It is, however, extremely difficult to calculate the spatially dependent geometric buckling from experimental data owing to the statistic fluctuation of the data. If the data could be smoothed out sufficiently, the local geometric bucklings in the axial and radial directions could be calculated by means of the finite difference method. The geometric bucklings could then be plotted as functions of position as sketched in Figure 2.8 for the axial buckling and in Figure 2.9 for the radial buckling. Appendix D describes a finite difference method for extracting the buckling values. The region where the bucklings (α^2 and γ^2) are independent of position and identical for the subcadmium and epicadmium neutrons is the asymptotic region.

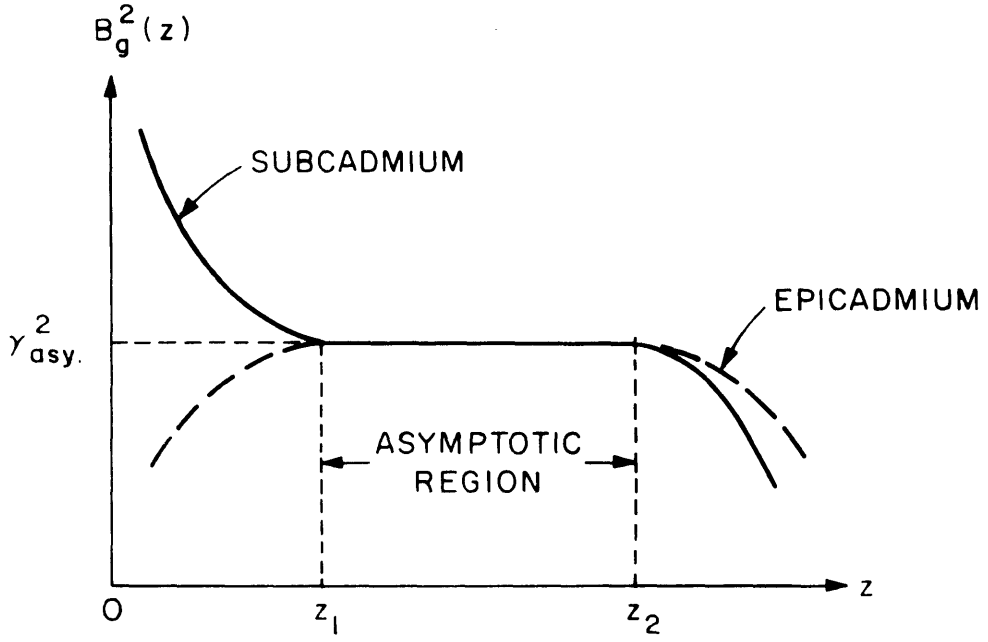

FIG. 2.8 AXIAL GEOMETRIC BUCKLING VS AXIAL POSITION.

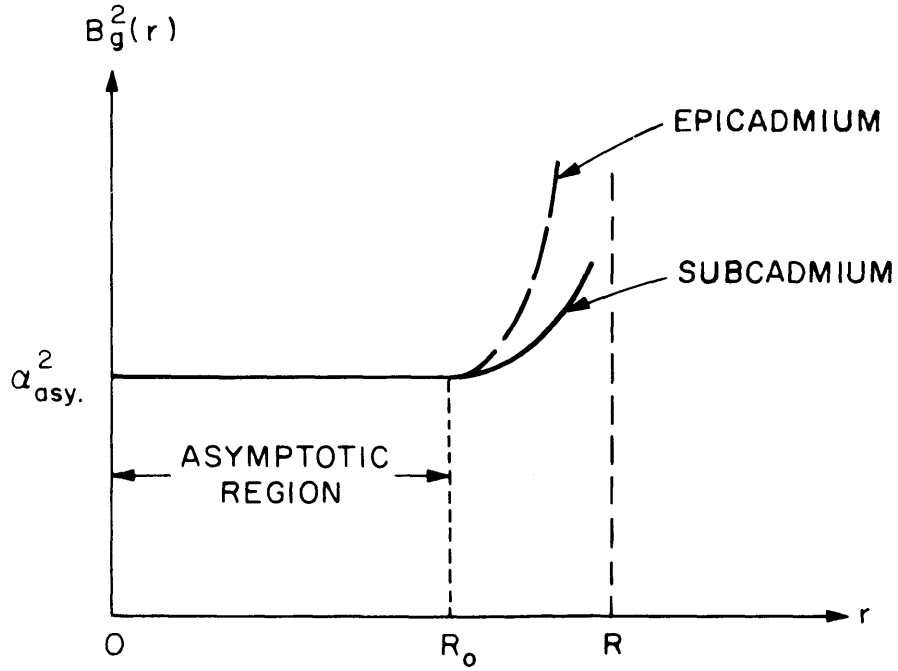

FIG. 2.9 RADIAL GEOMETRIC BUCKLING VS. RADIAL POSITION.

The procedure just described is possible in principle but difficult in practice. An alternative method is to calculate the buckling values from experimental activation data by using the Moments Method (to be developed in the next chapter), and successively dropping data points from the boundaries inward toward the central region. This process is used for both the subcadmium and epicadmium neutrons. Then the axial buckling is plotted as a function of the location of the first data point from the source; and the radial buckling is plotted as a function of the location of the first data point from the boundary. If there is an asymptotic region, the buckling values should level off as indicated in Figure 2.3. This procedure has been applied in the past (H9): with the conventional curve-fitting method it worked for the radial buckling but is less successful for the axial buckling because of the way it fixes the "best value" of the axial buckling. [Recall that at least three different sets of data points must be used in the curve-fitting method to analyze the axial buckling and that there is, in general, no uniquely specified first data point.] With the moments method this procedure is entirely feasible and simple and saves considerable computer time; it will be used in Chapter V to obtain the best value of the axial buckling of the miniature lattices.

2.5 CONCLUSIONS

We have discussed in considerable detail the asymptotic and equilibrium conditions for exponential experiments in general and the justification of these conditions for the miniature lattices in

particular. The following conclusions may be drawn from the discussion:

(a) The existence of spectral equilibrium is a difficult problem for exponential experiments in general and could be a serious problem for buckling measurements in the miniature lattices in particular. It is possible, however, to select (with great care) some appropriate position inside the miniature lattices where the neutron spectrum is essentially in equilibrium. This probably explains the reason why those lattice parameters such as ρ_{28}, δ_{25}, C^*, etc. which are measured at a single position could be measured with some success in the miniature lattices (S1) and why the material buckling could not be measured. As far as spectral equilibrium is concerned, the miniature lattices investigated at the M.I.T. Lattice Project are marginal but may just satisfy the necessary conditions. Increasing the diameter and/or the length of the system would improve the conditions significantly because of reduction in neutron leakage. Some kind of optimization can be made by considering the equilibrium condition, the asymptotic condition, and economy as functions of size.

(b) The diffusion approximation is generally well satisfied in heavy water lattices, even in the miniature lattices. The use of the moments method, which will be described in the next chapter, makes it possible to reduce significantly the transport effect in buckling measurements.

(c) The choice of the axial position where the radial flux distribution is to be measured is crucial. It should be inside the asymptotic and equilibrium region. For the miniature lattices, it is about 30 cm

from the neutron source. The axial flux distribution should be measured, if possible, along the axis of the cylinder, or at least near the center.

(d) Despite certain advantages of the diagonal buckling method (H6) recently investigated at the M.I.T. Lattice Project, there may be some serious problems with data analysis because the experimental data near the corners are not likely to be azimuthally symmetric; in addition, there may be a significant degree of nonseparability of the neutron flux.

(e) The constancy of the cadmium ratio provides only a rough check of spectral equilibrium. A more sensitive and reliable criterion would be the invariance of geometric buckling with respect to position and energy. The development of some method, such as a finite difference method, for calculating the local bucklings seems worth investigating.

Chapter III

THE ANALYSIS OF THE AXIAL BUCKLING AND THE EXTRAPOLATED HEIGHT WITH THE MOMENTS METHOD

3.1 INTRODUCTION

The shortcomings of the conventional curve-fitting method for buckling analysis have been discussed in Chapter I. In particular, its failure to provide consistent values of the buckling in small systems such as miniature lattices indicates the need for developing a new technique for buckling analysis. To show one of the difficulties with the curve-fitting method, curves of the axial buckling vs. extrapolated height for the miniature lattice ML2 are shown in Figure 3.1. There is no common intersection among the curves and, consequently, no way of fixing the best value of the axial buckling. The analysis made in Chapter II reveals that there should be an asymptotic region in the miniature lattices but that it may be too small for the curve-fitting method to be applicable. The measured axial flux distribution consists mainly of the asymptotic distribution predicted by diffusion theory, but it is contaminated by a significant contribution of source neutrons as well as by spatial and energy transients (S1). Thus, to infer buckling values from flux shapes in a small assembly, one must devise a method of eliminating, or at least reducing, the source and transient effects while retaining the asymptotic part of the flux distribution. To achieve this goal, we must analyze the spatial and energy transients in the neutron flux. This will be done in Chapter VI.

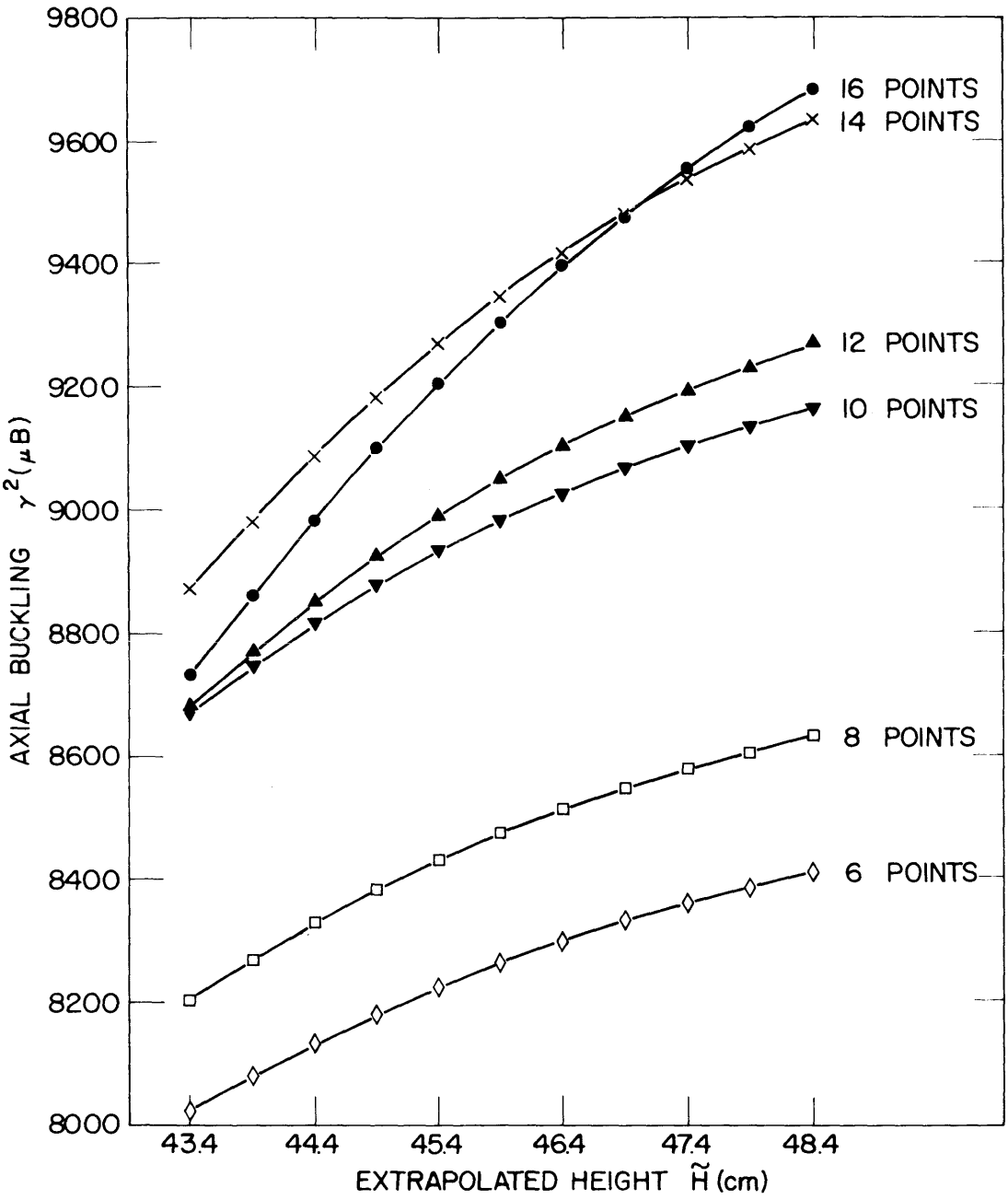

FIG. 3.1 CURVES OF THE AXIAL BUCKLING VS. THE EXTRAPOLATED HEIGHT FOR THE MINIATURE LATTICE ML2 CALCULATED WITH THE AXFIT CODE OF PALMEDO. NO COMMON INTERSECTION IS OBSERVED.

A possible method of analyzing the activation data is with the moments method used by Fermi in his early work on the slowing down of neutrons in paraffin (F2). This method has been used successfully to determine the Fermi age of neutrons in various moderators (B1, A3). Fano and Spencer have applied the method to the calculation of the deep penetration of X- or γ-rays in shields (F3, C1). Since the buckling is a measure of neutron leakage, which involves the mean-square distance $\overline{r^2}$ of neutron transport within an assembly, we may expect the buckling to be related to $\overline{r^2}$ and hence to the flux moments that are needed for the calculation of $\overline{r^2}$.

A moments method will be developed in this chapter, with this motivation in mind, for the axial buckling analysis in miniature lattices in particular, as well as for full-size lattices. The consistency of this method in the interpretation of axial buckling measurements will be tested by applying the method to several U-D_2O lattices as well as some UO_2-D_2O lattices. The corresponding moments analysis of the radial buckling will be described in Chapter IV, while its application to the miniature lattices will be given in Chapter V.

3.2 THE MOMENTS METHOD FOR THE ANALYSIS OF THE AXIAL BUCKLING AND EXTRAPOLATED HEIGHT

3.2.1 Theory

We start with the definition of the axial flux moments

$$\phi_n \equiv \int_a^b z^n \phi(z)\, dz\,, \qquad n = 0, 1, 2, \ldots, \infty. \tag{3.1}$$

The choice of the limits of integration deserves some discussion. If

one is interested in the calculation of the exact flux moments as required in the calculation of deep penetration in shields, the entire space associated with the system of interest must be covered, that is, a=0 and b=H, the physical boundary of the system. But, since our purpose here is to extract the value of the buckling from the asymptotic part of the neutron flux distribution, we need to know only the asymptotic flux moments. Thus, the choice of a and b can be left open; they will be chosen arbitrarily depending on the first and last data points selected for the analysis from the experimental data. The choice of a and b then provides us a way of determining the boundaries of an asymptotic region as we proposed in Chapter II.

In an asymptotic region, the neutron flux distribution in the axial direction may be represented by the expression

$$\phi(z) = A \sinh \gamma(\tilde{H}-z) , \tag{3.2}$$

where A is the normalization constant, γ^2 is the axial buckling, and $\tilde{H}$ is the extrapolated height. Now Eq. (3.2) is valid not only in simple diffusion theory (M1, W1, L1) but also in asymptotic transport theory (K4, D2). It is, therefore, rigorous under the asymptotic condition discussed in Chapter II.

When we evaluate the integral (3.1) by substituting Eq. (3.2) in Eq. (3.1), we get

$$\phi_n = \left[- \frac{b^n}{\gamma} \cosh \gamma(\tilde{H}-b) - \frac{nb^{n-1}}{\gamma^2} \sinh \gamma(\tilde{H}-b) \right] + \frac{n(n-1)}{\gamma^2} \phi_{n-2}$$

$$- \left[- \frac{a^n}{\gamma} \cosh \gamma(\tilde{H}-a) - \frac{na^{n-1}}{\gamma^2} \sinh \gamma(\tilde{H}-a) \right], \quad \text{for } n \geq 2 . \tag{3.3}$$

To simplify the analysis, it is desirable to have the lower limit a equal to zero, in which case Eq. (3.3) reduces to the simpler form

$$\phi'_n = -\frac{b'^n}{\gamma}\cosh\gamma(\tilde{H}'-b') - \frac{nb'^{n-1}}{\gamma^2}\sinh\gamma(\tilde{H}'-b') + \frac{n(n-1)}{\gamma^2}\phi'_{n-2} . \qquad (3.4)$$

Since this expression for ϕ'_n is important to the final result, its justification should be discussed. Equation (3.4) implies that the axial flux moments are defined by

$$\phi'_n = A\int_0^{b'} z'^n \sinh\gamma(\tilde{H}'-z')\,dz', \qquad n = 0, 1, 2, \ldots, \infty . \qquad (3.5)$$

We shall show that the definitions Eq. (3.1) and Eq. (3.5) are equivalent as far as the extraction of γ^2 and $\tilde{H}$ from experimental data is concerned. To do this, we translate the coordinate system along the z-axis so that the new axial coordinate z' is given by

$$z' = z - a \qquad (3.6)$$

as indicated in Figure 3.1a. Substitution of Eq. (3.6) into Eq. (3.1) yields

$$\phi_n = A\int_0^{(b-a)} (z'+a)^n \sinh\gamma[(\tilde{H}-a)-z']\,dz'$$

$$= A\int_0^{b'} (z'+a)^n \sinh\gamma(\tilde{H}'-z')\,dz' , \qquad (3.7)$$

where $b' = (b-a)$, and $\tilde{H}' = (\tilde{H}-a)$ is the new extrapolated height in the transformed coordinate system z'. The extrapolated height of the system under investigation is therefore given by

$$\tilde{H} = \tilde{H}' + a . \qquad (3.8)$$

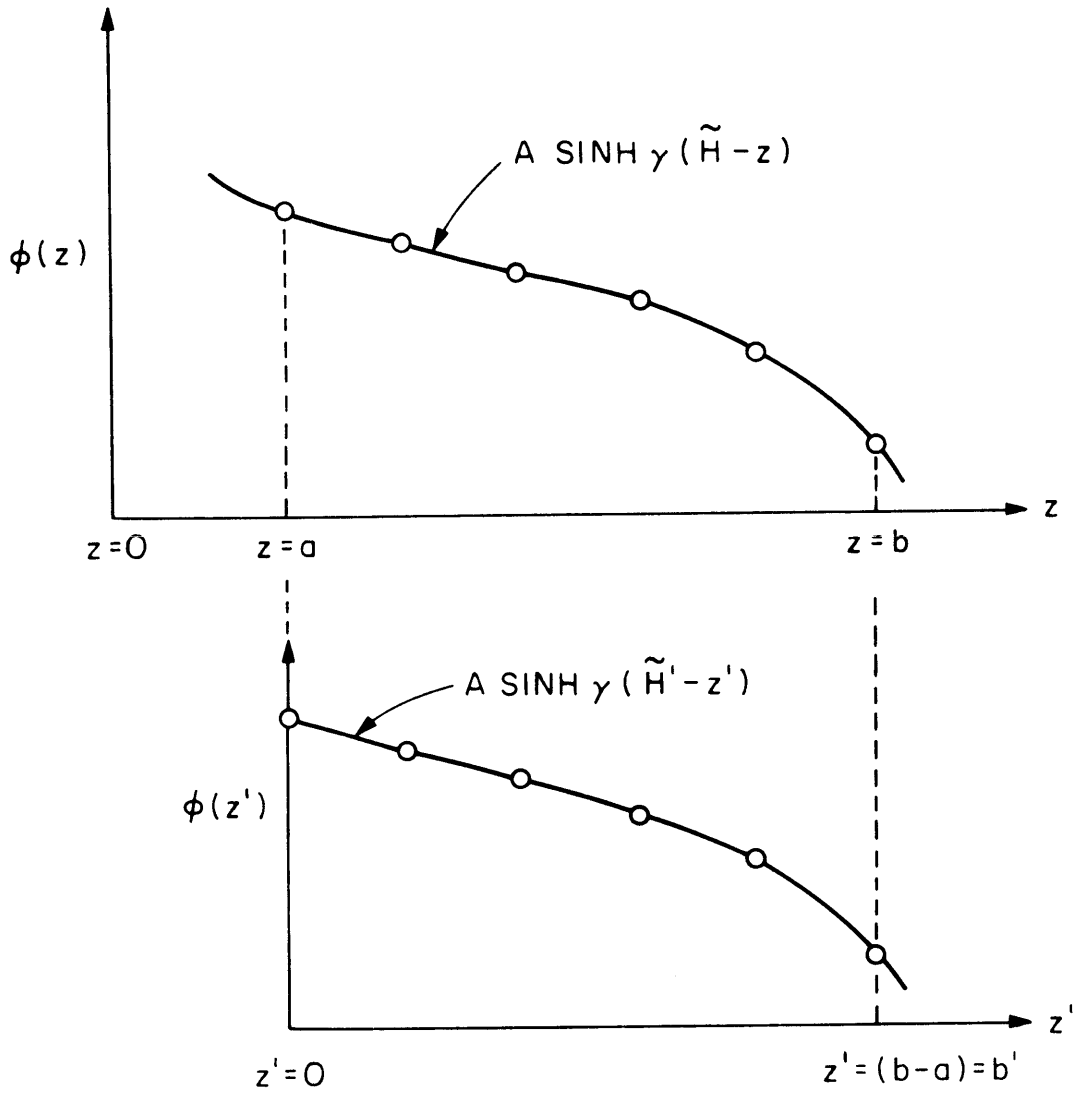

FIG. 3.1a TRANSLATIONAL TRANSFORMATION OF AXIAL COORDINATE SYSTEM.

We shall treat the moment index n as a variable integer, which acts as a weighting factor; it is therefore immaterial whether we use z' or (z'+a) as the base of the weighting factors of the flux moments. So we conclude that the definitions Eqs. (3.1) and (3.5) are equivalent for the parameters γ^2 and $\tilde{H}$. We shall use the definition (3.5); for ease of writing we shall drop the prime but shall bear in mind that the extrapolated height is actually given by Eq. (3.8).

Our major task is to derive an expression for the axial buckling γ^2 in terms of various axial flux moments. The essence of the moments method for the analysis of the axial buckling consists in the elimination of the functional forms cosh $\gamma(\tilde{H}-b)$ and sinh $\gamma(\tilde{H}-b)$ which appear in the axial flux moments by means of three independent equations involving three consecutive moment indices (n-1), n, and (n+1). To do this, we write the three axial flux moments:

$$\phi_{n-1} = -\frac{b^{n-1}}{\gamma}\cosh\gamma(\tilde{H}-b) - \frac{(n-1)b^{n-2}}{\gamma^2}\sinh\gamma(\tilde{H}-b) + \frac{(n-1)(n-2)}{\gamma^2}\phi_{n-3}\,, \tag{3.9}$$

$$\phi_{n} = -\frac{b^{n}}{\gamma}\cosh\gamma(\tilde{H}-b) - \frac{nb^{n-1}}{\gamma^2}\sinh\gamma(\tilde{H}-b) + \frac{n(n-1)}{\gamma^2}\phi_{n-2}\,, \tag{3.10}$$

$$\phi_{n+1} = -\frac{b^{n+1}}{\gamma}\cosh\gamma(\tilde{H}-b) - \frac{(n+1)b^{n}}{\gamma^2}\sinh\gamma(\tilde{H}-b) + \frac{n(n+1)}{\gamma^2}\phi_{n-1}\,. \tag{3.11}$$

To eliminate cosh $\gamma(\tilde{H}-b)$ and sinh $\gamma(\tilde{H}-b)$ from these three equations, we set the determinant

$$\begin{vmatrix} -\frac{b^{n-1}}{\gamma} & -\frac{(n-1)b^{n-2}}{\gamma^2} & \left[\phi_{n-1} - \frac{(n-1)(n-2)}{\gamma^2}\phi_{n-3}\right] \\ -\frac{b^{n}}{\gamma} & -\frac{nb^{n-1}}{\gamma^2} & \left[\phi_{n} - \frac{n(n-1)}{\gamma^2}\phi_{n-2}\right] \\ -\frac{b^{n+1}}{\gamma} & -\frac{(n+1)b^{n}}{\gamma^2} & \left[\phi_{n+1} - \frac{n(n+1)}{\gamma^2}\phi_{n-1}\right] \end{vmatrix} = 0 \qquad (3.12)$$

or

$$\begin{vmatrix} 1 & (n-1) & \left[\phi_{n-1} - \frac{(n-1)(n-2)}{\gamma^2}\phi_{n-3}\right] \\ b & nb & \left[\phi_{n} - \frac{n(n-1)}{\gamma^2}\phi_{n-2}\right] \\ b^2 & (n+1)b^2 & \left[\phi_{n+1} - \frac{n(n+1)}{\gamma^2}\phi_{n-1}\right] \end{vmatrix} = 0, \qquad (3.13)$$

which leads to the result for the axial buckling

$$\gamma^2(n) = \left\{ \frac{n(n+1)\phi_{n-1} - 2n(n-1)b\phi_{n-2} + (n-1)(n-2)b^2\phi_{n-3}}{\phi_{n+1} - 2b\phi_n + b^2\phi_{n-1}} \right\},$$

$$n = 3, 4, 5, 6, \ldots, \infty. \qquad (3.14)$$

The axial buckling is thus determined by the axial flux moments, the moment index, and the upper limit b. One of the major advantages of the moments method is that the usual difficulty of assuming a value of the extrapolated height, $\tilde{H}$, in order to obtain the axial buckling is removed. In fact, once the axial buckling has been determined, the extrapolated height can be calculated from it and various axial flux moments. To show this, we solve Eqs. (3.10) and (3.11) for $\cosh \gamma(\tilde{H}-b)$ and $\sinh \gamma(\tilde{H}-b)$:

$$\cosh \gamma(\tilde{H}-b) = \frac{\gamma}{b^{n+1}} \left\{ [n\phi_{n+1} - (n+1)b\phi_n] - \frac{n}{\gamma^2} [n(n+1)\phi_{n-1} - (n-1)(n+1)b\phi_{n-2}] \right\} , \quad (3.15)$$

and

$$\sinh \gamma(\tilde{H}-b) = - \frac{\gamma^2}{b^n} \left\{ [\phi_{n+1} - b\phi_n] - \frac{1}{\gamma^2} [n(n+1)\phi_{n-1} - n(n-1)b\phi_{n-2}] \right\} . \quad (3.16)$$

Forming the ratio, we get

$$\tanh \gamma(\tilde{H}-b) = \gamma b \left\{ \frac{\gamma^2[b\phi_n - \phi_{n+1}] + n(n+1)\phi_{n-1} - n(n-1)b\phi_{n-2}}{\gamma^2[n\phi_{n+1} - (n+1)b\phi_n] - n^2(n+1)\phi_{n-1} + n(n-1)(n+1)b\phi_{n-2}} \right\} ,$$

$$n = 2, 3, 4, 5, \ldots, \infty , \quad (3.17)$$

whence

$$\tilde{H}(n) = b + \frac{1}{\gamma} \tanh^{-1} \gamma b \left\{ \frac{\gamma^2[b\phi_n - \phi_{n+1}] + n(n+1)\phi_{n-1} - n(n-1)b\phi_{n-2}}{\gamma^2[n\phi_{n+1} - (n+1)b\phi_n] - n^2(n+1)\phi_{n-1} + n(n-1)(n+1)b\phi_{n-2}} \right\} ,$$

$$n = 2, 3, 4, \ldots, \infty . \quad (3.18)$$

The actual value of the extrapolated height is given by Eq. (3.8):

$$(\tilde{H})_{\text{actual}} = \tilde{H}(n) + a ,$$

where a is the distance from the external source to the first data point chosen for the analysis.

We can obtain a second expression for the extrapolated height by deriving an expression for $\tanh \gamma\tilde{H}$ instead of $\tanh \gamma(\tilde{H}-b)$ in terms of axial flux moments. This is feasible because the zeroth and first

axial flux moments contain cosh $\gamma\tilde{H}$ and sinh $\gamma\tilde{H}$. Thus, we evaluate the zeroth and first axial flux moments:

$$\phi_o = \frac{1}{\gamma}\left[-\cosh\gamma(\tilde{H}-b)+\cosh\gamma\tilde{H}\right], \tag{3.19}$$

$$\phi_1 = -\frac{b}{\gamma}\cosh\gamma(\tilde{H}-b) - \frac{1}{\gamma^2}\sinh\gamma(\tilde{H}-b) + \frac{1}{\gamma^2}\sinh\gamma\tilde{H}. \tag{3.20}$$

Now substitute Eqs. (3.15) and (3.16) in Eqs. (3.19) and (3.20), and then solve for cosh $\gamma\tilde{H}$ and sinh $\gamma\tilde{H}$:

$$\sinh\gamma\tilde{H} = \frac{1}{b^n}\left\{\gamma^2\left[(n-1)\phi_{n+1} - nb\phi_n + b^n\phi_1\right] - \left[n(n+1)(n-1)\phi_{n-1} - n^2(n-1)b\phi_{n-2}\right]\right\}, \tag{3.21}$$

$$\cosh\gamma\tilde{H} = \frac{1}{\gamma b^{n+1}}\left\{\gamma^2\left[n\phi_{n+1} - (n+1)b\phi_n + b^{n+1}\phi_o\right] - \left[n^2(n+1)\phi_{n-1} - n(n-1)(n+1)b\phi_{n-2}\right]\right\}. \tag{3.22}$$

Again, we form the ratio and invert the resulting expression for tanh $\gamma\tilde{H}$. The result is

$$\tilde{H}(n) = \frac{1}{\gamma}\tanh^{-1}\gamma b\left\{\frac{\gamma^2\left[(n-1)\phi_{n+1} - nb\phi_n + b^n\phi_1\right] - n\left[(n-1)(n+1)\phi_{n-1} - n(n-1)b\phi_{n-2}\right]}{\gamma^2\left[n\phi_{n+1} - (n+1)b\phi_n + b^{n+1}\phi_o\right] - n(n+1)\left[n\phi_{n-1} - (n-1)b\phi_{n-2}\right]}\right\}. \tag{3.23}$$

We prefer Eq. (3.18) to Eq. (3.23) because Eq. (3.23) determines $\tilde{H}$ directly through various axial flux moments while, in Eq. (3.18), the axial flux moments determine the much smaller value of $(\tilde{H}-b)$ with b being a fixed number. Hence, a larger error is incurred in $\tilde{H}$ by the use of Eq. (3.23) than by Eq. (3.18). We shall, therefore, use Eq. (3.18)

throughout this work to calculate the extrapolated height. The latter, together with the extrapolated radius, is important in the interpretation of pulsed neutron source experiments (C2, G1).

Both the axial buckling and the extrapolated height can be determined by means of the moments method with greater confidence than with the conventional curve-fitting method because they are uniquely defined when the moments index is fixed, and because they can be calculated independently through the axial flux moments. Moreover, the normalization constant A is not involved because only ratios of axial flux moments are required to compute the axial buckling and the extrapolated height, and A therefore drops out automatically.

If we could calculate the asymptotic axial flux moments by, say, the conventional moments method widely used in shielding calculations (F3, C1, B1), we could obtain the asymptotic axial buckling (hence the relaxation length) and extrapolated height by means of Eqs. (3.14) and (3.18). Such a calculation involves knowledge of the theoretical flux. However, we are concerned with inferring the axial buckling and extrapolated height from an experimental axial flux distribution. To do this, the theoretical axial flux moments that appear in Eqs. (3.14) and (3.18) are replaced by the corresponding experimental axial flux moments defined as

$$\phi_n^{exp} \equiv \int_0^b z^n A(z)\, dz \,, \tag{3.24}$$

where A(z) is the experimental axial activation distribution.

The experimental axial flux moments are to be evaluated from

equally spaced activation data by means of Simpson's rule for numerical integration. This choice is made because the accuracy of Simpson's rule is generally good enough for our purposes, while permitting flexibility in the selection of data (R2, H10).

3.2.2 The Choice of the Moment Index

Since the moment index n is treated as a variable parameter, there are many ways of calculating the axial buckling and extrapolated height in terms of axial flux moments. Which value of the moment index n will then yield the best values for the axial buckling and extrapolated height? We can answer this question in two different ways: by means of a physical argument and by means of a mathematical formulation.

From a physical point of view, the axial buckling γ^2 may be interpreted as the inverse square of the relaxation length, which is essentially the average distance from the external source and boundaries at which the neutron flux distribution becomes independent of source and boundary effects. In an infinite medium, there are no source or boundary effects, and the relaxation length is identical to the diffusion length, L, because the diffusion process describes the neutron behavior completely. The expression for the diffusion area, L^2, in an infinite medium is given in terms of the mean square distance, z^2, as (M1, B1, K6)

$$L^2 = \frac{1}{2}\overline{z^2} = \gamma^{-2} . \tag{3.25}$$

For a finite medium, the corresponding expression for γ^2 would be

expected to be more complicated but may be regarded, in general, as a function of various spatial moments, $\overline{z^n}$; namely,

$$\gamma^2 = \gamma^2(\overline{z}, \overline{z^2}, \ldots, \overline{z^n}) . \tag{3.26}$$

The functional dependence of γ^2 can be obtained from Eq. (3.14) by dividing the numerator and denominator by the zeroth axial flux moment ϕ_o; the result is

$$\gamma^2(n) = \frac{n(n+1)\overline{z^{n-1}} - 2n(n-1)b\overline{z^{n-2}} + (n-1)(n-2)b^2\,\overline{z^{n-3}}}{\overline{z^{n+1}} - 2b\overline{z^n} + b^2\overline{z^{n-1}}} , \tag{3.27}$$

where the average spatial moments $\overline{z^n}$ is, by definition,

$$\overline{z^n} \equiv \frac{\int z^n \phi(z)\, dz}{\int \phi(z)\, dz} = \frac{\phi_n}{\phi_o} . \tag{3.28}$$

To see if Eq. (3.27) for a finite system reduces to Eq. (3.25) for an infinite medium, we let $b \to \infty$ and find the limit of $\gamma^2(n)$:

$$\lim_{b\to\infty} \gamma^2(n) = (n-1)(n-2)\frac{\overline{z^{n-3}}}{\overline{z^{n-1}}} , \quad \text{for } n = 3, 4, 5, \ldots, \infty . \tag{3.29}$$

It is apparent that only if $n = 3$ does Eq. (3.29) lead to the correct infinite-medium result:

$$\lim_{b\to\infty} \gamma^2(3) = 2\left(\frac{1}{\overline{z^2}}\right) \tag{3.30}$$

or

$$\gamma^{-2}(3) = \frac{1}{2}\overline{z^2} = L^2 .$$

On the basis of this reasoning, therefore, the correct moment

index to be chosen for the axial buckling analysis should be n=3. One must not forget, however, that in a finite subcritical assembly there are spatial and energy transients in addition to the source neutron contribution. These additional contributions to the (asymptotic) flux distribution would perturb, to some extent, the result, Eq. (3.14) or Eq. (3.27), which is based on the asymptotic part of the neutron flux distribution alone. In other words, the conclusion that n may be equal to 3 is no longer true when the asymptotic part of the neutron flux distribution is significantly contaminated by various transients and by the source contribution.

The discussion up to this stage makes us doubt the applicability of Eqs. (3.14) and (3.18) to a small assembly where there may be only a small portion of the flux distribution that is asymptotic. Furthermore, the nature of the spatial and energy transients and the integral definition of the flux moments combine to make it possible for the transients and source neutron contribution to partly offset one another while the asymptotic part of neutron flux distribution remains. To see this, we have to understand the nature of the spatial and energy transients. These will be treated in Chapter VI. It suffices to say here that the transient fluxes appear to be positive near the source end and negative near the boundary z=H, as sketched in Figure 3.2 together with the asymptotic part and the source contribution. The corresponding distributions of the asymptotic flux moments, transient flux moments, and source moments are sketched in Figure 3.3. The transient flux moments tend to cancel in part; in addition, they will also offset a part of the source moments depending

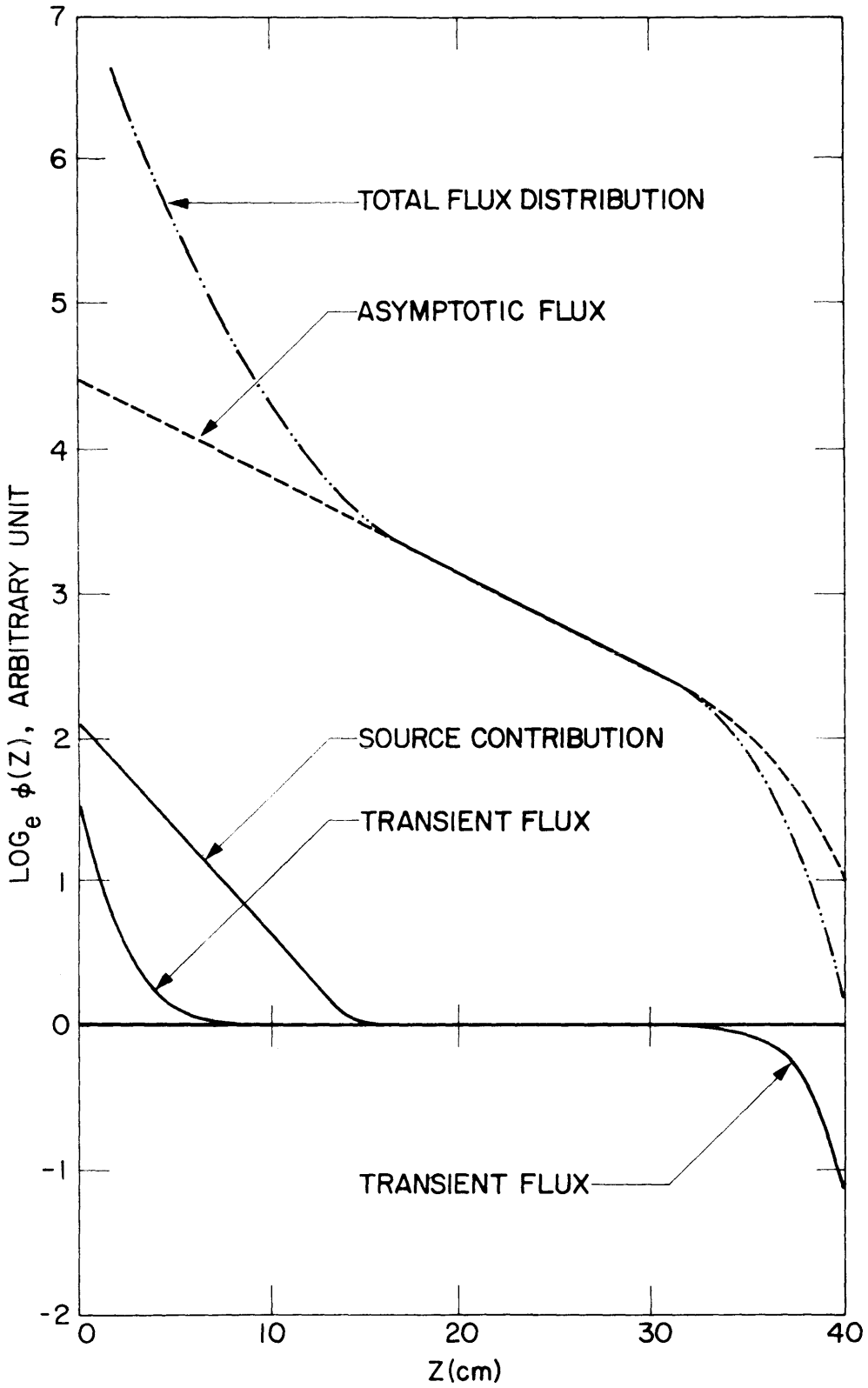

FIG. 3.2 SKETCH OF THE AXIAL FLUX DISTRIBUTION IN A TYPICAL MINIATURE LATTICE.

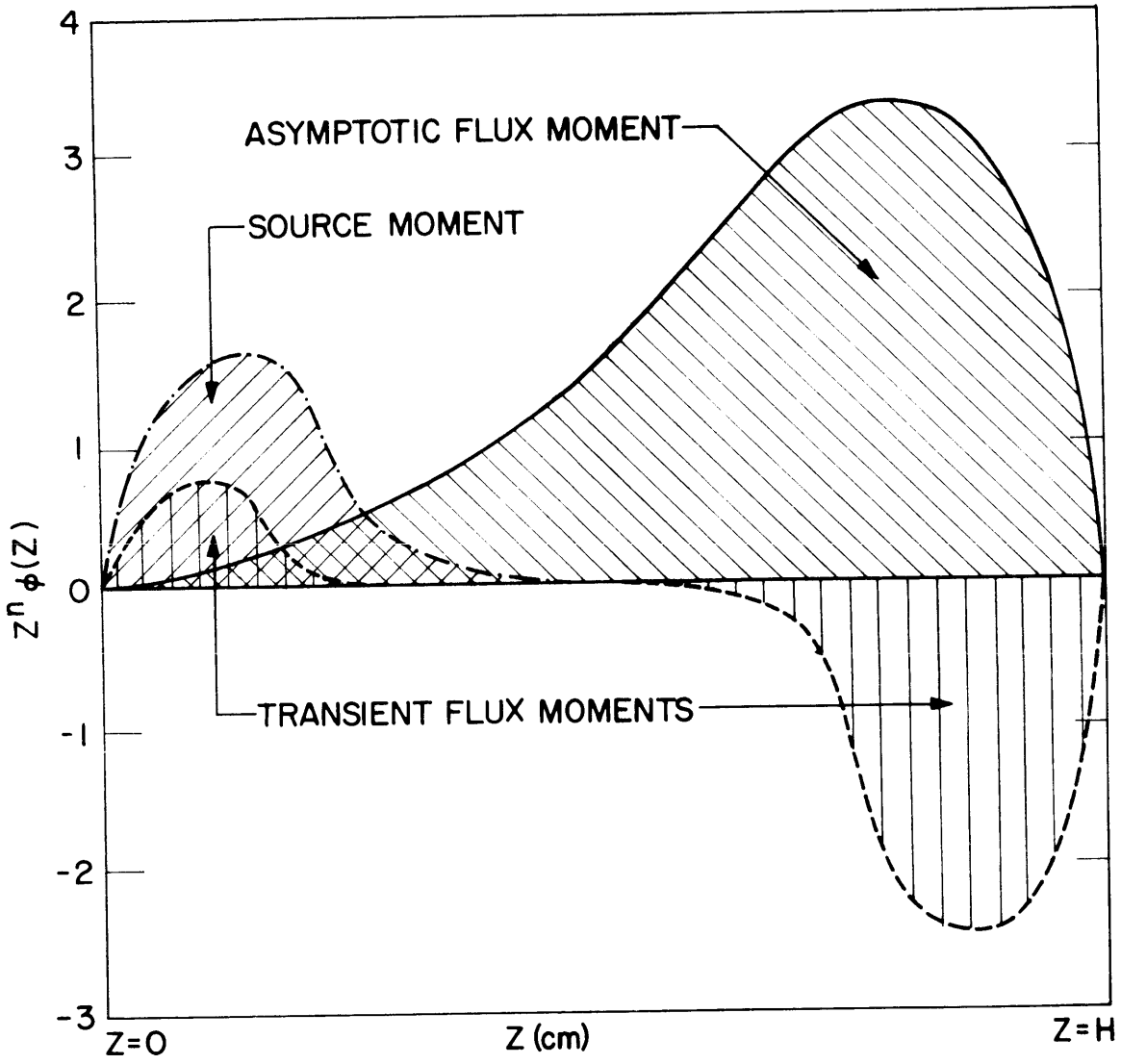

FIG. 3.3 DISTRIBUTIONS OF THE ASYMPTOTIC FLUX MOMENTS, SOURCE MOMENTS, AND TRANSIENT FLUX MOMENTS. THE AREAS UNDER THE CURVES ARE THE MOMENTS DESIRED.

on the weighting factor, i.e., the moment index. Hence, there should be a certain value of the moment index n that will mostly retain the asymptotic flux moments while minimizing the contribution of the source and transient flux moments.

This discussion leads to a mathematical method of determining the optimum value of n through an error analysis. A formal approach is to minimize the probable errors that may be incurred in γ^2 and $\tilde{H}$, with respect to the moment index n. This procedure will lead to an equation that determines the optimum value of n. But this approach is likely to be impractical, if not impossible, primarily because the dependence of the probable errors on the moment index is not clear. A practical way to get around this problem is to compute the probable errors for a series of values of n and then observe the variation of the error as a function of n. The moment index that yields the minimum probable errors is the one to be chosen. Thus, an error analysis is necessary to complete the moments method.

3.2.3 Error Analysis

There are primarily two kinds of errors associated with the calculation of the axial buckling and the extrapolated height by means of the moments method: (a) the experimental error, that is, the error incurred by replacing the theoretical asymptotic axial flux moments by the corresponding experimental axial flux moments (this error is, in a sense, a measure of how much the experimental flux distribution will deviate from the asymptotic); and (b) the truncation error, that is, the error incurred in the evaluation of the various axial flux moments by numerical integration.

The two kinds of errors combine to give the probable error which will be defined below (see Eq. (3.36)). The probable error is the error associated with the moments method itself and serves as a measure of the consistency of the moments method as well as a tool for selecting the best value of the axial buckling calculated by the moments method. It is important to distinguish the probable error from the standard deviation; they are entirely different quantities. The standard deviation, which is usually reported in the literature, is a measure of the reproducibility of a certain experiment; it will be defined in section 3.3.5 (see Eqs. (3.72) and (3.73)). The terms probable error and standard deviation will be used throughout the present work; their definitions and meanings should be distinguished wherever they appear.

First, we estimate the probable error in the axial buckling, γ^2. Consider γ^2 as a function of the axial flux moments:

$$\gamma^2 = \gamma^2(\phi_o, \phi_1, \phi_2, \cdots, \phi_N) \ . \tag{3.31}$$

Taking differentials, we obtain

$$\delta\gamma^2 = \sum_{j=1}^{N} \left(\frac{\partial \gamma^2}{\partial \phi_j} \right) \delta\phi_j \ . \tag{3.32}$$

Define the variance in axial buckling, $\sigma^2_{\gamma^2}$, in accord with the usual practice:

$$\sigma^2_{\gamma 2} = \sum_{j=1}^{N} \left(\frac{\partial \gamma^2}{\partial \phi_j} \right)^2 (\delta\phi_j)^2 \tag{3.33}$$

$$= \sum_{j=1}^{N} C_j (\delta\phi_j)^2 \ , \tag{3.34}$$

where

$$C_j \equiv \left(\frac{\partial \gamma^2}{\partial \phi_j}\right)^2 . \tag{3.35}$$

The probable error in γ^2 is defined as

$$\sigma_{\gamma^2} = \sqrt{\sum_{j=1}^{N} C_j (\delta\phi_j)^2} . \tag{3.36}$$

The deviations in the axial flux moments, $\delta\phi_j$, arise from two sources: experimental error and truncation error. If we consider that the two kinds of errors are independent, we have

$$(\delta\phi_j)^2 = \left(\delta\phi_j^{exp}\right)^2 + \left(\delta\phi_j^{tr}\right)^2 , \tag{3.37}$$

where $\delta\phi_j^{exp}$ is the experimental error in the ϕ_j, and $\delta\phi_j^{tr}$ is the truncation error in the ϕ_j.

The coefficients C_j can be obtained by differentiating Eq. (3.14) with respect to the ϕ_j. For brevity, we rewrite Eq. (3.14) as

$$\gamma^2(n) = \frac{N(n)}{D(n)} , \tag{3.38}$$

where

$$N(n) \equiv n(n+1)\,\phi_{n-1} - 2n(n-1)b\phi_{n-2} + (n-1)(n-2)b^2\phi_{n-3} , \tag{3.39}$$

and

$$D(n) \equiv \phi_{n+1} - 2b\phi_n + b^2\phi_{n-1} . \tag{3.40}$$

Then by differentiation we obtain, assuming that b is a fixed constant,

$$\frac{\partial \gamma^2(n)}{\partial \phi_{n-3}} = \frac{(n-1)(n-2)b^2}{D(n)} , \tag{3.41}$$

$$\frac{\partial \gamma^2(n)}{\partial \phi_{n-2}} = - \frac{2n(n-1)b}{D(n)} , \tag{3.42}$$

$$\frac{\partial \gamma^2(n)}{\partial \phi_{n-1}} = \frac{[n(n+1)D(n) - b^2 N(n)]}{[D(n)]^2} , \tag{3.43}$$

$$\frac{\partial \gamma^2(n)}{\partial \phi_{n}} = \frac{2bN(n)}{[D(n)]^2} , \tag{3.44}$$

$$\frac{\partial \gamma^2(n)}{\partial \phi_{n+1}} = - \frac{N(n)}{[D(n)]^2} . \tag{3.45}$$

There are five coefficients corresponding to the five axial flux moments, ϕ_{n-3}, ϕ_{n-2}, ϕ_{n-1}, ϕ_n, and ϕ_{n+1}, needed to compute the axial buckling. They can be combined in a single formula

$$C_{n+j-4} \equiv \left(\frac{\partial \gamma^2(n)}{\partial \phi_{n+j-r}} \right)^2 , \quad j = 1, 2, 3, 4, 5 . \tag{3.46}$$

Since the theoretical axial flux moments ϕ_j^{th} can be evaluated analytically, as in Eq. (3.10), it is possible to calculate the truncation errors incurred in the ϕ_j from the expression

$$\delta \phi_j^{tr} = \left[\phi_j^{th} \right]_{\substack{\text{analytical} \\ \text{integration}}} - \left[\phi_j^{th} \right]_{\substack{\text{numerical} \\ \text{integration}}} . \tag{3.47}$$

The experimental errors in the ϕ_j can be estimated from the relation

$$\delta \phi_j^{exp} = \left[\phi_j^{th} - \frac{\phi_j^{exp}}{A} \right] , \tag{3.48}$$

where both ϕ_j^{th} and ϕ_j^{exp} are to be evaluated by numerical integration, and A is the normalization constant to be determined.

The variance in γ^2 may then be written

$$\sigma^2_{\gamma 2}(n) = \left[\sigma^2_{\gamma^2}(n)\right]_{exp} + \left[\sigma^2_{\gamma^2}(n)\right]_{tr}$$

$$= \sum_{j=1}^{5} C_{n+j-4} \left\{ \left[\phi^{th}_{n+j-4} - \frac{\phi^{exp}_{n+j-4}}{A}\right]^2 + \left(\delta\phi^{tr}_{n+j-4}\right)^2 \right\} . \qquad (3.49)$$

The normalization constant, A, is to be determined by minimizing the probable error $\sigma_{\gamma 2}$ or, equivalently, $\sigma^2_{\gamma 2}$ with respect to A; that is, we set

$$\frac{d\sigma^2_{\gamma^2}(n)}{dA} = 0 . \qquad (3.50)$$

Realizing that $\left(\phi^{th}_{n+j-4}\right)^2$ is independent of A, we obtain the defining formula for A from Eq. (3.50):

$$A(n) = \frac{\sum_{j=1}^{5} C_{n+j-4}\left(\phi^{exp}_{n+j-4}\right)^2}{\sum_{j=1}^{5} C_{n+j-4}\left(\phi^{th}_{n+j-4}\right)\left(\phi^{exp}_{n+j-4}\right)} . \qquad (3.51)$$

We can now calculate the experimental errors $\left[\sigma_{\gamma^2}\right]_{exp}$, the truncation errors $\left[\sigma_{\gamma^2}\right]_{tr}$, and hence the probable errors $\sigma_{\gamma^2}(n)$ with the aid of Eq. (3.49). The theoretical axial flux moments must be used to calculate the coefficients C_{n+j-4} because of the way we define the experimental and truncation errors (see Eqs. (3.47) and (3.48)).

Following the same procedure, we can also estimate the

probable errors in the extrapolated height, $\tilde{H}$. To do this, we recall Eq. (3.18) and write

$$\tilde{H} = \tilde{H}(\phi_{n-2}, \phi_{n-1}, \phi_n, \phi_{n+1}; \gamma), \quad n = 2, 3, 4, 5, \ldots, \infty. \tag{3.52}$$

Again we differentiate and get

$$\delta\tilde{H} = \sum_{j=1}^{4} \left(\frac{\partial\tilde{H}}{\partial\phi_{n+j-3}}\right) \delta\phi_{n+j-3} + \frac{\partial\tilde{H}}{\partial\gamma}\,\delta\gamma \ . \tag{3.53}$$

The variance in $\tilde{H}$ is defined as

$$\sigma^2_{\tilde{H}}(n) = \sum_{j=1}^{4} H_{n+j-3}\left(\delta\phi_{n+j-3}\right)^2 + H_\gamma(\delta\gamma)^2 \ , \tag{3.54}$$

where

$$H_{n+j-3} \equiv \left(\frac{\partial\tilde{H}}{\phi_{n+j-3}}\right)^2 , \quad j = 1, 2, 3, 4, \tag{3.55}$$

and

$$H_\gamma \equiv \left(\frac{\partial\tilde{H}}{\partial\gamma}\right)^2 . \tag{3.56}$$

Since we have computed $\sigma^2_{\gamma 2}$ previously, we can determine $(\delta\gamma)^2$ from the relation $\gamma = (\gamma^2)^{1/2}$; hence,

$$\delta\gamma = \frac{1}{2}(\gamma^2)^{-1/2}\,\delta\gamma^2 \ ,$$

and

$$(\delta\gamma)^2 = \frac{\sigma^2_{\gamma^2}}{4\gamma^2} . \tag{3.57}$$

The calculation of the quantities $(\delta\phi_{n+j-3})^2$ remains the same as before. To compute the coefficients H_{n+j-3}, we differentiate Eq. (3.18) with respect to the ϕ_n. For simplicity, we rewrite Eq. (3.18) in the form

$$\tilde{H}(n) = b + \frac{1}{\gamma} \tanh^{-1} \gamma b \left[\frac{P(n)}{Q(n)}\right], \tag{3.58}$$

where

$$P(n) \equiv \gamma^2[b\phi_n - \phi_{n+1}] + n(n+1)\,\phi_{n-1} - n(n-1)\,b\phi_{n-2}, \tag{3.59}$$

and

$$Q(n) \equiv \gamma^2[n\phi_{n+1} - (n+1)b\phi_n] - n^2(n+1)\,\phi_{n-1} + n(n-1)(n+1)\,b\phi_{n-2},$$

$$n = 2, 3, 4, \ldots, \infty. \tag{3.60}$$

We again treat b as a constant and obtain the following results by differentiation:

$$\frac{\partial \tilde{H}(n)}{\partial \phi_{n-2}} = - \frac{n(n-1)b^2}{[Q^2(n) - \gamma^2 b^2 P^2(n)} [Q(n) + (n+1)P(n)], \tag{3.61}$$

$$\frac{\partial \tilde{H}(n)}{\partial \phi_{n-1}} = \frac{n(n+1)b}{[Q^2(n) - \gamma^2 b^2 P^2(n)} [Q(n) + nP(n)], \tag{3.62}$$

$$\frac{\partial \tilde{H}(n)}{\partial \phi_n} = \frac{b^2\gamma^2}{[Q^2(n) - \gamma^2 b^2 P^2(n)} [Q(n) + (n+1)P(n)], \tag{3.63}$$

$$\frac{\partial \tilde{H}(n)}{\partial \phi_{n+1}} = - \frac{b\gamma^2}{[Q^2(n) - \gamma^2 b^2 P^2(n)]} [Q(n) + nP(n)], \tag{3.64}$$

$$\frac{\partial \tilde{H}(n)}{\partial \gamma} = - \frac{(\tilde{H} - b)}{\gamma} + \frac{b}{\gamma} \cdot \frac{1}{[Q^2(n) - \gamma^2 b^2 P^2(n)]}$$

$$\left\{ P(n)Q(n) + 2\gamma^2 Q(n)[b\phi_n - \phi_{n+1}] - 2\gamma^2 P(n)[n\phi_{n+1} - (n+1)b\phi_n] \right\}. \tag{3.65}$$

The variance in the extrapolated height, $\sigma^2_{\tilde{H}}(n)$, is given by

$$\sigma^2_{\tilde{H}}(n) = \sum_{j=1}^{4} H_{n+j-3} \left\{ \left[\phi^{th}_{n+j-3} - \frac{\phi^{exp}_{n+j-3}}{A'} \right]^2 + \left(\delta\phi^{tr}_{n+j-3} \right)^2 \right\} + \left[H_\gamma \cdot \frac{\sigma^2_{\gamma^2}(n)}{4\gamma^2} \right]. \tag{3.66}$$

The normalization constant A′ for the extrapolation height is determined by minimizing the probable error in $\tilde{H}$, that is, setting

$$\frac{d\sigma^2_{\tilde{H}}(n)}{dA'} = 0 , \tag{3.67}$$

which yields the result for A′(n):

$$A'(n) = \frac{\sum_{j=1}^{4} H_{n+j-3}\left(\phi^{exp}_{n+j-3}\right)^2}{\sum_{j=1}^{4} H_{n+j-3}\left(\phi^{th}_{n+j-3}\right)\left(\phi^{exp}_{n+j-3}\right)} . \tag{3.68}$$

We separate the total probable error in $\tilde{H}$ into the experimental error and the truncation error and compute the two errors separately. To do this, we write Eq. (3.66) in the form

$$\sigma^2_{\tilde{H}}(n) = \left[\sigma^2_{\tilde{H}}(n)\right]_{exp} + \left[\sigma^2_{\tilde{H}}(n)\right]_{tr} , \tag{3.69}$$

where

$$\left[\sigma^2_{\tilde{H}}(n)\right]_{exp} = \sum_{j=1}^{4} H_{n+j-3}\left[\phi^{th}_{n+j-3} - \frac{\phi^{exp}_{n+j-3}}{A'}\right]^2 + H_\gamma \frac{\left[\sigma^2_{\gamma^2}(n)\right]_{exp}}{4\gamma^2} , \tag{3.70}$$

$$\left[\sigma^2_{\tilde{H}}(n)\right]_{tr} = \sum_{j=1}^{4} H_{n+j-3}\left\{\left[\phi^{th}_{n+j-3}\right]_{analytical} - \left[\phi^{th}_{n+j-3}\right]_{numerical}\right\}^2 + H_\gamma \frac{\left[\sigma^2_{\gamma^2}(n)\right]_{tr}}{4\gamma^2} . \tag{3.71}$$

Once again theoretical axial flux moments must be used to compute the coefficients H_{n+j-3}.

3.3 RESULTS

The procedure developed in the preceding section has been coded as "ABMOMENT" in FORTRAN IV language for the IBM Operating System 360 computer at the M.I.T. Computation Center. The details of the code are described in Appendix A. The code has been applied to several slightly enriched U-D_2O lattices and three slightly enriched UO_2-D_2O lattices investigated at the M.I.T. Subcritical Facility. The results as well as studies of some of the features of the moments method will be presented below.

3.3.1 Error Behavior of the Axial Buckling and Extrapolated Height As Functions of the Moment Index

Since the error behavior of the axial buckling and of the extrapolated height are crucial to the moments method, we study this problem first. On the basis of the discussion in section 3.2.2, we expect that there is an optimum value of the moment index that corresponds to the minimum experimental error in the quantities of interest. This has been verified for some typical lattices as shown in Figures 3.4 and 3.5. The optimum value of the moment index for these lattices is in the neighborhood of 6. It is also evident that the optimum moment indices for the axial buckling and extrapolated height are very nearly the same. This result has been found for most of the lattices studied. The truncation errors should increase with the moment index because the higher the moment index the greater is the truncation error that may be incurred in the axial flux moments through numerical integration. This is indicated in Figures 3.6 and 3.7. It is therefore desirable to

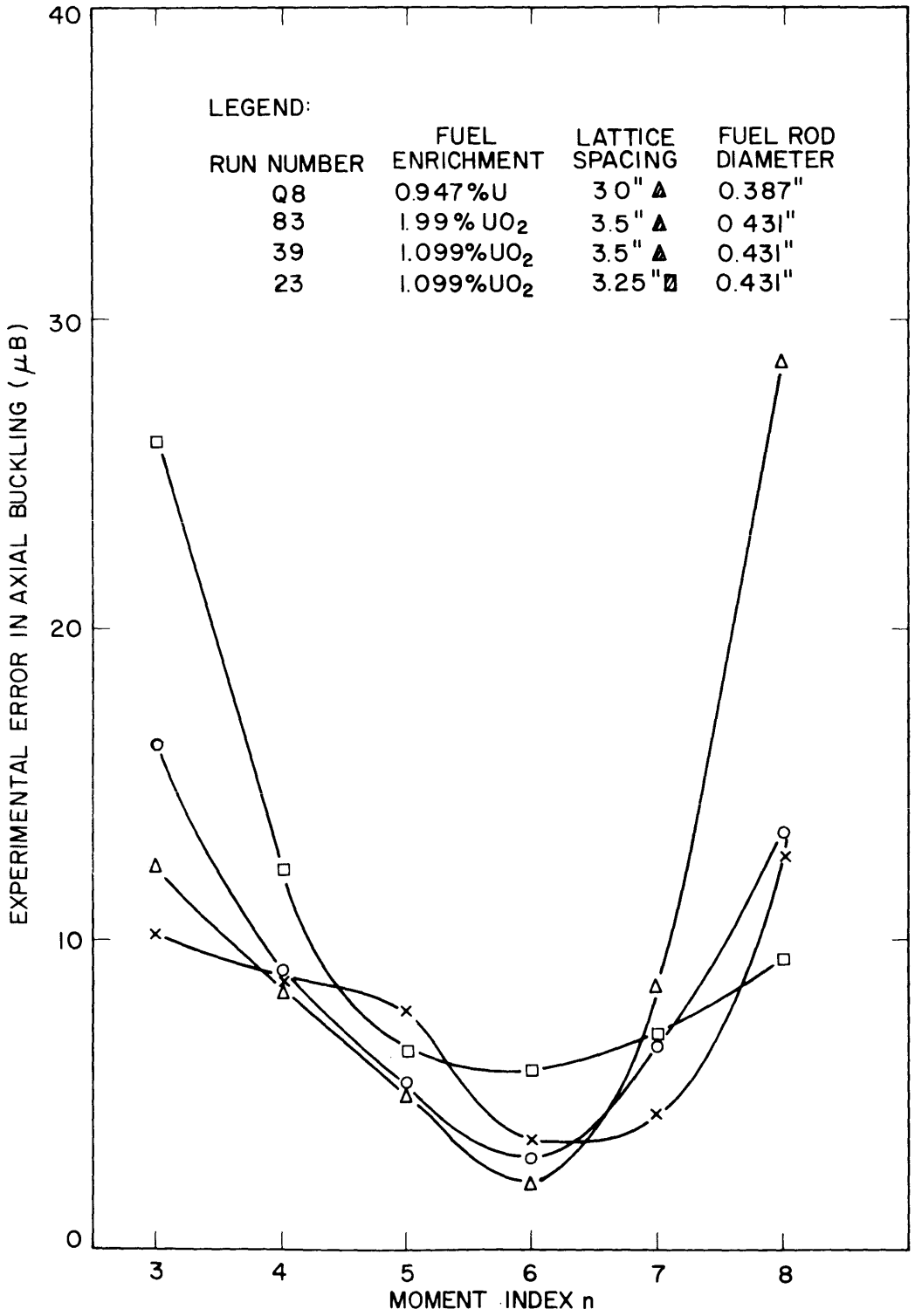

FIG. 3.4 BEHAVIOR OF THE EXPERIMENTAL ERROR IN THE AXIAL BUCKLING AS A FUNCTION OF THE INDEX.

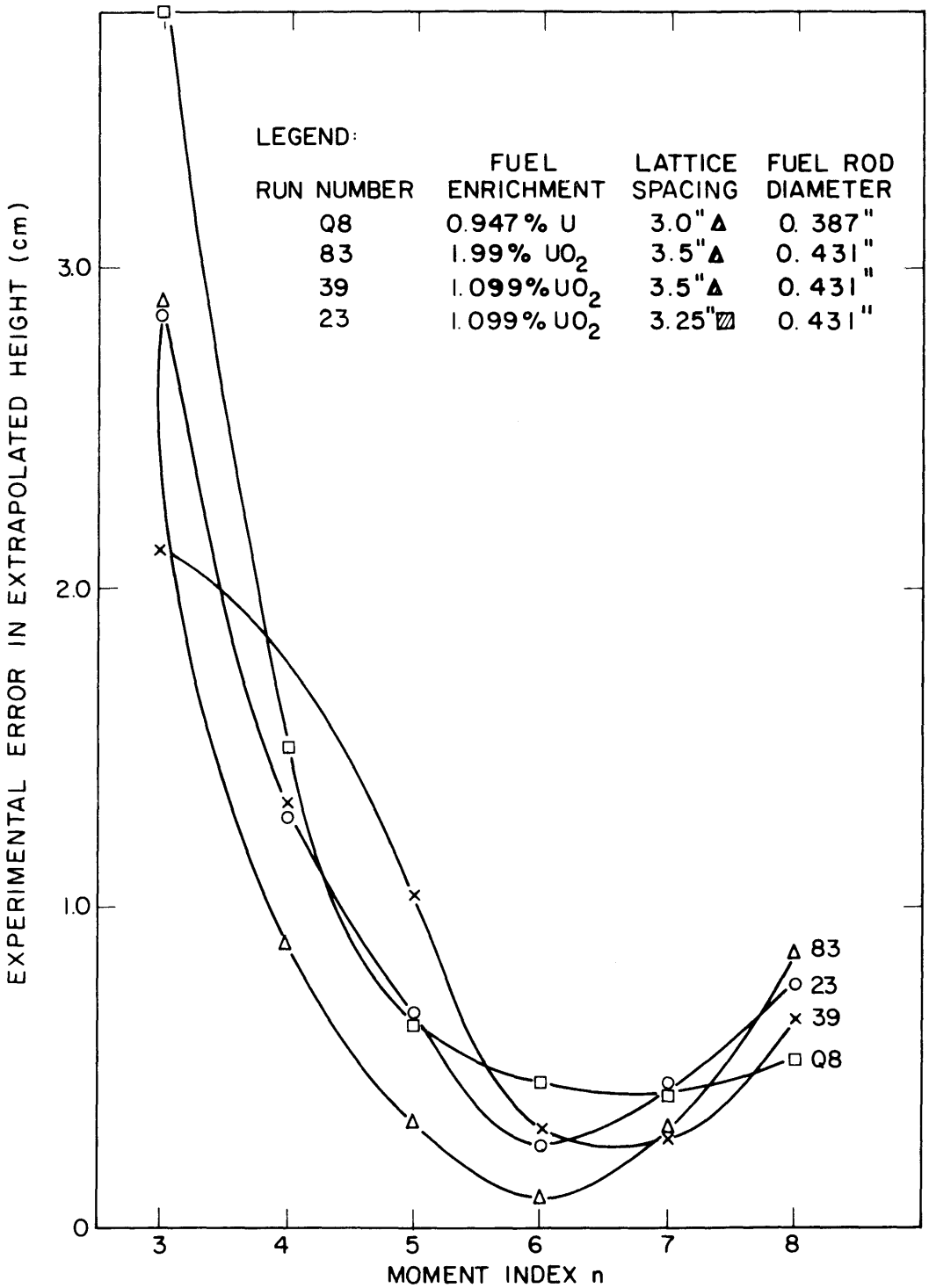

FIG. 3.5 BEHAVIOR OF THE EXPERIMENTAL ERROR IN THE EXTRAPOLATED HEIGHT AS A FUNCTION OF THE MOMENT INDEX.

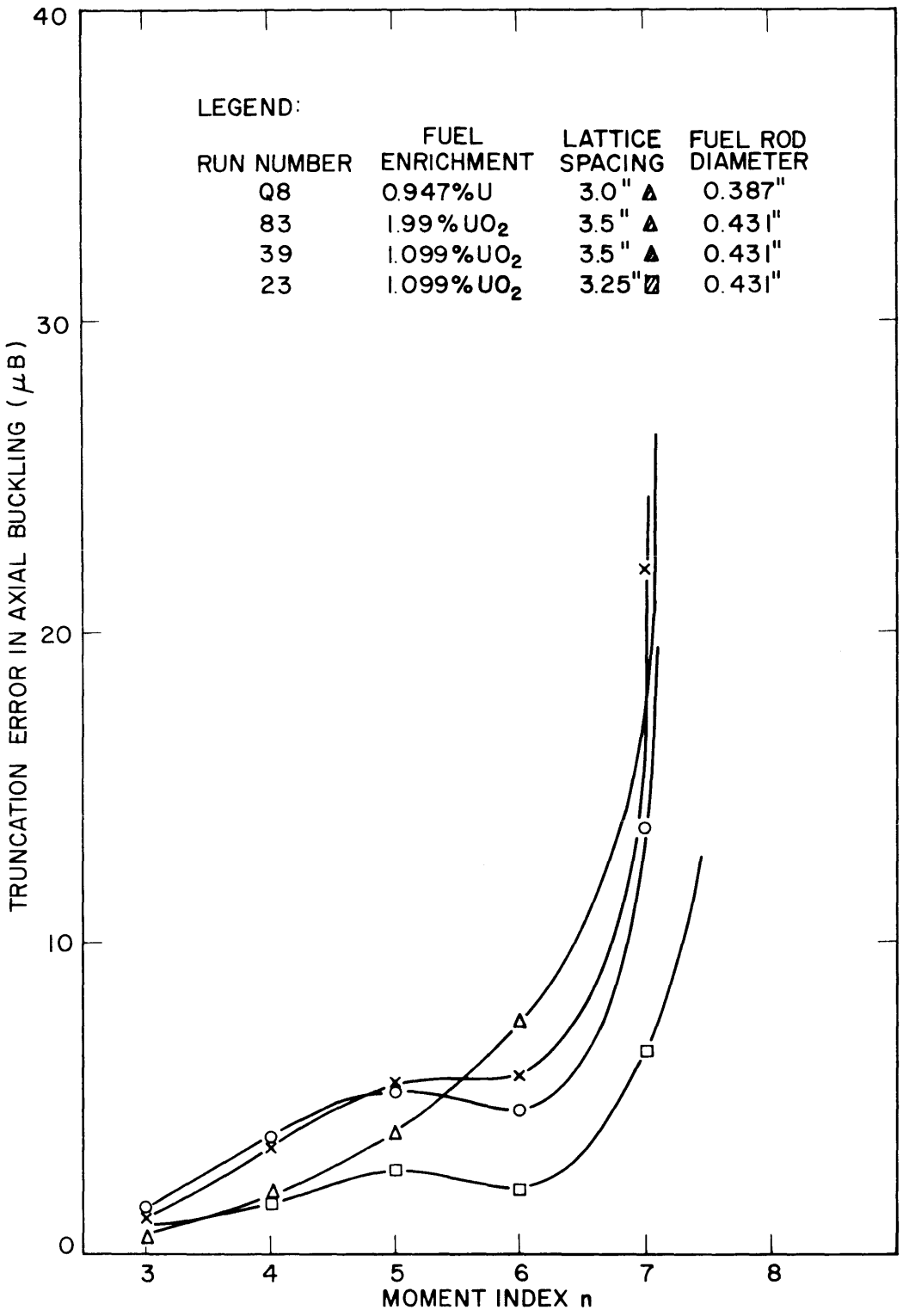

FIG. 3.6 BEHAVIOR OF THE TRUNCATION ERROR IN THE AXIAL BUCKLING AS A FUNCTION OF THE MOMENT INDEX.

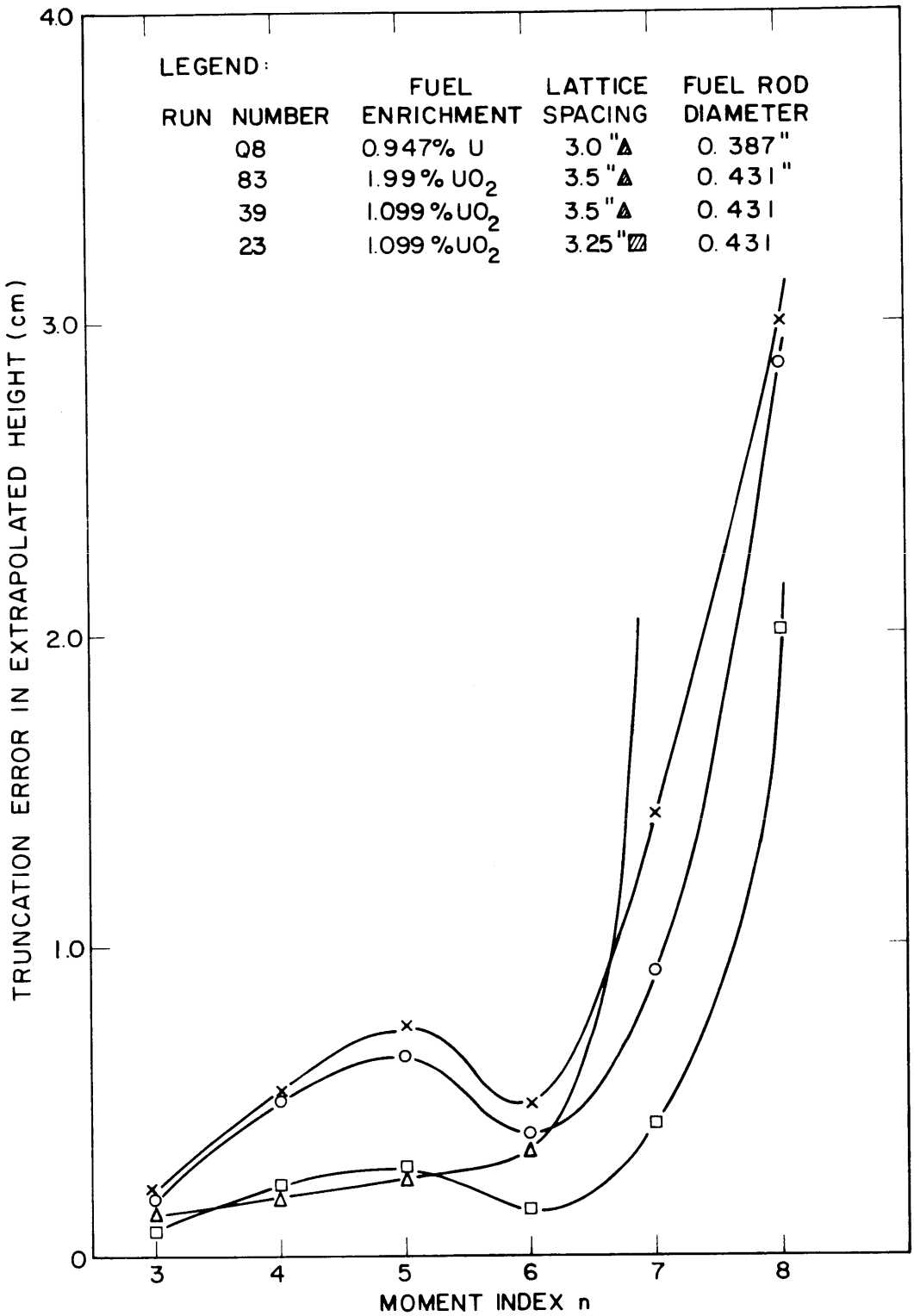

FIG. 3.7 BEHAVIOR OF THE TRUNCATION ERROR IN THE EXTRAPOLATED HEIGHT AS A FUNCTION OF THE MOMENT INDEX.

use the lowest moment index provided that the experimental error permits us to do so, but the presence of the source neutron contribution and various flux transients calls for a higher moment index to reduce their effects. A compromise must be made between these two kinds of errors. This can be accomplished through the combined probable errors defined in section 3.2.3. Figures 3.8 and 3.9 show the behavior of the combined probable error.

3.3.2 Optimization Study of the Choice of the Number of Data Points

The moments method has another degree of flexibility for the analysis of the axial buckling and extrapolated height, namely, the choice of the number of data points. As far as truncation error is concerned, the more data points are used the smaller the truncation error will be. However, because of the nature of the moments method this is not necessarily true for the experimental error. Rather, the choice of the positions of the first and last data points, that is, the lower and upper limits in the definition of the axial flux moments, turns out to be important for the experimental error. This choice provides a way of locating the boundaries of an asymptotic region, as has been discussed in section 3.2.1, and hence adds another degree of freedom to the moments method. Because of the way in which the moments method eliminates the transient effect and part of the source effect, as discussed in section 3.2.2, the asymptotic region would be enlarged by the moments method insofar as buckling experiments are concerned. This property of the method offers an appreciable advantage over the curve-fitting method, especially in small assemblies. Tables 3.1 and 3.2 serve to illustrate this advantage of the moments method in the

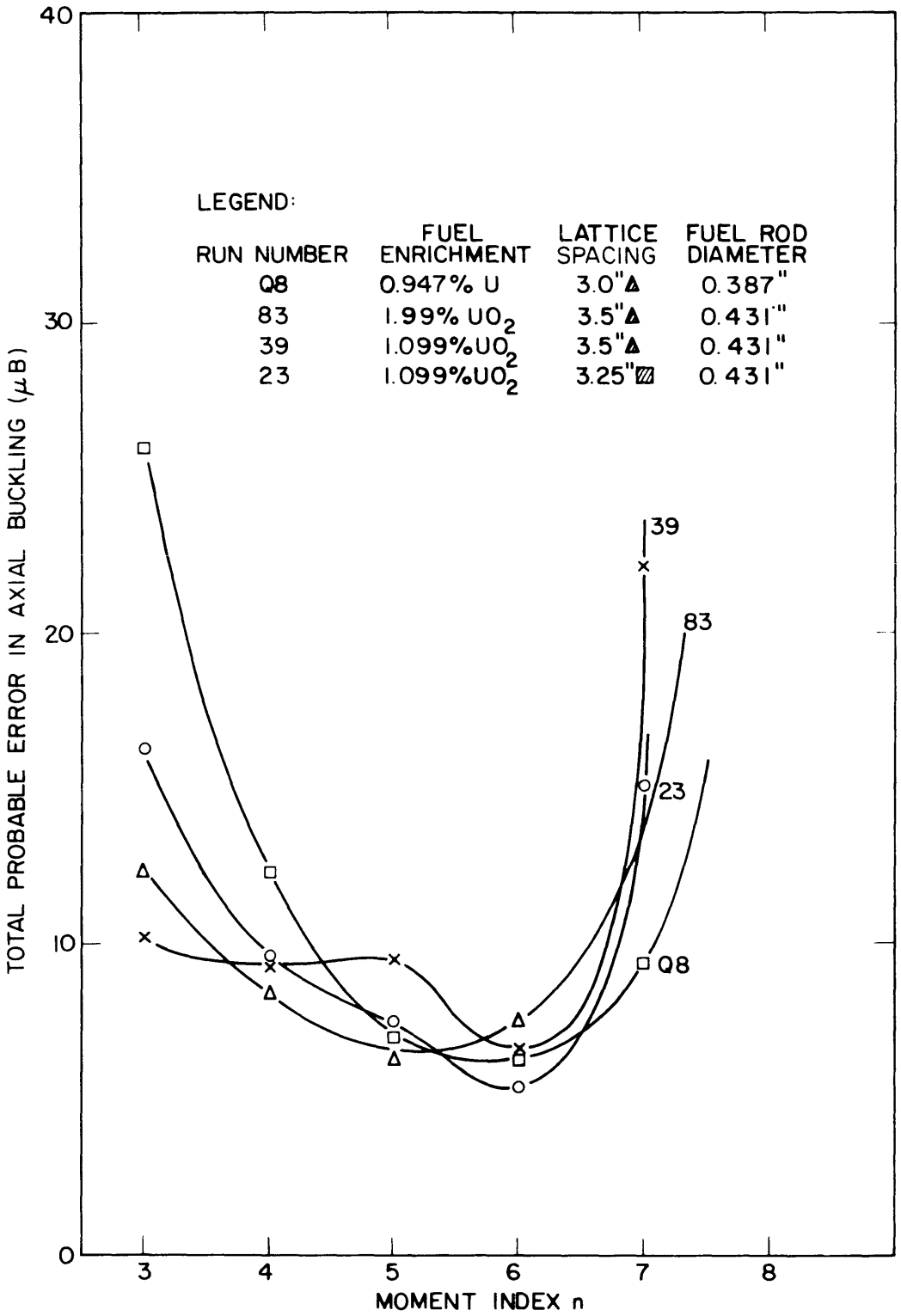

FIG. 3.8 BEHAVIOR OF THE TOTAL PROBABLE ERROR IN THE AXIAL BUCKLING AS A FUNCTION OF THE MOMENT INDEX.

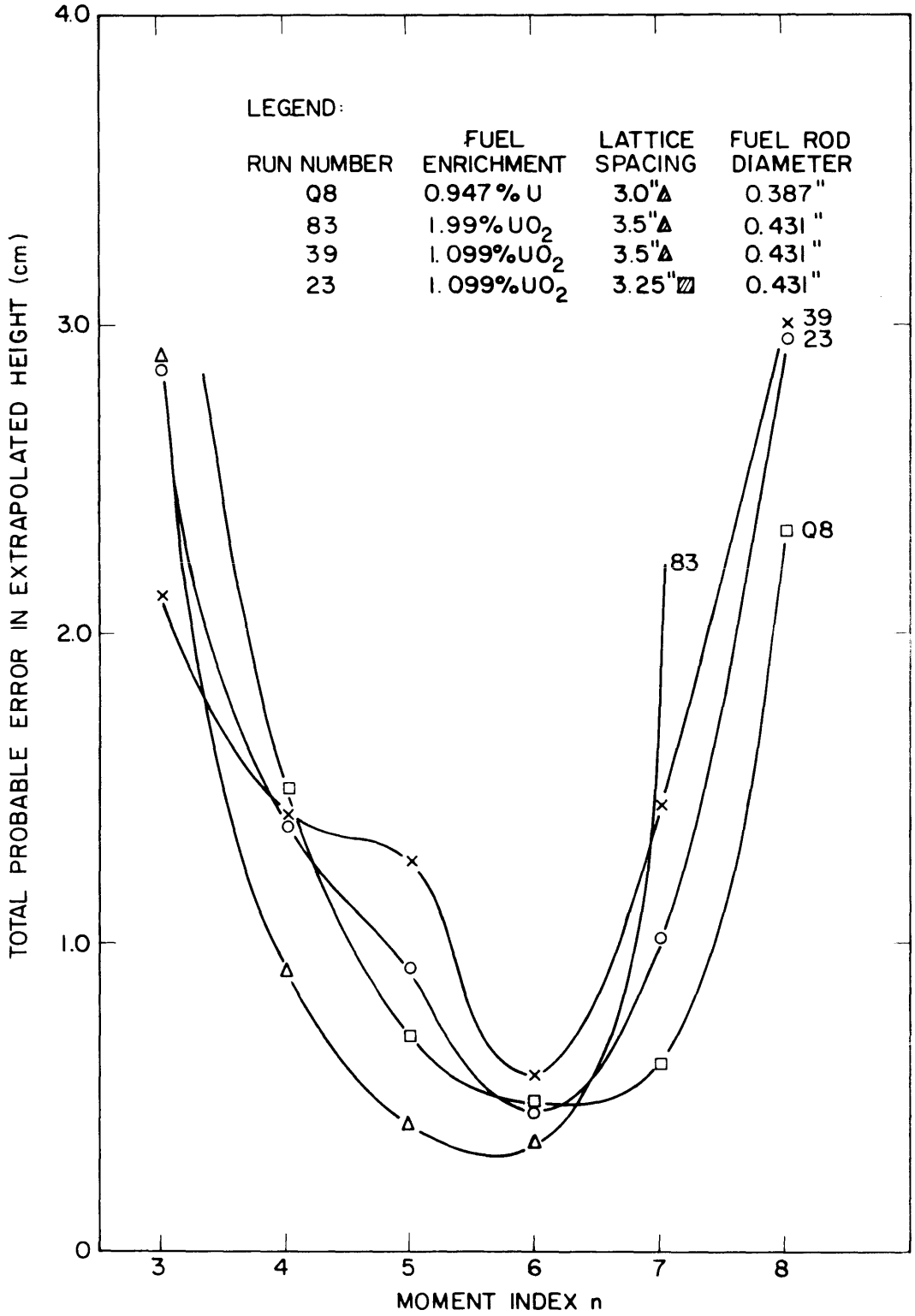

FIG. 3.9 BEHAVIOR OF THE TOTAL PROBABLE ERROR IN THE EXTRAPOLATED HEIGHT AS A FUNCTION OF THE MOMENT INDEX.

Table 3.1. The axial buckling vs. the first and end points calculated by means of the moments method for the Run R4 measured in a 3-foot tank.

Run R4: 0.947% enriched fuel, 3-inch triangular spacing, 0.387-inch rod diameter.

Number of Data Points	First Point (cm)	End Point (cm)	Axial Buckling γ^2 (μB)	Probable Error in γ^2 (μB)	Extrapolated Height $\tilde{H}$ (cm)	Probable Error in $\tilde{H}$ (cm)
17		101.60	1378	2.91	126.42	0.192
15		96.52	1375	4.94	126.51	0.401
15		91.44	1377	5.85	126.30	0.717
13		86.36	1379	9.41	127.10	1.490
13		81.28	1379	8.67	127.10	1.372
17	20.32		1378	2.91	126.42	0.192
15	25.40		1375	4.94	126.51	0.401
15	30.48		1383	3.66	126.70	0.369
13	35.56		1382	6.58	126.99	0.755
13	40.64		1389	6.19	127.45	0.752
11	45.72		1387	6.93	127.89	0.906

1 μB = 10^{-6} cm^{-2}

Table 3.2. The axial buckling vs. the first and end points calculated with the moments method for the Run I0 measured in a 4-foot tank.

RUN I0: 0.947% enriched U fuel, 5-inch triangular spacing, 0.75-inch rod diameter.

Number of Data Points	First Point (cm)	End Point (cm)	Axial Buckling γ^2 (μB)	Probable Error in γ^2 (μB)	Extrapolated Height $\tilde{H}$ (cm)	Probable Error in $\tilde{H}$ (cm)
17		101.50	286	0.76	125.66	0.052
15		96.42	291	1.13	126.35	0.124
15		91.34	298	0.90	127.04	0.137
13		86.26	292	1.72	126.63	0.257
13		81.18	298	3.72	127.69	0.574
17	20.22		286	0.76	125.66	0.052
15	25.30		291	1.13	126.35	0.124
15	30.38		285	0.67	125.85	0.073
13	35.46		275	4.12	125.24	0.229
13	40.54		276	0.40	125.22	0.023
11	45.62		294	0.74	126.07	0.047

1 μB = 10^{-6} cm^{-2}

case of the full-size exponential assemblies. It is evident from the results that we can use nearly all the experimental data for the buckling analysis and still get consistent results. Past experience with the AXFIT code indicated that, to get a consistent value of the axial buckling, the first data point could never be within about 40 cm from the source and the last data point had to be about 20 cm or more from the boundary (H9, P1). Figure 3.10 is a schematic diagram of the asymptotic regions permitted by the two different methods.

The increased extent of the asymptotic region made available by the moments method is an indication of the superiority of this method over the curve-fitting method for the analysis of the axial buckling in the full-size exponential lattices. It will be shown in Chapter V that the moments method offers real advantages in the analysis of experiments in miniature lattices.

3.3.3 Application of the Moments Method to Slightly Enriched U-D_2O Lattices

Seven slightly enriched U-D_2O lattices investigated at the M.I.T. Lattice Project have been analyzed with the aid of the moments method (with the code ABMOMENT). A typical good experimental run for each lattice (a run which yields the most precise value of the axial buckling with the conventional curve-fitting method and the AXFIT code developed by Palmedo (P1)) was chosen for the axial buckling analysis to test the reliability of the moments method. The results for the axial buckling and extrapolated height are given in Table 3.3 together with the corresponding values obtained by the AXFIT code. The agreement is excellent in all cases. The values given for the moments method are

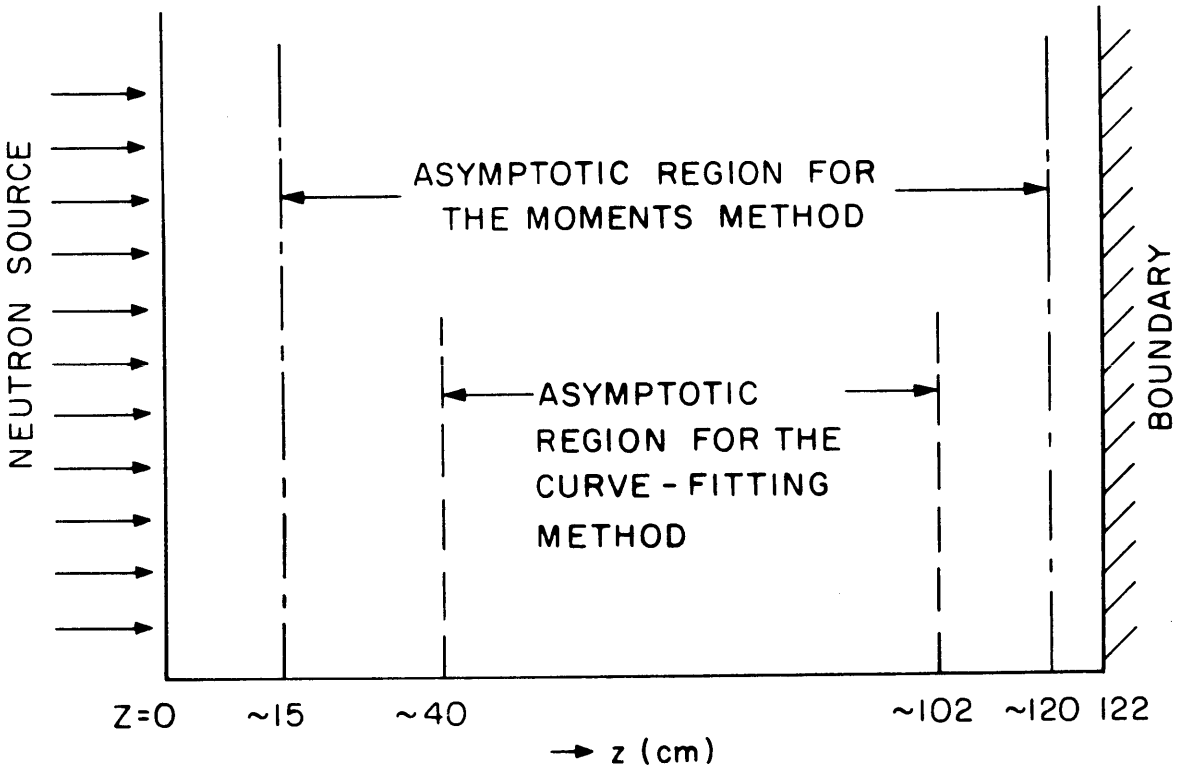

FIG. 3.10 ASYMPTOTIC REGION ALLOWED BY THE MOMENTS METHOD AND THE CURVE-FITTING METHOD.

Table 3.3. Values of the axial buckling and extrapolated height analyzed by the moments method for some U-D_2O lattices at the M.I.T. Lattice Project; in comparison with results obtained with the conventional curve-fitting method.

Run Number	Enrichment (%)	Lattice Spacing (Triangular) (inches)	Fuel Rod Diameter (inch)	AXIAL BUCKLING (μB)			EXTRAPOLATED HEIGHT (cm)		
				Moments Method		Curve-Fitting	Moments Method		Curve-Fitting
				γ^2 (μB)	σ_{γ^2} (μB)	γ^2 (μB)	$\tilde{H}$ (cm)	$\sigma_{\tilde{H}}$ (cm)	$\tilde{H}$ (cm)
81	1.150	1.25	0.250	972	3.93	987	128.985	0.707	128.0
D2	1.150	1.75	0.250	1006	2.78	1012	131.334	0.408	131.0
92	1.150	2.50	0.250	1391	6.50	1390	125.643	1.824	127.9
D8	0.947	2.50	0.750	1389	3.64	1389	127.260	0.760	129.5
R4	0.947	3.00	0.387	1383	3.66	1387	126.704	0.368	127.3
M3	0.947	3.50	0.750	48.7	5.85	48	125.002	0.302	125.0
I0	0.947	5.00	0.750	277	1.61	275	125.286	0.0825	125.5

σ_{γ^2} = Minimum probable error in axial buckling.

$\sigma_{\tilde{H}}$ = Minimum probable error in extrapolated height.

those that correspond to the minimum probable errors in the axial buckling and extrapolated height. The probable errors are also included for the moments method. They were computed with Eqs. (3.49) and (3.71), and are not to be confused with the usual standard deviations. The excellent agreement confirms the reliability of the moments method and also indicates that the AXFIT code based on the curve-fitting method indeed yields very reliable results when a common intersection among the three γ^2 vs. $\tilde{H}$ curves occurs as in Figure 1.1.

3.3.4 The Application to the Slightly Enriched UO_2-D_2O Lattices

Three slightly enriched UO_2-D_2O lattices recently investigated at the M.I.T. Lattice Project have also been analyzed by means of the moments method with the ABMOMENT code to test its versatility. Table 3.4 lists the results obtained from some good experimental runs. Again the agreement between the results of the two methods is very good, further indicating that both methods are reliable when the experimental data are well representable by the asymptotic flux (a definition of a good experimental run). However, if the total neutron flux is contaminated by the source neutron contributions and/or various flux transients, the curve-fitting method might run into trouble like that illustrated by Figures 1.2 and 1.3. In the latter cases, the moments method may be expected to yield more consistent results for the reasons discussed in section 3.2.2. Indeed, we have found that, in some cases, the moments method still could yield a consistent value of the axial buckling and of the extrapolated height when the curve-fitting method failed.

Table 3.4. Values of the axial buckling and extrapolated height analyzed by the moments method for some UO_2-D_2O lattices at the M.I.T. Lattice Project; in comparison with results obtained with the conventional curve-fitting method.

Run Number	Enrichment (%)	Lattice Spacing (Triangular) (inches)	Fuel Rod Diameter (inch)	AXIAL BUCKLING (μB)			EXTRAPOLATED HEIGHT (cm)		
				Moments Method		Curve-Fitting	Moments Method		Curve-Fitting
				γ^2 (μB)	σ_{γ^2} (μB)	γ^2 (μB)	$\tilde{H}$ (cm)	$\sigma_{\tilde{H}}$ (cm)	$\tilde{H}$ (cm)
42 (Bare)	1.099	3.50 △	0.431	1623	2.78	1632	135.268	0.680	136.9
37 (Cd-covered)	1.099	3.50 △	0.431	1613	1.26	1623	133.671	0.272	134.0
75 (Bare)	1.990	3.50 △	0.431	918	4.586	920	131.535	0.334	131.7
83 (Cd-covered)	1.990	3.50 △	0.431	926	4.749	947	134.212	0.299	134.7
30 (Bare)	1.099	3.25 ▨	0.431	1587	4.623	1595	136.696	0.497	136.0
23 (Cd-covered)	1.099	3.25 ▨	0.431	1647	5.433	1640	136.203	0.458	135.8

σ_{γ^2} = Minimum probable error in axial buckling.

$\sigma_{\tilde{H}}$ = Minimum probable error in extrapolated height.

3.3.5 The Study of the Consistency of the Data Analysis

It has been pointed out in Chapter I that the consistency of the conventional curve-fitting method would be relatively poor because of the way it fixes the "best values" of the axial buckling and extrapolated height. To find out whether this is the case, both the ABMOMENT code and the AXFIT code have been applied to a large number of experimental runs in three different U-D_2O lattices as well as to three UO_2-D_2O lattices. The consistency of each method is measured in terms of the standard deviations defined as (E1):

$$\epsilon_{\gamma^2} = \sqrt{\frac{1}{N(N-1)} \sum_{i=1}^{N} \left(\gamma_i^2 - \overline{\gamma^2}\right)^2} \tag{3.72}$$

for the axial buckling, and

$$\epsilon_{\widetilde{H}} = \sqrt{\frac{1}{N(N-1)} \sum_{i=1}^{N} \left(\widetilde{H}_i - \overline{\widetilde{H}}\right)^2} \tag{3.73}$$

for the extrapolated height, where

$$\overline{\gamma^2} \equiv \frac{1}{N} \sum_{i=1}^{N} \gamma_i^2 , \tag{3.74}$$

$$\overline{\widetilde{H}} \equiv \frac{1}{N} \sum_{i=1}^{N} \widetilde{H}_i , \tag{3.75}$$

and N is the number of experimental runs.

The results are given in Tables 3.5 through 3.10. The standard deviations in the axial buckling and extrapolated height are smaller by approximately a factor of 2 for the moments method than for the curve-fitting method. The moments method should, therefore, make it

Table 3.5. Comparison of the consistency of the moments and conventional curve-fitting methods.

Enrichment: 0.947%, Triangular Lattice Spacing: 3.0 inches, Uranium Rod Diameter: 0.387 inch.

Type of Run	Run Number	MOMENTS METHOD		CURVE-FITTING METHOD	
		Axial Buckling	Extrapolated Height	Axial Buckling	Extrapolated Height
		γ^2 (μB)	$\tilde{H}$ (cm)	γ^2 (μB)	$\tilde{H}$ (cm)
Axial, with bare foils	P9	1370	131.049	1382	135.30
	Q1	1380	128.263	1332	131.60
	Q5	1354	127.623	1348	126.60
	R4	1360	125.978	1387	127.30
	Average	1366 ± 5.7*	128.228 ± 1.1*	1362 ± 13	130.20 ± 2.03
Axial with Cd-covered foils	Q2	1389	127.241	1386	131.10
	Q6	1391	125.208	1384	130.40
	Q8	1387	126.594	1394	127.70
	Average	1389 ± 1.1	126.348 ± 0.6	1388 ± 3.1	129.40 ± 0.75

* The quantities are the standard deviations in γ^2 and $\tilde{H}$, respectively, defined in Eqs. (3.72) and (3.73).

Table 3.6. Comparison of the consistency of the moments and conventional curve-fitting methods for obtaining the axial buckling and the extrapolated height for the U-D_2O lattice.

Enrichment: 0.947%, Triangular Lattice Spacing: 3.5 inches, Uranium Rod Diameter: 0.75 inch.

Type of Run	Run Number	MOMENTS METHOD		CURVE-FITTING METHOD	
		Axial Buckling	Extrapolated Height	Axial Buckling	Extrapolated Height
		γ^2 (μB)	$\tilde{H}$ (cm)	γ^2 (μB)	$\tilde{H}$ (cm)
Axial, with Cd-covered foils	L9	44.19	124.295	40	124.5
	M1	33.92	123.919	65	126.3
	M3	39.43	124.091	48	125.0
	M5	26.71	124.044	32	125.0
	Average	36.06 ± 3.76*	124.087 ± 0.078*	46 ± 7.05	125.2 ± 0.385
Axial with bare foils	M0	20.48	124.956	5	124.4
	M2	20.63	124.942	35	126.6
	M4	17.96	125.007	45	126.5
	Average	19.69 ± 0.87	124.968 ± 0.020	28 ± 12.0	125.833 ± 0.51

* Standard deviations in γ^2 and $\tilde{H}$, respectively.

Table 3.7. Comparison of the consistency of the moments and conventional curve-fitting methods for obtaining the axial buckling and the extrapolated height for the U-D_2O lattice.

Enrichment: 0.947%, Triangular Lattice Spacing: 5.0 inches, Uranium Rod Diameter: 0.75 inch.

Type of Run	Run Number	MOMENTS METHOD		CURVE-FITTING METHOD	
		Axial Buckling	Extrapolated Height	Axial Buckling	Extrapolated Height
		γ^2 (μB)	$\tilde{H}$ (cm)	γ^2 (μB)	$\tilde{H}$ (cm)
Axial, with bare foils	H6	245.8	123.667	255	124.5
	H9	255.2	124.096	261	124.0
	I 0	282.4	125.267	275	125.5
	J9	252.5	122.899	260	122.2
	K1	258.9	124.343	298	125.4
	K4	281.6	123.761	250	123.6
	K6	279.3	124.406	300	126.2
	K7	284.5	125.349	285	124.2
	Average	267.5 ± 5.6*	124.223 ± 0.290*	273.0 ± 6.90	124.45 ± 0.433
Axial, with Cd-covered foils	H8	268.5	123.679	288	125.8
	J1	299.8	121.113	305	120.2
	J3	285.2	122.707	310	121.9
	J7	271.1	123.687	268	122.2
	K3	257.0	124.604	247	123.6
	K5	268.3	124.503	273	124.8
	Average	275 ± 6.2	123.382 ± 0.535	282.0 ± 9.75	123.08 ± 0.840

* Standard deviations in γ^2 and $\tilde{H}$, respectively.

Table 3.8. Comparison of the consistency of the moments and conventional curve-fitting methods for obtaining the axial buckling and the extrapolated height for the UO_2-D_2O lattice.

Enrichment: 1.99%, Triangular Lattice Spacing: 3.50 inches, Uranium Rod Diameter: 0.431 inch.

Type of Run	Run Number	MOMENTS METHOD		CURVE-FITTING METHOD	
		Axial Buckling	Extrapolated Height	Axial Buckling	Extrapolated Height
		γ^2 (μB)	$\tilde{H}$ (cm)	γ^2 (μB)	$\tilde{H}$ (cm)
Axial, with bare foils	75	918.3	131.535	920	131.7
	73	914.2	127.524	908	127.6
	71	918.1	132.971	930	133.7
	67	911.8	133.790	906	132.6
	62	915.9	132.342	925	133.5
	Average	915.7 ± 1.21*	131.632 ± 1.092*	917.8 ± 6.25	131.82 ± 1.120
Axial, with Cd-covered foils	83	954.1	136.287	947	134.7
	81	928.5	130.437	864	128.2
	79	950.0	132.690	906	128.2
	64	954.3	134.215	930	132.8
	Average	946.7 ± 6.17	133.407 ± 1.234	911.8 ± 18.0	130.98 ± 1.650

* Standard deviations in γ^2 and $\tilde{H}$, respectively.

Table 3.9. Comparison of the consistency of the moments and conventional curve-fitting methods for obtaining the axial buckling and the extrapolated height for the UO_2-D_2O lattice.

Enrichment: 1.099%, Square Lattice Spacing: 3.25 inches, Rod Diameter: 0.431 inch.

Type of Run	Run Number	MOMENTS METHOD		CURVE-FITTING METHOD	
		Axial Buckling	Extrapolated Height	Axial Buckling	Extrapolated Height
		γ^2 (μB)	$\tilde{H}$ (cm)	γ^2 (μB)	$\tilde{H}$ (cm)
Axial, with bare foils	35	1603	130.316	1623	139.3
	30	1587	135.398	1595	136.0
	17	1590	133.114	1602	134.5
	15	1587	132.650	1576	132.5
	13	1608	135.708	1628	137.5
	Average	1595 ± 4.43*	133.437 ± 0.985*	1605 ± 9.49	135.96 ± 1.177
Axial, with Cd-covered foils	32	1613	139.185	1655	143.0
	27	1622	135.524	1640	138.5
	23	1647	136.203	1640	135.8
	14	1625	138.987	1610	130.1
	Average	1627 ± 7.28	137.475 ± 0.941	1636 ± 9.48	136.85 ± 2.710

* Standard deviations in γ^2 and $\tilde{H}$, respectively.

Table 3.10. Comparison of the consistency of the moments and conventional curve-fitting methods for obtaining the axial buckling and the extrapolated height for the UO_2-D_2O lattice.

Enrichment: 1.099%, Triangular Lattice Spacing: 3.50 inches, Fuel Rod Diameter: 0.431 inch.

Type of Run	Run Number	MOMENTS METHOD		CURVE-FITTING METHOD	
		Axial Buckling	Extrapolated Height	Axial Buckling	Extrapolated Height
		γ^2 (μB)	$\tilde{H}$ (cm)	γ^2 (μB)	$\tilde{H}$ (cm)
Axial, with bare foils	58	1627	136.911	1633	141.9
	54	1617	139.667	1633	142.0
	49	1630	136.357	1638	138.5
	44	1624	135.387	1639	138.0
	42	1623	135.268	1632	136.9
	39	1633	136.782	1619	134.5
	Average	1625 ± 2.32*	136.729 ± 0.652*	1632 ± 2.91	138.633 ± 1.192
Axial, with Cd-covered foils	56	1630	139.892	1642	136.4
	41	1603	133.328	1590	132.9
	48	1630	131.809	1575	130.3
	47	1622	139.672	1629	142.4
	37	1613	133.671	1623	134.0
	Average	1620 ± 5.16	135.674 ± 1.705	1612 ± 12.52	135.20 ± 2.05

* Standard deviations in γ^2 and $\tilde{H}$, respectively.

possible to obtain values of the axial buckling and extrapolated height from a smaller number of measurements and with greater confidence than is possible with the conventional curve-fitting method.

3.4 DISCUSSION AND CONCLUSIONS

The study of the moments method described in this chapter for a variety of reactor lattices has shown that it provides a superior data reduction scheme for the analysis of the axial buckling and extrapolated height. Although the moments method has been tested only for heavy water lattices, it should be applicable equally well to light water lattices as well as to lattices moderated by graphite or beryllium because the moments method by itself does not impose any limitation on the type of moderator. It is expected that the moments method should be even better for the analysis of measurements of the diffusion length or relaxation length in pure moderator. We may also expect that such experiments can be made in small assemblies with the moments method available. This may turn out to be an appreciable advantage when it is not possible to use a large system.

The only serious drawback of the moments method, if any, arises when the number of experimental data available is relatively small, say less than 5, because the truncation errors incurred in the flux moments become predominant; but in such a case the least-squares curve-fitting method is also less reliable. For the axial buckling, this drawback does not present a serious problem because it is usually easy to have more than 10 experimental data points even in the miniature lattices (16 axial flux data have actually been obtained). In

the case of the radial buckling, however, the problem could become serious, particularly when the lattice spacing is large, because only a relatively small number of data points, say 5 or 7, may be available. This problem will be discussed in detail in the next chapter.

We close this chapter by summarizing some advantages of the moments method:

(a) The moments method for the analysis of the axial buckling and extrapolated height provides a way of reducing the source and boundary effects which become so severe in a small assembly such as a miniature lattice as to reduce seriously the value of the conventional curve-fitting method.

(b) The moments method avoids the necessity of assuming a value of the extrapolated height to begin the calculation of the axial buckling. The value of the extrapolated height computed by the curve-fitting method is less reliable and, in fact, quite indefinite in some cases. In contrast, the moments method does not require a value of the extrapolated height to calculate the axial buckling but is, in fact, able to obtain the extrapolated height once the axial buckling has been computed.

(c) The moments method yields a smaller standard deviation and is, therefore, more consistent in the interpretation of buckling measurements than the least-squares curve-fitting method primarily because of the reasons stated in (a) and (b).

(d) The moments method provides more information about the physics of neutron behavior inside the assembly than the curve-fitting technique which is primarily only a mathematical tool

(as discussed, for example, in section 3.2.2).

(e) The moments method makes possible the determination of the boundaries of an asymptotic region in the axial direction through the choice of the lower and upper limits in the definition of the axial flux moments.

(f) The moments method makes available a greater stretch of the asymptotic region for buckling measurements. This advantage will prove to be important in the case of small assemblies.

Chapter IV

THE ANALYSIS OF THE RADIAL BUCKLING AND EXTRAPOLATED RADIUS BY THE MOMENTS METHOD

4.1 INTRODUCTION

The moments method has been shown to be superior to the conventional curve-fitting method in the analysis of the axial buckling and extrapolated height. It remains uncertain whether this is also true in the case of the radial buckling. In this chapter we shall develop a moments method for the analysis of the radial buckling. The moments method will be used in two different ways: as a direct method and as an iterative method.

In general, the radial buckling can be inferred from experimental activation data by means of the least-squares curve-fitting method with reasonable consistency owing to the fact that a reasonably good estimate of the radial buckling is available from the size of the assembly through the relation (K6, M1)

$$\alpha^2 = \left(\frac{2.4048}{\tilde{R}}\right)^2 , \tag{4.1}$$

where $\tilde{R} = R + 0.7104\,\lambda_{tr}$ is the extrapolated (or effective) radius, and λ_{tr} is the transport mean free path. Problems arise, however, in the determination of the linear extrapolation distance from the experimental radial activation distribution: the experimental results extracted by the curve-fitting method are always larger than the theoretical result $0.7104\,\lambda_{tr}$ given by asymptotic transport theory

(H8, H9, H4), as will be seen later in this chapter. There is, therefore, a difficulty in the interpretation of exponential experiments (H7), as well as in the determination of the geometrical buckling in the pulsed neutron source experiments (G1). The problem is especially serious in small assemblies (S1) and is a general concern in reactor physics (K2, K7, K8). The basic difficulty underlying this problem is probably the presence of energy transients due to spectral inequilibrium and of spatial transients due to transport effects in the neighborhood of the boundaries. These effects are relatively small in large systems but can be important in small assemblies. For example, Windsor (W4) has demonstrated the significant effect of energy transients on the determination of the radial buckling when the buckling value is greater than 50 m^{-2} (i.e., 5000 μB) in a U-H_2O lattice.

In this chapter we shall, therefore, be concerned with the development of a moments method for the analysis of the radial buckling and extrapolated radius (hence the linear extrapolation distance) with two objectives in mind:

(a) To see if the consistency of the moments method is again better than that of the least-squares curve-fitting method, as was the case for the axial buckling.

(b) To find out if the method of data analysis is responsible, in part, for the sizable discrepancy existing between the experimental and theoretical values of the linear extrapolation distance.

The moments method will again be tested with data from the lattices used in the previous chapter; the method will be applied to the miniature lattices in Chapter V.

4.2 DIRECT MOMENTS METHOD

4.2.1 Theory

To parallel the approach in Chapter III, we define the radial flux moments as

$$\psi_n \equiv \int_0^R r^n \phi(r)\, dr \,, \tag{4.2}$$

where $\phi(r)$ is the radial flux distribution, and R is some appropriately chosen radial distance near the boundary which determines the boundary of the radial asymptotic region. In the actual calculation, R is determined by the position of the last data point of the radial activation distribution selected for the analysis of the radial buckling.

The definition (4.2) can be justified by the following argument. We start with the assumption, common to all techniques of analyzing buckling data, that the radial flux, $\phi(r)$, satisfies the diffusion equation

$$-D\nabla^2\phi(r) + (\Sigma_a - \nu\Sigma_f)\phi(r) = 0 \,, \tag{4.3}$$

where the nuclear constants have their usual meanings. Physically speaking, the radial buckling is a measure of the radial leakage of neutrons, which becomes increasingly important as the distance from the radial boundary decreases. This implies that the radial leakage of neutrons per unit volume and per unit time, $-D\nabla^2\phi(r)$, should be weighted more heavily as the radial distance from the center increases. The choice of the factor r^n as a weighting factor does just this.

Assuming azimuthal symmetry, we consider the element of volume at r, $2\pi r\, dr\, dz$, as shown in Figure 4.1. For convenience, let us set $|dz| = 1$ so that the element of volume becomes $2\pi r\, dr$. The

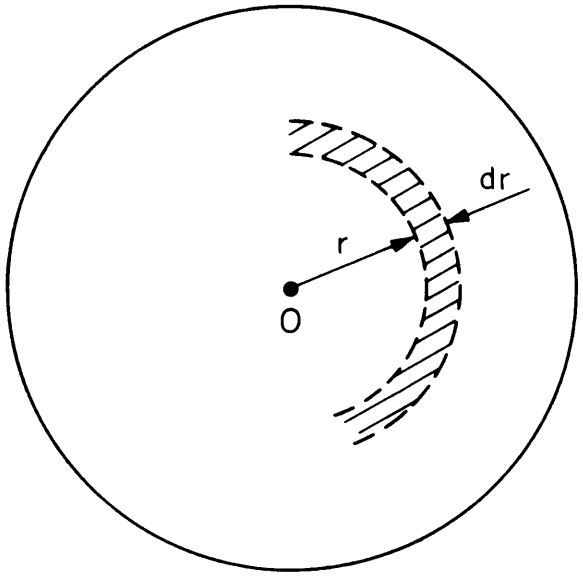

FIG. 4.1 THE ELEMENT OF AREA IN CYLINDRICAL COORDINATES.

number of neutrons that leak out of the assembly at the position r in the radial direction per unit time is given by $-D\nabla^2\phi(r) \cdot 2\pi r\, dr$; it is to be weighted by r^n to account for the relative importance of different locations. Hence, we focus on the quantity $r^n[-D\nabla^2\phi(r)]\, 2\pi r\, dr$. To include all the possible neutron leakages at all radial positions, we integrate the quantity over radial distance,

$$\int_0^R r^n[-D\nabla^2\phi(r)]\, 2\pi r\, dr\ . \tag{4.4}$$

But Eq. (4.3) gives $-D\nabla^2\phi(r) = (\nu\Sigma_f - \Sigma_a)$, and Eq. (4.4) becomes

$$2\pi(\nu\Sigma_f - \Sigma_a) \int_0^R r^{n+1}\phi(r)\, dr\ . \tag{4.5}$$

Since we shall use the <u>ratios</u> of radial flux moments to calculate the radial buckling, as will be seen later, the common factor $2\pi(\nu\Sigma_f - \Sigma_a)$ will cancel so that we can drop it without loss of generality. Finally, it is immaterial whether r^{n+1} or r^n is used as the weighting factor because we shall treat the moment index n as a variable parameter. We thus arrive at the definition of radial flux moments given by Eq. (4.2).

To derive the relationship between the radial flux moments and the radial buckling, α^2, we assume that

$$\phi(r) = A_r J_o(\alpha r)\ ; \tag{4.6}$$

this shape must describe the asymptotic radial flux distribution in order to justify radial buckling measurements. Again, the normalization constant A_r will not enter into the calculation of α^2, so we need consider only the normalized radial flux moments,

$$\psi_n = \int_0^R r^n J_o(\alpha r)\, dr , \qquad n = 1, 3, 5, \ldots, \text{odd} . \tag{4.7}$$

Only moments with odd indices are defined because the even radial flux moments cannot be evaluated analytically in closed form owing to the integration properties of Bessel functions (W3).

The flux value at the center of the assembly does not play a role in the calculation of ψ_n as its weight is zero. This proves to be helpful because central flux data are not available owing to the presence of a fuel rod. In addition, the true center of the system is usually not sharply defined. This causes a difficulty in the conventional curve-fitting method which is avoided in the moments method.

To evaluate Eq. (4.7), we use the identities (W3, A2):

$$\int x J_o(x)\, dx = x J_1(x) , \tag{4.8}$$

$$\int x^{n+1} J_o(x)\, dx = -n^2 \int x^{n-1} J_o(x)\, dx + x^{n+1} J_1(x) + n x^n J_o(x) . \tag{4.9}$$

The essence of the direct moments method is to eliminate the functional forms $J_o(\alpha x)$ and $J_1(\alpha r)$ by means of three equations corresponding to the (n-2)th, nth, and (n+2)th radial flux moments:

$$\psi_{n-2} = -\frac{(n-3)^2}{\alpha^2}\psi_{n-4} + \frac{R^{n-2}}{\alpha} J_1(\alpha R) + \frac{(n-3)R^{n-3}}{\alpha^2} J_o(\alpha R) , \tag{4.10}$$

$$\psi_n = -\frac{(n-1)^2}{\alpha^2}\psi_{n-2} + \frac{R^n}{\alpha} J_1(\alpha R) + \frac{(n-1)R^{n-1}}{\alpha^2} J_o(\alpha R) , \tag{4.11}$$

$$\psi_{n+2} = -\frac{(n+1)^2}{\alpha^2}\psi_n + \frac{R^{n+2}}{\alpha} J_1(\alpha R) + \frac{(n+1)R^{n+1}}{\alpha^2} J_o(\alpha R) , \tag{4.12}$$

$$n = 1, 3, 5, \ldots, \infty .$$

To eliminate $J_o(\alpha R)$ and $J_1(\alpha R)$, set the determinant

$$\begin{vmatrix} \frac{R^{n-2}}{\alpha} & \frac{(n-3)R^{n-3}}{\alpha^2}\left[\psi_{n-2} + \frac{(n-3)^2}{\alpha^2}\psi_{n-4}\right] \\ \frac{R^{n}}{\alpha} & \frac{(n-1)R^{n-1}}{\alpha^2}\left[\psi_{n} + \frac{(n-1)^2}{\alpha^2}\psi_{n-2}\right] \\ \frac{R^{n+2}}{\alpha} & \frac{(n+1)R^{n+1}}{\alpha^2}\left[\psi_{n+2} + \frac{(n+1)^2}{\alpha^2}\psi_{n}\right] \end{vmatrix} = 0 , \tag{4.13}$$

which yields the result

$$\alpha^2(n) = \frac{(n+1)^2\psi_n - 2R^2(n-1)^2\psi_{n-2} + R^4(n-3)^2\psi_{n-4}}{-\psi_{n+2} + 2R^2\psi_n - R^4\psi_{n-2}} ,$$

$$\text{for } n = 5, 7, 9, \ldots, \infty . \tag{4.14}$$

To infer the radial buckling α^2 from the foil activation data, we define the experimental radial flux moments as

$$\psi_n^{exp} \equiv \int_0^R r^n A(r)\, dr , \tag{4.15}$$

where A(r) is the measured foil activation distribution. The experimental radial buckling is then obtained from Eq. (4.14) by replacing the theoretical radial flux moments by the corresponding experimental radial flux moments. Once the radial buckling has been obtained, the extrapolated radius, $\tilde{R}$, can be readily calculated from the relation (K6, M1),

$$\tilde{R} = \frac{2.4048}{\sqrt{\alpha^2}} . \tag{4.16}$$

The linear extrapolation distance, d, is then given by

$$d = \tilde{R} - R \ , \tag{4.17}$$

where R is the physical radius of the system in question.

We could relax the definition of the radial flux moments as given by Eq. (4.7) at the expense of analytical elegance. From the standpoint of numerical calculations, there is no reason to restrict the moment index to odd integers. Thus, if we were to start with the definition

$$\psi_n \equiv \int_0^R r^n \phi(r)\, dr ; \qquad n = 0, 1, 2, 3, \ldots, \infty \ , \tag{4.18}$$

we would arrive at the following result for the radial buckling, for $\phi(r) = AJ_o(\alpha r)$:

$$\alpha^2(n) = \left\{ \frac{n^2\psi_{n-1} - 2R(n-1)^2\psi_{n-2} + R^2(n-2)^2\psi_{n-3}}{-\psi_{n+1} + 2R\psi_n - R^2\psi_{n-1}} \right\} , \tag{4.19}$$

$$\text{for } n = 3, 4, 5, \ldots, \infty .$$

The lowest possible moment index is actually 2. In this case, we would have

$$\alpha^2(z) = \frac{4\psi_1 - 2R\psi_o}{-\psi_3 + 2R\psi_2 - R^2\psi_1} . \tag{4.20}$$

Equation (4.20) should be preferable to Eq. (4.19) when only a few data points are available, for then the truncation error incurred in the numerical integration will predominate. This procedure was not used in the present work, but it is a possible one.

The choice of the moment index is again determined by the minimum probable error in radial buckling as found by means of the error analysis; this problem will be considered in the next section.

4.2.2 Error Analysis for the Radial Buckling and Extrapolated Radius

We shall use the same procedure that was used for the axial buckling and extrapolated height in Chapter III. Recall Eq. (4.14) and write

$$\alpha^2 = \alpha^2(\psi_{n-4}, \psi_{n-2}, \psi_n, \psi_{n+2}) \cdot \tag{4.21}$$

Taking the differential, we obtain

$$\delta\alpha^2 = \sum_{j=1}^{4} \left(\frac{\partial \alpha^2(n)}{\partial \psi_{n+2j-6}} \right) \delta\psi_{n+2j-6} \cdot \tag{4.22}$$

Define the variance in α^2 as

$$\sigma^2_{\alpha^2}(n) = \sum_{j=1}^{4} B_{n+2j-6} (\delta\psi_{n+2j-6})^2 , \tag{4.23}$$

where

$$B_{n+2j-6} \equiv \left(\frac{\partial \alpha^2(n)}{\partial \psi_{n+2j-6}} \right)^2 , \qquad j = 1, 2, 3, 4 ; \tag{4.24}$$

σ_{α^2} is then the probable error in the radial buckling.

To compute the coefficients B_{n+2j-6}, we rewrite Eq. (4.14) as

$$\alpha^2(n) = \frac{F(n)}{G(n)} , \tag{4.25}$$

where

$$F(n) = (n+1)^2\psi_n - 2R^2(n-1)^2\psi_{n-2} + R^4(n-3)^2\psi_{n-4} , \tag{4.26}$$

$$G(n) = -\psi_{n+2} + 2R^2\psi_n - R^4\psi_{n-2} ; \tag{4.27}$$

here R is a constant fixed by the choice of the last data point. By differentiation, we obtain the results:

$$\frac{\partial \alpha^2(n)}{\partial \psi_{n-4}} = \frac{(n-3)^2 R^4}{G(n)} , \tag{4.28}$$

$$\frac{\partial \alpha^2(n)}{\partial \psi_{n-2}} = \frac{-2(n-1)^2 R^2 G(n) + R^4 F(n)}{[G(n)]^2} , \tag{4.29}$$

$$\frac{\partial \alpha^2(n)}{\partial \psi_{n}} = \frac{(n+1)^2 G(n) - 2R^2 F(n)}{[G(n)]^2} , \tag{4.30}$$

$$\frac{\partial \alpha^2(n)}{\partial \psi_{n+2}} = \frac{F(n)}{[G(n)]^2} . \tag{4.31}$$

We consider again that the deviations in the radial flux moments are primarily composed of the experimental error, $\delta\psi_j^{exp}$ and the truncation error, $\delta\psi_j^{tr}$. These errors are defined as

$$\delta\psi_j^{exp} = \left[\psi_j^{th} - \frac{\psi_j^{exp}}{A_r} \right] , \tag{4.32}$$

and

$$\delta\psi_j^{tr} = \left[\psi_j^{th} \right]_{\substack{\text{analytical} \\ \text{integration}}} - \left[\psi_j^{th} \right]_{\substack{\text{numerical} \\ \text{integration}}} , \tag{4.33}$$

respectively, where ψ_j^{th} are the theoretical radial flux moments, and A_r is the normalization constant to be determined. The variance in α^2 may be written then

$$\sigma^2_{\alpha^2}(n) = \sum_{j=1}^{4} B_{n+2j-6} \left\{ \left[\psi^{th}_{n+2j-6} - \frac{\psi^{exp}_{n+2j-6}}{A_r} \right]^2 + \left(\delta\psi^{tr}_{n+2j-6} \right)^2 \right\} . \tag{4.34}$$

The normalization constant A_r is determined by setting

$$\frac{d\sigma^2_{\alpha^2}(n)}{dA_r} = 0 \tag{4.35}$$

to minimize the probable error in the radial buckling, σ_{α^2}. Equation (4.35) leads to the expression for A_r:

$$A_r(n) = \frac{\sum_{j=1}^{4} B_{n+2j-6}\left(\psi^{exp}_{n+2j-6}\right)^2}{\sum_{j=1}^{4} B_{n+2j-6}\left(\psi^{th}_{n+2j-6}\right)\left(\psi^{exp}_{n+2j-6}\right)} . \tag{4.36}$$

Notice that theoretical radial flux moments must be used to compute the coefficients B_{n+2j-6}, $j = 1, 2, 3, 4$ to be consistent with the definitions of the experimental and truncation errors.

The probable error in the extrapolated radius depends completely on σ_{α^2}. Their relationship can be found by taking the differential of Eq. (4.16):

$$\delta\tilde{R} = -1.2024\,(\alpha^2)^{-3/2}\,\delta\alpha^2 . \tag{4.37}$$

Hence the variance in $\tilde{R}$ is given by

$$\sigma^2_{\tilde{R}}(n) = \frac{1.4458}{(\alpha^2)^3}\,\sigma^2_{\alpha^2}(n) , \tag{4.38}$$

and the probable error in the extrapolated radius is given by

$$\sigma_{\tilde{R}}(n) = \frac{1.2024}{(\alpha^2)^{3/2}}\,\sigma_{\alpha^2}(n) . \tag{4.39}$$

The same error estimate can also be made when the definition of Eq. (4.18) is used. The results are formally the same except for the expressions for the coefficients B_j in which the moment indices would be changed appropriately.

Computer experience has indicated that the truncation errors incurred in the higher flux moments could so predominate, because of

the relatively few data points available for the numerical integration, as to reduce seriously the efficacy of the direct moments method. This will be shown later in Tables 4.1 and 4.2. We can avoid this problem by taking advantage of the fact that the radial buckling is more or less fixed by the simple formula of Eq. (4.1). An effort will, therefore, be made to improve the accuracy in the radial buckling by trying to determine the necessary correction to the value given by Eq. (4.1) by means of an iterative moments method rather than by trying to determine the radial buckling itself.

4.3 THE ITERATIVE MOMENTS METHOD

The iterative moments method is an iterative scheme which repeatedly corrects the radial buckling given by Eq. (4.1) by means of the experimental radial flux moments until a consistent value is obtained for the radial buckling.

4.3.1 Theory

Consider the asymptotic radial flux distribution given by Eq. (4.6). Suppose α_o^2 is a good approximate value to the desired radial buckling α^2. We can expand the radial flux $\phi(r)$ in a Taylor series around the initial value α_o:

$$\phi(r,\alpha) \approx \phi(r,\alpha_o) + (\alpha-\alpha_o)\frac{d}{d\alpha}\phi(r,\alpha)\Big|_{\alpha=\alpha_o} + \ldots \tag{4.40}$$

$$\approx A_r\{J_o(\alpha_o r) - (\alpha-\alpha_o)rJ_1(\alpha_o r)\}. \tag{4.41}$$

The radial flux moments defined in Eq. (4.2) become

$$\psi_n \simeq A_r \int_0^R r^n [J_o(\alpha_o r) - (\alpha-\alpha_o) r J_1(\alpha_o r)]\, dr\,, \quad n = 1, 3, 5, \ldots, \text{odd}\,. \tag{4.42}$$

Again we restrict the moment index to odd integers because none of the even radial flux moments can be evaluated in closed form. We should like to eliminate the normalization constant A_r by using the ratio of any two independent radial flux moments. The choice of these two radial flux moments is again arbitrary and would be governed by the results of the error analysis. The moments that yield the minimum probable error in the radial buckling should be the final choice. Unfortunately, owing to the arrangement of the fuel rods, the number of points at which measurements of the radial activation can be made is determined by the spacing of the lattice under study. For lattices of relatively wide spacing, the number of data points available is about six, and a significant truncation error in the radial buckling will be expected if we try to use higher radial flux moments. We are, therefore, limited to the lower radial flux moments and shall use the first three moments ψ_1, ψ_3, and ψ_5. On using Eqs. (4.8) and (4.9) together with the formulas

$$\int J_1(x)\, dx = -J_o(x) \tag{4.43}$$

and

$$\int x^n J_1(x)\, dx = -x^n J_o(x) + n \int x^{n-1} J_o(x)\, dx\,, \tag{4.44}$$

we obtain the three lowest possible radial flux moments

$$\psi_1 = A_r \left[\frac{R}{\alpha_o} J_1(\alpha_o R) - \left(\frac{\alpha-\alpha_o}{\alpha_o} \right) F \right], \tag{4.45}$$

$$\psi_3 = A_r\left[G - \left(\frac{\alpha-\alpha_o}{\alpha_o}\right)H\right] , \tag{4.46}$$

$$\psi_5 = A_r\left[U - \left(\frac{\alpha-\alpha_o}{\alpha_o}\right)V\right] , \tag{4.47}$$

where

$$F = -R^2 J_o(\alpha_o R) + \frac{2R}{\alpha_o} J_1(\alpha_o R) , \tag{4.48}$$

$$G = \frac{2R^2}{\alpha_o^2} J_o(\alpha_o R) + \frac{R}{\alpha_o}\left(R^2 - \frac{4}{\alpha_o^2}\right) J_1(\alpha_o R) , \tag{4.49}$$

$$H = R^2\left(\frac{8}{\alpha_o^2} - R^2\right) J_o(\alpha_o R) + \frac{4R}{\alpha_o}\left(R^2 - \frac{4}{\alpha_o^2}\right) J_1(\alpha_o R) , \tag{4.50}$$

$$U = \frac{4R^2}{\alpha_o^2}\left(R^2 - \frac{8}{\alpha_o^2}\right) J_o(\alpha_o R) + \frac{R}{\alpha_o}\left(\frac{64}{\alpha_o^4} + R^4 - \frac{16R^2}{\alpha_o^2}\right) J_1(\alpha_o R) , \tag{4.51}$$

$$V = -R^2\left(R^4 + \frac{192}{\alpha_o^4} - \frac{24R^2}{\alpha_o^2}\right) + \frac{6R}{\alpha_o}\left(\frac{64}{\alpha_o^4} + R^4 - \frac{16R^2}{\alpha_o^2}\right) J_1(\alpha_o R) . \tag{4.52}$$

The essence of the iterative moments method is to determine the quantity $\left(\frac{\alpha-\alpha_o}{\alpha_o}\right)$ by means of experimental radial flux moments, and hence correct the radial buckling repeatedly until a convergent value is obtained. This can be achieved by taking the ratio of any two radial flux moments given by Eqs. (4.45), (4.46) and (4.47). There are three possible cases:

Case 1

$$\frac{\psi_3}{\psi_1} = \frac{G - \left(\frac{\alpha-\alpha_o}{\alpha_o}\right) H}{\frac{R}{\alpha_o} J_1(\alpha_o R) - \left(\frac{\alpha-\alpha_o}{\alpha_o}\right) F} , \tag{4.53}$$

whence
$$\left(\frac{\alpha-\alpha_o}{\alpha_o}\right)_1 = \frac{\left[G - \left(\frac{\psi_3}{\psi_1}\right)\frac{R}{\alpha_o} J_1(\alpha_o R)\right]}{\left[H - \left(\frac{\psi_3}{\psi_1}\right) F\right]} ; \tag{4.54}$$

Case 2
$$\frac{\psi_5}{\psi_3} = \frac{U - \left(\frac{\alpha-\alpha_o}{\alpha_o}\right) V}{G - \left(\frac{\alpha-\alpha_o}{\alpha_o}\right) H} , \tag{4.55}$$

whence
$$\left(\frac{\alpha-\alpha_o}{\alpha_o}\right)_2 = \frac{\left[U - \left(\frac{\psi_5}{\psi_3}\right) G\right]}{\left[V - \left(\frac{\psi_5}{\psi_3}\right) H\right]} ; \tag{4.56}$$

Case 3
$$\frac{\psi_5}{\psi_1} = \frac{U - \left(\frac{\alpha-\alpha_o}{\alpha_o}\right) V}{\frac{R}{\alpha_o} J_1(\alpha_o R) - \left(\frac{\alpha-\alpha_o}{\alpha_o}\right) F} , \tag{4.57}$$

whence
$$\left(\frac{\alpha-\alpha_o}{\alpha_o}\right)_3 = \frac{\left[U - \left(\frac{\psi_5}{\psi_1}\right)\frac{R}{\alpha_o} J_1(\alpha_o R)\right]}{\left[V - \left(\frac{\psi_5}{\psi_1}\right) F\right]} . \tag{4.58}$$

The new radial buckling, α^2, is then given by

$$\alpha^2(i) = \alpha_o^2\left[1 + \left(\frac{\alpha-\alpha_o}{\alpha_o}\right)_i\right]^2 , \qquad i = 1, 2, 3 . \tag{4.59}$$

Since the method depends on the use of only the first-order term of the Taylor series, it is necessary to repeat the calculation with the newly computed α_1^2 replacing the initial value α_o^2. The procedure is

repeated until the following convergence criterion is satisfied:

$$\left| \frac{\alpha_{j+1}^2(i) - \alpha_j^2(i)}{\alpha_j^2(i)} \right| < \epsilon, \qquad i = 1, 2, 3, \tag{4.60}$$

where ϵ is some arbitrarily chosen small number, say 10^{-4}.

In this treatment we have terminated the Taylor expansion at the first-order term for simplicity, but this is by no means a limitation; we can actually extend the treatment to higher-order terms at the cost of increased complexity. We would then obtain a higher-order polynomial equation for the quantity $\left(\frac{\alpha-\alpha_o}{\alpha_o}\right)$ which could be solved numerically without difficulty. In contrast, a procedure of this kind would be more difficult for the least-squares curve-fitting method in which it is necessary to determine the normalization constant and the parameter α simultaneously. However, the extension to higher-order terms of the Taylor expansion turns out to be unnecessary when $J_o(\alpha r)$ represents the actual radial flux distribution reasonably well; Eq. (4.1) then gives a very good approximate value for the radial buckling.

An error analysis is now needed for the iterative moments method to select the best of the three possible cases considered above.

4.3.2 Error Analysis

To compute the probable error in α^2, we differentiate Eq. (4.59):

$$\delta\alpha^2(i) = \left[1 + \left(\frac{\alpha-\alpha_o}{\alpha_o}\right)_i\right]^2 \delta\alpha_o^2 + 2\alpha_o^2 \left[1 + \left(\frac{\alpha-\alpha_o}{\alpha_o}\right)_i\right] \delta\left(\frac{\alpha-\alpha_o}{\alpha_o}\right)_i, \tag{4.61}$$

where the value of α_o^2 appearing in Eq. (4.61) is not the initial value we

have chosen to start the iteration, but is rather the value that precedes the final convergent value of α^2. We define the probable error in α^2 as the magnitude of $\delta\alpha^2(i)$:

$$\sigma_{\alpha^2} \equiv \left|\delta\alpha^2(i)\right| \approx 2\alpha_o^2 \left|1 + \left(\frac{\alpha-\alpha_o}{\alpha_o}\right)_i\right| \cdot \left|\delta\left(\frac{\alpha-\alpha_o}{\alpha_o}\right)_i\right| \tag{4.62}$$

since $\delta\alpha_o^2 \approx 0$ when the iteration converges under the criterion, Eq. (4.60); ϕ_{α^2} is composed primarily of the possible deviations in the ratios ψ_j/ψ_k $(j, k = 1, 3, 5)$. Now,

$$\left|\delta\left(\frac{\psi_j}{\psi_k}\right)\right| = \left|\frac{\delta\psi_j}{\psi_k} - \frac{\psi_j}{\psi_k^2}\delta\psi_k\right|$$

$$\leq \sqrt{\frac{1}{\psi_k^2}(\delta\psi_j)^2 + \frac{\psi_j^2}{\psi_k^4}(\delta\psi_k)^2}\ , \tag{4.63}$$

where

$$\delta\psi_{j,k} = \left[\psi_{j,k}^{th} - \frac{\psi_{j,k}^{exp}}{A_r}\right], \tag{4.64}$$

$\psi_{j,k}^{th}$ are the theoretical radial flux moments calculated analytically so that there is no truncation error involved, and $\psi_{j,k}^{exp}$ are the experimental radial flux moments calculated numerically. Thus, the deviations $\delta\psi_{j,k}$ in Eq. (4.64) consist of the truncation error incurred in the numerical integration as well as the departure of the experimental data from the theoretical asymptotic flux given by Eq. (4.6).

The normalization constant A_r is determined by minimizing the total probable error in α^2, i.e., by setting

$$\frac{d}{dA_r}\,\sigma^2_{\alpha^2} = 0\ , \tag{4.65}$$

which leads to the result

$$A_r = \frac{\left(\psi_j^{th}\right)^2\left(\psi_k^{exp}\right)^2 + \left(\psi_j^{exp}\right)^2\left(\psi_k^{th}\right)^2}{\left(\psi_j^{th}\right)^2\left[\psi_k^{th}\psi_k^{exp}\right] + \left(\psi_k^{th}\right)^2\left[\psi_j^{th}\psi_j^{exp}\right]}\ ,\quad j,k = 1,3,5\ . \tag{4.66}$$

The deviations $\delta\left(\frac{\alpha-\alpha_o}{\alpha_o}\right)_i$ can be obtained from Eqs. (4.54), (4.56), and (4.58) by differentiation:

$$\delta\left(\frac{\alpha-\alpha_o}{\alpha_o}\right)_1 = \left\{\frac{-\frac{R}{\alpha_o}J_1(\alpha_o R)}{\left[H - \left(\frac{\psi_3}{\psi_1}\right)F\right]} + \frac{F\left[G - \left(\frac{\psi_3}{\psi_1}\right)\frac{R}{\alpha_o}J_1(\alpha_o R)\right]}{\left[H - \left(\frac{\psi_3}{\psi_1}\right)F\right]^2}\right\}\delta\left(\frac{\psi_3}{\psi_1}\right), \tag{4.67}$$

$$\delta\left(\frac{\alpha-\alpha_o}{\alpha_o}\right)_2 = \left\{\frac{-G}{\left[V - \left(\frac{\psi_5}{\psi_3}\right)H\right]} + \frac{H\left[U - \left(\frac{\psi_5}{\psi_3}\right)G\right]}{\left[V - \left(\frac{\psi_5}{\psi_3}\right)H\right]^2}\right\}\delta\left(\frac{\psi_5}{\psi_3}\right), \tag{4.68}$$

$$\delta\left(\frac{\alpha-\alpha_o}{\alpha_o}\right)_3 = \left\{\frac{-\frac{R}{\alpha_o}J_1(\alpha_o R)}{\left[V - \left(\frac{\psi_5}{\psi_1}\right)F\right]} + \frac{F\left[U - \left(\frac{\psi_5}{\psi_1}\right)\frac{R}{\alpha_o}J_1(\alpha_o R)\right]}{\left[V - \left(\frac{\psi_5}{\psi_1}\right)F\right]^2}\right\}\delta\left(\frac{\psi_r}{\psi_1}\right). \tag{4.69}$$

4.4 THE OFF-CENTER EFFECT

In the calculation of the radial buckling, we are faced with a possible "off-center effect" because the arrangement of the fuel rods does not allow the determination of the activation at the actual center of the assembly, as indicated in Figure 4.2. The off-center effect

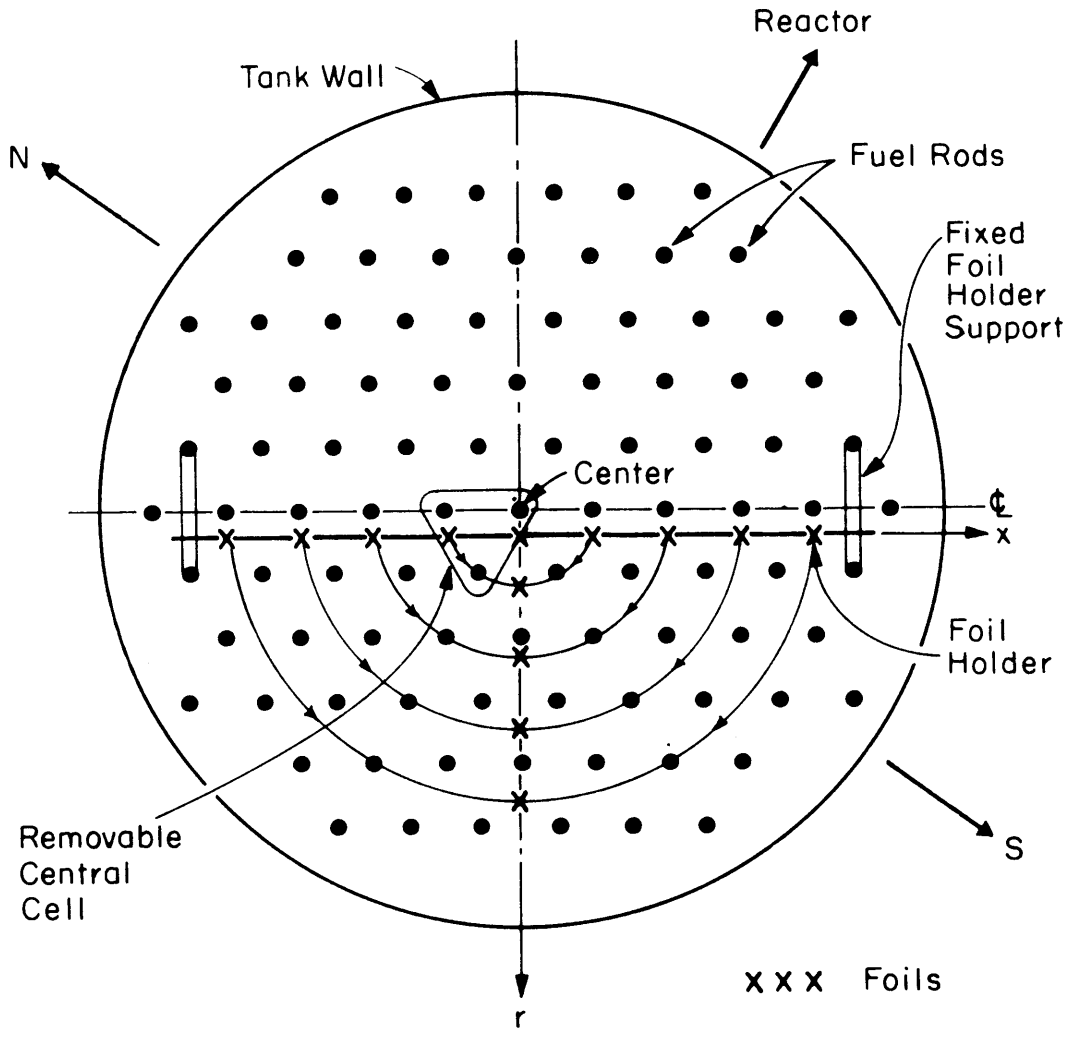

FIG. 4.2 CONFIGURATION OF 4 1/2 INCH SPACING LATTICE.

arises in the calculation of the experimental radial flux moments. To take this effect into account, we recall the assumption (Chapter II) that the radial flux distribution is azimuthally symmetric. We can then project the measured values of the activation on the x-axis on to the real radial axis r, as shown in Figure 4.2. To obtain the experimental radial flux moments along the radial axis r, we simply integrate the measured fluxes over r with unequal intervals, although the intervals are equally spaced on the x-axis. Simpson's rule may be used for the numerical integration, but the unequal-interval formula must be used; it is given in Appendix B. The off-center effect is generally small for large assemblies but may be significant in small assemblies.

Owing to the definition of the radial flux moments given by Eq. (4.2), we can use half of the measured radial activation data, as is evident from Figure 4.2. Throughout the present work, the arithmetic mean of the two activation data at the corresponding radial positions will be taken for the calculation of the radial flux moments. In most experiments, it turned out that foils at equal distances from the center of the assembly, but on opposite sides of the assembly, showed unequal activities (the differences being greater than those to be expected from counting statistics) owing primarily to the tilt of the foil holder (H9): one side of the foil holder is closer to the external neutron source than the other. An example is given in Figure 4.3. Harrington (H9) has shown that the desired radial activity in such a case is the arithmetic average of the two observed activities.

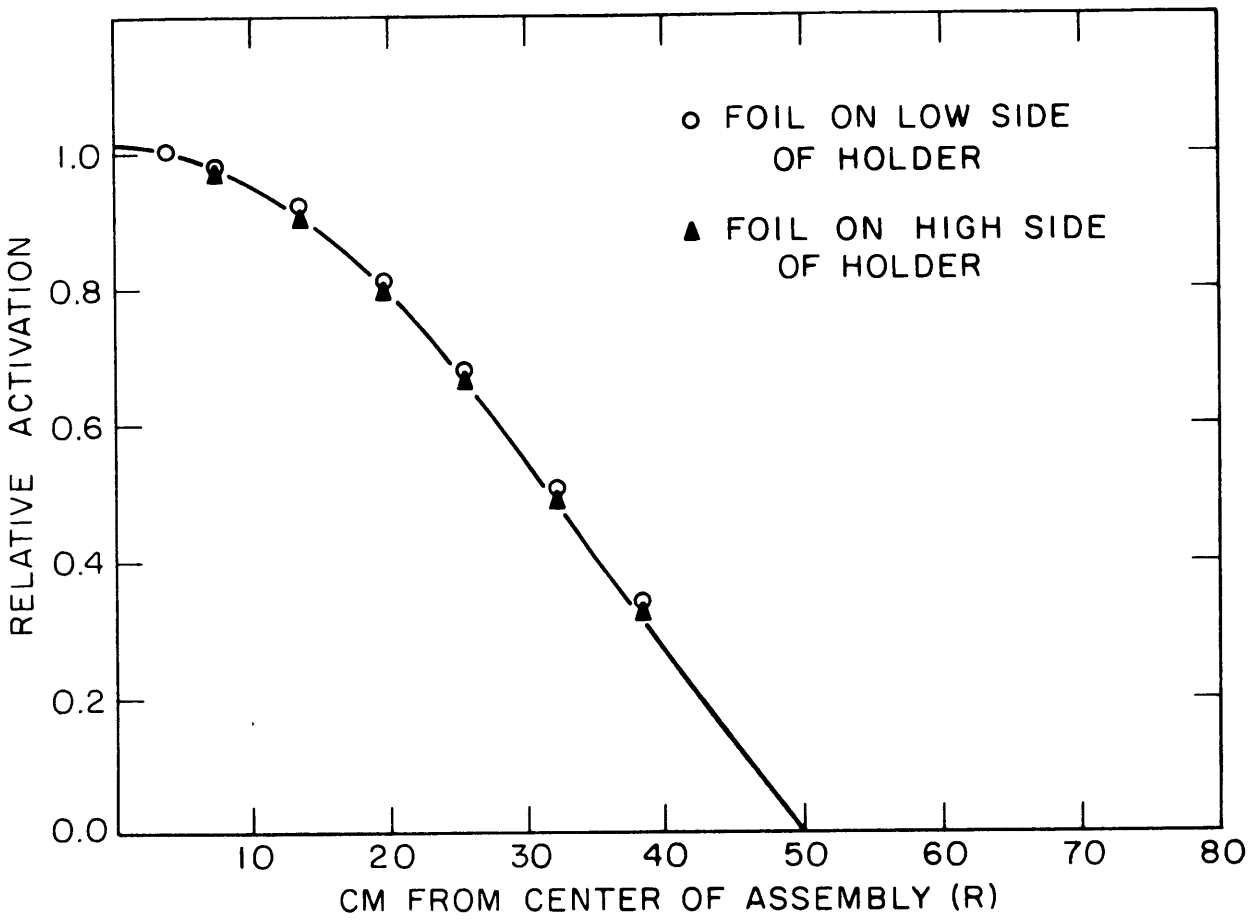

FIG. 4.3 RELATIVE ACTIVATION DISTRIBUTION AS A FUNCTION OF RADIAL POSITION (R), MEASURED IN ASSEMBLY 253A2 WITH BARE 0.010 INCH GOLD FOILS. FUNCTION $AJ_0(\alpha R)$ FITTED TO POINTS LESS THAN 22.5 CM. FROM CENTER; VALUE OF A IS 1.0065, VALUE OF α^2 IS 2313 μB. STANDARD DEVIATION IN FOIL ACTIVITIES DUE TO COUNTING STATISTICS 0.15%.

4.5 SOME FEATURES OF THE MOMENTS METHOD FOR THE ANALYSIS OF THE RADIAL BUCKLING

The analysis of radial buckling has been a challenging problem for some time (H7, W4, K8) because of spatial transients and energy transients associated with the asymptotic and equilibrium conditions discussed in Chapter II, and because of the reflector effect and heterogeneity effects (K8, N1). It is of great interest, therefore, to see if the use of the moments method can reduce various transient effects on the radial buckling as was the case with the axial buckling.

First, it is advisable to distinguish the higher spatial harmonics from the various transients. By spatial transients, we mean the extraneous contributions to the flux that arise from transport effects near the source and boundaries; these are sometimes called "current transients" (D3). Examples are the additional solutions, other than the fundamental, to the balance equation for the zeroth moment of the Legendre polynomials in the P_n approximation. By an energy transient is meant those eigen-functions besides the fundamental mode that are present because of spectral inequilibrium; for example, the additional solutions, other than the fundamental, to the balance equation of the zeroth moment of the Laguerre polynomials in the L_n approximation. Finally, we define the spatial harmonics as those eigen-functions, in addition to the fundamental, of the diffusion equation itself. These are separate from the transport effect which gives rise to the so-called current transients defined previously. In this section, we shall concentrate on the effect of the harmonic modes and leave the corresponding effect of various transients on the buckling determination to Chapter VI where they will be studied in greater detail.

We recall, for this purpose, that the complete solution of the diffusion equation (4.3) for a bare system is (W1, K6, S1, P2):

$$\phi(r) = \sum_{j=1}^{\infty} A_j J_o(\alpha_j r)$$

$$= A_1 J_o(\alpha_1 r) + \sum_{j=2}^{\infty} A_j J_o(\alpha_j r)$$

$$= [\text{Fundamental Mode}] + [\text{Harmonic Modes}], \tag{4.70}$$

where

$$\alpha_1 = \frac{2.4048}{\tilde{R}}, \tag{4.71}$$

$$\alpha_2 = \frac{5.5201}{\tilde{R}}, \tag{4.72}$$

$$\alpha_3 = \frac{8.6537}{\tilde{R}}, \tag{4.73}$$

$$\alpha_4 = \frac{11.7915}{\tilde{R}}, \tag{4.74}$$

etc.

The fundamental is the dominant mode, and the harmonics are usually small in large assemblies such as the M. I. T. Subcritical Assembly (P1). However, the effect of harmonic modes appears in small assemblies such as the miniature lattices. This is especially the case when the external neutron source contains various harmonics. Sefchovich made a harmonic analysis of the source distribution for the miniature lattices and concluded that the higher harmonics had a measurable contribution, with the third harmonic being the most significant (S1). His results are tabulated for reference:

Harmonic Index, j	Harmonic Coefficients, A_j
1	0.94130
2	-0.01455
3	0.03055
4	-0.01395
5	0.01679
6	-0.00316
7	0.00838
8	0.00184
9	0.00855

The higher harmonics of the source undoubtedly excite the spatial harmonics of the radial flux in the miniature lattices in addition to the fundamental mode. The quantitative study of this effect will be taken up in the next chapter.

To see the effect of harmonic modes on the radial flux distribution, we sketch the distribution of the higher harmonics as well as that of the fundamental in Figure 4.4. The corresponding moments distributions of the fundamental mode and of the harmonic modes are shown in Figure 4.5. It is evident that the integral definition of the radial flux moments again tends to reduce the higher harmonics and to extract mostly the asymptotic radial flux depending on the choice of the moment index. The harmonic modes are particularly influential near the boundary where the asymptotic flux decreases rapidly. Aside from the truncation error, the moments method would allow the use of more experimental data in the neighborhood of the boundary than the curve-fitting method. This is expected to be helpful in obtaining better results for

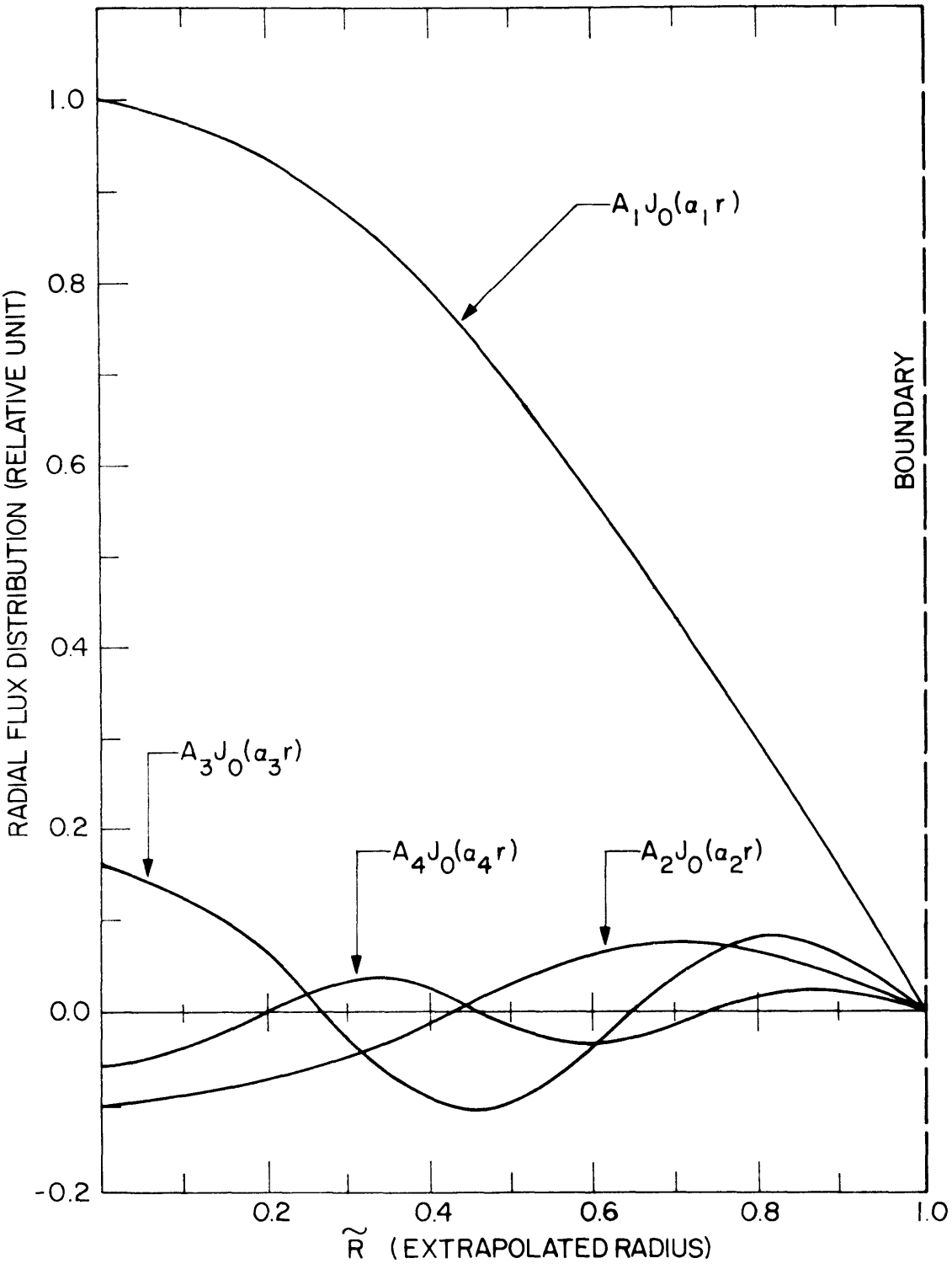

FIG. 4.4 THE FUNDAMENTAL MODE AND THE HIGHER HARMONICS OF RADIAL FLUX DISTRIBUTION.

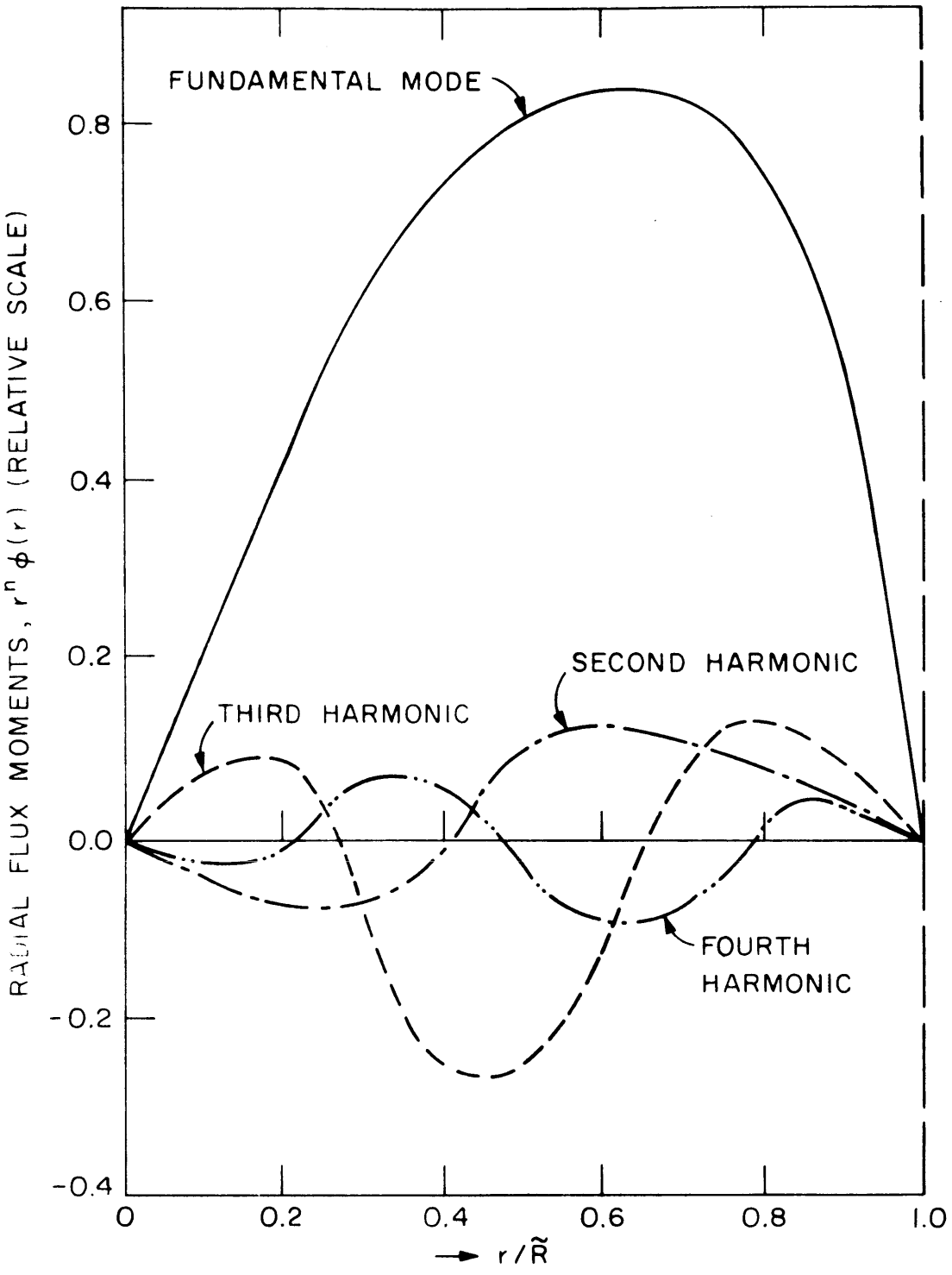

FIG. 4.5 DISTRIBUTION OF THE FLUX MOMENTS OF THE FUNDAMENTAL MODE AND THE HARMONIC MODES. NOTICE THAT THE AREAS UNDER THE CURVES ARE THE MOMENTS OF VARIOUS MODES.

the linear extrapolation distance than can be obtained with the curve-fitting method.

Finally, we mention the reflector effect, which is usually pronounced in a two-region lattice or a reflected assembly (P4, R2, S2). In such an assembly the radial flux cannot be fitted by the simple $J_o(\alpha r)$ and one has to take into account the $I_o(\beta r)$ term. This will be discussed in the next section.

4.6 THE REFLECTOR EFFECT

In a reflected cylindrical assembly, the radial flux is given by two-group theory as (K6, M1, S2)

$$\phi(r) = A_r[J_o(\alpha r) + cI_o(\beta r)], \tag{4.75}$$

where β^2 is the transient buckling corresponding to the reflector effect, and c is a coefficient which weights the I_o term relative to the J_o term. The other parameters have the same meanings as before.

We shall adopt the iterative moments method to infer the desired radial buckling α^2 from the experimental radial flux moments. To do this, we regard the radial flux as a function of the parameters α, β, and c, and expand it in a Taylor series around some appropriate initial set (α_o, β_o, c_o) that is supposed to be a good approximation to the true values of α, β, and c:

$$\begin{aligned}\phi(r, \alpha, \beta, c) \approx \phi(r, \alpha_o, \beta_o, c_o) &+ (\alpha-\alpha_o) \frac{d}{d\alpha} \phi(r, \alpha, \beta, c)\Big|_{\alpha_o, \beta_o, c_o} \\ &+ (\beta-\beta_o) \frac{d}{d\beta} \phi(r, \alpha, \beta, c)\Big|_{\alpha_o, \beta_o, c_o} \\ &+ (c-c_o) \frac{d}{dc} \phi(r, \alpha, \beta, c)\Big|_{\alpha_o, \beta_o, c_o} .\end{aligned} \tag{4.76}$$

Now,

$$\frac{d}{d\alpha}\,\phi(r,\alpha,\beta,c)\bigg|_{\alpha_o,\beta_o,c_o} = -A_r\, r J_1(\alpha_o r)\ , \tag{4.77}$$

$$\frac{d}{d\beta}\,\phi(r,\alpha,\beta,c)\bigg|_{\alpha_o,\beta_o,c_o} = A_r c_o\, r I_1(\beta_o r)\ , \tag{4.78}$$

$$\frac{d}{dc}\,\phi(r,\alpha,\beta,c)\bigg|_{\alpha_o,\beta_o,c_o} = A_r I_o(\beta_o r)\ . \tag{4.79}$$

Thus the radial flux is given approximately by

$$\begin{aligned}\phi(r,\alpha,\beta,c) \approx A_r\{&[J_o(\alpha_o r)+c_o I_o(\beta_o r)] - (\alpha-\alpha_o) r J_1(\alpha_o r)\\ &+ c_o(\beta-\beta_o) r I_1(\beta_o r)+(c-c_o) I_o(\beta_o r)\}\ .\end{aligned} \tag{4.80}$$

Substituting Eq. (4.80) in Eq. (4.2), we obtain the first three odd radial flux moments:

$$\psi_1 = A_r\left\{\frac{R}{\alpha_o} J_1(\alpha_o R) + c\,\frac{R}{\beta_o} I_1(\beta_o R) - \left(\frac{\alpha-\alpha_o}{\alpha_o}\right) F + c_o\left(\frac{\beta-\beta_o}{\beta_o}\right) f\right\}, \tag{4.81}$$

$$\psi_3 = A_r\left\{G + cg - \left(\frac{\alpha-\alpha_o}{\alpha_o}\right) H + c_o\left(\frac{\beta-\beta_o}{\beta_o}\right) h\right\}, \tag{4.82}$$

$$\psi_5 = A_r\left\{U + cu - \left(\frac{\alpha-\alpha_o}{\alpha_o}\right) V + c_o\left(\frac{\beta-\beta_o}{\beta_o}\right) v\right\}, \tag{4.83}$$

where F, G, H, U, and V are given by Eqs. (4.48) through (4.52), and

$$f = R^2 I_o(\beta_o R) - \frac{2R}{\beta_o} I_1(\beta_o R)\ , \tag{4.84}$$

$$g = -\frac{2R^2}{\beta_o^2} I_o(\beta_o R) + \frac{R}{\beta_o} I_1(\beta_o R)\left(R^2 + \frac{4}{\beta_o^2}\right), \tag{4.85}$$

$$h = R^2\left(R^2 + \frac{8}{\beta_o^2}\right)I_o(\beta_o R) - \frac{4R}{\beta_o}\left(R^2 + \frac{4}{\beta_o^2}\right)I_1(\beta_o R) \ , \tag{4.86}$$

$$u = -\frac{4R^2}{\beta_o^2}\left(R^2 + \frac{8}{\beta_o^2}\right)I_o(\beta_o R) + \frac{R}{\beta_o}\left(\frac{64}{\beta_o^4} + R^4 + \frac{16R^2}{\beta_o^2}\right)I_1(\beta_o R) \ , \tag{4.87}$$

$$v = R^2\left(R^4 + \frac{192}{\beta_o^4} + \frac{24R^2}{\beta_o^2}\right)I_o(\beta_o R) - \frac{6R}{\beta_o}\left(\frac{64}{\beta_o^4} + R^4 + \frac{16R^2}{\beta_o^2}\right)I_1(\beta_o R) \ . \tag{4.88}$$

The ratios ψ_3/ψ_1, ψ_5/ψ_3, and ψ_5/ψ_1 yield the following three equations, respectively:

$$\left(\frac{\alpha-\alpha_o}{\alpha_o}\right) - c_o\left(\frac{\beta-\beta_o}{\beta_o}\right)\frac{\left[h - \left(\frac{\psi_3}{\psi_1}\right)f\right]}{\left[H - \left(\frac{\psi_3}{\psi_1}\right)F\right]} - c\,\frac{\left[g - \left(\frac{\psi_3}{\psi_1}\right)\frac{R}{\beta_o}I_1(\beta_o R)\right]}{\left[H - \left(\frac{\psi_3}{\psi_1}\right)F\right]}$$

$$= \frac{\left[G - \left(\frac{\psi_3}{\psi_1}\right)\frac{R}{\alpha_o}J_1(\alpha_o R)\right]}{\left[H - \left(\frac{\psi_3}{\psi_1}\right)F\right]} \ , \tag{4.89}$$

$$\left(\frac{\alpha-\alpha_o}{\alpha_o}\right) - c_o\left(\frac{\beta-\beta_o}{\beta_o}\right)\frac{\left[v - \left(\frac{\psi_5}{\psi_3}\right)h\right]}{\left[V - \left(\frac{\psi_5}{\psi_3}\right)H\right]} - c\,\frac{\left[u - \left(\frac{\psi_5}{\psi_3}\right)g\right]}{\left[V - \left(\frac{\psi_5}{\psi_3}\right)H\right]}$$

$$= \frac{\left[U - \left(\frac{\psi_5}{\psi_3}\right)G\right]}{\left[V - \left(\frac{\psi_5}{\psi_3}\right)H\right]} \ , \tag{4.90}$$

$$\left(\frac{\alpha-\alpha_o}{\alpha_o}\right) - c_o\left(\frac{\beta-\beta_o}{\beta_o}\right)\frac{\left[v - \left(\frac{\psi_5}{\psi_1}\right)f\right]}{\left[V - \left(\frac{\psi_5}{\psi_1}\right)F\right]} - c\,\frac{\left[u - \left(\frac{\psi_5}{\psi_1}\right)\frac{R}{\beta_o}I_1(\beta_o R)\right]}{\left[V - \left(\frac{\psi_5}{\psi_1}\right)F\right]}$$

$$= \frac{\left[U - \left(\frac{\psi_5}{\psi_1}\right)\frac{R}{\alpha_o}J_1(\alpha_o R)\right]}{\left[V - \left(\frac{\psi_5}{\psi_1}\right)F\right]} \,. \tag{4.91}$$

We can solve these three equations for the three unknowns $\left(\frac{\alpha-\alpha_o}{\alpha_o}\right)$, $c_o\left(\frac{\beta-\beta_o}{\beta_o}\right)$, and c. For ease of writing, we set

$$B_1 = \left[G - \left(\frac{\psi_3}{\psi_1}\right)\frac{R}{\alpha_o}J_1(\alpha_o R)\right], \tag{4.92}$$

$$B_2 = \left[H - \left(\frac{\psi_3}{\psi_1}\right)F\right], \tag{4.93}$$

$$B_3 = \left[h - \left(\frac{\psi_3}{\psi_1}\right)f\right], \tag{4.94}$$

$$B_4 = \left[V - \left(\frac{\psi_5}{\psi_3}\right)H\right], \tag{4.95}$$

$$B_5 = \left[v - \left(\frac{\psi_5}{\psi_3}\right)h\right], \tag{4.96}$$

$$B_6 = \left[\left(\frac{\psi_5}{\psi_3}\right)G - U\right], \tag{4.97}$$

$$B_7 = \left[g - \left(\frac{\psi_3}{\psi_1}\right)\frac{R}{\beta_o}I_1(\beta_o R)\right], \tag{4.98}$$

$$B_8 = \left[\left(\frac{\psi_5}{\psi_3} \right) g - u \right] , \tag{4.99}$$

$$B_9 = \left[V - \left(\frac{\psi_5}{\psi_1} \right) F \right] , \tag{4.100}$$

$$B_{10} = \left[v - \left(\frac{\psi_5}{\psi_1} \right) f \right] , \tag{4.101}$$

$$B_{11} = \left[U - \left(\frac{\psi_5}{\psi_1} \right) \frac{R}{\alpha_o} J_1(\alpha_o R) \right] , \tag{4.102}$$

$$B_{12} = \left[u - \left(\frac{\psi_5}{\psi_1} \right) \frac{R}{\beta_o} I_1(\beta_o R) \right] . \tag{4.103}$$

Simultaneous solution of Eqs. (4.89), (4.90) and (4.91) yields:

$$\left(\frac{\alpha - \alpha_o}{\alpha_o} \right) = \frac{\begin{vmatrix} \frac{B_1}{B_2} & -\frac{B_3}{B_2} & -\frac{B_7}{B_2} \\ -\frac{B_6}{B_4} & -\frac{B_5}{B_4} & \frac{B_8}{B_4} \\ \frac{B_{11}}{B_9} & -\frac{B_{10}}{B_9} & -\frac{B_{12}}{B_9} \end{vmatrix}}{\begin{vmatrix} 1 & -\frac{B_3}{B_2} & -\frac{B_7}{B_2} \\ 1 & -\frac{B_5}{B_4} & \frac{B_8}{B_4} \\ 1 & -\frac{B_{10}}{B_9} & -\frac{B_{12}}{B_9} \end{vmatrix}} \equiv \frac{\Delta_1}{\Delta} , \tag{4.104}$$

$$c_o\left(\frac{\beta-\beta_o}{\beta_o}\right) = \frac{\begin{vmatrix} 1 & \frac{B_1}{B_2} & -\frac{B_7}{B_2} \\ 1 & -\frac{B_6}{B_4} & \frac{B_8}{B_4} \\ 1 & \frac{B_{11}}{B_9} & -\frac{B_{12}}{B_9} \end{vmatrix}}{\Delta} \equiv \frac{\Delta_2}{\Delta} \quad , \tag{4.105}$$

$$c = \frac{\begin{vmatrix} 1 & -\frac{B_3}{B_2} & \frac{B_1}{B_2} \\ 1 & -\frac{B_5}{B_4} & -\frac{B_6}{B_4} \\ 1 & -\frac{B_{10}}{B_9} & \frac{B_{11}}{B_9} \end{vmatrix}}{\Delta} \equiv \frac{\Delta_3}{\Delta} \tag{4.106}$$

The corrected radial buckling α^2 is given by

$$\alpha^2 = \alpha_o^2\left[1 + \left(\frac{\alpha-\alpha_o}{\alpha_o}\right)\right]^2 \quad , \tag{4.107}$$

and the corrected transient buckling β^2 is given by

$$\beta^2 = \beta_o^2\left[1 + \left(\frac{\beta-\beta_o}{\beta_o}\right)\right]^2 \quad . \tag{4.108}$$

The procedure must be repeated until the following convergence criteria are satisfied:

$$\left|\frac{\alpha_{j+1} - \alpha_j}{\alpha_j}\right| < \epsilon_1, \quad \left|\frac{\beta_{j+1} - \beta_j}{\beta_j}\right| < \epsilon_2, \quad \left|\frac{c_{j+1} - c_j}{c_j}\right| < \epsilon_3, \tag{4.109}$$

where ϵ_1, ϵ_2, and ϵ_3 are some arbitrarily specified small positive numbers.

Numerical experience indicates that the iteration on the parameter β converges slowly and even diverges in some cases depending upon the initial guess on β. This result is probably due to the non-linear nature of the parameter β as well as the divergent behavior of the modified Bessel function $I_o(\beta r)$ for large arguments (W3, A2). A similar difficulty has been reported by Serdula (S2). A common way of avoiding this problem is to use only those data in the central region where the reflector effect is negligible. This is, however, not always feasible, especially in a small assembly, because only a few data points are available.

We prefer to determine the parameter β by means of the two-group criticality equation indirectly and iterate on α and c alone. We assume that two-group diffusion theory gives a good representation of the reflector effect. The criticality equation in the two-group theory gives rise to two roots for the material buckling (K6):

$$B_{m1}^2 = \frac{1}{2}\left\{-\left(\frac{1}{L_1^2} + \frac{1}{L_2^2}\right) + \sqrt{\left(\frac{1}{L_1^2} + \frac{1}{L_2^2}\right)^2 + \frac{4(k_\infty - 1)}{L_1^2 L_2^2}}\right\}, \tag{4.110}$$

and

$$B_{m2}^2 = -\frac{1}{2}\left\{\left(\frac{1}{L_1^2} + \frac{1}{L_2^2}\right) + \sqrt{\left(\frac{1}{L_1^2} + \frac{1}{L_2^2}\right)^2 + \frac{4(k_\infty - 1)}{L_1^2 L_2^2}}\right\}, \tag{4.111}$$

where $L_1^2 = \frac{D_1}{\Sigma_1}$ is the diffusion area, $L_2^2 = \frac{D_2}{\Sigma_2}$ is the age, and k_∞ is the multiplication factor for an infinite medium; B_{m1}^2 is the usual material buckling corresponding to the fundamental mode, while B_{m2}^2 is the transient buckling corresponding to the reflector effect. Under the assumption of the azimuthal symmetry of the neutron flux, the two roots of the material buckling can be expressed in terms of the axial and radial bucklings:

$$B_{m1}^2 = \alpha^2 - \gamma^2 , \tag{4.112}$$

and

$$B_{m2}^2 = -(\beta^2 + \gamma^2) . \tag{4.113}$$

The sum of Eqs. (4.112) and (4.113) yields

$$\beta^2 = -\left(\beta_{m1}^2 + \beta_{m2}^2\right) + \alpha^2 - 2\gamma^2 ; \tag{4.114}$$

the addition of Eqs. (4.110) and (4.111) gives

$$-\left(B_{m1}^2 + B_{m2}^2\right) = \frac{1}{L_1^2} + \frac{1}{L_2^2} . \tag{4.115}$$

Thus,

$$\beta^2 = \left(\frac{1}{L_1^2} + \frac{1}{L_2^2}\right) + \alpha^2 - 2\gamma^2 . \tag{4.116}$$

The transient buckling β^2 is therefore determined by the radial and axial bucklings as well as the diffusion area and Fermi age (or slowing-down area). To calculate β^2, we assume that L_1^2 and L_2^2 are known and that the axial buckling γ^2 has been obtained by, say, the moments method in Chapter III. The value of β^2 is thus corrected in accordance with the radial buckling α^2.

Another way of deriving β^2 is to eliminate γ^2 between Eqs. (4.112) and (4.113):

$$\beta^2 = \left(B_{m1}^2 - B_{m2}^2\right) - \alpha^2$$

$$= \sqrt{\left(\frac{1}{L_1^2} + \frac{1}{L_2^2}\right)^2 + \frac{4(k_\infty - 1)}{L_1^2 L_2^2}} - \alpha^2 \,. \tag{4.117}$$

This formula requires the knowledge of k_∞ and may be undesirable when k_∞ is not well known. Since we can obtain γ^2 with good accuracy, we prefer Eq. (4.116) to Eq. (4.117).

On fixing β^2 through the two-group criticality equation as Eq. (4.116), we then use Eqs. (4.89) and (4.90) to determine the quantities $\left(\frac{\alpha-\alpha_o}{\alpha_o}\right)$ and c without the terms involving $\left(\frac{\beta-\beta_o}{\beta_o}\right)$:

$$\left(\frac{\alpha-\alpha_o}{\alpha_o}\right) - c\,\frac{B_7}{B_2} = \frac{B_1}{B_2}\,, \tag{4.118}$$

and

$$\left(\frac{\alpha-\alpha_o}{\alpha_o}\right) + c\,\frac{B_8}{B_4} = -\frac{B_6}{B_4}\,. \tag{4.119}$$

Solving Eqs. (4.118) and (4.119) for $\left(\frac{\alpha - \alpha_o}{\alpha_o}\right)$ and c, we get:

$$\left(\frac{\alpha-\alpha_o}{\alpha_o}\right) = \frac{\begin{vmatrix} \frac{B_1}{B_2} & -\frac{B_7}{B_2} \\ \frac{B_6}{B_4} & \frac{B_8}{B_4} \end{vmatrix}}{\begin{vmatrix} 1 & -\frac{B_7}{B_2} \\ 1 & \frac{B_8}{B_4} \end{vmatrix}} = \left(\frac{B_1B_8 - B_6B_7}{B_4B_7 - B_2B_8}\right)\,, \tag{4.120}$$

and

$$c = \frac{\begin{vmatrix} 1 & \frac{B_1}{B_4} \\ 1 & -\frac{B_6}{B_4} \end{vmatrix}}{\begin{vmatrix} 1 & -\frac{B_7}{B_6} \\ 1 & \frac{B_8}{B_7} \end{vmatrix}} = \left(\frac{-(B_1 B_4 + B_2 B_6)}{(B_4 B_7 + B_2 B_8)} \right). \tag{4.121}$$

Thus we iterate the calculation on the parameters α and c alone; the iteration is terminated when the convergence criteria given by Eq. (4.109) are met.

The consistency of the method can be tested by means of an error analysis following the same procedure as section 4.3. The derivation is tedious and is given in Appendix E.

There is some difficulty in guessing the value of c at the beginning of the iteration. To avoid this difficulty, we shall estimate the value of c from the experimental data by means of a least-squares technique; this procedure is described in Appendix F.

4.7 RESULTS

The direct moments method and the iterative moments method have been coded as RADBUCK and RAMBLER, respectively, in FORTRAN IV language for an IBM Operating System 360 Model 65 computer at the M.I.T. Computation Center. These codes are

described in Appendix A and have been applied to the same slightly enriched U-D_2O and UO_2-D_2O lattices as were analyzed in the calculation of the axial buckling in Chapter III. We present the results in the following subsections.

4.7.1 Application to the Slightly Enriched U-D_2O Lattices

Four different slightly enriched, triangular, U-D_2O lattices investigated in the M. I. T. Subcritical Facility have been analyzed by means of the iterative moments method with the RAMBLER code and also by means of the direct moments method with the RADBUCK code. Both the radial buckling and the extrapolated radius (hence the linear extrapolation distance) are computed. The results are given in Tables 4.1 through 4.4 for the radial buckling and in Tables 4.5 through 4.8 for the extrapolated radius and linear extrapolation distance. The average value of a number of experimental runs and its standard deviation are calculated by means of Eqs. (3.72) through (3.75) with γ^2 and $\tilde{H}$ replaced by α^2 and $\tilde{R}$, respectively. The corresponding values of α^2 and $\tilde{R}$ computed by the curve-fitting method with Palmedo's RADFIT code are also included for comparison. The standard deviations obtained with the moments method are again smaller by as much as a factor of about 2 in some cases than those obtained with the curve-fitting method. This result indicates that the internal consistency of the moments method is greater than that of the conventional curve-fitting method in the interpretation of the radial buckling measurements, just as it is in the case of the axial buckling. The values of the radial buckling inferred by means of the moments method are consistently

about 40 μB or 50 μB larger than the corresponding values obtained with the curve-fitting method. The difference is appreciably greater than the experimental error quoted and seems to be related to the method of data analysis. It is difficult to resolve this apparent discrepancy quantitatively, but it may be explained qualitatively:
(a) The curve-fitting method has been found to be sensitive to the position of the true center of the cylindrical assembly (P1). A difference as large as 100 μB has been obtained with the RADFIT code by varying the position of the center by one or two centimeters in the case of full-size lattices, and the difference can be even greater (a few hundred μB) in the case of the miniature lattices (to be seen in Table 5.2). The moments method described in the present chapter removes this difficulty by giving a zero weight to the flux at the center on the physical reasoning that the radial leakage of neutrons is zero at the center. (b) Another possible cause of the discrepancies is the truncation error incurred in the numerical integration involved in the moments method, but this error should be small, if the iterative moments method is used, as is implied by the relatively small values of the computed probable error in the radial buckling. (See Table 4.4, for example.) The probable error is expected to be small because the iterative moments method computes a correction term $\left(\frac{\alpha-\alpha_o}{\alpha_o}\right)$ which is a much smaller number than the radial buckling itself, and therefore the value of α^2 obtained with the iterative moments method is insensitive to the truncation error incurred in the calculation of the various radial flux moments. In any case, the values obtained by means of the moments method are in better agreement with the theoretical

asymptotic value given by Eq. (4.1) than are those obtained with the curve-fitting method. This can be seen by comparing the results of the analysis listed in Tables 4.1 through 4.8 with the theoretical values of α^2 and $\tilde{R}$ for the 3-foot tank and 4-foot tank, respectively:

3-Foot Tank: Physical Radius = 45.72 cm

$\lambda_{tr} = 2.60 \pm 0.06$ cm at thermal energy

$\tilde{R} = 47.50$ cm

$\alpha^2 = 2560\ \mu B$

4-Foot Tank: Physical Radius = 60.96 cm

$\lambda_{tr} = 2.60 \pm 0.06$ cm at thermal energy

$\tilde{R} = 62.81$ cm

$\alpha^2 = 1463\ \mu B$

Because of the good agreement with the theoretical value of the radial buckling, the moments method makes it possible to compare the (usually controversial) experimental values of the linear extrapolation distance with the theoretical values. To this end, we list a range of values of the transport mean-free path which may characterize the lattices investigated in the present work:

For thermal neutrons (H8, H9, P2, S1, B3),

$\lambda_{tr} = 2.40$ to 3.20 cm,

$d = 0.71\ \lambda_{tr} = 1.71$ to 2.27 cm.

For epithermal neutrons (thermal to 180 Kev) (A4),

$\lambda_{tr} = 3.72$ to 3.95 cm,

$d = 0.71\ \lambda_{tr} = 2.64$ to 2.80 cm.

It is evident that the agreement is satisfactory.

Finally, the values of the radial buckling and extrapolated radius extracted by means of the iterative moments method and the direct moments method agree well with each other, although the probable error incurred with the direct moments method is appreciably greater than that of the iterative moments method.

4.7.2 Application to the Slightly Enriched UO_2-D_2O Lattices

The RAMBLER code has also been applied to the three slightly enriched UO_2-D_2O lattices analyzed in Chapter III for the axial buckling. Here, only the iterative moments method has been used because only five data points are available in most measurements, and the direct moments method usually incurs a large truncation error as has been shown in section 4.7.1. The results, paralleling those of section 4.7.1, are presented in Tables 4.9 through 4.14. The conclusions are similar to those reached in section 4.7.1.

All the results obtained except those for the lattice with square spacing are calculated with Case 1 of the iterative moments method described in section 4.3 because this case yields the smallest probable errors in the radial buckling among the three cases. For the UO_2-D_2O lattice with square spacing, Case 2 gives the smallest probable errors. Case 2 not only yields a smaller probable error but also provides a value of the radial buckling much closer to the theoretical value.

There are also consistent significant differences between the values of the radial buckling inferred by means of the moments method and those obtained with the curve-fitting method. The reasons are

believed to be associated with the methods used for the analysis of the experimental data as have been discussed in section 4.7.1. Nevertheless, the values extracted by means of the moments method are in better agreement with the theoretical values.

It is also evident that, for each of the two triangular UO_2-D_2O lattices, there is a difference of about 50 μB between the value of the radial buckling obtained with bare foils and that obtained with cadmium-covered foils (the radial buckling for epicadmium neutrons). The corresponding difference is about 75 μB for the square UO_2-D_2O lattice. The differences may be indicative of a slightly nonasymptotic spectrum in these lattices.

We are now in a position to compute the values of the material buckling of all the lattices we have investigated so far. This will be done in the next section.

4.8 THE MATERIAL BUCKLING

In this section we shall calculate the values of the material bucklings of the three U-D_2O lattices and of the three UO_2-D_2O lattices by means of Eq. (2.3), without the component B_θ^2:

$$B_m^2 = \alpha^2 - \gamma^2 . \tag{4.122}$$

This is permissible if the neutron flux is azimuthally symmetric. The possible contribution of the component B_θ^2 has been investigated experimentally for the M.I.T. Exponential Assembly by measuring the radial buckling at different angles θ and was found negligible (P1, H8). At the M.I.T. Lattice Project, the values of the radial buckling of each lattice

have actually been inferred from a number of radial flux traverses measured at different azimuthal angles. The fact that the differences observed are within the experimental uncertainty indicates the validity of the assumption of azimuthal symmetry.

The results for the U-D_2O lattices are given in Table 4.15, while those for the UO_2-D_2O lattices are given in Table 4.16. The corresponding results obtained with the curve-fitting method are included for comparison. The values of the standard deviation quoted are calculated by combining the standard deviations in the radial and axial bucklings (B2, P5):

$$\epsilon_{B_m^2} = \sqrt{\epsilon_{\alpha^2}^2 + \epsilon_{\gamma^2}^2} \quad , \tag{4.123}$$

where ϵ denotes the standard deviation.

The standard deviation in the material buckling measurement analyzed by the moments method is smaller by approximately a factor of 2 than that of the curve-fitting method, indicating that the moments method is more consistent than the curve-fitting method for the analysis of the material buckling. However, the values of the material buckling inferred by the moments method are consistently larger than those obtained by the curve-fitting method (45 to 150 μB). The differences come, in large part, from the difference in the values of the radial buckling (discussed in section 4.7.1). It is difficult to judge which method is more accurate. The best way of testing the two different methods would be to compare the values obtained in the critical experiments. It has not, so far, been possible to make such a comparison.

4.9 CONCLUSIONS

In this chapter we have developed the iterative moments method and the direct moments method for the analysis of the radial buckling and extrapolated radius. The two methods are equivalent and should yield the same value of the radial buckling whenever the truncation error is not significant. If the number of data points is relatively large, the direct moments method is superior because it gives a unique definition for the radial buckling and no iteration is necessary. When only a few data points (say, ≤ 7) are available, the iterative moments method is not only preferable but, in fact, is necessary. The method converges very rapidly; in most cases, two or three iterations are sufficient. When nine or more data points are available, the two methods give practically the same results. (See Tables 4.1 and 4.3.)

The values of the radial buckling of all the lattices studied in the present chapter, which are extracted by means of the moments method, are consistently about 40 μB to 100 μB greater than those inferred by means of the curve-fitting method. In each case, the value obtained with the moments method agrees better with the theoretical value given by Eq. (4.1) than the curve-fitting method and is more consistent for the analysis of the radial buckling. As a consequence, it is possible to obtain a consistent value of the linear extrapolation distance experimentally and to compare it with the theoretical value predicted by asymptotic neutron transport theory. The cause of a discrepancy between the two methods of analyzing the radial buckling is not well understood, but some possible reasons were discussed in section 4.7.1.

Analogous systematic discrepancies, due to the use of different methods for the analysis of the radial buckling (and hence the material buckling) of light water-moderated lattices, have been found at the Brookhaven National Laboratory (H7). The analysis of the radial buckling has been the major problem associated with the measurement of the material buckling by means of exponential experiments and is still a problem of concern. A study of both the experimental techniques as well as the theoretical methods used in connection with this problem seems still necessary.

It seems reasonable to conclude that the moments method is a more consistent scheme for analysis of both the axial and radial bucklings than the conventional curve-fitting method.

Table 4.1. Radial buckling values for 0.75-inch-diameter, 0.947% U^{235} enriched, uranium rods in a 3.5-inch triangular lattice, moderated by D_2O at a temperature of 27°C. Density of uranium = 18.9 gm/cm^3.

Type of Detector	Experimental Run Number	Iterative Moments Method		Direct Moments Method		Curve-Fitting Method
		α^2 (μB)	σ_{α^2}* (μB)	α^2 (μB)	σ_{α^2} (μB)	α^2 (μB)
Bare gold foils	K9	1467	0.012	1467	45.6	1399
	L0	1466	0.005	1463	45.7	1416
	L2	1454	0.006	1454	46.0	1398
	L6	1440	0.013	1442	46.4	1382
	L7	1456	0.008	1455	46.0	1425
	Average	1457 ± 4.9**		1456 ± 4.4		1404 ± 8
Cadmium-covered gold foils	L1	1435	0.015	1434	46.7	1398
	L3	1426	0.027	1425	46.9	1380
	L5	1436	0.021	1435	46.6	1412
	L8	1426	0.024	1425	47.0	1388
	Average	1431 ± 2.8		1430 ± 2.6		1395 ± 7

* σ_{α^2} is the probable error in α^2 associated with the method of data analysis itself as defined in section 4.3.

** Standard deviation of the mean of a number of experimental runs (not to be confused with the probable error σ_{α^2}).

Table 4.2. Radial buckling values for 0.75-inch-diameter, 0.947% U^{235} enriched, uranium rods in a 5-inch triangular lattice, moderated by D_2O at a temperature of 27°C. Density of uranium = 18.9 grams/cm^3.

Type of Detector	Experimental Run Number	Iterative Moments Method		Direct Moments Method		Curve-Fitting Method
		α^2	σ_{α^2}*	α^2	σ_{α^2}	α^2
		(μB)	(μB)	(μB)	(μB)	(μB)
Bare gold foils	G9	1448	0.002	1459	100.5	1408
	H2	1458	0.002	1468	99.8	1420
	H5	1458	0.003	1469	99.7	1415
	I 1	1437	0.006	1450	101.3	1394
	I 2	1447	0.006	1460	100.5	1404
	I 3	1463	0.010	1474	99.4	1425
	I 4	1467	0.029	1595	89.7	1437
	I 5	1457	0.007	1468	99.8	1412
	I 6	1452	0.011	1463	100.3	1413
	J 2	1432	0.001	1444	101.8	1387
	J 4	1432	0.005	1444	101.8	1389
	J 5	1430	0.004	1441	102.0	1388
	J 8	1464	0.002	1474	99.4	1428
	K0	1459	0.005	1470	99.7	1418
	Average	1450 ± 3.4**		1470 ± 10		1410 ± 4
Cadmium-covered gold foils	H3	1431	0.0003	1439	102.3	1396
	H4	1426	0.004	1436	102.5	1387
	H7	1435	0.013	1444	101.9	1396
	Average	1430 ± 2.5		1440 ± 2.3		1393 ± 3

* σ_{α^2} is the probable error in α^2 defined in section 4.3.

** Standard deviation of the mean of a number of experimental runs.

Table 4.3. Radial buckling values for 0.387-inch-diameter, 0.947% U^{235} enriched, uranium rods in a 1.5-inch triangular lattice moderated by D_2O at a temperature of 26°C. Density of uranium = 18.9 grams/cm^3.

Type of Detector	Experimental Run Number	Iterative Moments Method		Direct Moments Method		Curve-Fitting Method
		α^2 (μB)	σ_{α^2}* (μB)	α^2 (μB)	σ_{α^2} (μB)	α^2 (μB)
Bare gold foils	N4	2427	0.059	2424	45.0	2375
	N6	2416	0.088	2414	45.1	2373
	N7	2426	0.081	2425	45.1	2382
	N9	2416	0.095	2414	45.2	2373
	P3	2430	0.051	2425	44.9	2390
	P6	2425	0.079	2423	45.0	2374
	Average	2424 ± 2.4**		2421 ± 2.3		2378 ± 3
Cadmium-covered gold foils	N3	2415	0.117	2410	44.9	2364
	N5	2396	0.143	2391	45.2	2347
	P0	2389	0.132	2387	45.4	2335
	P2	2390	0.145	2387	45.3	2342
	P4	2405	0.129	2399	45.0	2354
	Average	2399 ± 4.9		2395 ± 4.5		2348 ± 5

* σ_{α^2} is the probable error in α^2 defined in section 4.3.

** Standard deviation of the mean of a number of experimental runs.

Table 4.4. Radial buckling values for 0.387-inch-diameter, 0.947% U^{235} enriched, uranium rods in a 3-inch triangular lattice moderated by D_2O at a temperature of 25°C. Density of uranium = 18.9 grams/cm^3.

Type of Detector	Experimental Run Number	Iterative Moments Method		Curve-Fitting Method
		α^2	σ_{α^2} *	α^2
		(μB)	(μB)	(μB)
Bare gold foils	Q9	2606	0.178	2446
	R1	2596	0.108	2444
	R3	2576	0.090	2415
	R6	2607	0.076	2473
	R8	2586	0.111	2448
	Average	2594 ± 5.9**		2445 ± 9
Cadmium-covered gold foils	Q4	2522	0.021	2346
	Q7	2567	0.055	2420
	R0	2523	0.013	2375
	R2	2546	0.035	2399
	R5	2567	0.021	2348
	R7	2558	0.042	2427
	Average	2547 ± 8.4		2386 ± 15

* σ_{α^2} is the probable error in α^2 defined in section 4.3.

** Standard deviation of the mean.

Table 4.5. Values of the extrapolated radius and linear extrapolation length for 0.75-inch-diameter, 0.947% U-235 enriched, uranium rods in a 3.5-inch triangular lattice, moderated by D_2O at a temperature of 27°C. Density of uranium = 18.9 grams/cm^3.

Type of Detector	Experimental Run Number	Extrapolated Radius (cm)		Linear Extrapolation Distance (cm)	
		Iterative Moments Method	Curve-Fitting Method	Iterative Moments Method	Curve-Fitting Method
Bare gold foils	K9	62.776	64.40	1.816	3.44
	L0	62.809	63.99	1.849	3.03
	L2	63.077	64.39	2.117	3.43
	L6	63.364	64.70	2.404	3.74
	L7	63.031	63.75	2.071	2.79
	Average	63.011 ± 0.110	64.20 ± 0.173	2.051 ± 0.106	3.24 ± 0.17
Cadmium-covered gold foils	L1	63.485	64.39	2.525	3.43
	L3	63.689	64.75	2.729	3.79
	L5	63.468	64.03	2.508	3.07
	L8	63.692	64.50	2.732	3.54
	Average	63.583 ± 0.062	64.45 ± 0.156	2.623 ± 0.06	3.49 ± 0.16

Table 4.6. Values of the extrapolated radius and linear extrapolation distance for 0.75-inch-diameter, 0.947% U-235 enriched, uranium rods in a 5-inch triangular lattice, moderated by D_2O at a temperature of 27°C. Density of uranium = 18.9 grams/cm^3.

Type of Detector	Experimental Run Number	Extrapolated Radius (cm)		Linear Extrapolation Distance (cm)	
		Iterative Moments Method	Curve-Fitting Method	Iterative Moments Method	Curve-Fitting Method
Bare gold foils	G9	63.192	64.15	2.232	3.190
	H2	62.970	63.80	2.010	2.840
	H5	62.988	64.00	2.028	3.040
	I 1	63.428	64.49	2.468	3.540
	I 2	63.211	64.20	2.251	3.240
	I 3	62.872	63.71	1.912	2.750
	I 4	62.592	63.50	1.632	2.540
	I 5	63.004	64.02	2.045	3.060
	I 6	63.103	64.02	2.143	3.060
	J 2	63.553	64.55	2.593	3.590
	J 4	63.551	64.53	2.591	3.570
	J 5	63.603	64.54	2.643	3.580
	J 8	62.854	63.70	1.894	2.740
	K0	62.966	63.99	2.006	3.030
	Average	63.135 ± 0.081	64.09 ± 0.095	2.175 ± 0.081	3.130 ± 0.095
Cadmium-covered gold foils	H3	63.578	64.48	2.618	3.520
	H4	63.677	64.55	2.717	3.590
	H7	63.486	64.48	2.526	3.520
	Average	63.580 ± 0.055	64.50 ± 0.067	2.620 ± 0.055	3.540 ± 0.067

Table 4.7. Values of the extrapolated radius and linear extrapolation distance for 0.387-inch-diameter, 0.947% U-235 enriched, uranium rods in a 3.0-inch triangular lattice, moderated by D_2O at a temperature of 25°C. Density of uranium = 18.9 grams/cm^3.

Type of Detector	Experimental Run Number	Extrapolated Radius (cm)		Linear Extrapolation Distance (cm)	
		Iterative Moments Method	Curve-Fitting Method	Iterative Moments Method	Curve-Fitting Method
Bare gold foils	Q9	47.110	48.72	1.390	3.00
	R1	47.199	48.70	1.479	2.98
	R3	47.383	49.10	1.663	3.38
	R6	47.102	48.40	1.382	2.68
	R8	47.294	48.74	1.574	3.02
	Average	47.218 ± 0.054	48.71 ± 0.092	1.498 ± 0.054	2.99 ± 0.09
Cadmium-covered gold foils	Q4	47.886	49.75	2.166	4.03
	Q7	47.461	49.00	1.741	3.28
	R0	47.876	49.40	2.156	3.68
	R2	47.662	49.20	1.942	3.48
	R5	47.467	49.70	1.747	3.98
	R7	47.544	48.80	1.824	3.08
	Average	47.649 ± 0.079	49.30 ± 0.141	1.929 ± 0.079	3.58 ± 0.14

Table 4.8. Values of the extrapolated radius and linear extrapolation distance for 0.387-inch-diameter, 0.947% U-235 enriched, uranium rods in a 1.5-inch triangular lattice, moderated by D_2O at a temperature of 26°C. Density of uranium = 18.9 grams/cm^3.

Type of Detector	Experimental Run Number	Extrapolated Radius (cm)		Linear Extrapolation Distance (cm)	
		Iterative Moments Method	Curve-Fitting Method	Iterative Moments Method	Curve-Fitting Method
Bare gold foils	N4	48.816	49.35	3.096	3.63
	N6	48.921	49.38	3.201	3.66
	N7	48.820	49.29	3.100	3.57
	N9	48.922	49.38	3.202	3.66
	P3	48.781	49.21	3.061	3.49
	P6	48.832	49.36	3.112	3.64
	Average	48.849 ± 0.024	49.30 ± 0.031	3.129 ± 0.022	3.58 ± 0.031
Cadmium-covered gold foils	N3	48.933	49.56	3.213	3.84
	N5	49.131	49.74	3.411	4.02
	P0	49.200	49.82	3.479	4.10
	P2	49.189	49.76	3.469	4.04
	P4	49.035	49.60	3.315	3.88
	Average	49.098 ± 0.051	49.73 ± 0.051	3.378 ± 0.051	4.01 ± 0.051

Table 4.9. Values of the radial buckling for 0.431-inch-diameter, 1.99% UO_2 (density of 10.2 grams/cm^3) in a 3.5-inch triangular lattice, moderated by D_2O at a temperature of 30°C.

Type of Detector	Experimental Run Number	RADIAL BUCKLING (μB)	
		Iterative Moments Method	Curve-Fitting Method
Bare gold foils	65	2544	2457
	69	2439	2342
	72	2542	2458
	82	2528	2504
	86	2562	2531
	Average	2523 ± 23.1	2458 ± 32.4
Cadmium-covered gold foils	61	2467	2361
	74	2467	2365
	84	2455	2344
	Average	2463 ± 3.9	2357 ± 6.5

Table 4.10. Values of the radial buckling for 0.431-inch-diameter, 1.099% UO_2 rods (density of 10.2 grams/cm^3) in a 3.5-inch triangular lattice, moderated by D_2O at a temperature of 26°C.

Type of Detector	Experimental Run Number	RADIAL BUCKLING (μB)	
		Iterative Moments Method	Curve-Fitting Method
Bare gold foils	36	2570	2486
	40	2552	2465
	46	2546	*
	60	2540	*
	Average	2552 ± 6.5	2476 ± 11
Cadmium-covered gold foils	38	2436	2324
	43	2436	*
	45	2414	2311
	Average	2429 ± 7.3	2318 ± 7

* Not listed in the 1968 Lattice Project Annual Report.

Table 4.11. Values of the radial buckling for 0.431-inch-diameter, 1.099% UO_2 rods (density of 10.2 grams/cm^3) in a 3.25-inch square lattice, moderated by D_2O at a temperature of 30°C.

Type of Detector	Experimental Run Number	RADIAL BUCKLING (μB)	
		Iterative Moments Method	Curve-Fitting Method
Bare gold foils	12	2579	2484
	20	2568	2475
	24	2541	2453
	29	2584	2490
	34	2564	2474
	Average	2567 ± 7.4	2475 ± 6.3
Cadmium-covered gold foils	11	2324	2255
	16	2379	2304
	26	2374	2306
	31	2365	2305
	Average	2361 ± 12.2	2293 ± 13

Table 4.12. Values of the extrapolated radius and linear extrapolation distance for 0.431-inch-diameter, 1.99% UO_2 rods (density of 10.2 gm/cm^3) in a 3.5-inch triangular lattice, moderated by D_2O at a temperature of 30°C.

Type of Detector	Experimental Run Number	Extrapolated Radius (cm)		Linear Extrapolation Distance (cm)	
		Iterative Moments Method	Curve-Fitting Method	Iterative Moments Method	Curve-Fitting Method
Bare gold foils	65	47.675	48.50	1.955	2.78
	69	48.695	49.75	2.975	4.03
	72	47.699	48.49	1.979	2.47
	82	47.834	48.02	2.114	2.30
	86	47.513	47.81	1.793	2.09
	Average	47.883 ± 0.935	48.514 ± 1.51	2.163 ± 0.935	2.794 ± 1.51
Cadmium-covered gold foils	61	48.422	49.50	2.702	3.78
	74	48.422	49.48	2.702	3.76
	84	48.537	49.75	2.817	4.03
	Average	48.460 ± 0.09	49.58 ± 0.22	2.740 ± 0.09	3.86 ± 0.22

Table 4.13. Values of the extrapolated radius and linear extrapolation distance for 0.431-inch-diameter, 1.099% UO_2 rods (density of 10.2 gm/cm^3) in a 3.5-inch triangular lattice, moderated by D_2O at a temperature of 26°C.

Type of Detector	Experimental Run Number	Extrapolated Radius (cm)		Linear Extrapolation Distance (cm)	
		Iterative Moments Method	Curve-Fitting Method	Iterative Moments Method	Curve-Fitting Method
Bare gold foils	36	47.439	48.22	1.719	2.50
	40	47.603	48.46	1.883	2.74
	46	47.658	*	1.938	*
	60	47.720	*	2.000	*
	Average	47.605 ± 0.021	48.34 ± 0.12	1.885 ± 0.021	2.62 ± 0.12
Cadmium-covered gold foils	38	48.728	49.90	3.008	4.18
	43	48.723	*	3.003	*
	45	48.945	50.02	3.225	4.30
	Average	48.798 ± 0.018	49.96 ± 0.06	3.078 ± 0.018	4.24 ± 0.06

* Not listed in the 1968 Lattice Project Annual Report.

Table 4.14. Values of the extrapolated radius and linear extrapolation distance for 0.431-inch-diameter, 1.099% UO_2 rods (density of 10.2 gm/cm^3) in a 3.25-inch triangular lattice, moderated by D_2O at a temperature of 30°C.

Type of Detector	Experimental Run Number	Extrapolated Radius (cm)		Linear Extrapolation Distance (cm)	
		Iterative Moments Method	Curve-Fitting Method	Iterative Moments Method	Curve-Fitting Method
Bare gold foils	12	47.350	48.21	1.630	2.49
	20	47.452	48.31	1.732	2.59
	24	47.703	48.50	1.983	2.78
	29	47.309	48.20	1.589	2.48
	34	47.488	48.32	1.768	2.60
	Average	47.460 ± 0.031	48.31 ± 0.023	1.740 ± 0.031	2.59 ± 0.023
Cadmium-covered gold foils	11	49.887	50.70	4.167	4.98
	16	49.299	50.10	3.579	4.38
	26	49.357	50.02	3.637	4.30
	31	49.447	50.04	3.727	4.32
	Average	49.498 ± 0.133	50.22 ± 0.17	3.778 ± 0.133	4.50 ± 0.17

Table 4.15. Values of the material buckling of the slightly enriched, uranium-fueled and heavy water-moderated, triangular lattices obtained by means of the moments method and the conventional curve-fitting method.

Enrichment (%)	Lattice Spacing (inches)	Fuel Rod Diameter (inch)	MOMENTS METHOD		CURVE-FITTING METHOD	
			Material Buckling B_m^2 (μB)	Standard Deviation $\epsilon_{B_m^2}$ (μB)	Material Buckling B_m^2 (μB)	Standard Deviation $\epsilon_{B_m^2}$ (μB)
0.947	3.00	0.387	1228*	8.2	1083	15.8
			1159**	8.5	998	15.3
0.947	3.50	0.750	1437	4.9	1376	14.4
			1394	4.7	1349	9.9
0.947	5.00	0.750	1183	6.6	1137	8.1
			1156	6.7	1111	10.4

* The top values are those for bare gold foils.

** The bottom values are those for cadmium-covered gold foils.

Table 4.16. Values of the material buckling of the slightly enriched UO_2-D_2O lattices at the M.I.T. Lattice Project obtained by means of the moments method and the conventional curve-fitting method.

Enrichment (%)	Lattice Spacing (inches)	Fuel Rod Diameter (inch)	MOMENTS METHOD		CURVE-FITTING METHOD	
			Material Buckling B_m^2 (μB)	Standard Deviation $\epsilon_{B_m^2}$ (μB)	Material Buckling B_m^2 (μB)	Standard Deviation $\epsilon_{B_m^2}$ (μB)
1.990	3.50 △	0.431	1607*	23.2	1540	32.8
			1517**	7.7	1445	19.0
1.099	3.50 △	0.431	926	6.9	844	11.4
			809	8.9	706	14.4
1.099	3.25 ▨	0.431	972	8.6	870	11.2
			734	14.2	657	16.1

* The top values are those for bare gold foils.

** The bottom values are those for cadmium-covered gold foils.

Chapter V

APPLICATION OF THE MOMENTS METHOD TO THE MINIATURE LATTICES

5.1 INTRODUCTION

The use of small subcritical assemblies for the measurement of reactor parameters has appeared attractive for some time. Wikdahl and Akerhielm (W5), in Sweden, used miniature lattices to measure disadvantage factors in single rods and clusters of UO_2 rods in D_2O. Relatively small assemblies were also used by Kouts and coworkers (K10) at the Brookhaven National Laboratory to measure quantities related to k_∞ in lattices of slightly enriched U-metal rods in ordinary water. Peak (P2) and Sefchovich (S1) at M.I.T. demonstrated the feasibility of using U-D_2O miniature lattices to measure intracellular flux distributions as well as lattice parameters such as ρ_{28}, δ_{28}, δ_{25}, C^*, etc. In all cases the results were encouraging.

At the M.I.T. Lattice Project, Sefchovich (S1) tried to infer values of the axial and radial bucklings (and hence the material buckling) from measured flux shapes in miniature lattices by means of the conventional curve-fitting method but failed to obtain consistent results. The main difficulty seemed to be the axial buckling; the presence of an external source, the effect of the boundary, and the relatively short length of the miniature lattice assembly combined to make the axial flux distribution deviate from the asymptotic hyperbolic

sine shape over a considerably wide region as indicated in Figure 5.1 for a typical miniature lattice ML4. This behavior was also observed in the other miniature lattices studied. Up to about 24 cm from the source, the axial flux was significantly contaminated by the source neutron contribution and by flux transients due to transport and/or energy effects. As a consequence, the curve-fitting method always yielded a value for the axial buckling that is considerably larger than the theoretical value. This result is illustrated in Figure 5.2 for the miniature lattice ML2. No common intersection is observed and hence there is no way of determining a unique value of the axial buckling and extrapolated height. Table 5.1 lists the results obtained with the AXFIT code developed by Palmedo (P1) for the cases of the 16-point fit, 10-point fit, and 6-point fit corresponding to Figure 5.2. It is evident from Table 5.1 that in all of the cases analyzed with the AXFIT code the value of the axial buckling turns out to be larger than 8000 μB with a probable error in the fit of 170 μB to 490 μB. The results obtained with the AXFIT code are physically unreasonable because the value of the axial buckling obtained with the AXFIT code is greater than that of the radial buckling (the theoretical value of which is about 7600 μB), so that a negative value is obtained for the material buckling.

In the analysis of the radial flux distribution in the miniature lattices, the harmonic and reflector effects also present a problem in that the experimental activation data near the boundary are greater than the values corresponding to the asymptotic J_o function, as shown in Figure 5.3. The RADFIT code written by Palmedo (P1) has also been used to infer values of the radial buckling of the ML2. The

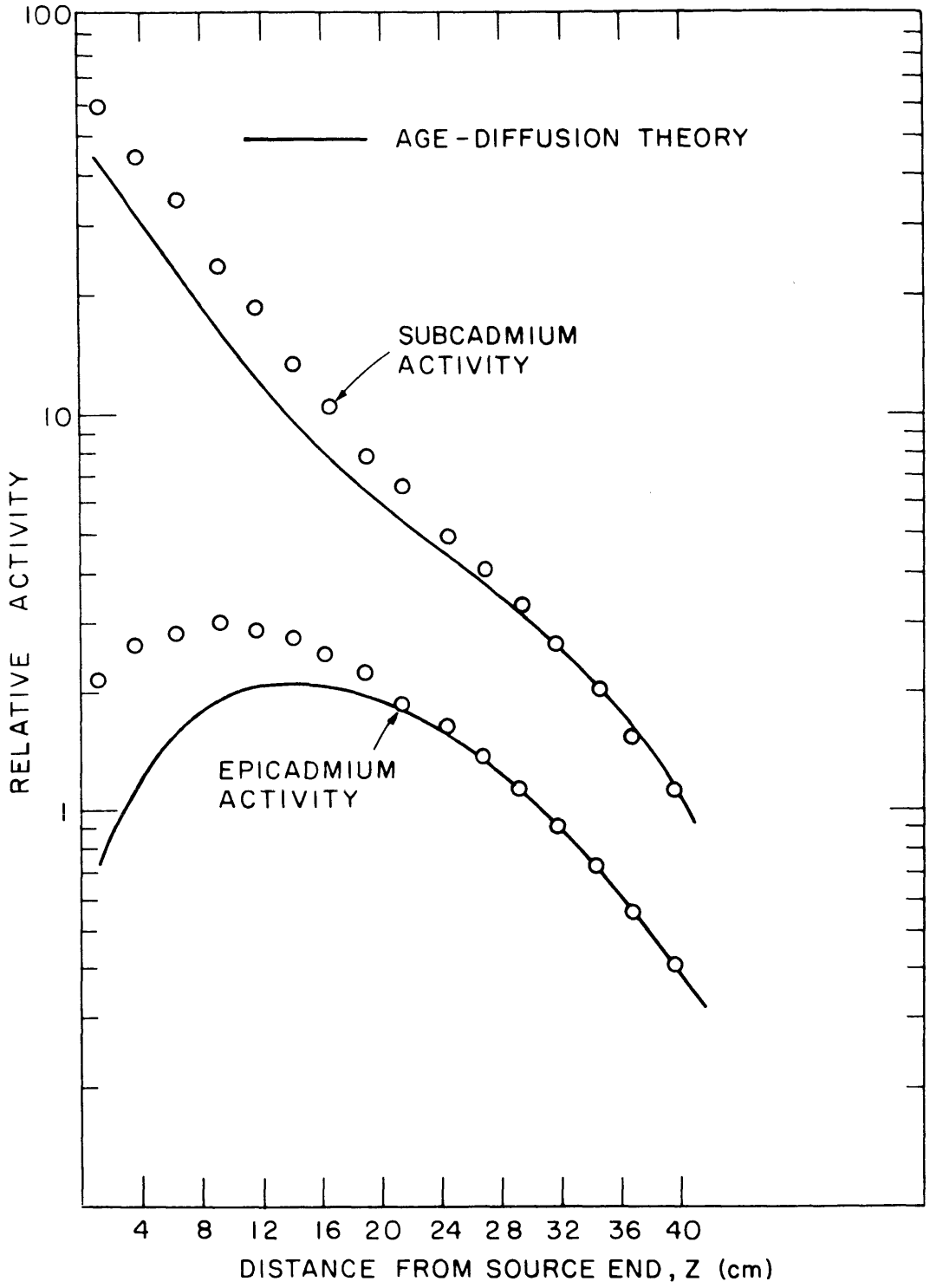

FIG. 5.1 AXIAL DISTRIBUTION OF THE EPICADMIUM AND SUBCADMIUM ACTIVITIES OF GOLD IN ML4
ML4: 1.027% ENRICHED FUEL, D_2O MODERATED 1.25-INCH LATTICE SPACING.

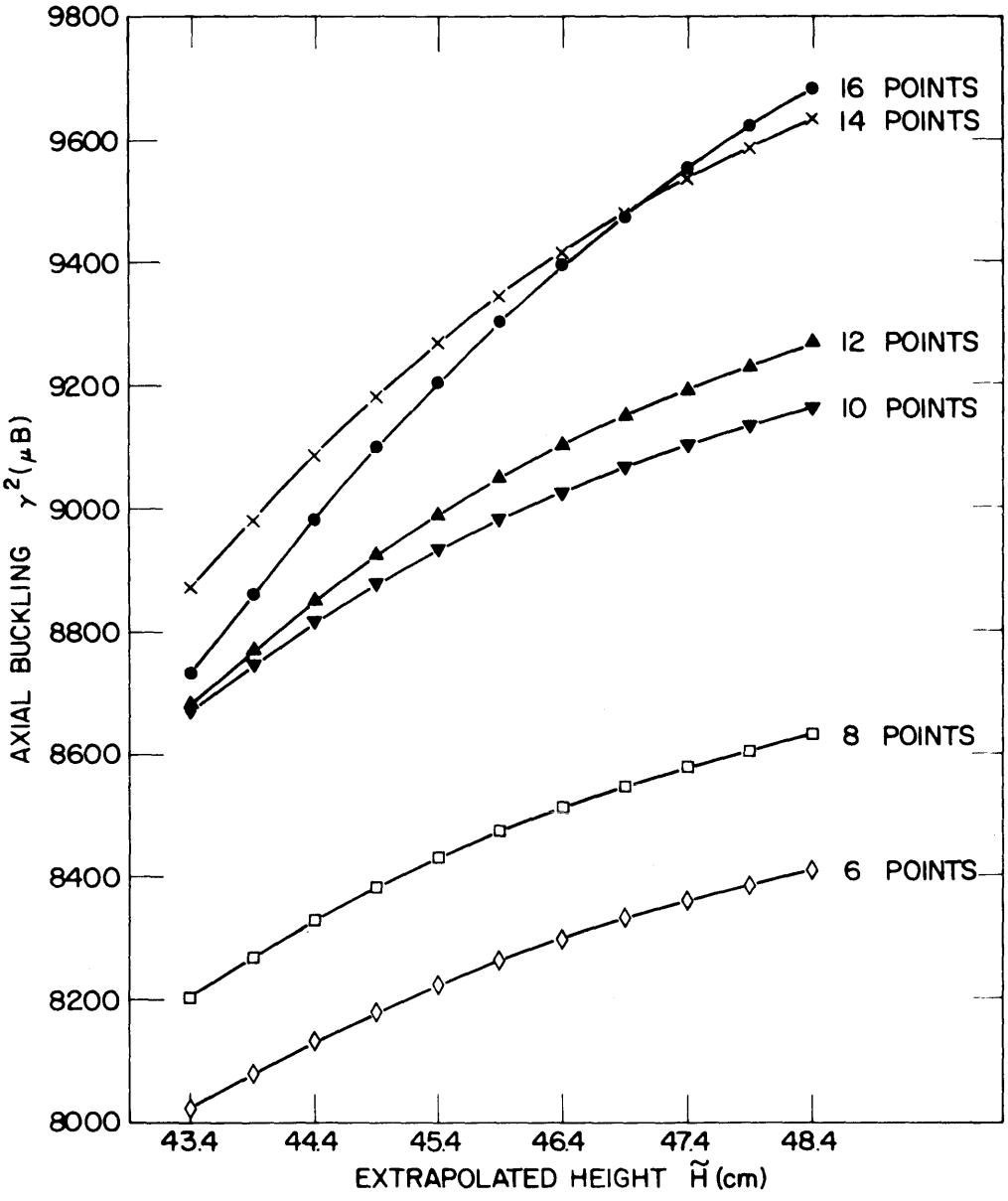

Fig. 5.2 CURVES OF THE AXIAL BUCKLING VS. THE EXTRAPOLATED HEIGHT FOR THE MINIATURE LATTICE ML2 CALCULATED WITH THE AXFIT CODE OF PALMEDO. NO COMMON INTERSECTION IS OBSERVED.

Table 5.1. Values of the axial buckling of the miniature lattice ML2 for the subcadmium activation data calculated with the AXFIT code developed by Palmedo (P1).

Assumed Values of Extrapolated Height, $\tilde{H}$ (cm)	AXIAL BUCKLING AND DEGREE OF FIT					
	16-Point Fit		10-Point Fit		6-Point Fit	
	Axial Buckling (μB)	Degree of Fit (μB)	Axial Buckling (μB)	Degree of Fit (μB)	Axial Buckling (μB)	Degree of Fit (μB)
43.4	8735	487	8674	376	8023	398
43.9	8864	425	8750	351	8082	378
44.4	8987	373	8818	328	8135	359
44.9	9102	330	8879	308	8183	343
45.4	9209	294	8934	290	8227	327
45.9	9307	265	8983	274	8266	313
46.4	9398	239	9028	259	8301	299
46.9	9480	218	9068	246	8333	287
47.4	9555	200	9103	233	8361	275
47.9	9623	184	9136	222	8387	264
48.4	9684	170	9165	211	8411	253
48.9	8871	420	8206	344	10118	178
49.4	8986	379	8271	323	10143	169

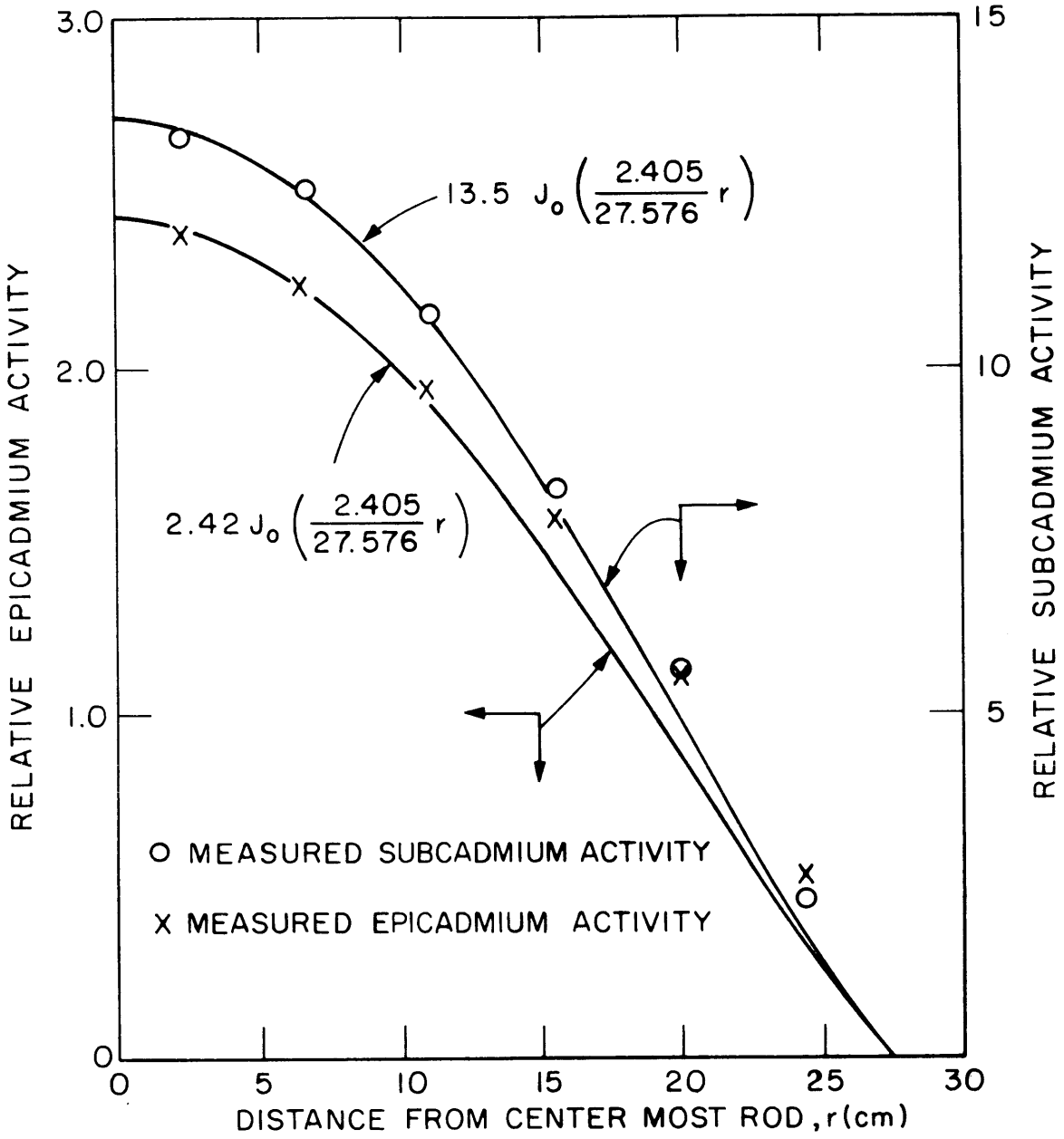

FIG. 5.3 RELATIVE RADIAL ACTIVITY DISTRIBUTION OF GOLD IN ML7, 9.75 INCHES FROM SOURCE END. ML7: 1.143% ENRICHED FUEL, D_2O MODERATED 1.75 - INCH SPACING.

results for the 8-point fit, the 7-point fit, and the 6-point fit are given in Table 5.2. It is evident that a difference of 1000 μB can be obtained by varying the position of the center for different numbers of data points. Furthermore, the best value (6643 μB) obtained with the RADFIT code is about 1000 μB smaller than the theoretical value (about 7600 μB) calculated from Eq. (4.1). This discrepancy may be due to the presence of harmonic modes in addition to the fundamental, since the source used for the measurements in the miniature lattices contains a measurable fraction of various harmonic modes, as has been shown in section 4.5 of Chapter IV. The harmonic modes will be investigated further in section 5.3. The reflection of neutrons from outside the assembly may also contribute to the discrepancy; this possibility will also be studied in section 5.3.

In Chapter II we have investigated the asymptotic condition in the miniature lattices by studying the asymptotic solutions of the neutron transport equations. The results seem to indicate the existence of an asymptotic region which may be too small for the curve-fitting method to be applicable, but may be sufficient for the moments method. It will be shown in section 5.2 that this is indeed the case.

Some features of the moments method seem to imply that this general method may be applied to the miniature lattices with some hope of success. In this chapter we shall try to derive values of the material buckling of the miniature lattices by inferring the values of the axial buckling and the radial buckling by means of the moments methods described in Chapters III and IV. In particular, we shall exemplify some important features of the moments methods discussed

Table 5.2. Values of the radial buckling of the miniature lattice ML2 for the subcadmium activation data calculated with the RADFIT code developed by Palmedo (P1).

Radial Shift of Center Position (cm)	RADIAL BUCKLING AND DEGREE OF FIT					
	8-Point Fit		7-Point Fit		6-Point Fit	
	Radial Buckling (μB)	Degree of Fit (μB)	Radial Buckling (μB)	Degree of Fit (μB)	Radial Buckling (μB)	Degree of Fit (μB)
-1.00	7176	0.66×10^{-3}	6310	0.23×10^{-3}	6803	0.23×10^{-3}
-0.75	7149	0.41×10^{-3}	6437	0.13×10^{-3}	6806	0.13×10^{-3}
-0.50	7113	0.23×10^{-3}	6553	0.56×10^{-4}	6779	0.58×10^{-4}
-0.25	7067	0.1×10^{-3}	6659	0.14×10^{-4}	6724	0.17×10^{-4}
0.00	7012	0.4×10^{-4}	6752	0.64×10^{-5}	6643	0.49×10^{-5}
+0.25	6949	0.36×10^{-4}	6832	0.35×10^{-4}	6538	0.20×10^{-4}
+0.50	6877	0.85×10^{-4}	6898	0.1×10^{-3}	6412	0.60×10^{-4}
+0.75	6796	0.19×10^{-3}	6949	0.2×10^{-3}	6267	0.12×10^{-3}
+1.00	6710	0.34×10^{-3}	6984	0.36×10^{-3}	6107	0.20×10^{-3}

in the preceding two chapters by making some numerical experiments. The purpose of these "experiments" is to shed some light on the applicability of the moments methods in the presence of flux transients, harmonic modes, and reflected neutrons.

The specifications of the six miniature lattices to be analyzed in the present chapter are described in Table 5.3.

5.2 THE EXTRACTION OF THE AXIAL BUCKLING

5.2.1 A Preliminary Study of the Source and Transport Effects

Before we apply the moments method described in Chapter III to experimental activation data of the miniature lattices, it seems desirable to test the moments method with a set of theoretical flux values with two objectives in mind:

(a) To see if the ABMOMENT code based on the moments method can reproduce the input values of the axial buckling and the extrapolated height corresponding to the set of theoretical flux values.

(b) To investigate the applicability of the moments method in the presence of significant transport and source effects.

The total axial flux distribution of a subcritical assembly in the presence of the source effect, the energy effect, and the transport effect may be described by the general expression

$$\phi_o(z) = A\left\{ \sum_{g=1}^{\infty} S_g e^{-\Sigma_{t,g} z} + \sinh \gamma_1(\tilde{H}_1 - z) + \sum_{i=2}^{\infty} c_i \sinh \gamma_i(\tilde{H}_i - z) \right\} , \tag{5.1}$$

where the source neutron contribution consists of infinitely many terms corresponding to infinitely many energy groups of source neutrons; S_g

Table 5.3. Description of the Miniature Lattices*

U^{235} Concentration of Fuel (%)	Triangular Lattice Spacing (Inches)	Denomination of Lattice
1.143	1.25	ML2
1.143	1.75	ML7
1.143	2.50	ML3
1.027	1.25	ML4
1.027	1.75	ML6
1.027	2.50	ML5

* All the lattices are moderated by 99.75 mole percent D_2O. Fuel rods are 0.25 inch in diameter in aluminum tubes of 0.318-inch O. D.

represents the contribution of the g^{th} group of source neutrons relative to the asymptotic flux (the second term in Eq. (5.1)), while the third term represents the flux transients, with the c_i being the coefficients of the transients relative to the asymptotic contribution. In a one-group P_3 approximation, Eq. (5.1) reduces to

$$\phi_o(z) = A\left[S_1 e^{-\Sigma_t z} + \sinh \gamma_1(\tilde{H}_1 - z) + c \sinh \gamma_3(\tilde{H}_3 - z)\right], \tag{5.2}$$

where γ_1^2 is the axial buckling corresponding to the asymptotic flux and $\tilde{H}_1$ is the corresponding extrapolated height; γ_3^2 is the axial buckling corresponding to the transient flux and $\tilde{H}_3$ is the position where the transient flux vanishes. These quantities, as well as the constants S_1 and c, can be determined by means of the spherical harmonics method (P6, C1, D2) together with Marshak's boundary conditions. Since the derivation is too lengthy to be presented here, we shall give only the final quantitative result obtained with Eq. (5.2) for one miniature lattice (say, ML3) for illustration and refer the reader to section 6.2.3 of Chapter VI for details. Equation (5.2) leads to the following quantitative expression for the relative total axial flux distribution of ML3 (see Eq. (6.104)):

$$\frac{\phi_o(z)}{A} = 11.053\, e^{-0.4476z} + \sinh\left[0.08072(41.715 - z)\right] + 0.1025\, e^{-15.994} \sinh\left[0.8804(22.89 - z)\right], \tag{5.3}$$

where z is in centimeters. The asymptotic axial buckling γ_1^2 is then

$$\gamma_1^2 = (0.08072)^2 = 0.0065163 \text{ cm}^{-2} \text{ or } 6516.3\ \mu\text{B},$$

and the extrapolated height is

$$\tilde{H}_1 = 41.715 \text{ cm}.$$

Table 5.4 lists the theoretical values of the asymptotic flux and of the relative total flux as functions of the axial distance, computed with Eq. (5.3).

The theoretical values of the asymptotic flux listed in Table 5.4 have been used to extract the values of the asymptotic axial buckling and the extrapolated height by means of the moments method as applied in the code ABMOMENT. The purpose of this calculation is to test the ability of the moments method to reproduce the theoretical values. The results are

$$\gamma_1^2 = 6518 \pm 8\ \mu B,$$

and

$$\tilde{H}_1 = 41.711 \pm 0.01\ \text{cm},$$

respectively, in excellent agreement with the input values ($\gamma_1^2 = 6516.3\ \mu B$ and $\tilde{H} = 41.715$ cm). The errors quoted are the probable errors incurred in the analysis with the moments method per se, not the experimental uncertainties.

To see the extent to which the source and transport effects can affect the calculation of the axial buckling and extrapolated height with the moments method, the ABMOMENT code has also been used to analyze the theoretical values of the total axial flux in Table 5.4 by selecting the locations of the first and last data points. The results are given in Table 5.5. The last two cases yield values of γ_1^2 and $\tilde{H}_1$ that agree with the corresponding exact asymptotic values within the probable errors quoted. The results of Table 5.5 are also plotted in Figure 5.4 for ease of comparison.

It seems reasonable to conclude that the moments method can

Table 5.4. Values of the asymptotic axial flux and the total axial flux of the miniature lattice ML3 as functions of the axial distance in a one-group P_3 approximation.

z (cm)	Normalized Asymptotic Flux	Relative Total Axial Flux
0.0	1.45004	2.88331
2.0	1.22536	1.73135
4.0	1.04893	1.24568
6.0	0.89129	0.96989
8.0	0.75760	0.78953
10.0	0.64382	0.65688
12.0	0.54594	0.55130
14.0	0.46361	0.46581
16.0	0.39263	0.39354
18.0	0.33178	0.33215
20.0	0.27991	0.28006
22.0	0.23538	0.23544
24.0	0.19697	0.19699
26.0	0.16373	0.16374
28.0	0.13475	0.13475
30.0	0.10931	0.10931
32.0	0.08671	0.08671
34.0	0.06639	0.06638
36.0	0.04778	0.04773
38.0	0.03044	0.03009
40.0	0.01388	0.01186

Table 5.5. Reduction of the source and transport effects on the extraction of the axial buckling and the extrapolated height for the miniature lattice ML3 by means of the ABMOMENT code.

Number of Data Points Used	First Data Point (cm)	Last Data Point (cm)	Axial Buckling γ_1^2 (μB)	Probable* Error in γ_1^2 (μB)	Extrapolated Height $\tilde{H}_1$ (cm)	Probable Error in $\tilde{H}_1$ (cm)
19	2.0	38.0	7023	3843	42.006	7.080
19	4.0	40.0	6554	49	41.615	0.030
17	8.0	40.0	6547	48	41.623	0.030
13	14.0	38.0	6496	41	41.667	0.035
13	16.0	40.0	6508	34	41.680	0.029

* The probable error is the error that may be incurred in the quantity of interest in the analysis by means of the moments method (not to be confused with the experimental uncertainty usually expressed in terms of a standard deviation of the mean).

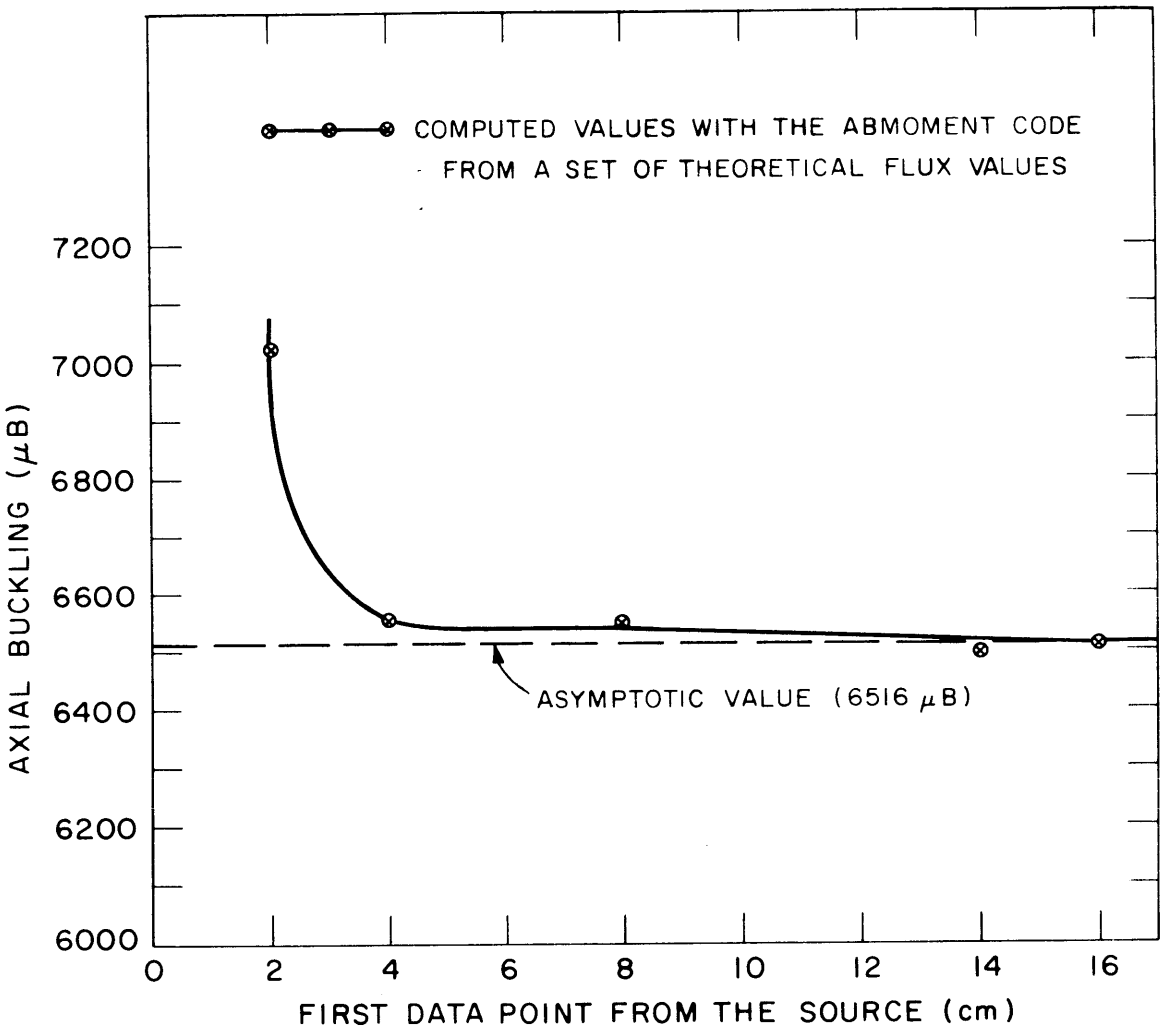

FIG. 5.4 VARIATION OF THE AXIAL BUCKLING WITH THE FIRST THEORETICAL DATA POINT FROM THE SOURCE OF THE MINIATURE LATTICE ML3. THE CIRCLED BUCKLING VALUES ARE OBTAINED WITH THE MOMENTS METHOD AS APPLIED TO A SET OF THEORETICAL FLUX VALUES CALCULATED BY A ONE-GROUP P_3 APPROXIMATION. ML3: 1.143% ENRICHED FUEL, D_2O MODERATED, 2.5-INCH LATTICE SPACING.

reproduce theoretical values of the axial buckling and extrapolated height; the method can be applied successfully to the miniature lattices if care is taken in the choice of the first and last data points.

5.2.2 Application of the Moments Method to the Miniature Lattices

Axial activation data have been obtained with bare and cadmium-covered gold goils in the miniature lattices at 16 locations with successive separations of one inch (S1). Since the source effect is the major problem, we analyze the measured axial flux data by dropping the first data point from the source successively, until we obtain a nearly constant value of the axial buckling (as we proposed in section 2.4 of Chapter II). This is probably the most satisfactory way of removing the source effect: for when the axial buckling becomes independent of the location of the first data point, the axial flux distribution is free not only of the source neutron contribution but also of other transients. If this were not the case, the axial buckling would vary with position, according to the analysis in section 2.4. In this chapter, therefore, we shall adopt the point-dropping procedure together with an error analysis to derive the best values of the axial buckling of the miniature lattices.

The method outlined has been applied to the analysis of the activation distributions of the six miniature lattices; the moments method, in the form of the ABMOMENT code, has been used to infer the best value of the axial buckling. The results are given in Table 5.6 for the activation data with bare gold foils; in Table 5.7 the results are given for the activation data with cadmium-covered gold foils, and in Table 5.8 for the subcadmium activation data. The variation of the

Table 5.6. Values of the axial buckling and the extrapolated height for the activation of bare gold foils of the six miniature lattices investigated at the M.I.T. Lattice Project, fueled with slightly enriched uranium and moderated by heavy water.

Lattice Designator	Fuel Enrichment (%)	Lattice Spacing (Inches)	Fuel Rod Diameter (Inch)	Axial Buckling γ^2 (μB)	Probable Error $\sigma_{\gamma 2}$ (μB)	Extrapolated Height $\tilde{H}$ (cm)	Probable Error $\sigma_{\tilde{H}}$ (cm)
ML2	1.143	1.25	0.25	5844.1	69.1	47.725	0.197
ML7	1.143	1.75	0.25	6139.5	35.2	44.721	0.052
ML3	1.143	2.50	0.25	6984.4	72.4	46.408	0.169
ML4	1.027	1.25	0.25	5760.2	78.4	47.135	0.110
ML6	1.027	1.75	0.25	6425.7	69.8	44.976	0.113
ML5	1.027	2.50	0.25	7294.7	98.2	46.955	0.257

Table 5.7. Values of the axial buckling and the extrapolated height for the activation of Cd-covered gold foils of the six miniature lattices, fueled with slightly enriched uranium and moderated by heavy water.

Lattice Designator	Fuel Enrich-ment (%)	Lattice Spacing (Inches)	Fuel Rod Diameter (Inch)	Axial Buckling γ^2 (μB)	Probable Error $\sigma_{\gamma 2}$ (μB)	Extrapolated Height $\tilde{H}$ (cm)	Probable Error $\sigma_{\tilde{H}}$ (cm)
ML2	1.143	1.25	0.25	4226.8	87.0	47.379	0.127
ML7	1.143	1.75	0.25	3484.1	82.5	45.058	0.068
ML3	1.143	2.50	0.25	3386.3	69.4	46.709	0.084
ML4	1.027	1.25	0.25	4285.5	82.2	47.015	0.111
ML6	1.027	1.75	0.25	3464.6	66.6	45.124	0.056
ML5	1.027	2.50	0.25	3312.8	72.7	46.480	0.084

Table 5.8. Values of the axial buckling and the extrapolated height for the subcadmium activation data of the six miniature lattices, fueled with slightly enriched uranium and moderated by 99.75% D_2O.

Lattice Designator	Fuel Enrichment (%)	Lattice Spacing (Inches)	Fuel Rod Diameter (Inch)	Axial Buckling γ^2 (μB)	Probable Error σ_{γ^2} (μB)	Extrapolated Height $\tilde{H}$ (cm)	Probable Error $\sigma_{\tilde{H}}$ (cm)
ML2	1.143	1.25	0.25	6398	80	47.180	0.234
ML7	1.143	1.75	0.25	6285	165	44.440	0.625
ML3	1.143	2.50	0.25	6934	152	45.628	0.186
ML4	1.027	1.25	0.25	6252	234	47.864	0.350
ML6	1.027	1.75	0.25	6404	71	43.786	0.270
ML5	1.027	2.50	0.25	7380	84	46.021	0.095

axial buckling for the epicadmium neutrons as a function of the location of the first data point from the source is presented in Figure 5.5. The results for the axial buckling obtained from the activation of bare gold foils have been given in Figure 2.3 and are repeated in Figure 5.6. The values of the axial buckling obtained with the activation data of cadmium-covered gold foils do not become quite constant even at 24 cm from the source, while the corresponding values obtained with the activation data of bare gold foils level off at about 15 cm from the source. The shapes of the two curves turn out to be much as expected from the qualitative discussion in section 2.4.

A sizable difference between the value of the axial buckling for the activation of bare gold foils and that for the activation of cadmium-covered gold foils is observed, in contrast to the smaller difference obtained from measurements in the corresponding full-size lattices. This result may be indicative of a nonasymptotic neutron spectrum in the miniature lattices: the subcadmium and epicadmium fluxes may not be separable in space and energy. But the investigation in section 2.3 seems to indicate that the effect of spectral inequilibrium should be too small to account for the large differences observed here in the miniature lattices. A more convincing explanation might be the loose coupling of the subcadmium neutrons and the epicadmium neutrons owing to the large neutron leakage. To see how this might come about, we apply two-group diffusion theory. The neutron balance equation is

[Neutron Leakage] + [Neutron Absorption] = [Neutron Production],

which becomes, in two-group theory,

$$-D_1\nabla^2\phi_1 + \Sigma_{a1}\phi_1 = P_1 + S_1 , \tag{5.4}$$

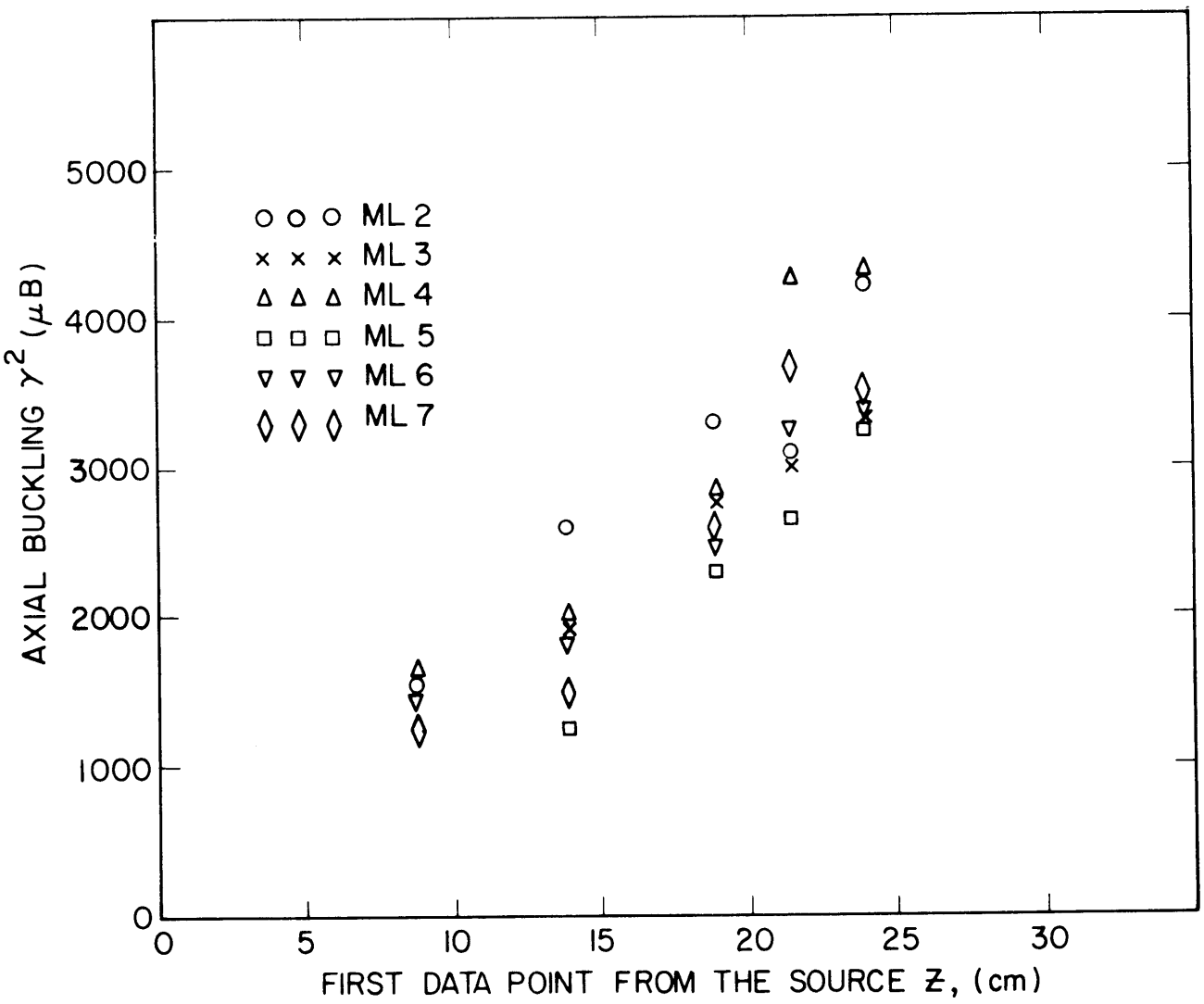

FIG. 5.5 VARIATION OF THE AXIAL BUCKLING FOR ACTIVATION DATA OF CADMIUM COVERED GOLD FOILS WITH THE FIRST DATA POINT FROM THE SOURCE OF THE MINIATURE LATTICES.

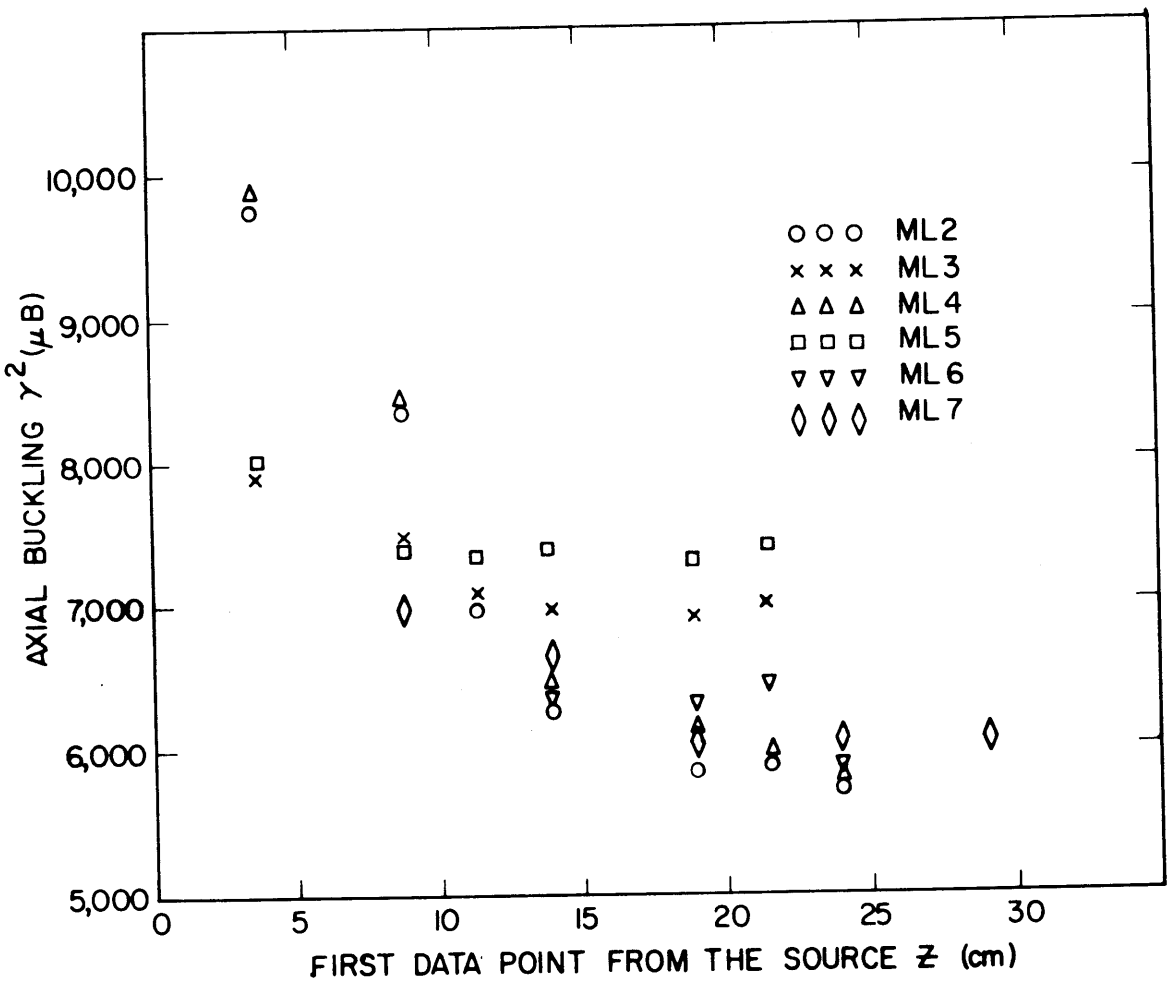

Fig. 5.6 VARIATION OF THE AXIAL BUCKLING FOR THE ACTIVATION DATA OF BARE GOLD FOILS WITH THE FIRST DATA POINT FROM THE SOURCE OF THE MINIATURE LATTICES.

and

$$-D_2\nabla^2\phi_2 + \Sigma_{a2}\phi_2 = P_2 + S_2 \ , \tag{5.5}$$

where the subscript 1 denotes the epicadmium group, the subscript 2 denotes the subcadmium group, and the constants have their usual meanings; in particular, S represents the external source and P stands for the production of neutrons due to fissions and the slowing-down process.

The coupling between the two groups of neutrons is established by the slowing-down process and fissions through the production terms P_1 and P_2. Now, if the assembly is so small that the leakage terms dominate in the neutron balance equations, ϕ_1 and ϕ_2 are loosely coupled and behave nearly independently. An analogous behavior would be expected in a highly absorbing system when the absorption terms dominate the neutron balance equation. If the assembly is both very small and highly absorbing, the two groups of neutrons may be entirely decoupled. On the other hand, if the system is sufficiently large, and if the neutron absorption is weak, the groups of neutrons are strongly coupled through the production terms; the eigenvalues corresponding to the fundamental modes for the various groups of neutrons become the same.

To show that the fast and slow neutron groups are loosely coupled in the miniature lattices, we choose ML3 for illustration:

$$\Sigma_{a2} = 0.00406 \text{ cm}^{-1} \ ,$$

$$\nu\Sigma_{f2} = 0.00493 \text{ cm}^{-1} \ ,$$

$$D_2 = 0.804 \text{ cm} \ ,$$

$$D_1 = 1.130 \text{ cm} ,$$

$$\tau_{th} = 124 \text{ cm} .$$

These numbers are taken, or derived, from the report by Sefchovich et al. (S1) except the value of D_1 which is taken from Ref. M4.

Under the assumption that fast neutrons are produced by thermal fissions alone, the production terms may be written

$$P_1 = \nu\Sigma_{f2}\phi_2 ,$$

and

$$P_2 = p\Sigma_r\phi_1 ,$$

where Σ_r is the removable cross section and p is the resonance escape probability. We can estimate the removable cross section from the expression (M1)

$$\Sigma_r = \frac{D_1}{\tau_{th}} = \frac{1.130}{124} = 0.00912 \text{ cm}^{-1} .$$

For the purpose of illustration, we choose p = 0.9. We then have the ratio of the production term to the sum of the leakage and absorption terms of the thermal group:

$$\frac{P_2}{-D_2\nabla^2\phi_2 + \Sigma_{a2}\phi_2} = \left(\frac{\phi_1}{\phi_2}\right)\left[\frac{p\Sigma_r}{\left(D_2B^2 + \Sigma_{a2}\right)}\right] \approx 0.79\left(\frac{\phi_1}{\phi_2}\right) .$$

Foil activation data obtained with bare gold foils and with cadmium-covered gold foils in the miniature lattice indicate that the ratio of the subcadmium to epicadmium activity ranges from 4 to 12 (S1):

$$\frac{\phi_1}{\phi_2} \approx 0.1 \sim 0.25,$$

and

$$\frac{P_2}{-D_2\nabla^2\phi_2 + \Sigma_{a2}\phi_2} \approx 0.079 \sim 0.197 .$$

Thus the two groups of neutrons in ML3 are indeed loosely coupled; this implies that the subcadmium group has to be supplied mainly by the external source to maintain a steady state.

5.3 THE EXTRACTION OF THE RADIAL BUCKLING

5.3.1 A Preliminary Study on the Nature of the Radial Flux Distribution in the Miniature Lattices

The radial activation distributions, measured with bare and cadmium-covered gold foils, in the miniature lattice ML7 have been shown in Figure 5.3. The experimental points agree well with the theoretical $J_o(\alpha r)$ curve for $r < 15$ cm, but deviate from the J_o function near the boundary. The deviation of the epicadmium activation distribution is greater than that of the subcadmium activation distribution. It seems evident that the subcadmium and epicadmium neutrons have different flux shapes (and hence different values of the radial buckling and extrapolated radius). We can think of at least four reasons for this:

(a) Energy Effect

The radial buckling depends on the linear extrapolation distance d through the relationship:

$$\alpha^2 = \left(\frac{2.4048}{R + d}\right)^2 , \qquad (5.6)$$

where R is the physical radius. The fact that d is a function of neutron

energy indicates that different groups of neutrons have different values of the radial buckling. Since $d_{epicm} > d_{subcd}$, $\alpha^2_{epicd} < \alpha^2_{subcd}$ as Figure 5.3 implies. This fact is practically hidden in a large assembly whose radius R is much greater than the linear extrapolation distance d, and d has little effect on the buckling. But d is important in the determination of the radial buckling in a small assembly such as a miniature lattice. To illustrate, let us take the miniature lattice ML7 as an example:

$$R = 25.40 \text{ cm},$$

$$d_{subcd} = 2.176 \text{ cm} \quad \text{(from Ref. S1)}.$$

The results obtained in Chapter IV for the linear extrapolation distance of several full-size lattices indicate that d_{epicd} can be larger than d_{subcd} by as much as 0.6 cm. If we use this value, we have

$$d_{epicd} = 2.776 \text{ cm},$$

and

$$\alpha^2_{subcd} = \left(\frac{2.4048}{25.4 + 2.176}\right)^2 = 7610 \ \mu B,$$

while

$$\alpha^2_{epicd} = \left(\frac{2.4048}{25.4 + 2.776}\right)^2 = 7300 \ \mu B.$$

The values of the radial buckling of the subcadmium and epicadmium neutrons may differ by 300 μB because of the energy dependence of the linear extrapolation distance.

(b) Reflector Effect

The miniature-lattice assembly is bare with respect to subcadmium neutrons but not with respect to epicadmium neutrons because

the tank containing the lattices was surrounded by a sheet of cadmium and two 3-inch-thick layers of paraffin (S1). (See Figure 2.1.) The effect of neutron reflection in such a case can be studied by means of the albedo concept. The linear extrapolation distance in the presence of the reflector effect is increased by a factor given by (G2)

$$\frac{(d)_{\text{reflect}}}{(d)_{\text{vacuum}}} = \frac{1 + \beta}{1 - \beta}, \tag{5.7}$$

where $(d)_{\text{vacuum}}$ is the linear extrapolation distance without neutron reflection, $(d)_{\text{reflect}}$ is that with neutron reflection, and β is the albedo defined as the ratio of the number of neutrons reflected from a medium surface to the number of neutrons incident upon it. The value of β for the miniature lattice assembly is difficult to determine. In the diffusion approximation, the albedo β is given by (A3)

$$\beta = \frac{1 - \Sigma_t L \ln (1 - 1/\Sigma_t L)}{-1 - \Sigma_t L \ln (1 - 1/\Sigma_t L)}, \tag{5.8}$$

where L is the diffusion length and Σ_t is the macroscopic total cross section. In the case of weak absorption ($\Sigma_t L \gg 1$), we may expand the logarithm and obtain the result (W7, H13)

$$\beta = 1 - \frac{4}{\sqrt{3}} \sqrt{\frac{\Sigma_a}{\Sigma_t}}, \tag{5.9}$$

where Σ_a is the macroscopic absorption cross section. For pure paraffin, $\Sigma_a/\Sigma_t = 1/180$, and $\beta = 0.827$. This value of β is actually too high because there are two sheets of cadmium and a sheet of borated plastic between the two layers of paraffin (see Fig. 2.1). The paraffin tends to soften the spectrum of fast leakage neutrons through

moderation, while the cadmium and borated plastic absorb some of the moderated leakage neutrons. Consequently, the effective value of the ratio Σ_a/Σ_t for the escape neutrons in the actual reflector would be much larger than that for pure paraffin. To estimate the value of β in our case, we plot the value of β as a function of the ratio Σ_a/Σ_t in Figure 5.7 with Eq. (5.9). The value of the albedo decreases rapidly as the neutron absorption increases. For example, suppose that the presence of the cadmium sheets and the borated plastic makes $\Sigma_a/\Sigma_t = 0.1$; then $\beta \approx 0.2$, and

$$\frac{1+\beta}{1-\beta} = \frac{1.2}{0.8} = 1.5 \ .$$

Thus we have

$$(d)_{reflect} = 1.5\,(d)_{vacuum} = 1.5 \times 2.776 = 4.16 \text{ cm},$$

and

$$\left(\alpha^2_{epicd}\right)_{reflect} = \left(\frac{2.4048}{25.4+4.16}\right)^2 = 6620\ \mu B,$$

which is about 1000 μB less than α^2_{subcd}. Although this example may overestimate the reflector effect, it indicates the importance of this effect in a small assembly. Table 5.9 gives three cases for the reflector effect; the influence is significant.

The reflection of neutrons from outside the lattice gives rise to an $I_o(\beta r)$ term in addition to the asymptotic J_o distribution (K6). We can estimate quantitatively the importance of the neutron reflection relative to the asymptotic flux by fitting the radial activation data with the function

$$\phi(r) = A[J_o(\alpha r) + cI_o(\beta r)] \qquad (5.10)$$

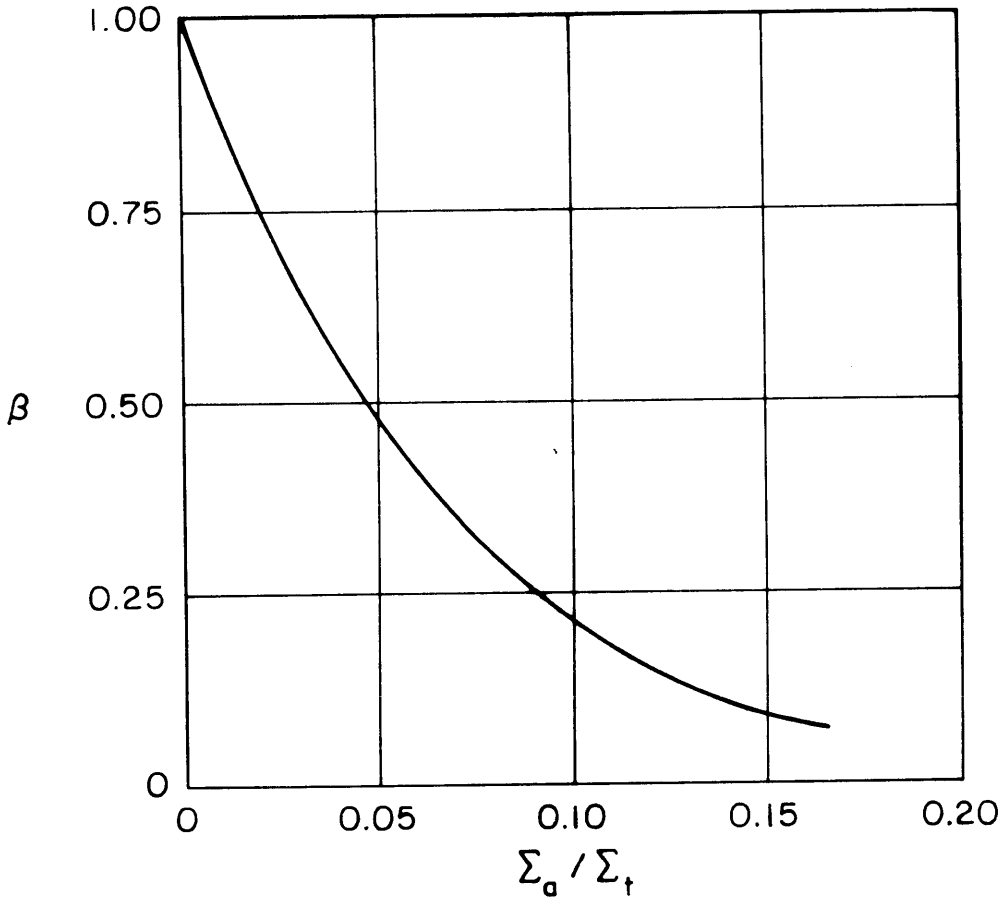

FIG. 5.7 VARIATION OF THE ALBEDO AS A FUNCTION OF THE Σ_a / Σ_t RATIO.

Table 5.9. Effect of the epicadmium neutron reflection from outside the miniature lattices on the calculation of the radial buckling for epicadmium neutrons. $\left(\alpha_{epi}\right)_{vacuum} = 2.776$ cm.

Albedo β	$\left(\alpha_{epi}\right)_{reflect}$ (cm)	$\left(\alpha^2_{epi}\right)_{reflect}$ (μB)	$\left(\alpha^2_{epi}\right)_{vacuum}$ (μB)	$\Delta\alpha^{2\,*}_{epi}$ (μB)
0.05	3.072	7100	7300	200
0.10	3.397	6970	7300	330
0.20	4.160	6620	7300	680

* $\Delta\alpha^2_{epi} = \left(\alpha^2_{epi}\right)_{vacuum} - \left(\alpha^2_{epi}\right)_{reflect}$.

by means of a least-squares technique on the basis of relative flux values; this technique is described in Appendix F. The results for the coefficient c are given in Table 5.10 for data obtained with both the bare and cadmium-covered foils. In most cases, the value of the coefficient c is about 0.05 or less but can be significant for the data points near the boundary owing to the rapid increase of the I_o function near the boundary.

Fortunately, the iterative moments method developed in Chapter IV can reduce the contribution of the harmonic modes and the I_o term through the choice of the moment index and the position of the last data point. We shall demonstrate this property of the iterative moments method in the next section by means of some numerical "experiments." In addition, transport effects near the boundary give rise to a negative I_o contribution (see section 6.3 for reference) that would cancel part of the positive I_o contribution due to the reflector effect.

(c) Transport Effects

Spatial transients may be excited in the neighborhood of boundaries due to transport effects. The effect of the spatial transients on the determination of the radial buckling will be studied quantitatively by means of the spherical harmonics method in section 6.3.3. It suffices to mention here that radial spatial transients are negative in nature and can be expressed in terms of an I_o function. The resulting spatial transients tend to reduce the reflector effect.

Table 5.10. Values of the coefficient of the I_o term relative to the fundamental mode of the radial flux distributions in the miniature lattices.

Lattice Designator	Coefficient c	
	Bare	Cd-covered
ML2	0.0032	0.0202
ML3	0.0470	0.0540
ML4	0.0005	0.0038
ML5	0.0531	0.0627
ML6	0.0023	0.0069
ML7	0.0033	0.0092

(d) Harmonic Effects

Sefchovich (S1) has shown that the source for the miniature lattice experiments contains a measurable amount of harmonics, as discussed in section 4.5. We therefore expect harmonics to be excited in the radial flux distributions of the miniature lattices. To investigate the extent of these harmonic modes, a radial harmonic analysis must be made for a cylinder. We suppose that the measured radial activation distribution $\phi(r)$ may be represented by

$$\phi(r) = \sum_{j=1}^{\infty} A_j J_o\left(\frac{\mu_j}{\tilde{R}} r\right), \tag{5.11}$$

where A_j is the coefficient of the j^{th} harmonic, and the μ_j are the roots of the transcendental equation

$$J_o(\mu_j) = 0 . \tag{5.12}$$

To estimate the coefficients A_j from the experimental activation data $\phi(r)$, we multiply both sides of Eq. (5.11) by $rJ_o\left(\frac{\mu_k}{\tilde{R}} r\right)$ and integrate over r from r = 0 to r = R:

$$\int_0^R r\phi(r)\, J_o\left(\frac{\mu_k}{\tilde{R}} r\right) dr = \sum_{j=1}^{\infty} \int_0^R A_j r\, J_o\left(\frac{\mu_j}{\tilde{R}} r\right) J_o\left(\frac{\mu_k}{\tilde{R}} r\right) dr . \tag{5.13}$$

The Bessel function J_o has the orthogonality properties (A2):

$$\int t J_o(\alpha_m t)\, J_o(\alpha_n t)\, dt = 0, \quad \text{if } m \neq n , \tag{5.14}$$

and

$$\int_0^z t J_o^2(t)\, dt = \frac{z^2}{2}\left[J_o^2(z) + J_1^2(z)\right]. \tag{5.15}$$

The right-hand side of Eq. (5.13) therefore reduces to a single term corresponding to j = k:

$$\int_0^R r\phi(r) J_o\left(\frac{\mu_k}{\tilde{R}} r\right) dr = A_k \int_0^R r J_o^2\left(\frac{\mu_k}{\tilde{R}} r\right) dr$$

$$= A_k \frac{R^2}{2} \left\{ J_o^2\left(\frac{\mu_k}{\tilde{R}} R\right) + J_1^2\left(\frac{\mu_k}{\tilde{R}} R\right) \right\} , \qquad (5.16)$$

whence

$$A_k = \frac{2}{R^2 \left[J_o^2\left(\frac{\mu_k}{\tilde{R}} R\right) + J_1^2\left(\frac{\mu_k}{\tilde{R}} R\right) \right]} \int_0^R r\phi(r) J_o\left(\frac{\mu_k}{\tilde{R}} r\right) dr ,$$

$$k = 1, 2, 3, \ldots, \infty . \qquad (5.17)$$

The value of R is arbitrary and is fixed by the choice of the last data point used for the harmonic analysis.

Since we are interested in the relative importance of the harmonic modes with respect to the fundamental, we normalize the coefficient of the fundamental so that $A_1 = 1$ and

$$\phi(r) = J_o\left(\frac{2.4048}{\tilde{R}} r\right) + \sum_{k=2}^{\infty} a_k J_o\left(\frac{\mu_k}{\tilde{R}} r\right) , \qquad (5.18)$$

where

$$a_k = \frac{A_k}{A_1} = \frac{\left[J_o^2\left(\frac{2.4048}{\tilde{R}} R\right) + J_1^2\left(\frac{2.4048}{\tilde{R}} R\right) \right]}{\left[J_o^2\left(\frac{\mu_k}{\tilde{R}} R\right) + J_1^2\left(\frac{\mu_k}{\tilde{R}} R\right) \right]} \int_0^R r\phi(r) J_o\left(\frac{\mu_k}{\tilde{R}} r\right) dr ,$$

$$k = 2, 3, 4, \ldots, \infty . \qquad (5.19)$$

The integral in Eq. (5.19) is to be evaluated numerically by means of a rectangular rule described in Figure 5.8. The RADIAL HARMONICS

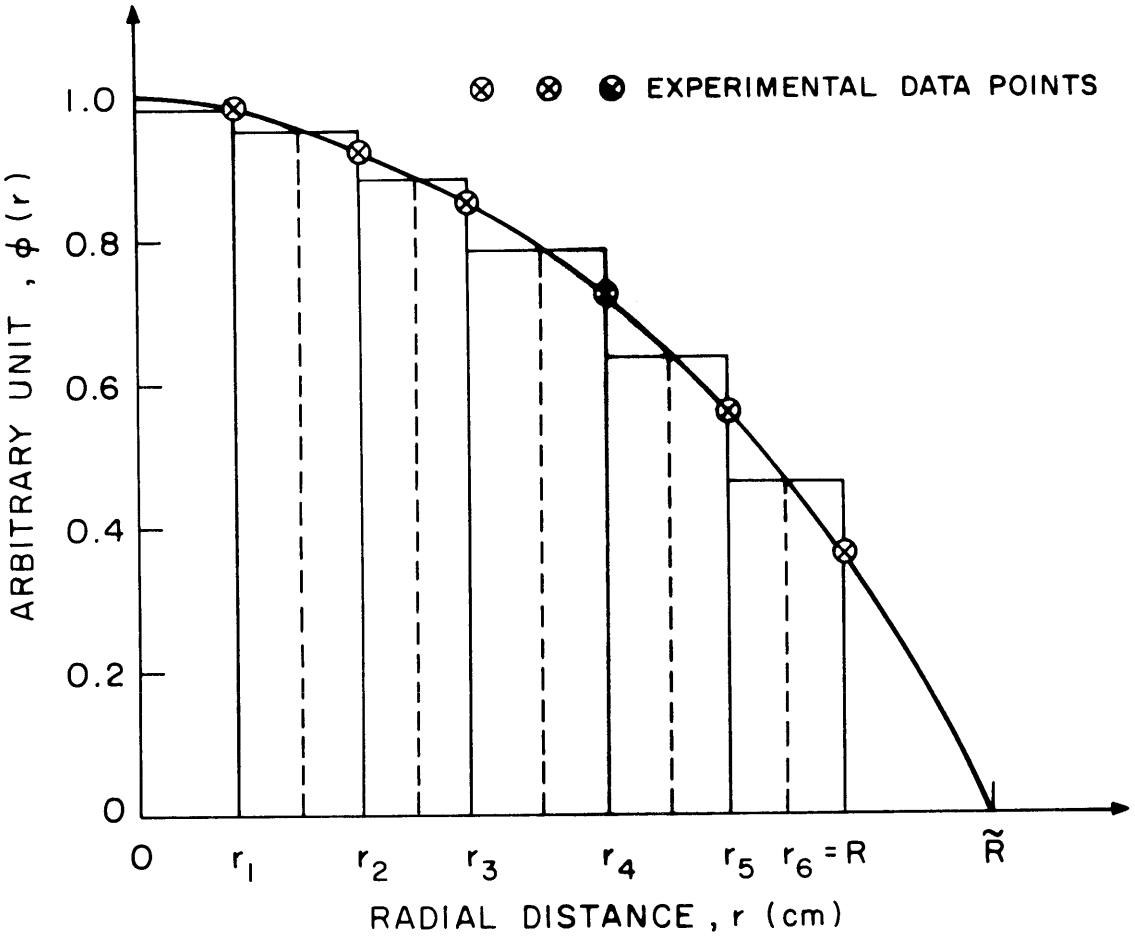

FIG. 5.8 A RECTANGULAR RULE FOR NUMERICAL INTEGRATION USED FOR THE HARMONIC ANALYSIS.

code of Sefchovich (S1), which computes the integral, has been modified according to Eq. (5.19) for the case of unequal intervals to make the harmonic analysis for the miniature lattices. The results are given in Table 5.11 for the activation of bare gold foils and in Table 5.12 for the activation of cadmium-covered gold foils. It is evident that the harmonic modes make a measurable contribution to the radial activation data obtained with both bare and cadmium-covered gold foils. For the lattices ML2, ML4, ML6, and ML7, the second, the third, and the fourth harmonics are the most significant, amounting in some cases to as much as 10 percent. For the lattices ML3 and ML5 with 2.5-inch lattice spacing, the seventh harmonic is the largest, while the fourth and sixth harmonics are also significant; the seventh harmonic may amount to about 15 percent.

To see how the harmonic modes may affect the extraction of the radial buckling from the radial flux shape, the fundamental mode as well as the first three harmonic modes of the lattice ML2 are drawn approximately to scale in Figure 5.9. The corresponding distributions of the moments of the various harmonic modes are sketched in Figure 5.10. It is evident that the harmonic moments tend to cancel one another while the fundamental moment is retained. Furthermore, the higher the order of the harmonic mode, the greater is the extent of cancellation of the moment of the mode owing to the decrease of the J_o function from cycle to cycle (W3, A2). The fact that only the higher harmonics are troublesome in the miniature lattices ML3 and ML5 probably explains the reason why the ratio of the flux moments ψ_3/ψ_1 yields a better value of the radial buckling than the ratio ψ_5/ψ_3 for ML3

Table 5.11. Values of the coefficients of the various harmonic modes relative to the fundamental mode of the bare radial activation distribution of the miniature lattices.

A_j Coefficient \ Lattice Designator	ML2	ML3	ML4	ML5	ML6	ML7
A_1	1.0000	1.0000	1.0000	1.0000	1.0000	1.0000
A_2	0.0730	0.0257	0.0700	0.0374	0.0985	0.0984
A_3	-0.0634	0.00661	-0.0640	0.00688	-0.0676	-0.0696
A_4	0.0538	0.0589	0.0538	0.0590	0.0454	0.0488
A_5	-0.0110	-0.0283	-0.00802	-0.0231	0.0093	0.0104
A_6	0.00105	0.0759	-0.000095	0.0738	0.00612	0.00084
A_7	0.0168	0.1440	0.0120	0.1454	0.0123	0.0132

Table 5.12. Values of the coefficients of the various harmonic modes relative to the fundamental mode of the epicadmium radial activation distribution of the miniature lattices.

A_j Coefficient \ Lattice Designator	ML2	ML3	ML4	ML5	ML6	ML7
A_1	1.0000	1.0000	1.0000	1.0000	1.0000	1.0000
A_2	0.0585	0.0148	0.0500	0.00339	0.0849	0.0849
A_3	-0.0656	0.0145	-0.0710	0.0155	-0.0686	-0.0637
A_4	0.0559	0.0542	0.0607	0.0628	0.0529	0.0490
A_5	-0.0105	-0.0284	-0.0082	-0.0305	0.00808	0.00664
A_6	0.00363	0.0783	0.00035	0.0752	0.00074	0.00960
A_7	0.0167	0.1387	0.0163	0.1363	0.0122	0.0110

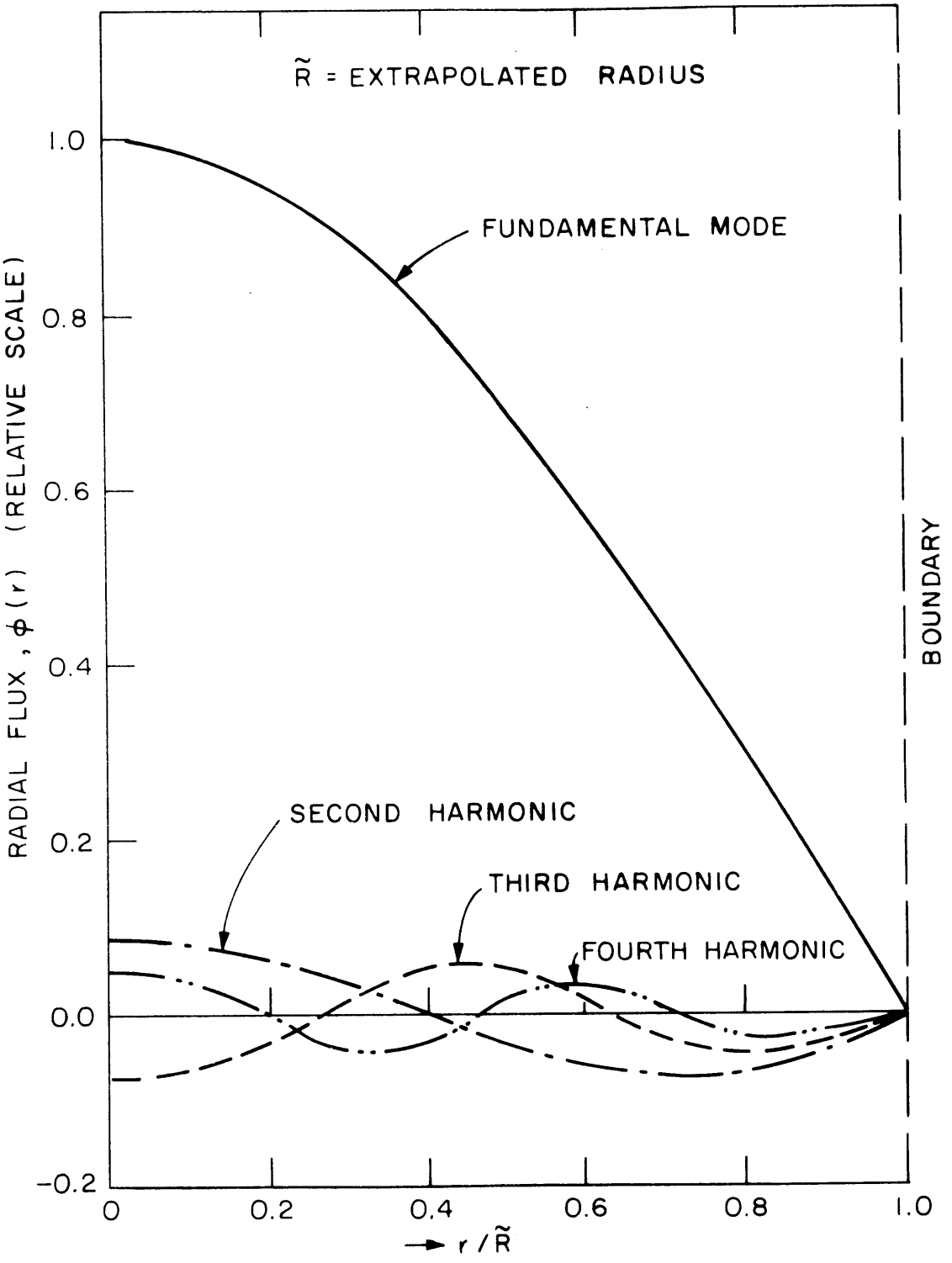

FIG. 5.9 RADIAL FLUX DISTRIBUTION OF THE FUNDAMENTAL MODE AND VARIOUS HARMONIC MODES OF THE MINIATURE LATTICE ML2. APPROXIMATELY DRAWN TO SCALE.

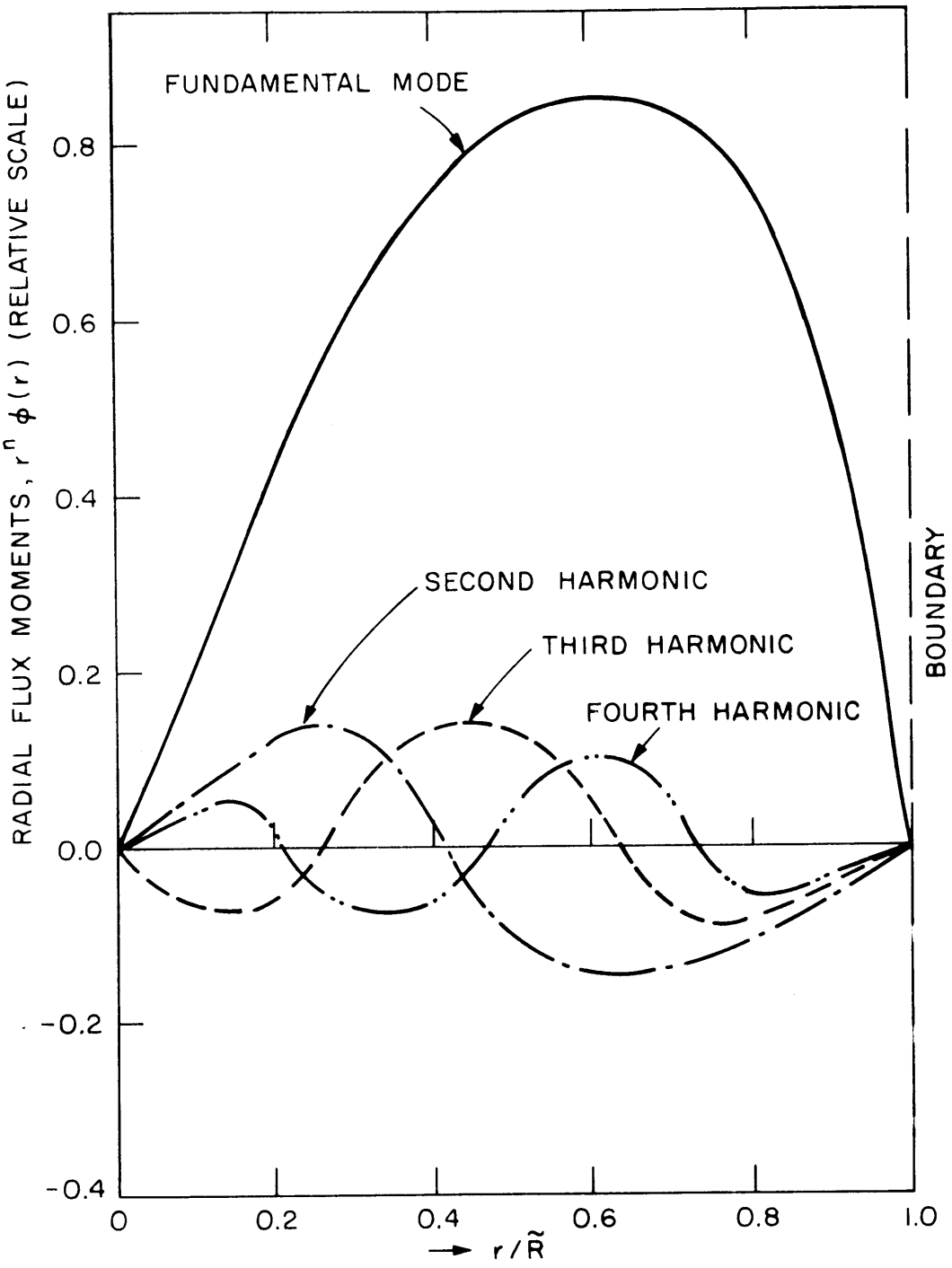

FIG. 5.10 DISTRIBUTION OF THE FLUX MOMENTS OF THE FUNDAMENTAL MODE AND THE HARMONIC MODES OF THE MINIATURE LATTICE ML2. NOTICE THAT THE AREAS UNDER THE CURVES ARE THE MOMENTS OF VARIOUS MODES.

and ML5 (as will be seen in the next section): a moment with lower index weighs the data points near the boundary less heavily than a moment with higher index. The same explanation may account for the analogous results obtained in Chapter IV for the full-size lattices: the ratio ψ_3/ψ_1 gives a better value of the radial buckling for the U-D_2O and UO_2-D_2O lattices with a triangular spacing, while the ratio ψ_5/ψ_3 yields a better value for the UO_2-D_2O lattices with a square spacing. The harmonics seem to contribute more in the case of the square lattices than in the case of the triangular lattices.

The fact that the iterative moments method involves significant cancellation of the contributions of the harmonic modes is crucial for the applicability of the method to a small assembly. We shall study this property further together with the reflector effect in section 5.3.2.

Finally, the results of the harmonic analysis are sensitive to the choice of the last data point as well as to the value of the extrapolated radius. The position of the last data point (i.e., the value of R appearing in Eq. (5.19)) determines the contribution of the harmonic modes. The results listed in Tables 5.10 and 5.11 were obtained with the use of the theoretical value of the extrapolated radius, $R = R + 0.71\lambda_{tr}$, taken from Reference S1.

5.3.2 The Reduction of the Harmonic and Reflector Effects by the Iterative Moments Method

In this section we shall test two important characteristics of the iterative moments method by means of some numerical experiments:

(a) The ability of the method to reproduce input values of the radial buckling and the extrapolated radius,

(b) The reduction of the harmonic and reflector effects.

To this end, we make up a set of artificial data with the fundamental mode alone, $J_o\left(\frac{2.4048}{\tilde{R}} r\right)$; and another set of artificial data according to the formula

$$\phi(r) = J_o\left(\frac{2.4048}{\tilde{R}} r\right) + \sum_{k=2}^{7} a_k J_o\left(\frac{\mu_k}{\tilde{R}} r\right) + c I_o(\beta r) , \qquad (5.20)$$

with $a_2 = 0.07$, $a_3 = -0.06$, $a_4 = 0.05$, $a_5 = -0.01$, $a_6 = 0.001$, $a_7 = 0.017$, $c = 0.02$, $\beta = 0.1$, and $\tilde{R} = 27.50$ cm. These values, chosen in accord with Tables 5.10, 5.11, and 5.12, are representative of the miniature lattices; so the results should be sufficient for our purpose. The two sets of artificial data are given in Table 5.13.

The RAMBLER code based on the iterative moments method described in section 4.3 has been used to analyze the two sets of artificial data. The results for the radial buckling and the extrapolated radius are given in Table 5.14 for the data from the fundamental mode alone; the results for the data including the harmonics and the reflector effect are given in Table 5.15. The exact values of the radial buckling and the extrapolated radius corresponding to the fundamental mode are also included for comparison. We see that the iterative moments method can reproduce the input values of the radial buckling and the extrapolated radius in the case of a pure J_o distribution within the practical accuracy of a computer. Furthermore, this method can also yield satisfactory values of the radial buckling and the extrapolated radius, even in the presence of the harmonic and reflector effects, when the moment index and the position of the last data point are chosen in accordance with the method developed in section 4.3.

Table 5.13. Two sets of artificial data based on Equation 5.20 and the fundamental mode.

j	r_j (cm)	$J_o\left(\frac{2.4048}{\tilde{R}} r_j\right)$	$\phi(r_j)$
1	0.00	1.000000	1.088000
2	2.54	0.987640	1.057801
3	5.08	0.951183	0.998755
4	7.62	0.892010	0.938338
5	10.16	0.811565	0.856571
6	12.70	0.714850	0.754307
7	15.24	0.600330	0.640388
8	17.78	0.480050	0.508471
9	20.32	0.351612	0.355270
10	22.86	0.223891	0.227691
11	25.40	0.099272	0.138355
12	27.50	0.000000	0.080124

Table 5.14. Values of the radial buckling and the extrapolated radius analyzed by the RAMBLER code for the artificial data based on the fundamental mode alone.

Number of Data Points Used	Position of Last Data Point (cm)	Radial* Buckling α^2 (μB)	Extrapolated** Radius $\tilde{R}$ (cm)
7	17.78	7695.3	27.414
9	22.86	7672.7	27.454
11	27.50	7663.5	27.471

* The exact value of the radial buckling is 7656.3 μB.

** The exact value of the extrapolated radius is 27.50 cm.

Table 5.15. Values of the radial buckling and the extrapolated radius analyzed by the RAMBLER code for the set of artificial data with the presence of the harmonic and reflector effects.

Number of Data Points Used	Position of Last Data Point (cm)	Radial* Buckling α^2 (μB)	Extrapolated** Radius $\tilde{R}$ (cm)
7	17.78	7582.8	27.616
9	25.40	7564.1	27.650
11	27.50	7678.7	27.443

* The exact value of the radial buckling corresponding to the fundamental mode is 7656.3 μB. The curve-fitting method yields 7817 μB.

** The exact value of the extrapolated radius corresponding to the fundamental mode is 27.50 cm.

To see if the iterative moments method extracts the asymptotic J_o function from the total radial flux distribution, another numerical experiment has been performed by deliberately describing the radial activation distribution by means of the function

$$(r) = A[J_o(\alpha r) + cJ_o(\beta r)]; \tag{5.21}$$

here α^2 is the radial buckling, β^2 is an artificially introduced "buckling" which might correspond to some harmonic mode, and c is a coefficient giving the contribution of the function $J_o(\beta r)$ relative to the desired function $J_o(\alpha r)$. An iterative moments method similar to that developed in section 4.6 for the reflector effect was used to infer α^2, β^2, and c from the experimental data. The initial value of α^2 was calculated by Eq. (4.1) and that of β^2 was chosen arbitrarily. For each chosen initial value of β^2, the following results were obtained whenever the iteration converged:

$$\beta^2 \approx \alpha^2 ,$$

and

$$c \approx 1.0 .$$

These results mean that the iterative moments method yields a single J_o function whose radial buckling is α^2 when it is applied to the analysis of the measured radial activation distribution in a miniature lattice. The results of the two numerical examples imply that the moments method does indeed have the property of reducing the effect of the harmonic modes and the reflector effect. In contrast, the curve-fitting method tends to emphasize the harmonic and the reflector effects, especially in the neighborhood of the boundary.

In conclusion, the iterative moments method developed in section 4.3 can be applied to the miniature lattices provided that the value of the moment index and the position of the last data point are varied; the best values of the radial buckling and extrapolated radius are determined by means of an error analysis as described in section 4.3.

5.3.3 Application of the Iterative Moments Method to the Miniature Lattices

The iterative moments method was chosen to extract the values of the radial buckling of the miniature lattices from the foil activation data because only a few data points are available. The RAMBLER code was used for the analysis. It turns out that the use of the ratio of the fifth to third flux moments yields a smaller probable error and hence a better value of the radial buckling for all of the miniature lattices except ML3 and ML5. For the latter, the ratio of the third to first flux moments gives a smaller probable error.

Owing to differences in the lattice spacing, eight radial data points were available for the miniature lattices ML2 and ML4, six data points for the miniature lattices ML6 and ML7, and only five data points for ML3 and ML5. In each lattice the radial activation distributions of the bare gold foils and the cadmium-covered gold foils were measured at two different axial positions: one at 6.75 inches from the source and the other at 9.75 inches from the source. One experimental run was made for each of the six lattices. For the lattices ML2 and ML4, the inner seven data points and the outer seven

data points were used in separate calculations of the radial buckling in order to remove the boundary and harmonic contributions. The results for ML2 and ML4 are given in Tables 5.16 and 5.17, respectively. A similar procedure was used for the lattices ML6 and ML7: both the inner five data points and the outer five data points were used to extract the values of the radial buckling by means of the iterative moments method. The results are given in Tables 5.18 and 5.19 for ML6 and ML7, respectively. For the lattices with 2.5-inch spacing, ML3 and ML5, all five data points were used. The results are given in Tables 5.20 and 5.21 together with the results for the other lattices; the latter values are obtained from Tables 5.16 through 5.19 by taking the average of various runs at different axial positions. Tables 5.20 and 5.21 give the best values of the radial buckling and extrapolated radius of the miniature lattices obtained by means of the iterative moments method. These values will be used to calculate the values of the material buckling in the next section. The corresponding values of the radial buckling and extrapolated radius for the subcadmium neutrons are given in Table 5.22.

The results obtained by means of the iterative moments method are consistent. The use of the ratio of the fifth moment to the third moment seems to reduce most the effect of the harmonic modes. This is indicated by the small difference between the values of the radial buckling obtained by using the outer data points and the inner data points. It seems reasonable to conclude that the harmonic modes and the reflector effect have a measurable contribution to the radial flux shapes and that the use of the iterative moments method reduces the

harmonic contribution to the extent that all the experimental data can be used; the outermost data point was only about 2 cm from the boundary.

For the purpose of comparison, we list the theoretical values of the radial buckling and extrapolated radius for the miniature lattice ML2 for thermal neutrons:

Physical radius = 25.40 cm,

Transport mean-free path, λ_{tr} = 3.534 cm (Ref. B3, p. 182),

Extrapolated radius = 27.910 cm,

Radial buckling = 7420 μB.

It is seen that the theoretical value of the radial buckling is greater than the experimental value for the bare gold foils (see Table 5.20) by about 400 μB for this lattice ML2. As a consequence, the experimental value of the extrapolated radius is approximately 1 cm larger than the theoretical value. The discrepancy is probably due to the fact that the theoretical value is only good for the thermal neutrons, while the experimental value includes both thermal and epithermal neutrons. The presence of epithermal neutrons tends to increase the extrapolated radius and hence to decrease the radial buckling. To see this, two typical sets of subcadmium data for the miniature lattice ML2 have been analyzed by the iterative moments method. The results are tabulated for convenience of discussion:

Radial Buckling (μB)	Extrapolated Radius (cm)
7310.1	28.127
7367.4	28.017

These values agree reasonably well with the theoretical value for thermal neutrons.

Significant discrepancies, ranging from 600 μB to 1200 μB, have been observed between the values of the radial buckling obtained from the activation of bare gold foils and of cadmium-covered gold foils. (Compare Tables 5.20 and 5.21.) We have shown in section 5.3.1 that the energy dependence of the linear extrapolation distance may introduce discrepancies as large as 300 μB. Another contribution may be due to differences in the reflection of subcadmium and epicadmium neutrons from the wall of the room back into the assembly containing a miniature lattice. One reason for such a difference is the presence of two thick layers of paraffin around the assembly. The contribution due to the reflection of epicadmium neutrons may be as much as 700 μB, as is shown in Table 5.9. It would seem desirable to replace the paraffin by a good absorber of epicadmium neutrons.

Table 5.16. Values of the radial buckling and the extrapolated radius of the miniature lattice ML2 calculated with the RAMBLER code based on the iterative moments method.

ML2: 1.143% enriched fuel, D_2O moderated, 1.25-inch lattice spacing.

Type of Detector	Run Number	OUTER DATA POINTS USED			INNER DATA POINTS USED		
		Radial Buckling		Extrapolated Radius	Radial Buckling		Extrapolated Radius
		α^2 (μB)	$\sigma_{\alpha 2}$* (μB)	$\tilde{R}$ (cm)	α^2 (μB)	$\sigma_{\alpha 2}$ (μB)	$\tilde{R}$ (cm)
Bare gold foils	ML2A	7124.2	0.0036	28.491	6996.6	0.0388	28.750
	ML2B	7063.0	0.0161	28.614	7868.0	0.0273	27.111
	ML2C	6919.1	0.0127	28.911	6817.4	0.0250	29.125
	ML2D	6917.9	0.0203	28.913	6896.1	0.0078	28.750
Cd-covered gold foils	ML2E	6455.1	0.0179	29.931	6381.9	0.0190	30.103
	ML2F	6480.5	0.0372	29.873	6456.8	0.0360	29.928

* The σ's are the probable errors defined in section 4.3, not the standard deviations. They are devised for the choice of the best values of the radial buckling.

Table 5.17. Values of the radial buckling and the extrapolated radius of the miniature lattice ML4 calculated with the RAMBLER code based on the iterative moments method.

ML4: 1.027% enriched fuel, D_2O moderated, 1.25-inch lattice spacing.

Type of Detector	Run Number	OUTER DATA POINTS USED			INNER DATA POINTS USED		
		Radial Buckling		Extrapolated Radius	Radial Buckling		Extrapolated Radius
		α^2 (μB)	$\sigma_{\alpha 2}$* (μB)	$\tilde{R}$ (cm)	α^2 (μB)	$\sigma_{\alpha 2}$ (μB)	$\tilde{R}$ (cm)
Bare gold foils	ML4A	7084.3	0.0053	28.571	6884.2	0.071	28.984
	ML4B	6975.6	0.022	28.793	6846.9	0.040	29.062
Cd-covered gold foils	ML4C	6585.0	0.0056	29.635	6550.3	0.059	29.713
	ML4D	6337.3	0.015	30.721	6292.6	0.033	30.315

* The σ's are the probable errors defined in section 4.3, not the standard deviations. They are devised for choosing the best values of α^2.

Table 5.18. Values of the radial buckling and the extrapolated radius of the miniature lattice ML6 calculated with the RAMBLER code based on the iterative moments method.

ML6: 1.027% enriched fuel, D_2O moderated, 1.75-inch lattice spacing.

Type of Detector	Run Number	OUTER DATA POINTS USED			INNER DATA POINTS USED		
		Radial Buckling		Extrapolated Radius	Radial Buckling		Extrapolated Radius
		α^2 (μB)	$\sigma_{\alpha 2}$* (μB)	$\tilde{R}$ (cm)	α^2 (μB)	$\sigma_{\alpha 2}$ (μB)	$\tilde{R}$ (cm)
Bare gold foils	ML6A	7267.0	0.0092	28.210	7029.6	0.014	28.682
	ML6B	7228.4	0.0101	28.285	7209.5	0.010	28.322
	ML6C	7221.8	0.0127	28.298	7192.2	0.014	28.356
Cd-covered gold foils	ML6D	6560.5	0.0102	29.690	6615.8	0.0098	29.566
	ML6E	6393.1	0.0227	30.076	6620.9	0.0076	29.554

* The σ's are the probable errors defined in section 4.3, not the standard deviations. They are devised for choosing the best values of α^2.

Table 5.19. Values of the radial buckling and the extrapolated radius of the miniature lattice ML7 calculated with the RAMBLER code based on the iterative moments method.

ML7: 1.143% enriched fuel, D_2O moderated, 1.75-inch lattice spacing.

Type of Detector	Run Number	OUTER DATA POINTS USED			INNER DATA POINTS USED		
		Radial Buckling		Extrapolated Radius	Radial Buckling		Extrapolated Radius
		α^2 (μB)	$\sigma_{\alpha 2}$* (μB)	$\tilde{R}$ (cm)	α^2 (μB)	$\sigma_{\alpha 2}$ (μB)	$\tilde{R}$ (cm)
Bare gold foils	ML7A	7107.7	0.0210	28.524	7439.9	0.0215	27.880
	ML7B	7072.3	0.0193	28.596	7427.6	0.0221	27.903
	ML7C	7195.4	0.0100	28.350	7287.6	0.0217	28.170
	ML7D	7191.1	0.0072	28.358	7222.6	0.0096	28.296
Cd-covered gold foils	ML7E	6433.3	0.0095	29.982	6070.6	0.0230	30.865
	ML7F	6393.0	0.0158	30.076	6430.0	0.0103	29.990

* The σ's are the probable errors defined in section 4.3, not the standard deviations. They are devised for the choice of the best values of the radial buckling.

Table 5.20. Average values* of the radial buckling and the extrapolated radius of the six miniature lattices calculated with the RAMBLER code for the activation of bare gold foils.

Lattice Designator	Fuel Enrichment (%)	Lattice Spacing (Inches)	Fuel Rod Diameter (Inch)	Radial Buckling α^2 (μB)	Standard Deviation ϵ_{α^2} (μB)	Extrapolated Radius $\tilde{R}$ (cm)	Standard Deviation $\epsilon_{\tilde{R}}$ (cm)
ML2	1.143	1.25	0.25	7006	52	28.732	0.107
ML7	1.143	1.75	0.25	7344.8	53	28.062	0.102
ML3	1.143	2.50	0.25	7930.4	123	27.007	0.211
ML4	1.027	1.25	0.25	7030	54	28.682	0.333
ML6	1.027	1.75	0.25	7239	14	28.264	0.027
ML5	1.027	2.50	0.25	8242.3	56	26.489	0.130

* The average of the two radial flux traverses at two different axial positions.

Table 5.21. Average values* of the radial buckling and the extrapolated radius of the six miniature lattices calculated with the RAMBLER code for the activation of cadmium-covered gold foils.

Lattice Designator	Fuel Enrichment (%)	Lattice Spacing (Inches)	Fuel Rod Diameter (Inch)	Radial Buckling α^2 (μB)	Standard Deviation ϵ_{α^2} (μB)	Extrapolated Radius $\tilde{R}$ (cm)	Standard Deviation $\epsilon_{\tilde{R}}$ (cm)
ML2	1.143	1.25	0.25	6468	13.0	29.902	0.054
ML7	1.143	1.75	0.25	6413	20.0	30.029	0.217
ML3	1.143	2.50	0.25	7291.2	–	28.163	–
ML4	1.027	1.25	0.25	6461	124	30.178	0.738
ML6	1.027	1.75	0.25	6619	2.5	29.555	0.001
ML5	1.027	2.50	0.25	7033	–	28.676	–

* The average of the two radial flux traverses at two different axial positions.

Table 5.22. Average values* of the radial buckling and the extrapolated radius of the six miniature lattices calculated with the RAMBLER code for the activation of subcadmium neutrons.

Lattice Designator	Fuel Enrichment (%)	Lattice Spacing (Inches)	Fuel Rod Diameter (Inch)	Radial Buckling α^2 (μB)	Standard Deviation $\epsilon_{\alpha 2}$ (μB)	Extrapolated Radius $\tilde{R}$ (cm)	Standard Deviation $\epsilon_{\tilde{R}}$ (cm)
ML2	1.143	1.25	0.25	7210	76	28.325	0.151
ML7	1.143	1.75	0.25	7670	65	27.462	0.128
ML3	1.143	2.50	0.25	8002	158	26.887	0.267
ML4	1.027	1.25	0.25	7188	63	28.364	0.127
ML6	1.027	1.75	0.25	7519	60	27.735	0.155
ML5	1.027	2.50	0.25	8389	42	26.256	0.100

* The average of the two radial flux traverses at two different axial positions.

5.4 THE MATERIAL BUCKLING OF THE MINIATURE LATTICES

We now obtain the values of the material buckling for the miniature lattices from the difference between the radial buckling and the axial buckling:

$$B_m^2 = \alpha^2 - \gamma^2 .$$

The results are listed in Table 5.23 for the activation data obtained with bare gold foils. The values for the corresponding full-size exponential lattices measured at the M.I.T. Lattice Project as well as those calculated by means of the two-group criticality equation (Eq. (4.111)) are also included for comparison. The agreement is good for the miniature lattices ML3, ML4, and ML5. For the other three lattices ML2, ML6, and ML7, the values of the material buckling are about 200 μB to 400 μB lower than the values for the corresponding full-size lattices. The discrepancies seem to come largely from the uncertainties in the values of the radial buckling because of the presence of the four possible effects discussed in section 5.3.1. The results presented in this chapter are derived from single measurements on each lattice and hence should be considered preliminary. More measurements are needed before the reasons for the discrepancies can be firmly established. Nevertheless, the methods of analysis developed in this report have made it possible, for the first time, to infer values of the material buckling from measurements in miniature lattices.

According to the results shown in Figure 5.5, the values of the axial buckling corresponding to the distribution of epicadmium neutrons do not approach a constant value even at 25 cm from the source.

Table 5.23. Values of the material buckling of the six miniature lattices calculated with the RAMBLER code together with the values of the corresponding full-size lattices and the two-group theoretical values.

Type of Detector	Lattice Designator	Fuel Enrichment (%)	Lattice Spacing (Inches)	Fuel Rod Diameter (Inch)	Experimental Material Buckling: Miniature Lattice B_m^2 (μB)	Experimental Material Buckling: Full-Size Lattice B_m^2 (μB)	Theoretical: Two-Group Material Buckling (μB)
Bare gold foils	ML2	1.143	1.25	0.25	1162	1444	1525
	ML7	1.143	1.75	0.25	1205	1405	1485
	ML3	1.143	2.50	0.25	946	1007	1050
	ML4	1.027	1.25	0.25	1270	1177	1400
	ML6	1.027	1.75	0.25	813	1200	1320
	ML5	1.027	2.50	0.25	948	891	960

Hence, no asymptotic value of the axial buckling can be deduced; the values given in Table 5.7 are "nonasymptotic" values. For this reason, we do not present any values of the material buckling as obtained from experimental data for epicadmium neutrons.

It is evident from Figure 5.6 that the miniature lattice assembly is large enough so that the subcadmium neutrons can attain an asymptotic distribution. The cadmium ratio is sufficiently large so that the total neutron density also seems to approach an asymptotic distribution even though the epicadmium neutrons do not. The asymptotic region is too small for the conventional curve-fitting method to be applicable but seems large enough for the moments method. Since the theoretical values of the material buckling given in Table 5.23 are actually those for the thermal neutrons, we have calculated the values of the material buckling for the subcadmium neutrons. Table 5.24 gives the results of such a calculation. The results for the 1.75-inch and 2.50-inch lattices (ML6, ML7, ML3, and ML5) agree better with the theoretical values cited as well as with the corresponding values obtained from full-size exponential lattices. For the more tightly packed lattices ML2 and ML4, the results appear to be too low primarily due to apparently larger values of the axial buckling obtained. (Compare Tables 5.6 and 5.8.)

5.5 CONCLUSIONS

In this chapter we have analyzed both the axial and radial bucklings (and hence the material buckling) of the miniature lattices by means of the moments methods developed in Chapters III and IV. The applicability of the moments methods to the miniature lattices has been

Table 5.24. Values of the material buckling for the subcadmium neutrons of the miniature lattices calculated with the RAMBLER code together with the values of the corresponding full-size lattices and the two-group theoretical values.

Lattice Designator	Fuel Enrichment (%)	Lattice Spacing (Inches)	Fuel Rod Diameter (Inch)	Experimental Material Buckling		Theoretical
				Miniature Lattice B_m^2 (μB)	Full-Size Lattice B_m^2 (μB)	Two-Group Material Buckling (μB)
ML2	1.143	1.25	0.25	812	1444	1525
ML7	1.143	1.75	0.25	1385	1405	1485
ML3	1.143	2.50	0.25	1068	1007	1050
ML4	1.027	1.25	0.25	936	1177	1400
ML6	1.027	1.75	0.25	1115	1200	1320
ML5	1.027	2.50	0.25	1009	891	960

tested by comparing the values obtained with the values of the material buckling of the corresponding full-sized exponential lattices as well as with theoretical values. The reasonably good agreement found shows that measurement of the material buckling can be made in miniature lattices, although with less precision than in a large exponential assembly. The conventional curve-fitting method cannot be used for the analysis of the data for the miniature lattices; the moments methods developed in the present work turn out to be applicable to miniature lattices as well as to full-size exponential assemblies.

For the analysis of the axial buckling of the miniature lattices, the source effect is the most troublesome. The choice of the first data point at 20 cm from the source yielded the best results for the bare-foil data in the sense that the value of the axial buckling become very nearly independent of position at this point for most of the miniature lattices; a reasonable number of data points were still available for the analysis. The values of the axial buckling for the epicadmium data did not level even at a distance of 25 cm from the source (see Figure 5.5).

On the other hand, for the analysis of the radial buckling of the miniature lattices, the harmonic and reflector effects seem to disturb the radial flux shape near the boundary. Fortunately, the iterative moments method developed in section 4.3 reduces the harmonic and reflector effects simultaneously to an important extent. Further analysis showed that the radial harmonics are more important than the reflector effect. The use of the ratio of the fifth to third flux moments instead of the ratio of the third to first flux moments for the analysis

of the radial buckling yields consistent results for all the miniature lattices except ML3 and ML5; in the latter cases, the ratio of the third to first flux moments yielded a better value of the radial buckling. The difference is probably due to differences in the relative contributions of different harmonic modes.

Chapter VI

STUDY OF THE EFFECT OF SPATIAL TRANSIENTS ON BUCKLING MEASUREMENTS BY MEANS OF THE SPHERICAL HARMONICS METHOD

6.1 INTRODUCTION

In Chapter II we mentioned that spatial transients can be excited in the neighborhood of the source and boundaries owing to the directional dependence of the neutron flux. These transients are sometimes called "current transients" (D3) and are much less persistent than the asymptotic flux – the fundamental mode.

Similarly, the nonseparability of neutron flux in space and energy can excite extraneous fluxes which are often called "energy transients" (W1, B4). These usually die out within a short distance from the source and boundaries.

The spatial and energy transients are generally negligible in a well-thermalized large assembly, but they can cause difficulties in small assemblies such as the miniature lattices. Little work has been done on the possible effects of these flux transients on the determination of buckling values from activation data by means of the flux-shape method. Hellens and Anderson (H7) made a four-group analysis of the radial buckling in water-reflected, light-water moderated, uranium metal-fueled lattices and found that energy transients can be serious in the neighborhood of the interface between the core and the reflector. Windsor (W4) demonstrated the effect of the energy transients

on the determination of the radial buckling in H_2O-U lattices and found that the energy effects start to appear when the value of the radial buckling becomes greater than about 5000 μB.

In this chapter we shall investigate the effect of the spatial transients on the determination of the buckling by means of the flux-shape method. The spherical harmonics method (C1, P6, D2, K11, N2, T1) will be applied to the miniature lattice ML3 in a one-group P_3 approximation. No attempt will be made here to study the effect of the energy transients, although further research is needed on that general problem.

6.2 THE USE OF THE SPHERICAL HARMONICS METHOD FOR THE STUDY OF SPATIAL TRANSIENTS IN THE AXIAL FLUX DISTRIBUTION

6.2.1 General Theory

This section is concerned with the solution of the time-independent, linear neutron transport equation in the z-direction:

$$\mu \frac{\partial}{\partial z} \phi(z, E, \mu) + \Sigma_t^*(z, E)\, \phi(z, E, \mu) = \int_{-1}^{1} d\mu' \int_{0}^{\infty} dE'\, \Sigma_c(z, E' \rightarrow E ; \mu_o)\, \phi(z, E', \mu') \,, \qquad (6.1)$$

where all the quantities have been defined in section 2.3 of Chapter II; the integral term combines the scattering and fission processes, and the Σ_c denotes the collision kernel. Equation (6.1) is valid under the assumption that the radial part of the neutron flux is asymptotic at the radial position where the axial flux distribution is measured. Figure 6.1 is a sketch of the experimental arrangement. The radial

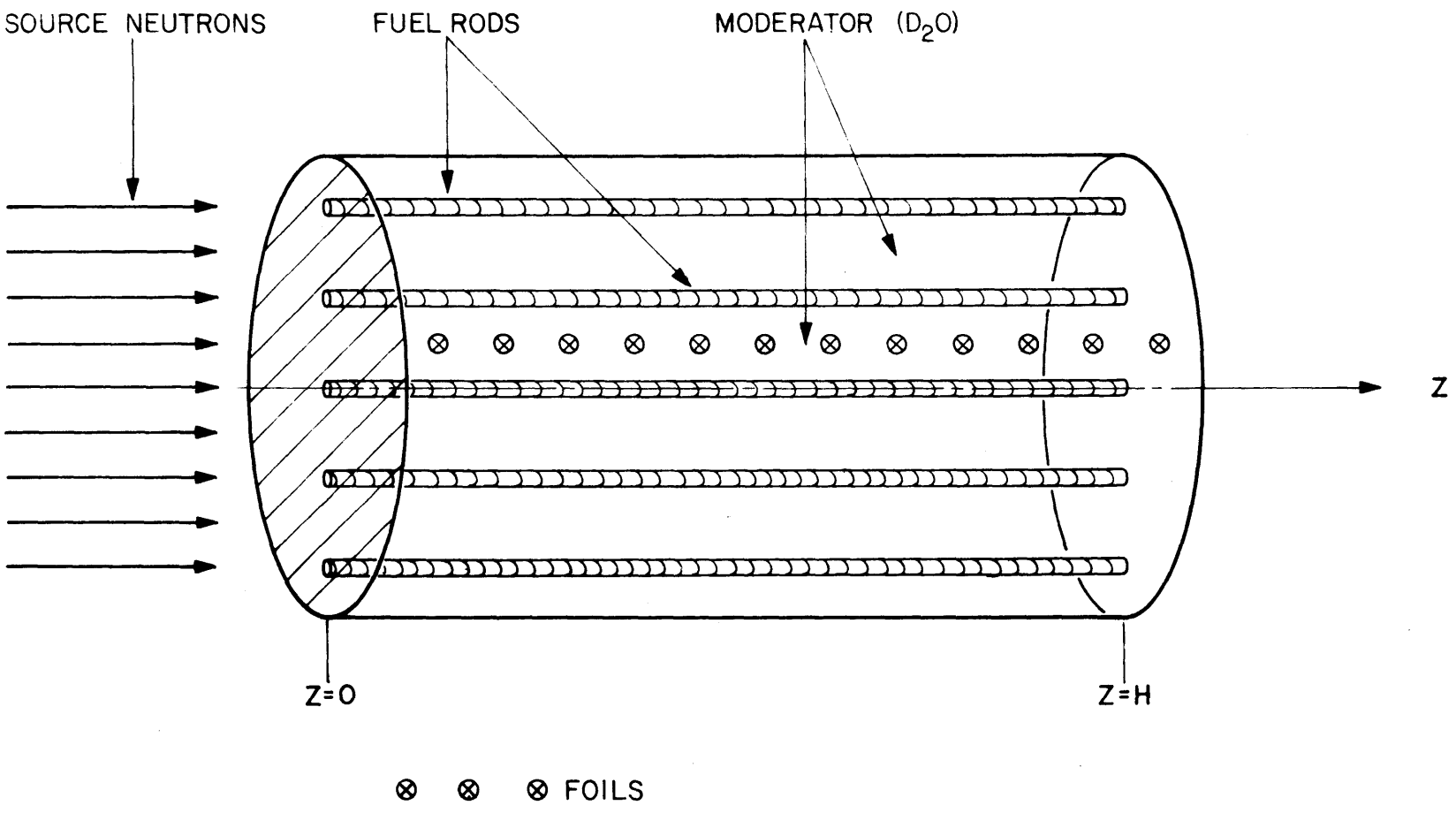

FIG. 6.1 SKETCH OF THE MINIATURE LATTICE ASSEMBLY

flux distribution is truly asymptotic at r=0; but it is practically asymptotic in the neighborhood of the axis, as we have verified in section 2.3. The external neutron source is located at z=0 and will enter as a boundary condition. The radial leakage is included in the modified total cross section Σ_t^* defined by Eq. (2.16).

Another assumption is necessary before we can solve the equation, Eq. (6.1): the medium under consideration is homogeneous and isotropic. The nuclear cross sections are then independent of position and the scattering kernel is a function of the angle $\theta_o = \cos^{-1}(\vec{\Omega}\cdot\vec{\Omega}_z)$ alone. The presence of fuel rods violates the assumption; but, if a properly homogenized set of nuclear cross sections is used for the flux calculation, and if the axial flux distribution is measured at positions in the moderator region about which the flux is symmetric, the assumption represents a good approximation.

To account for anisotropic scattering in an approximate fashion, the collision kernel $\Sigma_c(E'\to E;\mu_o)$ is expanded in a truncated series of Legendre polynomials:

$$\Sigma_c(E'\to E;\mu_o) = \sum_{m=0}^{M} \left(\frac{2m+1}{2}\right) \Sigma_{cm}(E'\to E)\, P_m(\mu_o) , \tag{6.2}$$

where, because of the orthogonality of the Legendre polynomials,

$$\Sigma_{cm}(E'\to E) = 2\pi \int_{-1}^{1} d\mu_o\, P_m(\mu_o)\, \Sigma_c(E'\to E;\mu_o) . \tag{6.3}$$

In the case of a multiplying assembly, $\Sigma_{cm}(E'\to E)$ is composed of two terms corresponding to scattering and fission, respectively:

$$\Sigma_{cm}(E'\to E) = 2\pi \int_{-1}^{1} d\mu_o \, P_m(\mu_o)\, \Sigma_s(E')\, f(E'\to E;\mu_o)$$

$$+ 2\pi \int_{-1}^{1} d\mu_o \, P_m(\mu_o)\, \nu\Sigma_f(E')\, \chi(E'\to E;\mu_o)$$

$$= \Sigma_s(E')\, f_m(E'\to E) + \nu\Sigma_f(E')\, \chi_m(E'\to E)\ ; \tag{6.4}$$

here,

$$f_m(E'\to E) = 2\pi \int_{-1}^{1} d\mu_o \, P_m(\mu_o)\, f(E'\to E;\mu_o), \tag{6.5}$$

and

$$\chi_m(E'\to E) = 2\pi \int_{-1}^{1} d\mu_o \, P_m(\mu_o)\, \chi(E'\to E;\mu_o)$$

$$= \begin{cases} \chi_o(E'\to E) & \text{for } m = 0 \\ 0 & \text{otherwise,} \end{cases} \tag{6.6}$$

because the fission neutrons are emitted isotropically. The use of the addition theorem for the Legendre polynomials (C1) together with Eqs. (6.3) and (6.1) yields the equation

$$\mu \frac{\partial}{\partial z}\, \phi(z,E,\mu) + \Sigma_t^*(E)\, \phi(z,E,\mu)$$

$$= \sum_{m=0}^{M} \left(\frac{2m+1}{2}\right) P_m(\mu) \int_{-1}^{1} d\mu' P_m(\mu') \int_{0}^{\infty} dE'\, \Sigma_{cm}(E'\to E)\, \phi(z,E',\mu')$$

$$\text{for } z > 0\ . \tag{6.7}$$

To treat the source effect, we separate the neutron flux into two parts, the uncollided flux and the collided flux:

$$\phi(z,E,\mu) = \phi^{uc}(z,E,\mu) + \phi^{c}(z,E,\mu)\ . \tag{6.8}$$

The uncollided flux satisfies Eq. (6.7) with the integral term set equal to zero:

$$\mu \frac{\partial}{\partial z}\, \phi^{uc}(z,E,\mu) + \Sigma_t^*(E)\, \phi(z,E,\mu) = 0\ . \tag{6.9}$$

The solution is

$$\phi^{uc}(z, E, \mu) = A\, e^{-\Sigma_t^*(E)z/\mu} . \tag{6.10}$$

Since the external source is very nearly unidirectional, we can express the source as

$$S(z=0, E, \mu) = Q_o S(E)\, \delta(\mu-1) , \tag{6.11}$$

where Q_o is the source intensity, and S(E) is the energy distribution of the source neutrons. The boundary condition at z=0 gives

$$A = \phi^{uc}(0, E, \mu) = Q_o S(E)\, \delta(\mu-1) . \tag{6.12}$$

The uncollided flux may then be written as

$$\phi^{uc}(z, E, \mu) = Q_o S(E)\, \delta(\mu-1)\, e^{-\Sigma_t^*(E)z/\mu} . \tag{6.13}$$

The balance equation for the collided flux can be obtained by substituting Eq. (6.8) into Eq. (6.7). The result is

$$\mu \frac{\partial}{\partial z} \phi^c(z, E, \mu) + \Sigma_t^*(E)\, \phi^c(z, E, \mu)$$

$$= \sum_{m=0}^{M} \left(\frac{2m+1}{2}\right) P_m(\mu) \int_{-1}^{1} d\mu' P_m(\mu') \int_0^{\infty} dE' \Sigma_{cm}(E' \to E)\, \phi^c(z, E', \mu')$$

$$+ \sum_{m=0}^{M} \left(\frac{2m+1}{2}\right) P_m(\mu) \int_0^{\infty} dE' \Sigma_{cm}(E' \to E)\, Q_o S(E')\, e^{-\Sigma_t^*(E')z} . \tag{6.14}$$

We see that the uncollided flux in the integral term acts as a distributed source for the collided flux.

Equation (6.14) can be solved approximately by means of several methods: for example, the multigroup P_N method, the multigroup B_N method, the multigroup S_N method. Since we are concerned with the

spatial transients caused by the directional dependence of the neutron flux, we shall use the multigroup P_N method. First, the directional flux is expanded in a series of Legendre polynomials:

$$\phi^c(z, E, \mu) = \sum_{m=0}^{\infty} \left(\frac{2m+1}{2}\right) \phi_m^c(z, E)\, P_m(\mu) \,. \tag{6.15}$$

Inserting the expansion (6.15) in Eq. (6.14), we find that

$$\sum_{m=0}^{\infty} \left(\frac{2m+1}{2}\right)\left[\mu P_m(\mu) \frac{d}{dz} \phi_m^c(z, E) + \Sigma_t^*(E)\, P_m(\mu)\, \phi_n^c(z, E)\right]$$

$$= \sum_{m=0}^{M} \left(\frac{2m+1}{2}\right)\Bigg[P_m(\mu) \int_0^{\infty} dE'\, \Sigma_{cm}(E' \to E)\, \phi_m^c(z, E')$$

$$+ P_m(\mu)\, Q_o \int_0^{\infty} dE'\, \Sigma_{cm}(E' \to E)\, S(E')\, e^{-\Sigma_t^*(E')z} \Bigg] . \tag{6.16}$$

To derive the equation for each Legendre moment, we multiply Eq. (6.16) by $P_n(\mu)$ and integrate over μ. The term in $\mu P_m(\mu)$ is eliminated by use of the recurrence formula

$$\mu P_m(\mu) = \frac{(m+1)P_{m+1}(\mu) + m P_{m-1}(\mu)}{(2m+1)} \,. \tag{6.17}$$

The orthogonality property of the Legendre polynomials,

$$\int_{-1}^{1} d\mu\, P_m(\mu)\, P_n(\mu) = \begin{cases} 0 & \text{if } m \neq n \\ \dfrac{2}{2m+1} & \text{if } m = n \,, \end{cases} \tag{6.18}$$

leads to the P_N equations

$$\frac{n+1}{2n+1}\frac{d}{dz}\phi^c_{n+1}(z,E) + \frac{n}{2n+1}\frac{d}{dz}\phi^c_{n-1}(z,E) + \Sigma^*_t(E)\,\phi^c_n(z,E)$$

$$= \int_0^\infty dE'\,\Sigma_{cn}(E'\to E)\,\phi^c_n(z,E') + Q_o\int_0^\infty dE'\,\Sigma_{cn}(E'\to E)S(E')\,e^{-\Sigma^*_t(E')z},$$

$$(0 \leq n < \infty)\,. \qquad (6.19)$$

An approximate solution is obtained by truncating this infinite set of equations by setting

$$\phi^c_n(z,E) = 0\,, \quad (n > N)\,. \qquad (6.20)$$

The multigroup treatment of the energy dependence of the neutron flux consists in dividing the energy scale into a finite number of energy groups and in defining the n^{th} Legendre moment of the g^{th}-group directional flux as

$$\phi^c_{n,g}(z) \equiv \int_{E_g}^{E_{g-1}} dE\,\phi^c_n(z,E)\,, \qquad (6.21)$$

where $E_g \leq E \leq E_{g-1}$ for the g^{th} group. Thus, if we integrate Eq. (6.19) over E from E_g to E_{g-1}, we arrive at the multigroup P_N equations

$$\frac{n+1}{2n+1}\frac{d}{dz}\phi^c_{n+1,g}(z) + \frac{n}{2n+1}\frac{d}{dz}\phi^c_{n-1,g}(z) + \Sigma^{*g}_t\,\phi^c_{n,g}(z)$$

$$= \sum_{g'=1}^{G}\Sigma^{gg'}_{cn}\,\phi^c_{n,g'}(z) + Q_o\sum_{g'=1}^{G}\Sigma^{gg'}_{cn}\,S^{g'}\,e^{-\Sigma^{*g'}_t z}\,, \quad (0\leq n\leq N\,;\,1\leq g\leq G)\,, \qquad (6.22)$$

where G represents the total number of energy groups, N is the order of the P_N approximation, and S^g is the fraction of source neutrons that are in the g^{th} group. The calculation of the group constants has recently been discussed by Pomraning (P6). In general, these constants are

weighted flux averages of the quantities of interest in a particular group. The weight function is sometimes chosen as the adjoint flux. The choice of unity as the weight function leads to the following expressions for the group constants:

$$\Sigma_t^{*g} = \frac{\int_{E_g}^{E_{g-1}} dE\ \Sigma_t^*(E)\ \phi_n^c(E)}{\int_{E_g}^{E_{g-1}} dE\ \phi_n^c(E)} , \tag{6.23}$$

and

$$\Sigma_{cn}^{gg'} = \frac{\int_{E_g}^{E_{g-1}} dE \int_{E_{g'}}^{E_{g'-1}} dE'\ \Sigma_{cn}(E'\to E)\ \phi_n^c(E')}{\int_{E_{g'}}^{E_{g'-1}} dE'\ \phi_n^c(E')} . \tag{6.24}$$

Since the conventional flux shape method for analyzing buckling measurements is based on the total flux distribution, we shall focus on the calculation of the integral quantity for the g^{th} energy group,

$$\begin{aligned}\Phi_g^c(z) &\equiv \int_{-1}^{1} \phi_g^c(z,\mu)\ d\mu \\ &= \int_{-1}^{1} \sum_{m=0}^{\infty} \left(\frac{2m+1}{2}\right) \phi_{m,g}^c(z)\ P_m(\mu)\ d\mu \\ &= \phi_{0,g}^c(z) , \qquad 1 \leq g \leq G ,\end{aligned} \tag{6.25}$$

owing to the orthogonality of the Legendre polynomials Eq. (6.18). Hence, the calculation of the total neutron flux is identical to the calculation of the zeroth Legendre moment of the directional flux.

By spatial transients we mean the extraneous contributions to the asymptotic flux that arise from transport effects near the

source and boundaries. Examples are the additional solutions, other than the fundamental, to the balance equation for the zeroth moment of the Legendre polynomials in the P_N approximation. With this definition of the spatial transients, the multigroup P_N equations we have derived can be used to calculate the spatial transients as well as the eigenvalues corresponding to the spatial transients for each energy group. Such a calculation should help us understand some of the problems associated with the flux shape method for the analysis of the axial buckling or, equivalently, of the relaxation length. To show this, we consider the P_N approximation with N odd. The equations (6.22) for the g^{th} group can be rewritten in the form

$$\frac{d}{dz}\phi^c_{1,g}(z)+\Sigma^{*g}_t\phi^c_{0,g}(z)=\sum_{g'=1}^{G}\Sigma^{gg'}_{c0}\phi^c_{0,g'}(z)+Q_o\sum_{g'=1}^{G}\Sigma^{gg'}_{c0}S^{g'}e^{-\Sigma^{*g'}_t z}$$

$$\frac{2}{3}\frac{d}{dz}\phi^c_{2,g}(z)+\frac{1}{3}\frac{d}{dz}\phi^c_{0,g}(z)+\Sigma^{*g}_t\phi^c_{1,g}(z)=\sum_{g'=1}^{G}\Sigma^{gg'}_{c1}\left[\phi^c_{1,g'}(z)+Q_oS^{g'}e^{-\Sigma^{*g'}_t z}\right]$$

$$\frac{3}{5}\frac{d}{dz}\phi^c_{3,g}(z)+\frac{2}{5}\frac{d}{dz}\phi^c_{1,g}(z)+\Sigma^{*g}_t\phi^c_{2,g}(z)=\sum_{g'=1}^{G}\Sigma^{gg'}_{c2}\left[\phi^c_{2,g'}(z)+Q_oS^{g'}e^{-\Sigma^{*g'}_t z}\right]$$

$$\vdots \qquad\qquad \vdots$$

$$\frac{N}{2N-1}\frac{d}{dz}\phi^c_{N,g}(z)+\frac{N-1}{2N-1}\frac{d}{dz}\phi^c_{N-2,g}(z)+\Sigma^{*g}_t\phi^c_{N-1,g}(z)$$

$$=\sum_{g'=1}^{G}\Sigma^{gg'}_{cN-1}\left[\phi^c_{N-1,g'}(z)+Q_oS^{g'}e^{-\Sigma^{*g'}_t z}\right]$$

$$\frac{N}{2N+1}\frac{d}{dz}\phi^c_{N-1,g}(z)+\Sigma^{*g}_t\phi^c_{N,g}(z)=\sum_{g'=1}^{G}\Sigma^{gg'}_{cN}\left[\phi^c_{N,g'}(z)+Q_oS^{g'}e^{-\Sigma^{*g'}_t z}\right].$$

(6.26)

The elimination of all the higher Legendre moments except the zeroth in the g^{th} group as well as all the Legendre moments in the other groups yields an ordinary differential equation of order (2G+N+1) for $\phi^c_{0,g}(z)$. This equation may be written in the form

$$a_o \frac{d^n}{dz^n} \phi^c_{0,g}(z) + a_1 \frac{d^{n-1}}{dz^{n-1}} \phi^c_{0,g}(z) + a_2 \frac{d^{n-2}}{dz^{n-2}} \phi^c_{0,g}(z) + \ldots + a_n \phi^c_{0,g}(z) = f(z) \ , \tag{6.27}$$

where $N = 2G+N+1$, and the coefficients a_i's are made up of the group constants. The inhomogeneous term f(z) comes from the external source contribution. The axial buckling or the relaxation length, characteristic of the assembly of interest, is determined by the coefficients a_i's through the characteristic equation of the scalar flux $\phi^c_{0,g}(z)$

$$a_o \gamma^n + a_1 \gamma^{n-1} + \ldots + a_{n-1} \gamma + a_n = 0 \ , \tag{6.28}$$

where the value of γ^2 that corresponds to the most persistent mode is the axial buckling (to be inferred by means of the flux shape method) and the corresponding value of γ^{-1} is the relaxation length. Notice that $n = 2G+N+1$ is always an even number when N is odd, so that Eq. (6.28) can be solved for γ^2 directly. The values of γ always appear in pairs: for a positive value of γ there exists always a negative value of γ with the same magnitude. This result also implies the existence of a solution of the type

$$\left(c_1 e^{-\gamma z} + c_2 e^{\gamma z}\right) = A \sinh \gamma(\tilde{H}-z) \ .$$

There are $\left(\frac{2G+N+1}{2}\right)$ solutions of this type for the flux $\phi^c_{0,g}(z)$; the

most persistent one is the asymptotic solution, often called the fundamental mode; we denote the corresponding eigenvalue by γ_1. The solutions corresponding to the characteristic equation (6.28) are the homogeneous solutions for $\phi^c_{0,g}(z)$; there is also a particular solution corresponding to the inhomogeneous term f(z). The complete solution for $\phi^c_{0,g}(z)$ can be written in the general form:

$$\phi^c_{0,g}(z) = A_1 \sinh \gamma_1(\tilde{H}_1 - z) + \sum_{i=2}^{\left(\frac{2G+N+1}{2}\right)} A_i \sinh \gamma_i(\tilde{H}_i - z) + p(z)$$

$$= [\text{Asymptotic Flux}] + [\text{Spatial Transients}]$$

$$+ [\text{Source Neutron Contribution}] . \qquad (6.29)$$

6.2.2 The Boundary Conditions

The specification of the boundary conditions for obtaining the complete solution of the type Eq. (6.29) is crucial and difficult. The usual zero-flux boundary conditions at both ends of the assembly are not enough to permit the determination of all the coefficients that appear in Eq. (6.29). If we next consider just the collided flux and assume that the directional collided flux vanishes at the boundaries, the exact boundary conditions are

$$\phi^c_g(0,\mu) = 0 \quad \text{for } \mu > 0 , \qquad (6.30)$$

and

$$\phi^c_g(H,\mu) = 0 \quad \text{for } \mu < 0 . \qquad (6.31)$$

These two equations provide an infinite number of conditions (since there are infinitely many possible values of μ) which cannot be all

exactly satisfied in an approximation of finite order. We shall therefore use Marshak's boundary conditions (D2):

$$\int_0^1 \phi_g^c(0,\mu)\, P_{2n-1}(\mu)\, d\mu = 0 \quad \text{at } z = 0 , \tag{6.32}$$

and

$$\int_{-1}^0 \phi_g^c(H,\mu)\, P_{2n-1}(\mu)\, d\mu = 0 \quad \text{at } z = H , \tag{6.33}$$

where $n = 1, 2, 3, \ldots, \frac{1}{2}(N+1)$. It is evident that there are just enough boundary conditions for the determination of the coefficients in a P_N approximation.

6.2.3 A One-Group P_3 Approximation

We wish, at this point, to separate the problem of the spatial transients from that of the energy transients. We shall, therefore, reduce the number of energy groups to one, and treat the spatial problem for the case of monoenergetic neutrons. For exploratory purposes, and to keep the problem amenable to analytic treatment, we shall use the lowest order P_n approximation that will help us understand the transport effects, namely, the P_3 approximation. Hence, we shall derive expressions for the axial buckling, the total axial flux distribution, the extrapolated height, and the geometric buckling in the one-energy group, P_3 approximation.

Equation (6.22) for $G = 1$ and $N = 3$ gives the following set of equations:

$$\frac{d}{dz}\phi_1^c(z) + (\Sigma_t^* - \Sigma_{co})\phi_o^c(z) = Q_o\Sigma_{co}\, e^{-\Sigma_t^* z}$$

$$\frac{2}{3}\frac{d}{dz}\phi_2^c(z) + \frac{1}{3}\frac{d}{dz}\phi_o^c(z) + (\Sigma_t^* - \Sigma_{c1})\phi_1^c(z) = Q_o\Sigma_{c1}\, e^{-\Sigma_t^* z}$$

$$\frac{3}{5}\frac{d}{dz}\phi_3^c(z) + \frac{2}{5}\frac{d}{dz}\phi_1^c(z) + (\Sigma_t^* - \Sigma_{c2})\phi_2^c(z) = Q_o\Sigma_{c2}\, e^{-\Sigma_t^* z}$$

$$\frac{3}{7}\frac{d}{dz}\phi_2^c(z) + (\Sigma_t^* - \Sigma_{c3})\phi_3^c(z) = Q_o\Sigma_{c3}\, e^{-\Sigma_t^* z}\,, \tag{6.34}$$

where

$$\Sigma_{cn} \equiv f_n\Sigma_s + \chi_n\nu\Sigma_f\,, \tag{6.35}$$

$$\chi_n \equiv \begin{cases} 1 & \text{for } n = 0 \\ 0 & \text{otherwise}\,, \end{cases}$$

and

$$f_n \equiv \int_{-1}^{1} d\mu_o\, f(\mu_o)\, P_n(\mu_o)\,; \tag{6.36}$$

in particular, $f_o = 1$ and $f_1 = \overline{\mu_o}$. If the scattering is not strongly anisotropic, we may assume that $f_n = 0$ for $n \geq 2$. Under this assumption, the elimination of $\phi_1^c(z)$, $\phi_2^c(z)$, and $\phi_3^c(z)$ from Eq. (6.34) yields a fourth-order differential equation for the scalar flux $\phi_o^c(z)$:

$$\frac{d^4}{dz^4}\phi_o^c(z) - a\frac{d^2}{dz^2}\phi_o^c(z) + b\phi_o^c(z) = f(z)\,, \tag{6.37}$$

where

$$f(z) = \frac{35}{9}\Sigma_t^* Q_o\, e^{-\Sigma_t^* z}\left\{-\frac{4}{5}\left(\Sigma_t^*\right)^2(\nu\Sigma_f + \Sigma_s) + \frac{78}{35}\Sigma_t^*[\overline{\mu_o}\,\Sigma_s\Sigma_t^* + \Sigma_{tr}(\nu\Sigma_f + \Sigma_s)]\right\}\,, \tag{6.38}$$

$$a = \frac{35}{9}\left(\Sigma_t^*\right)^2 + 3\Sigma_{tr}(\Sigma_a - \nu\Sigma_f) + \frac{28}{9}\Sigma_t^*(\Sigma_a - \nu\Sigma_f)\,, \tag{6.39}$$

and

$$b = \frac{35}{3}\,\Sigma_{tr}\left(\Sigma_t^*\right)^2(\Sigma_a - \nu\Sigma_f)\ . \tag{6.40}$$

A. The Axial Buckling

For the homogeneous solution of Eq. (6.37), we seek a solution of the form $e^{\gamma z}$ where γ satisfies the characteristic equation

$$\gamma^4 - a\gamma^2 + b = 0\ , \tag{6.41}$$

or

$$\gamma^2 = \frac{1}{2}\left[a \pm \sqrt{a^2 - 4b}\ \right]. \tag{6.42}$$

The value of γ^2 with smaller magnitude is the asymptotic axial buckling; the other value of γ^2 is the eigenvalue corresponding to the transient flux. The complete solution for the flux $\phi_o^c(z)$ is given by

$$\phi_o^c(z) = S_o e^{-\Sigma_t^* z} + A_1 e^{\gamma_1 z} + A_2 e^{-\gamma_1 z} + A_3 e^{\gamma_3 z} + A_4 e^{-\gamma_3 z}\ , \tag{6.43}$$

where

$$\gamma_1^2 = \frac{1}{2}\left[a - \sqrt{a^2 - 4b}\ \right],\ \text{asymptotic axial buckling}\ , \tag{6.44}$$

$$\gamma_3^2 = \frac{1}{2}\left[a + \sqrt{a^2 - 4b}\ \right],\ \text{transient axial buckling}\ , \tag{6.45}$$

and

$$S_o = \frac{\frac{35}{9}\,Q_o(\Sigma_t^*)^2}{\left(\Sigma_t^{*4} - a\Sigma_t^{*2} + b\right)} - \frac{4}{5}\,\Sigma_t^*(\nu\Sigma_f + \Sigma_s) + \frac{78}{35}\left[\overline{\mu_o}\Sigma_s\Sigma_t^* + \Sigma_{tr}(\nu\Sigma_f + \Sigma_s)\right]\ . \tag{6.46}$$

The coefficients A_i are to be determined by the boundary conditions. The use of Eqs. (6.32) and (6.33) for n = 1 and 2 yields the following four boundary conditions:

$$\phi_o^c(0) + 2\phi_1^c(0) + \frac{5}{4}\phi_2^c(0) = 0 , \tag{6.47}$$

$$\phi_o^c(0) - 5\phi_2^c(0) - 8\phi_3^c(0) = 0 , \tag{6.48}$$

$$\phi_o^c(H) - 2\phi_1^c(H) + \frac{5}{4}\phi_2^c(H) = 0 , \tag{6.49}$$

$$\phi_o^c(H) - 5\phi_2^c(H) + 8\phi_3^c(H) = 0 . \tag{6.50}$$

It is seen that the determination of the coefficients by means of Marshak's boundary conditions requires the knowledge of the higher Legendre moments. However, the solutions for ϕ_1^c, ϕ_2^c, and ϕ_3^c can be obtained readily through Eq. (6.34):

$$\phi_1^c(z) = -(\Sigma_a - \nu\Sigma_f)\left[\frac{A_1}{\gamma_1} e^{\gamma_1 z} - \frac{A_2}{\gamma_1} e^{-\gamma_1 z} + \frac{A_3}{\gamma_3} e^{\gamma_3 z} - \frac{A_4}{\gamma_3} e^{-\gamma_3 z}\right]$$

$$+ \left[S_o(\Sigma_a - \nu\Sigma_f) - Q_o(\nu\Sigma_f + \Sigma_s)\right] \frac{1}{\Sigma_t^*} e^{-\Sigma_t^* z} , \tag{6.51}$$

$$\phi_2^c(z) = -\frac{M}{\gamma_1}\left(A_1 e^{\gamma_1 z} + A_2 e^{-\gamma_1 z}\right) - \frac{N}{\gamma_3}\left(A_3 e^{\gamma_3 z} + A_4 e^{-\gamma_3 z}\right) - \frac{P}{\Sigma_t^*} e^{-\Sigma_t^* z} , \tag{6.52}$$

and

$$\phi_3^c(z) = \frac{3}{7}\frac{1}{\Sigma_t^*}\left[M\left(A_1 e^{\gamma_1 z} - A_2 e^{-\gamma_1 z}\right) + N\left(A_3 e^{\gamma_3 z} - A_4 e^{-\gamma_3 z}\right)\right] - \frac{3}{7}\cdot\frac{P}{\Sigma_t^*} e^{-\Sigma_t^* z} , \tag{6.53}$$

where

$$M = \frac{1}{2}\left[\gamma_1 - 3\frac{\Sigma_{tr}}{\gamma_1}(\Sigma_a - \nu\Sigma_f)\right] , \tag{6.54}$$

$$N = \frac{1}{2}\left[\gamma_3 - 3\,\frac{\Sigma_{tr}}{\gamma_3}\,(\Sigma_a - \nu\Sigma_f)\right] , \tag{6.55}$$

$$P = Q_o\left[\frac{3}{2}\,\overline{\mu_o}\,\Sigma_s + \frac{3}{2}\,\frac{\Sigma_{tr}}{\Sigma_t^*}\,(\nu\Sigma_f + \Sigma_s)\right] + \frac{1}{2}\,\Sigma_t^*\,S_o , \tag{6.56}$$

and S_o is given by Eq. (6.46). Substitution of Eqs. (6.43), (6.51), (6.52), and (6.53) into Eqs. (6.47) through (6.50) gives four simultaneous equations for the four unknowns A_1, A_2, A_3, and A_4:

$$A_1\lambda_1 e^{\gamma_1 H} + A_2\lambda_2 e^{-\gamma_1 H} + A_3\lambda_3 e^{\gamma_3 H} + A_4\lambda_4 e^{-\gamma_3 H} = q_1 e^{-\Sigma_t^* H} ,$$

$$A_1\rho_1 e^{\gamma_1 H} + A_2\rho_2 e^{-\gamma_1 H} + A_3\rho_3 e^{\gamma_3 H} + A_4\rho_4 e^{-\gamma_3 H} = q_2 e^{-\Sigma_t^* H} ,$$

$$A_1\lambda_2 + A_2\lambda_1 + A_3\lambda_4 + A_4\lambda_3 = q_3 ,$$

$$A_1\rho_2 + A_2\rho_1 + A_3\rho_4 + A_4\rho_3 = q_4 , \tag{6.57}$$

where

$$\lambda_1 = \left[1 - \frac{2}{\gamma_1}\,(\nu\Sigma_f - \Sigma_a) - \frac{5}{4}\,\frac{M}{\gamma_1}\right] , \tag{6.58}$$

$$\lambda_2 = \left[1 + \frac{2}{\gamma_1}\,(\nu\Sigma_f - \Sigma_a) - \frac{5}{4}\,\frac{M}{\gamma_1}\right] , \tag{6.59}$$

$$\lambda_3 = \left[1 - \frac{2}{\gamma_3}\,(\nu\Sigma_f - \Sigma_a) - \frac{5}{4}\,\frac{N}{\gamma_3}\right] , \tag{6.60}$$

$$\lambda_4 = \left[1 + \frac{2}{\gamma_3}\,(\nu\Sigma_f - \Sigma_a) - \frac{5}{4}\,\frac{N}{\gamma_3}\right] , \tag{6.61}$$

$$\rho_1 = \left[1 + 5\,\frac{M}{\gamma_1} + \frac{24}{7}\,\frac{M}{\Sigma_t^*}\right] , \tag{6.62}$$

$$\rho_2 = \left[1 + 5\,\frac{M}{\gamma_1} - \frac{24}{7}\,\frac{M}{\Sigma_t^*}\right] , \tag{6.63}$$

$$\rho_3 = \left[1 + 5 \frac{N}{\gamma_3} + \frac{24}{7} \frac{N}{\Sigma_t^*} \right], \tag{6.64}$$

$$\rho_4 = \left[1 + 5 \frac{N}{\gamma_3} - \frac{24}{7} \frac{N}{\Sigma_t^*} \right], \tag{6.65}$$

$$q_1 = 2\left[\frac{(\Sigma_a - \nu\Sigma_f)}{\Sigma_t^*} - 1 \right] S_o - 2 \frac{(\nu\Sigma_f + \Sigma_s)}{\Sigma_t^*} Q_o + \frac{5}{4} \frac{P}{\Sigma_t^*}, \tag{6.66}$$

$$q_2 = -\left[\frac{11}{7} \frac{P}{\Sigma_t^*} + S_o \right], \tag{6.67}$$

$$q_3 = -\left[2 \frac{(\Sigma_a - \nu\Sigma_f)}{\Sigma_t^*} + 1 \right] S_o + 2 \frac{(\nu\Sigma_f + \Sigma_s)}{\Sigma_t^*} Q_o + \frac{5}{4} \frac{P}{\Sigma_t^*}, \tag{6.68}$$

$$q_4 = -\left[\frac{59}{7} \frac{P}{\Sigma_t^*} + S_o \right]. \tag{6.69}$$

The set of simultaneous equations Eq. (6.57) can be solved for the A_i by means of Cramer's rule. The results may be written in the form

$$A_i = \frac{\Delta_i}{\Delta} \qquad (i = 1, 2, 3, 4), \tag{6.70}$$

where

$$\Delta = \begin{vmatrix} \lambda_1 e^{\gamma_1 H} & \lambda_2 e^{-\gamma_1 H} & \lambda_3 e^{\gamma_3 H} & \lambda_4 e^{-\gamma_3 H} \\ \rho_1 e^{\gamma_1 H} & \rho_2 e^{-\gamma_1 H} & \rho_3 e^{\gamma_3 H} & \rho_4 e^{-\gamma_3 H} \\ \lambda_2 & \lambda_1 & \lambda_4 & \lambda_3 \\ \rho_2 & \rho_1 & \rho_4 & \rho_3 \end{vmatrix}$$

$$\approx -(\lambda_1\rho_3 - \lambda_3\rho_1)^2 e^{(\gamma_1+\gamma_3)H} + (\lambda_2\rho_3 - \lambda_3\rho_2)^2 e^{(\gamma_3-\gamma_1)H}, \tag{6.71}$$

$$\Delta_1 = \begin{vmatrix} q_1 e^{-\Sigma_t^* H} & \lambda_2 e^{-\gamma_1 H} & \lambda_3 e^{\gamma_3 H} & \lambda_4 e^{-\gamma_3 H} \\ q_2 e^{-\Sigma_t^* H} & \rho_2 e^{-\gamma_1 H} & \rho_3 e^{\gamma_3 H} & \rho_4 e^{-\gamma_3 H} \\ q_3 & \lambda_1 & \lambda_4 & \lambda_3 \\ q_4 & \rho_1 & \rho_4 & \rho_3 \end{vmatrix}$$

$$\approx (\lambda_2\rho_3 - \lambda_3\rho_2)(q_3\rho_3 - q_4\lambda_3)\, e^{(\gamma_3-\gamma_1)H}$$

$$+ (\lambda_1\rho_3 - \lambda_3\rho_1)(q_2\lambda_3 - q_1\rho_3)\, e^{(\gamma_3-\Sigma_t^*)H}, \qquad (6.72)$$

$$\Delta_2 = \begin{vmatrix} \lambda_1 e^{\gamma_1 H} & q_1 e^{-\Sigma_t^* H} & \lambda_3 e^{\gamma_3 H} & \lambda_4 e^{-\gamma_3 H} \\ \rho_1 e^{\gamma_1 H} & q_2 e^{-\Sigma_t^* H} & \rho_3 e^{\gamma_3 H} & \rho_4 e^{-\gamma_3 H} \\ \lambda_2 & q_3 & \lambda_4 & \lambda_3 \\ \rho_2 & q_4 & \rho_4 & \rho_3 \end{vmatrix}$$

$$\approx (\lambda_1\rho_3 - \lambda_3\rho_1)(q_3\rho_3 - q_4\lambda_3)\, e^{(\gamma_1+\gamma_3)H}$$

$$+ (\lambda_2\rho_3 - \lambda_3\rho_2)(q_1\rho_3 - q_2\lambda_3)\, e^{(\gamma_3-\Sigma_t^*)H}, \qquad (6.73)$$

$$\Delta_3 = \begin{vmatrix} \lambda_1 e^{\gamma_1 H} & \lambda_2 e^{-\gamma_1 H} & q_1 e^{-\Sigma_t^* H} & \lambda_4 e^{-\gamma_3 H} \\ \rho_1 e^{\gamma_1 H} & \rho_2 e^{-\gamma_1 H} & q_2 e^{-\Sigma_t^* H} & \rho_4 e^{-\gamma_3 H} \\ \lambda_2 & \lambda_1 & q_3 & \lambda_3 \\ \rho_2 & \rho_1 & q_4 & \rho_4 \end{vmatrix}$$

$$\approx (\lambda_1\rho_2 - \lambda_2\rho_1)(q_3\rho_3 - q_4\lambda_3)$$

$$+ (\lambda_1\rho_3 - \lambda_3\rho_1)(q_1\rho_1 - q_2\lambda_1)\, e^{-(\Sigma_t^* - \gamma_1)H}, \qquad (6.74)$$

$$\Delta_4 = \begin{vmatrix} \lambda_1 e^{+\gamma_1 H} & \lambda_2 e^{-\gamma_1 H} & \lambda_3 e^{\gamma_3 H} & q_1 e^{-\Sigma_t^* H} \\ \rho_1 e^{+\gamma_1 H} & \rho_2 e^{-\gamma_1 H} & \rho_3 e^{\gamma_3 H} & q_2 e^{-\Sigma_t^* H} \\ \lambda_2 & \lambda_1 & \lambda_4 & q_3 \\ \rho_2 & \rho_1 & \rho_4 & q_4 \end{vmatrix}$$

$$\approx -(\lambda_1\rho_3 - \lambda_3\rho_1)(q_4\lambda_1 - q_3\rho_1)\, e^{(\gamma_1+\gamma_3)H}$$

$$+ (\lambda_2\rho_3 - \lambda_3\rho_2)(q_4\lambda_2 - q_3\rho_2)\, e^{(\gamma_3-\gamma_1)H}. \qquad (6.75)$$

B. The Total Axial Flux Distribution

The total axial flux is, by definition,

$$\phi_o(z) = \int_{-1}^{1} d\mu\ \phi(z,\mu) = \int_{-1}^{1} d\mu[\phi^{uc}(z,\mu)+\phi^{c}(z,\mu)] = Q_o\, e^{-\Sigma_t^* z} + \phi_o^c(z)$$

$$= (Q_o+S_o)\, e^{-\Sigma_t^* z} + \left[\frac{\Delta_1}{\Delta} e^{\gamma_1 z} + \frac{\Delta_2}{\Delta} e^{-\gamma_1 z}\right] + \left[\frac{\Delta_3}{\Delta} e^{\gamma_3 z} + \frac{\Delta_4}{\Delta} e^{-\gamma_3 z}\right] . \tag{6.76}$$

Here the first term is the source neutron contributions, the second term represents the asymptotic axial flux distribution, and the third term is the spatial transient in the one-group P_3 approximation. It is advisable to express the asymptotic flux and the transient flux in terms of hyperbolic functions. To do this, recall that

$$e^{\pm\gamma z} = \cosh \gamma z \pm \sinh \gamma z\ . \tag{6.77}$$

Thus,

$$\phi_o^{asy.}(z) = \frac{\Delta_1}{\Delta} e^{\gamma_1 z} + \frac{\Delta_2}{\Delta} e^{-\gamma_1 z}$$

$$= \frac{\sqrt{(\Delta_2-\Delta_1)^2 - (\Delta_1+\Delta_2)^2}}{\Delta} \left\{ \frac{(\Delta_1+\Delta_2)}{\sqrt{(\Delta_2-\Delta_1)^2 - (\Delta_1+\Delta_2)^2}} \cosh \gamma_1 z \right.$$

$$\left. - \frac{(\Delta_2-\Delta_1)}{\sqrt{(\Delta_2-\Delta_1)^2 - (\Delta_1+\Delta_2)^2}} \sinh \gamma_1 z \right\} . \tag{6.78}$$

Now, define

$$\sinh \gamma_1 \tilde{H}_1 \equiv \frac{(\Delta_1+\Delta_2)}{\sqrt{(\Delta_2-\Delta_1)^2 - (\Delta_1+\Delta_2)^2}} = \frac{(\Delta_1+\Delta_2)}{2\sqrt{-\Delta_1\Delta_2}}\ ; \tag{6.79}$$

then

$$\cosh \gamma_1 \tilde{H}_1 = \sqrt{1 + \sinh^2 \gamma_1 \tilde{H}_1} = \frac{(\Delta_2 - \Delta_1)}{\sqrt{(\Delta_2 - \Delta_1)^2 - (\Delta_1 + \Delta_2)^2}} \, . \tag{6.80}$$

Equation (6.78) reduces to

$$\phi_o^{asy.}(z) = \frac{2\sqrt{-\Delta_1 \Delta_2}}{\Delta} \sinh \gamma_1 (\tilde{H}_1 - z) \, . \tag{6.81}$$

Similarly, we can express the transient flux as

$$\phi_o^{tr}(z) = \frac{2\sqrt{-\Delta_3 \Delta_4}}{\Delta} \sinh \gamma_3 (\tilde{H}_3 - z) \, , \tag{6.82}$$

where

$$\sinh \gamma_3 \tilde{H}_3 \equiv \frac{(\Delta_3 + \Delta_4)}{2\sqrt{-\Delta_3 \Delta_4}} \, . \tag{6.83}$$

It can be shown either by a numerical calculation or by the expressions given by Eqs. (6.71) through (6.75) that

$$\frac{\Delta_1}{\Delta} = \text{negative}, \qquad \frac{\Delta_2}{\Delta} = \text{positive} \, ;$$

and

$$\frac{\Delta_3}{\Delta} = \text{negative}, \qquad \frac{\Delta_4}{\Delta} = \text{positive} \, .$$

These results must be true if the expressions, Eqs. (6.81) and (6.82) for the asymptotic flux and the transient flux, respectively, are to be physically meaningful; for then the factors $\frac{\sqrt{-\Delta_1 \Delta_2}}{\Delta}$ and $\frac{\sqrt{-\Delta_3 \Delta_4}}{\Delta}$ are real. To avoid confusion, we write

$$\frac{\sqrt{-\Delta_1\Delta_2}}{\Delta} = \frac{\sqrt{|\Delta_1| \cdot |\Delta_2|}}{|\Delta|} \quad , \quad \text{which is positive and real,}$$

and

$$\frac{\sqrt{-\Delta_3\Delta_4}}{\Delta} = \frac{\sqrt{|\Delta_3| \cdot |\Delta_4|}}{|\Delta|} \quad , \quad \text{which is positive and real.}$$

The total axial flux becomes

$$\phi_o(z) = (Q_o+S_o)\, e^{-\Sigma_t^* z} + \frac{2\sqrt{|\Delta_1| \cdot |\Delta_2|}}{|\Delta|} \sinh \gamma_1(\tilde{H}_1-z)$$

$$\frac{2\sqrt{|\Delta_3| \cdot |\Delta_4|}}{|\Delta|} \sinh \gamma_3(\tilde{H}_3-z) \; . \qquad (6.84)$$

C. The Extrapolated Height

Equation (6.79) suggests a way of calculating the extrapolated height $\tilde{H}_1$ for the asymptotic axial flux:

$$\tilde{H}_1 = \frac{1}{\gamma_1} \sinh^{-1}\left[\frac{\Delta_1 + \Delta_2}{2\sqrt{|\Delta_1| \cdot |\Delta_2|}}\right] . \qquad (6.85)$$

This expression includes the boundary effect as well as the source effect and is, consequently, more suitable for estimating the extrapolated height of a miniature lattice than the usual formula given by the asymptotic transport theory

$$\tilde{H} = H + 0.7104\, \lambda_{tr} \; , \qquad (6.86)$$

which neglects the source effect.

Another formula for the extrapolated height $\tilde{H}_1$ can be obtained by forming the ratio of Eqs. (6.79) and (6.80):

$$\tilde{H}_1 = \frac{1}{\gamma_1} \tanh^{-1}\left(\frac{\Delta_1+\Delta_2}{\Delta_2-\Delta_1}\right) . \tag{6.87}$$

The functional form is exact; the approximations enter in the calculation of the Δ_i. Equation (6.87) is similar to the expression for the extrapolated height derived by means of the moments method in Chapter III, namely, Eq. (3.23).

Equation (6.83) also suggests a way of calculating the axial position at which the transient flux vanishes:

$$\tilde{H}_3 = \frac{1}{\gamma_3} \sinh^{-1}\left[\frac{(\Delta_3+\Delta_4)}{2\sqrt{|\Delta_3|\cdot|\Delta_4|}}\right] , \tag{6.88}$$

or, alternatively,

$$\tilde{H}_3 = \frac{1}{\gamma_3} \tanh^{-1}\left(\frac{\Delta_3+\Delta_4}{\Delta_4-\Delta_3}\right) . \tag{6.89}$$

D. The Axial Geometric Buckling

We have shown in Chapter II that the geometric buckling is a sensitive parameter for testing the asymptotic condition; when the axial flux becomes asymptotic, the geometric buckling is equal to γ_1^2. We shall estimate the position at which the geometric buckling becomes equal to γ_1^2. To do this, we define the geometric buckling as

$$B_g^2(z) = \frac{1}{\phi_o(z)} \frac{d^2}{dz^2} \phi_o(z) . \tag{6.90}$$

Substitution of Eq. (6.84) into Eq. (6.90) yields

$$B_g^2(z) = \gamma_1^2 \left\{ \frac{1 + \frac{\gamma_3^2}{\gamma_1^2} \cdot \frac{F_2(z)}{F_1(z)} + \frac{\Sigma_t^{*2}}{\gamma_1^2} \cdot \frac{(Q_o+S_o)}{F_1(z)} e^{-\Sigma_t^* z}}{1 + \frac{F_2(z)}{F_1(z)} + \frac{(Q_o+S_o)}{F_1(z)} e^{-\Sigma_t^* z}} \right\} , \tag{6.91}$$

where

$$F_1(z) = \frac{2\sqrt{|\Delta_1| \cdot |\Delta_2|}}{|\Delta|} \sinh \gamma_1(\tilde{H}_1 - z) , \tag{6.92}$$

and

$$F_2(z) = \frac{2\sqrt{|\Delta_3| \cdot |\Delta_4|}}{|\Delta|} \sinh \gamma_3(\tilde{H}_3 - z) . \tag{6.93}$$

In the neighborhood of the boundary, z=H, Eq. (6.91) reduces to

$$B_g^2(z) \approx \gamma_1^2 \left[1 + \left(\frac{\gamma_3^2 - \gamma_1^2}{\gamma_1^2} \right) \frac{F_2(z)}{F_1(z)} \right] . \tag{6.94}$$

When $e^{-\Sigma_t^* z} \approx 0$ and $\frac{F_2(z)}{F_1(z)} \approx 0$, we have the asymptotic condition

$$B_g^2(z) \approx \gamma_1^2 = \text{independent of } z .$$

E. Numerical Calculations for the Miniature Lattice ML3

The miniature lattice ML3 was chosen for the quantitative study of the effects of the spatial transient and the source contributions on the determination of the asymptotic axial buckling.

(i) Calculations of the Macroscopic Nuclear Cross Sections and Diffusion Parameters

The homogenized set of macroscopic nuclear cross sections is calculated by means of the formula

$$\Sigma_j = \frac{\bar{\Sigma}_j^F V_F \bar{\phi}_F + \bar{\Sigma}_j^C V_C \bar{\phi}_C + \bar{\Sigma}_j^M V_M \bar{\phi}_M}{V_F \bar{\phi}_F + V_C \bar{\phi}_C + V_M \bar{\phi}_M} , \tag{6.95}$$

where

j = a for the macroscopic absorption cross section,

j = s for the macroscopic scattering cross section,

j = f for the macroscopic fission cross section,

$j = t_r$ for the macroscopic transport cross section,

j = t for the macroscopic total cross section,

and the superscripts F, C and M stand for fuel, cladding and moderator, respectively. The average macroscopic cross sections for the i^{th} region, the $\bar{\Sigma}_j^i$, were computed with the THERMOS code which gives

$$\bar{\Sigma}_j^i V_i \bar{\phi}_i = \int_i d\underline{r} \int_0^{v^*} dv\, vN(\underline{r}, v)\, \Sigma_j^i(v) , \tag{6.96}$$

where V_i and $\bar{\phi}_i$ are the volume and the average flux in the i^{th} region, respectively; the average flux is given by:

$$V_i \bar{\phi}_i = \int_i d\underline{r} \int_0^{v^*} dv\, vN(\underline{r}, v) . \tag{6.97}$$

In Eqs. (6.96) and (6.97), $N(\underline{r}, v)$ denotes the neutron density as a function of space and velocity, and v^* represents the upper limit of the velocity range under consideration. To account for the fast

fissions in U^{238} as well as the epicadmium fissions in U^{235}, the average macroscopic fission cross section $\bar{\Sigma}_f^F$ was calculated from the formula

$$\bar{\Sigma}_f^F = \varepsilon \bar{\Sigma}_f^{25}(1+\delta_{25})(1+\delta_{28}) + (1-\varepsilon)\bar{\Sigma}_f^{28} , \tag{6.98}$$

where ε is the concentration (atom fraction) of U^{235} in the fuel and the quantities δ_{25} and δ_{28} have been defined in Chapter I. To correct for the epicadmium capture in U^{238}, the average macroscopic absorption cross section in the fuel $\bar{\Sigma}_a^F$ was defined as

$$\bar{\Sigma}_a^F = \varepsilon \bar{\Sigma}_a^{25} + (1-\varepsilon)\bar{\Sigma}_a^{28}(1+\rho_{28}) , \tag{6.99}$$

where ρ_{28} is the ratio of the epicadmium to subcadmium capture rates in U^{238} averaged over the fuel.

The diffusion length L was computed from the formula

$$L = \frac{1}{\sqrt{3\Sigma_a \Sigma_{tr}}} , \tag{6.100}$$

and the diffusion coefficient D from

$$D = \frac{1}{3\Sigma_{tr}} . \tag{6.101}$$

The radial leakage of neutrons was taken into account by defining the "leakage cross section" in the diffusion approximation:

$$\Sigma_{Lr} = D\alpha^2 = D\left(\frac{2.4048}{\tilde{R}}\right)^2 = 0.00614 \text{ cm}^{-1} .$$

The modified macroscopic absorption cross section including the radial leakage is then

$$\Sigma_a^* = \Sigma_a + \Sigma_{Lr} = 0.0102 \text{ cm}^{-1},$$

and the modified macroscopic total cross section becomes

$$\Sigma_t^* = \Sigma_s + \Sigma_a^* = 0.44713 \text{ cm}^{-1}.$$

The values of the homogenized nuclear cross sections and diffusion parameters are listed in Table 6.1 together with measured values of the quantities δ_{25}, δ_{28}, and ρ_{28}.

Table 6.1. Values of the parameters used in the one-group P_3 calculation for the miniature lattice ML3.

ML3: 1.143% enriched uranium fuel, D_2O moderated, and 2.50-inch triangular spacing.

Parameter	Value
Σ_a (cm^{-1})	0.00406
Σ_a^* (cm^{-1})	0.01020
Σ_f (cm^{-1})	0.00203
Σ_s (cm^{-1})	0.43693
Σ_t^* (cm^{-1})	0.44713
Σ_{tr} (cm^{-1})	0.41456
D (cm)	0.80407
L (cm)	15.70500
ν	2.430
$\overline{\mu}_o$	0.116
V_M/V_F	108.34
$\widetilde{R}$ (cm)	27.522
ρ_{28} [1]	0.2510
δ_{28} [1]	0.0174
δ_{25} [1]	0.0153

[1] Taken from the report by Sefchovich et al. (S1).

(ii) Calculation of the Axial Buckling (or the Eigenvalues)

The axial bucklings corresponding to the asymptotic flux and the transient mode were calculated by means of Eqs. (6.44) and (6.45); the coefficients a and b were calculated from Eqs. (6.39) and (6.40). The results are:

$$a = 0.7816619 \text{ cm}^{-2},$$

$$b = 0.00505104 \text{ cm}^{-4},$$

$$\gamma_1^2 = 0.00651627 \text{ cm}^{-2},$$

$$\gamma_3^2 = 0.775146 \text{ cm}^{-2},$$

where $\gamma_1^2 = 6516.3\ \mu B$ is the asymptotic axial buckling. The corresponding value obtained by means of the moments method from the experimental data is 6984.4 μB (see Table 5.7 of Chapter V). The discrepancy is probably due mainly to the uncertainty in the various cross sections, especially the transport cross section. The effect of uncertainties in cross sections is aggravated by the fact that the asymptotic axial buckling γ_1^2 is calculated as the small difference between two relatively large numbers. For the lattice ML3,

$$\gamma_1^2 = \left(\frac{a}{2}\right) - \sqrt{\left(\frac{a}{2}\right)^2 - b}$$

$$= 0.39083097 - 0.3843147 = 0.00651627 \text{ cm}^{-2}.$$

It is evident that small uncertainties in the various cross sections could lead to a significant error in the value of γ_1^2. This example emphasizes the importance of measurements of the axial buckling. The same argument applies to the determination of the material buckling. Another contribution of the discrepancy may come from the inadequacy of low-order approximate theory used — the one-group P_3 approximation — and particularly from the boundary conditions.

(iii) Calculation of the Total Axial Flux Distribution

Equation (6.84) was used to calculate the total axial flux distribution. The physical height used in this calculation was 40 cm, the actual height of the miniature lattices. The following values were obtained for the constants in Eq. (6.84):

$$S_o = 2.084316\, Q_o,$$

$$\Delta_1 = 177.762\, Q_o\, e^{31.988},$$

$$\Delta_2 = -234.249\, Q_o\, e^{38.446},$$

$$\Delta_3 = 8.28496\, Q_o,$$

$$\Delta_4 = -52.8974\, Q_o\, e^{38.446} - 37.0314\, Q_o\, e^{31.988},$$

$$\Delta = -54.8102\, e^{38.446} + 31.5633\, e^{31.988}.$$

Since only a relative flux distribution is needed for the analysis of the axial buckling by the moment method, the total axial flux in Eq. (6.84) was normalized with respect to the asymptotic axial flux:

$$[\phi_o(z)]_{rel.} = \frac{|\Delta|\,(Q_o+S_o)}{2\sqrt{|\Delta_1|\cdot|\Delta_2|}}\, e^{-\Sigma_t^* z} + \sinh \gamma_1(\tilde{H}_1 - z) + c \sinh \gamma_3(\tilde{H}_3 - z), \tag{6.102}$$

where

$$c = \frac{\sqrt{|\Delta_3|\cdot|\Delta_4|}}{\sqrt{|\Delta_1|\cdot|\Delta_2|}}. \tag{6.103}$$

The extrapolated height was calculated from Eq. (6.85):

$$\frac{(\Delta_1+\Delta_2)}{2\sqrt{|\Delta_1|\cdot|\Delta_2|}} = 14.50,$$

and

$$\tilde{H}_1 = \frac{1}{\gamma_1} \sinh^{-1}(14.50) = \frac{3.3674}{0.08072} = 41.715 \text{ cm}.$$

The corresponding value, obtained with the ABMOMENT code through the analysis for a set of theoretical values calculated by Eq. (6.102), was 41.711 cm. The good agreement confirms the reproducibility of the ABMOMENT code. The exact value predicted by the asymptotic transport theory is given by

$$\tilde{H}_1 = H + 0.7104\, \lambda_{tr}$$

$$= 40.0 + 0.7104 \cdot (2.4122) = 41.713 \text{ cm},$$

which agrees very well with the value computed by means of Eq. (6.85). The experimental value of $\tilde{H}_1$ has been obtained in section 5.3 of Chapter V (see Table 5.7):

$$\left(\tilde{H}_1\right)_{exp.} = 46.408 \text{ cm},$$

which is greater than the theoretical value. The discrepancy may be attributed to the presence of a layer of D_2O at the bottom of the cylindrical tank during the course of experiments (S1). By taking into account the reflector savings, the value of the extrapolated height was calculated to be 48.476 cm (S1), which is in better agreement with the experimental value. Similarly, for the transient flux, we have

$$\sinh \gamma_3 \tilde{H}_3 = \frac{(\Delta_3 + \Delta_4)}{2\sqrt{|\Delta_3| \cdot |\Delta_4|}} = \frac{1}{2} \cdot \frac{52.957}{20.92} e^{19.223},$$

since

$$\sinh \gamma_3 \tilde{H}_3 \approx \frac{1}{2} e^{\gamma_3 \tilde{H}_3} \quad \text{for } \gamma_3 \tilde{H}_3 \gg 1,$$

$$e^{\gamma_3 \tilde{H}_3} \approx \frac{52.957}{20.92} e^{19.223} \approx e^{20.151},$$

and

$$\tilde{H}_3 \simeq \frac{20.151}{\gamma_3} = \frac{20.151}{0.8804} = 22.888 \text{ cm}.$$

The transient flux should therefore vanish near the middle of the assembly. We finally obtain for the total relative flux:

$$[\phi_o(z)]_{rel.} \simeq 11.053\, e^{-0.4476z} + \sinh[0.08072(41.715-z)] + 0.1025\, e^{-15.994} \sinh[0.8804(22.888-z)]. \quad (6.104)$$

The total flux distribution just obtained is plotted on a semilog scale in Figure 6.2. Table 6.2 lists theoretical values of the asymptotic flux, the transient flux, the source neutron contributions, and the total axial flux.

(iv) Calculation of the Geometric Buckling

The geometric buckling was calculated from Eq. (6.91); the results are listed in Table 6.3 and are plotted in Figure 6.3. The same figure has been shown previously in Chapter II as Figure 2.2. It is seen that the geometric buckling should become very nearly independent of position at about 20 cm from the source and should remain constant to about 34 cm where the boundary effect begins to appear. The result indicates that there should be an asymptotic region of about 15 cm in the miniature lattice ML3.

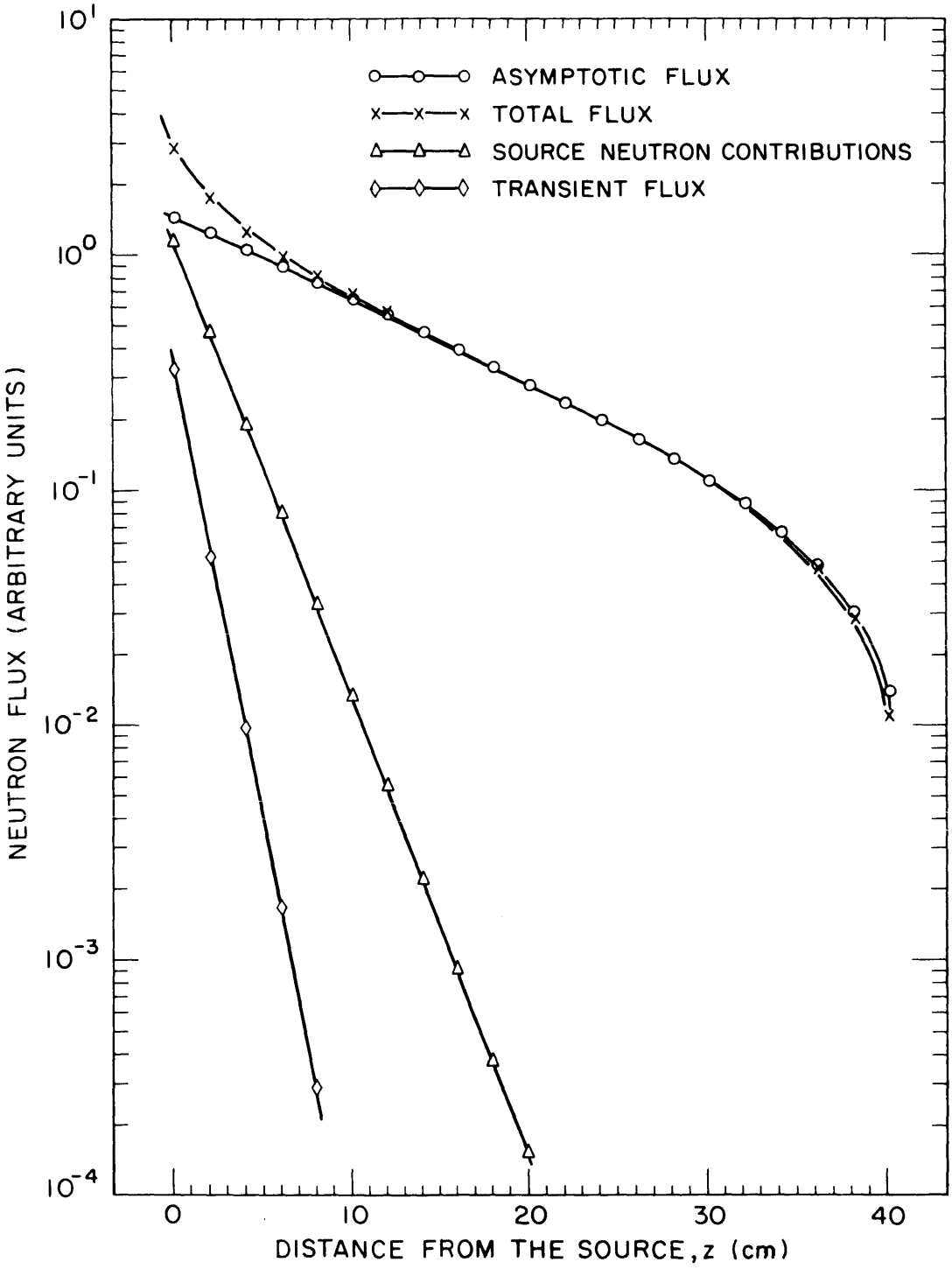

FIG. 6.2 DISTRIBUTIONS OF THE ASYMPTOTIC FLUX, THE TRANSIENT FLUX, THE SOURCE NEUTRON CONTRIBUTIONS, AND THE TOTAL FLUX OF THE MINIATURE LATTICE ML3 IN A ONE-GROUP P_3 APPROXIMATION.

Table 6.2. Values of the theoretical fluxes calculated with Equation 6.104 for the miniature lattice ML3.

ML3: 1.143% enriched fuel, D_2O moderated, 2.50-inch spacing.

z (cm)	Asymptotic Flux	Transient Flux	Source Neutron Contribution	Total Flux
0.0	1.450040	0.327973	1.105300	2.883313
2.0	1.225363	0.051635	0.454352	1.731350
4.0	1.048927	0.009676	0.187072	1.245675
6.0	0.891293	0.001665	0.076929	0.969887
8.0	0.757596	0.000286	0.031645	0.789527
10.0	0.643821	0.000049	0.013009	0.656879
12.0	0.545935		0.005361	0.551296
14.0	0.463609		0.002201	0.465810
16.0	0.392627		0.000910	0.393537
18.0	0.331776		0.000371	0.332147
20.0	0.279905		0.000153	0.280058
22.0	0.235376		0.000063	0.235439
24.0	0.196969		0.000024	0.196993
26.0	0.163733		0.000009	0.163742
28.0	0.134754			0.134754
30.0	0.109312			0.109312
32.0	0.086710			0.086710
34.0	0.066386	-0.000011		0.066375
36.0	0.047784	-0.000057		0.047727
38.0	0.030442	-0.000349		0.030093
40.0	0.013884	-0.002026		0.011858

Table 6.3. Values of the geometric buckling as a function of axial position in terms of the asymptotic axial buckling γ_1^2 for the miniature lattice ML3.

Axial Position z (cm)	$\left[\frac{B_g^2(z)}{\gamma_1^2}\right]$
0.0	25.8000
2.0	12.3200
4.0	6.3800
6.0	3.5600
8.0	2.2350
10.0	1.5950
12.0	1.2900
14.0	1.1400
16.0	1.0690
18.0	1.0332
20.0	1.0162
22.0	1.0080
24.0	1.0036
26.0	1.0016
//	//
34.0	0.98037
36.0	0.85920
38.0	-0.3765
40.0	-19.1500

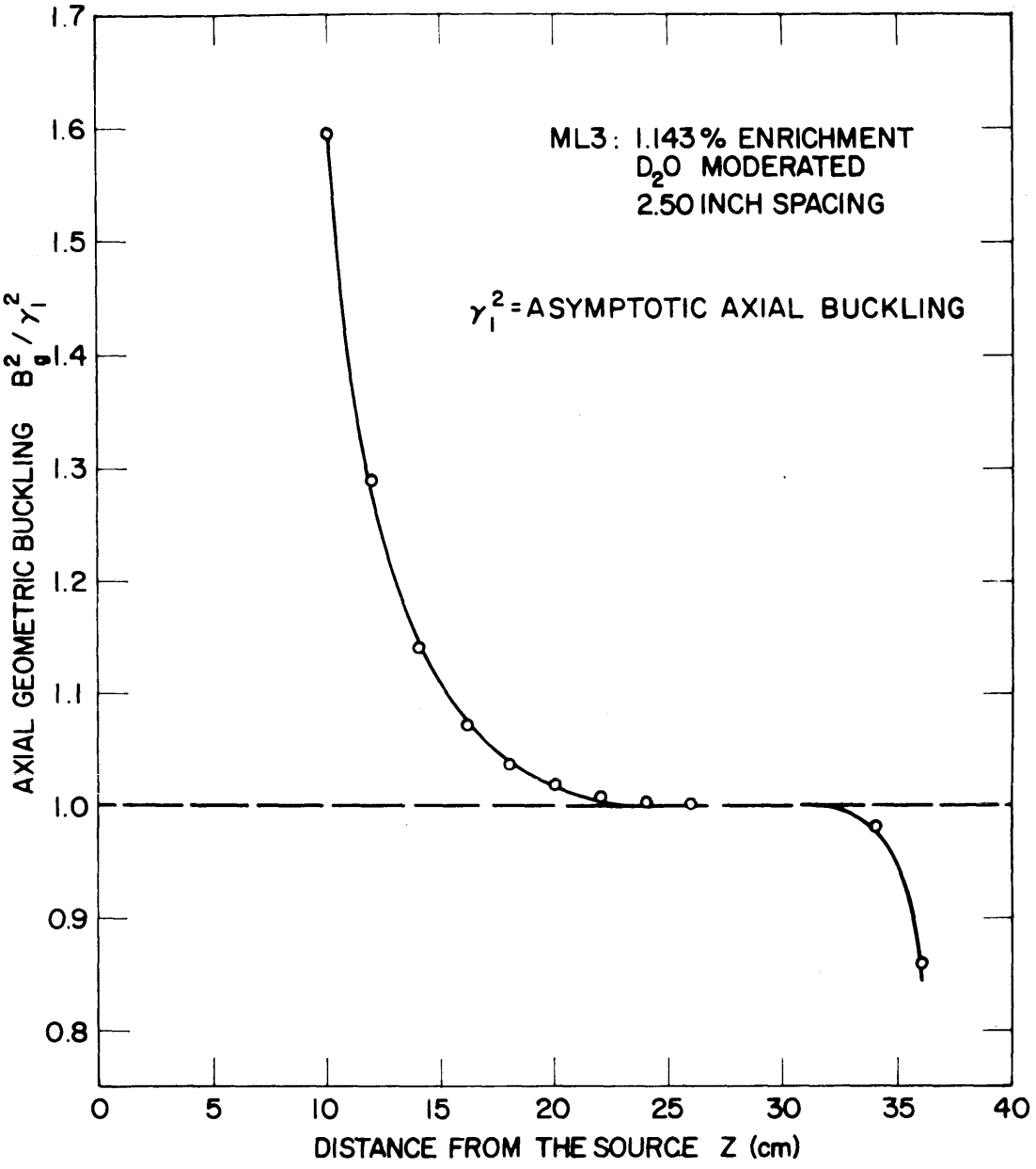

Fig. 6.3 DISTRIBUTION OF THE AXIAL GEOMETRIC BUCKLING AS A FUNCTION OF THE DISTANCE FROM THE SOURCE OF THE MINIATURE LATTICE ML3 IN A ONE-GROUP P3 APPROXIMATION.

6.3 A SPATIAL TRANSIENT ANALYSIS OF THE RADIAL FLUX DISTRIBUTION BY MEANS OF THE SPHERICAL HARMONICS METHOD

6.3.1 Introduction

A complete spherical harmonics solution of the Boltzmann equation for neutron transport in an infinite homogeneous cylinder has been obtained by Kofink (K11). Tralli and Agresta (T1) have also worked out the corresponding solution for a cylindrical cell of finite height. Noble (N2) has studied some conditions for the unsymmetric spherical harmonics method in cylindrical geometry. In this section we shall apply the spherical harmonics solution to the miniature-lattice assembly for the analysis of radial spatial transients.

6.3.2 General Theory

We wish to analyze the radial flux distribution measured in a plane where the axial flux distribution has become asymptotic. We shall assume that the axial leakage of neutrons is accounted for by means of an axial leakage cross section as in section 2.4 of Chapter II. We may then consider that the radial flux distribution is independent of z. We assume further that the system is well thermalized so that a one-group treatment is sufficient. Under these assumptions, the Boltzmann equation for monoenergetic neutron transport in a cylinder has the form (K11, T1, N2):

$$\sin\theta\left[\cos\phi\,\frac{\partial}{\partial r}-\frac{\sin\phi}{r}\,\frac{\partial}{\partial\phi}\right]f(r,\theta,\phi)+\Sigma_t^{**}\,f(r,\theta,\phi)$$

$$=\int_0^{2\pi}d\phi\int_0^{\pi}d\theta\,\sin\theta\,\Sigma_c(\mu_o)\,f(r,\theta,\phi)\,, \qquad (6.105)$$

where Σ_t^{**} is the modified macroscopic total cross section including the axial leakage as given by Eq. (2.42), $\Sigma_c(\mu_o)$ is a kernel which combines the scattering collisions and the fission events, and $\mu_o = \vec{\Omega} \cdot \vec{\Omega}'$.

To derive the spherical-harmonics component form of the Boltzmann equation (6.105), we expand the flux and the kernel in terms of the associated spherical harmonics $P_{\ell m}(\vec{\Omega})$:

$$f(r, \theta, \phi) = \sum_{\ell=0}^{\infty} \sum_{m=-\ell}^{+\ell} f_{\ell m}(r)\, P_{\ell m}(\vec{\Omega}), \tag{6.106}$$

and

$$\Sigma_c(\mu_o) = \sum_{\ell=0}^{\infty} \Sigma_{c\ell}\, P_\ell(\mu_o), \tag{6.107}$$

where, with the help of the addition theorem,

$$P_\ell(\mu_o) = \sum_{m=-\ell}^{+\ell} P_{\ell m}(\vec{\Omega})\, P^*_{\ell m}(\vec{\Omega}'). \tag{6.108}$$

We use the orthogonality property of the associated spherical harmonics $P_{\ell m}(\vec{\Omega})$:

$$\int d\vec{\Omega}\, P_{\ell m}(\vec{\Omega})\, P^*_{\ell' m'}(\vec{\Omega}) = \left(\frac{4\pi}{2\ell+1}\right) \delta_{\ell\ell'}\, \delta_{mm'}, \tag{6.109}$$

where the δ_{ij} are the Kronecker deltas, and the recursion relations (N2)

$$\sin\theta\, e^{i\phi}\, P_{\ell m}(\vec{\Omega}) = \frac{2}{2\ell+1}\left[(2\ell-1)C_{\ell m} P_{\ell-1,m+1}(\vec{\Omega}) - (2\ell+3)\, A_{\ell m} P_{\ell+1,m+1}(\vec{\Omega})\right], \tag{6.110}$$

$$\sin\theta\, e^{-i\phi} P_{\ell m}(\vec{\Omega}) = \frac{2}{2\ell+1}\left[(2\ell+3)B_{\ell m} P_{\ell+1,m-1}(\vec{\Omega}) - (2\ell-1)D_{\ell m} P_{\ell-1,m-1}(\vec{\Omega})\right], \tag{6.111}$$

$$\cos\theta\, P_{\ell m}(\vec{\Omega}) = \frac{1}{2\ell+1}\left[(2\ell+3)E_{\ell m} P_{\ell+1,m}(\vec{\Omega}) + (2\ell-1)F_{\ell m} P_{\ell-1,m}(\vec{\Omega})\right], \tag{6.112}$$

to obtain the following set of the spherical harmonics equations (K11, N2, T1):

$$A_{\ell m}\left[\frac{d}{dr}+\frac{m+1}{r}\right]f_{\ell+1,m+1}(r) - B_{m\ell}\left[\frac{d}{dr}-\frac{m-1}{r}\right]f_{\ell+1,m-1}(r)$$

$$-C_{\ell m}\left[\frac{d}{dr}+\frac{m+1}{r}\right]f_{\ell-1,m+1}(r) + D_{\ell m}\left[\frac{d}{dr}-\frac{m-1}{r}\right]f_{\ell-1,m-1}(r)$$

$$-\left[1 - \frac{4\pi}{2\ell+1}\cdot\frac{\Sigma_{c\ell}}{\Sigma_t^{**}}\right]f_{\ell m}(r) = 0 , \qquad (6.113)$$

where

$$A_{\ell m} = \frac{\sqrt{(\ell+m+1)(\ell+m+2)}}{2(2\ell+3)} , \qquad (6.114)$$

$$B_{\ell m} = \frac{\sqrt{(\ell-m+1)(\ell-m+2)}}{2(2\ell+3)} , \qquad (6.115)$$

$$C_{\ell m} = \frac{\sqrt{(\ell-m-1)(\ell-m)}}{2(2\ell-1)} , \qquad (6.116)$$

$$D_{\ell m} = \frac{\sqrt{(\ell+m-1)(\ell+m)}}{2(2\ell-1)} , \qquad (6.117)$$

Instead of solving the set of equations (6.113) directly, we adopt the usual approach of assuming a solution of the form

$$f_{\ell m}(r) = A_1 R_{\ell m}(\alpha)\, I_m(\alpha\Sigma_t^{**} r) + A_2 S_{\ell m}(\alpha)\, K_m(\alpha\Sigma_t^{**} r) , \qquad (6.118)$$

where A_1, A_2 are two arbitrary constants, the coefficients $R_{\ell m}(\alpha)$ and $S_{\ell m}(\alpha)$ are functions of some arbitrary parameter α, and I_m, K_m are the modified Bessel functions. Substituting Eq. (6.118) into Eq. (6.113) and comparing coefficients of like terms obtains recursion relations for the coefficients $R_{\ell m}(\alpha)$ and $S_{\ell m}(\alpha)$:

$$\alpha[A_{\ell m}R_{\ell+1,m+1}(\alpha) - B_{\ell m}R_{\ell+1,m-1}(\alpha) - C_{\ell m}R_{\ell-1,m+1} + D_{\ell m}R_{\ell-1,m-1}] = \beta_\ell R_{\ell m} , \tag{6.119}$$

and

$$S_{\ell m} = (-1)^m R_{\ell m} , \tag{6.120}$$

where

$$\beta_\ell = 1 - \frac{4\pi}{2\ell+1} \cdot \frac{\Sigma_{c\ell}}{\Sigma_t^{**}} . \tag{6.121}$$

The symmetry condition $f(r, \theta, \phi) = f(r, \theta, -\phi)$ requires that

$$f_{\ell,-m}(r) = (-1)^m f_{\ell,m}(r) , \tag{6.122}$$

and hence

$$R_{\ell,-m}(\alpha) = (-1)^m R_{\ell,m}(\alpha) . \tag{6.123}$$

The eigenvalue, α, of the problem is obtained from Eq. (6.119), and the spherical harmonics moment $f_{\ell m}(r)$ of the directional radial flux is given by Eq. (6.118). The eigenvalue α may be real, imaginary, or complex depending on the composition of the medium.

We shall use the Marshak boundary conditions as an approximation to the exact boundary condition: Marshak's conditions require that the inward angular flux at a free surface r=R vanish. In the present problem the conditions may be written:

$$\int_{\pi/2}^{3\pi/2} d\phi \int_0^{\pi} d\theta \, \sin\theta \, f(R, \theta, \phi) \, P_{\ell m}(\vec{\Omega}) = 0,$$

$$\ell = 1, 3, 5, \ldots, \text{odd} \; ; \quad m = 0, 1, 2, \ldots, \ell . \tag{6.124}$$

6.3.3 A P_3 Approximation for Linearly Anisotropic Scattering

In a P_3 approximation for the case of linear anisotropic scattering ($\Sigma_{c\ell} = 0$ for $\ell > 2$), ten homogeneous equations in ten unknowns are obtained for the $R_{\ell m}(\alpha)$ in Eq. (6.119) by setting $R_{\ell m}(\alpha) = 0$ for $\ell > 3$. In order for a nontrivial solution to exist, the determinant of the coefficients of the $R_{\ell m}(\alpha)$ must vanish, and the following roots of the resulting characteristic equation are obtained (N2, T1):

$$\alpha_1^2 = -\left(\frac{35g}{18}\right)\left[1 - \sqrt{1 - \frac{108\beta_o\beta_1}{(35g)^2}}\right], \tag{6.125}$$

$$\alpha_2^2 = -\left(\frac{35g}{18}\right)\left[1 + \sqrt{1 - \frac{108\beta_o\beta_1}{(35g)^2}}\right], \tag{6.126}$$

$$\alpha_3^2 = 7\ , \tag{6.127}$$

$$\alpha_4^2 = \frac{35\beta_1}{(8\beta_1+7)}\ , \tag{6.128}$$

where

$$g = 1 + \beta_o\left(\frac{4}{5} + \frac{27\beta_1}{35}\right)\ . \tag{6.129}$$

The lowest eigenvalue, α_1^2, corresponds to the asymptotic radial buckling, and the other eigenvalues correspond to the spatial transients in the radial flux due to the transport effect.

In the case of the miniature lattices, α_1^2 must be negative to have a physically realizable solution, and the other α_i^2 are positive. These statements will be verified in a calculation that will be made later in this section. We must also satisfy the condition

$$f_{\ell m}(r) \neq \infty \quad \text{at } r = 0\ ,$$

which rules out the terms $K_m(r)$ and $Y_m(r)$. Thus, the spherical harmonics moment $f_{\ell m}(r)$ for the miniature lattices in a P_3 approximation can be written as

$$f_{\ell m}(r) = A_1 R_{\ell m}(\alpha_1)\, J_m\left(|\alpha_1|\Sigma_t^{**} r\right) + \sum_{i=2}^{4} A_i R_{\ell m}(\alpha_i)\, I_m(\alpha_i \Sigma_t^{**} r) \ . \tag{6.130}$$

In the measurement of the radial buckling, we are concerned with the total radial flux alone. This is, with the aid of the orthogonality property, Eq. (6.109), of the associated spherical harmonics:

$$\begin{aligned} f(r) &= \int_{4\pi} f(r,\vec{\Omega})\, d\vec{\Omega} \\ &= \int \sum_{\ell=0}^{\infty} \sum_{m=-\ell}^{+\ell} f_{\ell m}(r)\, P_{\ell m}(\vec{\Omega})\, d\vec{\Omega} \\ &= 4\pi\, f_{o,o}(r) \ . \end{aligned} \tag{6.131}$$

Thus, we need to consider only the moment $f_{o,o}(r)$, and Eq. (6.130) reduces to

$$f_{o,o}(r) = A_1 R_{o,o}(\alpha_1)\, J_o\left(|\alpha_1|\Sigma_t^{**} r\right) + \sum_{i=2}^{4} A_i R_{o,o}(\alpha_i)\, I_o(\alpha_i \Sigma_t^{**} r) \ , \tag{6.132}$$

where the coefficients $R_{o,o}(\alpha_i)$ have been found by Noble (N2) and Tralli (T1) to be:

$$R_{o,o}(|\alpha_1|) = R_{o,o}(\alpha_2) = 1 \ ,$$

and

$$R_{o,o}(\alpha_3) = R_{o,o}(\alpha_4) = 0 \ .$$

Finally, we have

$$f_{o,o}(r) = A_1 J_o(|\alpha_1| \Sigma_t^{**} r) + A_2 I_o(\alpha_2 \Sigma_t^{**} r) \ . \tag{6.133}$$

We see that the transport effect may give rise to an I_o term in the total radial flux even in a bare assembly.

To determine the relative importance of the I_o term in Eq. (6.133) with respect to the J_o term, that is, the ratio A_2/A_1, we apply Marshak's boundary conditions, Eq. (6.124), for the cases of $P_{1,1}$ and $P_{3,1}$ because these are the only combinations that can involve the constants A_1 and A_2 (N2). Two boundary conditions at r=R are thus obtained:

$$\text{For } P_{1,1}: \quad f_{oo} + \frac{2\sqrt{2}}{3} f_{11} - \frac{1}{8} f_{20} + \frac{\sqrt{6}}{8} f_{22} = 0 \ , \tag{6.134}$$

$$\text{for } P_{3,1}: \quad \frac{1}{4} f_{oo} + \frac{7}{16} f_{20} - \frac{\sqrt{6}}{48} f_{22} + \frac{8\sqrt{3}}{21} f_{31} = 0 \ . \tag{6.135}$$

To evaluate the $f_{\ell m}$, we need to know the coefficients $R_{\ell m}(\alpha_i)$. Table 6.4 lists the values of the $R_{\ell m}(\alpha_i)$ from Ref. (N2) for the P_3 approximation. Equations (6.134) and (6.135) lead to the two equations:

$$A_1 b_1 J_o(|\alpha_1| \Sigma_t^{**} R) + A_2 b_2 I_o(\alpha_2 \Sigma_t^{**} R) + A_3 b_3 I_o(\alpha_3 \Sigma_t^{**} R) = 0 \ , \tag{6.136}$$

and

$$A_1 C_1 J_o(|\alpha_1| \Sigma_t^{**} R) + A_2 C_2 I_o(\alpha_2 \Sigma_t^{**} R) + A_3 C_3 I_o(\alpha_3 \Sigma_t^{**} R) = 0 \ , \tag{6.137}$$

where

$$b_i = 1 + \frac{2\sqrt{2}}{3} R_{11}(\alpha_i) - \frac{1}{8} R_{20}(\alpha_i) + \frac{\sqrt{6}}{8} R_{22}(\alpha_i), \quad i = 1, 2 \ , \tag{6.138}$$

$$b_3 = -\frac{1}{8} + \frac{\sqrt{6}}{8} R_{22}(\alpha_3) \ , \tag{6.139}$$

$$c_i = \frac{1}{4} + \frac{7}{16} R_{20}(\alpha_i) - \frac{\sqrt{6}}{48} R_{22}(\alpha_i) + \frac{8\sqrt{3}}{21} R_{31}(\alpha_i) \ , \quad i = 1, 2 \ , \tag{6.140}$$

Table 6.4. Values of the coefficients, $R_{\ell m}(\alpha_i)$, in P_3 Approximation

ℓ	m	$R_{\ell m}(\alpha_i)$ $i = 1, 2$	$R_{\ell m}(\alpha_3)$	$R_{\ell m}(\alpha_4)$
0	0	1	0	0
1	0	0	0	1
1	1	$3\beta_o\alpha_i/a_i\sqrt{2}$	0	0
2	0	$-a_iN_i$	1	0
2	1	0	0	$5a_4M/\sqrt{6}$
2	2	$\alpha_i^2N_i\sqrt{6}/2$	$7/\alpha_3^2\sqrt{6}$	0
3	0	0	0	$-\beta_1$
3	1	$-3\sqrt{3}\,\alpha_i^2N_i/10$	$7/2\alpha_3\sqrt{3}$	0
3	2	0	0	$5\beta_1/\sqrt{30}$
3	3	$3\alpha_i^3N_i/2\sqrt{5}$	$7/2\alpha_3\sqrt{5}$	0

$$a_1 = \alpha_1^2\,, \quad a_2 = \alpha_2^2\,, \quad a_3 = \alpha_3^2 = 7\,, \quad a_4 = \alpha_4^2$$

$$N_i = \frac{(a_i - 3\beta_o\beta_1 - 7\beta_o)}{a_i(a_i - 7)} \qquad (i = 1, 2)$$

$$M = \frac{\beta_1}{a_4\alpha_4}$$

and

$$c_3 = \frac{7}{16} - \frac{\sqrt{6}}{48} R_{22}(\alpha_3) + \frac{8\sqrt{3}}{21} R_{31}(\alpha_3) \ . \tag{6.141}$$

Eliminating the $A_3 I_o(\alpha_3 \Sigma_t^{**} R)$ term from Eqs. (6.136) and (6.137), we obtain

$$A_1 b_1 c_3 J_o(|\alpha_1| \Sigma_t^{**} R) + A_2 b_2 c_3 I_o(\alpha_2 \Sigma_t^{**} R)$$

$$= A_1 c_1 b_3 J_o(|\alpha_1| \Sigma_t^{**} R) + A_2 c_2 b_3 I_o(\alpha_2 \Sigma_t^{**} R) \ , \tag{6.142}$$

whence

$$\left(\frac{A_2}{A_1}\right) = - \frac{J_o(|\alpha_1| \Sigma_t^{**} R)}{I_o(\alpha_2 \Sigma_t^{**} R)} \cdot \frac{(b_1 c_3 - c_1 b_3)}{(b_2 c_3 - c_2 b_3)} \ . \tag{6.143}$$

A. The Radial Geometric Buckling

We define the radial geometric buckling as

$$B_r^2(r) \equiv - \frac{1}{f_{o,o}(r)} \cdot \frac{d^2}{dr^2} f_{o,o}(r) \ . \tag{6.144}$$

Substitution of Eq. (6.133) into Eq. (6.144) yields

$$B_r^2(r) = \alpha^2 \left\{ \frac{1 - \left(\frac{A_2}{A_1}\right)\left(\frac{\alpha_2^2}{\alpha_1^2}\right) \frac{I_o(\alpha_2 \Sigma_t^{**} r)}{J_o(|\alpha_1| \Sigma_t^{**} r)}}{1 + \left(\frac{A_2}{A_1}\right) \frac{I_o(\alpha_2 \Sigma_t^{**} r)}{J_o(|\alpha_1| \Sigma_t^{**} r)}} \right\} \ , \tag{6.145}$$

where $\alpha^2 = |\alpha_1|^2 (\Sigma_t^{**})^2$ is the asymptotic radial buckling. This expression enables us to locate the radial position at which the spatial transient is negligible and $B_r^2(r) \simeq |\alpha_1|^2$, independent of position.

B. Numerical Calculations for the Miniature Lattice ML3

(i) Calculation of the Eigenvalues

We shall use the cross section data listed in Table 6.1 for the following calculations. In particular,

$$\Sigma_t^{**} = \Sigma_t - D\gamma_1^2 = 0.43575 \text{ cm}^{-1} ,$$

$$\Sigma_{co} = \Sigma_s + \nu\Sigma_f = 0.44186 \text{ cm}^{-1} ,$$

$$\Sigma_{c1} = \bar{\mu}_o\Sigma_s = 0.05069 \text{ cm}^{-1} .$$

Thus, we have

$$\beta_o = 1 - 4\pi\left(\frac{\Sigma_{co}}{\Sigma_t^{**}}\right) = - 11.730$$

and

$$\beta_1 = 1 - \frac{4\pi}{3}\left(\frac{\Sigma_{c1}}{\Sigma_t^{**}}\right) = 0.5125 .$$

From Eq. (6.129) we get

$$g = - 13.02 .$$

The eigenvalues, α_i^2, can be calculated by means of Eqs. (6.125) through (6.128). First, the square-root term is

$$\sqrt{1 - \frac{108\beta_o\beta_1}{(35g)^2}} = \sqrt{1.003125714} = 1.0015616 ,$$

so that

$$\alpha_1^2 = - 0.039484 ,$$

$$\alpha_2^2 = 50.5995 ,$$

$$\alpha_3^2 = 7 ,$$

$$\alpha_4^2 = 1.6162 .$$

Only α_1^2 is negative as mentioned earlier. This indicates that α_1^2 corresponds to a solution in terms of the J_o function since

$$I_o(i|\alpha_1|\,r) = J_o(|\alpha_1|\,r)\ , \qquad i = \sqrt{-1}\ .$$

The asymptotic radial buckling in the P_3 approximation is then given by

$$\alpha^2 = |\alpha_1^2| \cdot \left(\Sigma_t^{**}\right)^2 = (0.039484) \cdot (0.43575)^2$$
$$= 0.0074973\ \text{cm}^{-2} \quad \text{or} \quad 7497.3\ \mu\text{B}\ . \qquad (6.146)$$

The expression (6.146) is expected for the asymptotic radial buckling because of the way in which we defined the eigenvalue α_1 in Eq. (6.133) for the asymptotic solution of the scalar radial flux. For comparison, we recall that the radial buckling, in diffusion theory, is given by the expression

$$(\alpha^2)_{\text{diff.}} = \left(\frac{2.4048}{R + d}\right)^2 \qquad (6.147)$$

with $d = 0.7104\ \lambda_{tr}$. The value of (R+d) for the miniature lattice ML3 is 27.522 cm (see Table 6.1), and we obtain

$$(\alpha^2)_{\text{diff.}} = 0.0076348\ \text{cm}^{-2} \quad \text{or} \quad 7634.8\ \mu\text{B}\ ,$$

which is 138 μB higher than the value resulting from the P_3 approximation. The usual difficulty associated with the expression Eq. (6.147) is the uncertainty involved in the value of d, the linear extrapolation distance: in a small assembly the radial buckling is sensitive to the value of d.

The value of the material buckling in the P_3 approximation is just the difference between Eq. (6.146) and Eq. (6.44):

$$B_m^2 = \alpha^2 - \gamma_1^2\ .$$

The value of γ_1^2 has been calculated to be 6516.3 μB in section 6.2.3. Thus, we have

$$B_m^2 = 7497.3 - 6516.3 = 981 \ \mu B ,$$

which agrees reasonably well with the experimental values: 1007 μB in the full-size lattice and 946 μB in the miniature lattice.

(ii) Calculation of the Radial Flux Distribution

The radial scalar flux distribution in the P_3 approximation is given by Eq. (6.133) which can be rewritten as

$$f_{o,o}(r) = A_1 \ J_o(|\alpha_1| \Sigma_t^{**} r) + \frac{A_2}{A_1} \ I_o(\alpha_2 \Sigma_t^{**} r) \quad ,$$

where the ratio A_2/A_1 is given by Eq. (6.143) and is found to be

$$\left(\frac{A_2}{A_1}\right) \simeq -108 \ e^{-78.8} .$$

Table 6.5 lists the values of the relative radial flux, $f_{o,o}(r)/A_1$, as a function of the radial distance. Because of the large argument in the I_o term, the following asymptotic formula for the I_o function is used in the calculations:

$$I_o(\chi) \approx \frac{0.3989}{\sqrt{\chi}} e^{\chi} , \qquad (6.148)$$

for $\chi > 10$. It is seen that the spatial transient is negative, and is important only within a centimeter or two from the physical boundary. This general result has also been observed in the study of Milne's problem. The negative nature of the spatial transient in the radial flux distribution could be helpful in reducing the reflector effect somewhat.

Table 6.5. Values of the relative radial flux $f_{o,o}(r)/A_1$ as a function of radial distance in a P_3 approximation for the miniature lattice ML3.

r (cm)	$J_o(\alpha_1 \Sigma_t^{**} r)$	$\left(\frac{A_2}{A_1}\right) I_o(\alpha_2 \Sigma_t^{**} r)$	$\frac{f_{o,o}(r)}{A_1}$
0.0	1.00000	~0.0	1.000000
2.0	0.99202	~0.0	0.992020
4.0	0.96969	~0.0	0.969690
6.0	0.93347	~0.0	0.933470
8.0	0.88366	~0.0	0.883660
10.0	0.82110	~0.0	0.821100
12.0	0.74740	~0.0	0.747400
14.0	0.66498	~0.0	0.664980
16.0	0.57490	~0.0	0.574900
18.0	0.47910	~0.0	0.479100
20.0	0.38060	-0.0000003	0.380600
22.0	0.28160	-0.000130	0.281470
22.4	0.25863	-0.000472	0.258158
23.0	0.22970	-0.002820	0.226880
23.4	0.20898	-0.009300	0.199680
24.0	0.17810	-0.061300	0.116800
24.4	0.16098	-0.202000	
25.0	0.13180	-1.334900	
25.4	0.11036	-4.860000	

(iii) Calculation of the Radial Geometric Buckling

For the miniature lattice ML3, Eq. (6.145) becomes

$$\frac{B_r^2(r)}{\alpha^2} = \left\{ \frac{1 + 1.388 \times 10^5 \; e^{-78.8 \frac{I_o(3.10r)}{J_o(0.0865r)}}}{1 - 1.08 \times 10^2 \; e^{-78.8 \frac{I_o(3.10r)}{J_o(0.0865r)}}} \right\}.$$

The values of the radial geometric buckling are listed in Table 6.6 at different radial distances from the center. The results are also plotted in Figure 6.4. It is evident that the geometric buckling is a highly sensitive parameter for testing for the asymptotic condition. In the particular miniature lattice ML3, the asymptotic region in the radial direction is given by $0 \leq r < 22$ cm. The spatial transient resulting from the transport effect has a substantial effect on the geometric buckling only within a centimeter or two from the physical boundary.

6.4 SUMMARY AND CONCLUSIONS

We have made separate spatial transient analyses for the axial and radial flux distributions by means of the spherical harmonics method. In both cases, a general theory was presented, but only a one-group P_3 approximation was used to calculate the eigenvalues, the total flux distribution, and the distribution of the geometric buckling for the miniature lattice ML3.

We can draw several conclusions from the results obtained:

(a) The transport effect does not seem to perturb the measurement of either the axial or radial buckling in the miniature lattice ML3, when the flux shape method is used, except within a few total mean free

Table 6.6. Values of the radial geometric buckling as a function of radial distance for the miniature lattice ML3.

Radial Position r (cm)	Radial Geometric Buckling $B_r^2(r)/\alpha^2$
0.0	1.000000
4.0	1.000000
8.0	1.000000
12.0	1.000000
14.0	1.000000
16.0	1.000000
18.0	1.000000
20.0	1.000092
22.0	1.059700
22.4	1.234800
23.0	2.601600
23.4	5.954000
24.0	67.200000

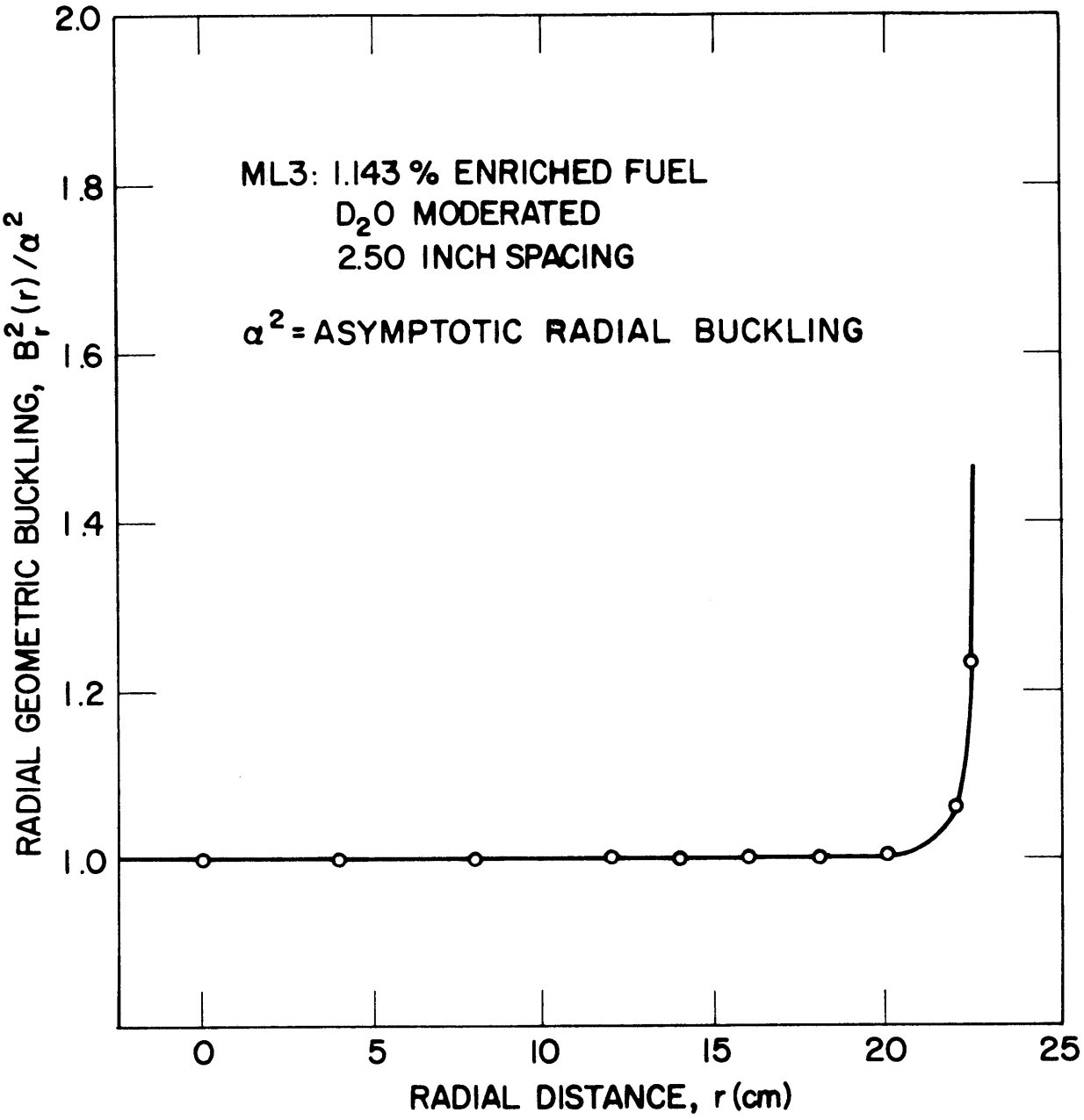

FIG. 6.4 DISTRIBUTION OF THE RADIAL GEOMETRIC BUCKLING AS A FUNCTION OF THE RADIAL DISTANCE FOR THE MINIATURE LATTICE ML3 IN A ONE-GROUP P3 APPROXIMATION.

paths from boundaries. Similar results should also be expected for the other miniature lattices although the transport effect may be more annoying for a tightly packed lattice because of the greater absorption of neutrons. The transport effect should be more severe in a light water lattice than in a heavy water lattice owing to larger neutron absorption in H_2O and to the greater anisotropic neutron scattering in H_2O.

(b) The spherical harmonics method yields expressions for the asymptotic axial and radial bucklings and, therefore, provides a way of calculating the values of these quantities in the presence of transport effects. However, the uncertainties involved in the nuclear data may lead to a significant error in the calculation of the asymptotic eigenvalues as we have shown. This difficulty emphasizes the importance of measurement of the asymptotic eigenvalues.

(c) A theoretical calculation of the flux distributions by means of the spherical harmonics method is, in general, faced with a difficulty in the boundary conditions. Although Marshak's boundary conditions appear to be the most convenient ones to use, they may not be suitable for all assemblies, depending on the composition of the assembly. Miniature lattices provide a good assembly for the study of boundary conditions.

Finally, we mention the energy transients arising from the non-separability of the neutron flux in space and energy. It should be possible to study these transients with the aid of expansions in terms of Laguerre polynomials (W2). This type of analysis would provide a parallel to the use of the spherical harmonics method in the study of spatial transients.

Chapter VII

SUMMARY, CONCLUSIONS AND RECOMMENDATIONS FOR FUTURE WORK

7.1 SUMMARY

The asymptotic conditions associated with buckling measurements in a subcritical assembly have been investigated, and practical criteria have been established for locating the asymptotic regions for the axial and radial flux distributions. These conditions have been derived from the neutron transport equations (Chapter II). They should be useful in the design of an exponential assembly for the measurement of the material buckling and also for the measurement of other lattice parameters.

Motivated by the difficulty of the conventional curve-fitting method in the analysis of the axial buckling and the extrapolated height, we have developed a moments method for these purposes (in Chapter III) and have applied it to several full-size lattices as well as to the miniature lattices studied at M.I.T. The results indicate that the moments method is more consistent than the curve-fitting method for the determination of the axial buckling and the extrapolated height. The standard deviations in these quantities have been reduced by as much as a factor of 2 by the use of the moments method.

An iterative moments method and a direct moments method have been developed for the analysis of the radial buckling (Chapter IV). These methods have been applied to several lattices and have turned

out to be more consistent than the curve-fitting method. These two methods are equivalent but the iterative moments method is much less affected by the truncation errors incurred in the numerical integration required to evaluate the flux moments. The consistency of the methods makes it possible to determine experimental values of the linear extrapolation distance and to compare them with the theoretical values predicted by asymptotic neutron transport theory.

Finally, a spatial transient analysis has been made for both the axial and radial flux distributions by means of the spherical harmonics method. A general theory has been given in both cases; a one-group P_3 approximation was used to analyze quantitatively the miniature lattice ML3, and was found sufficient. For the analysis of the spatial transients, the use of geometric buckling as a parameter for testing the asymptotic conditions has been found to be useful and sensitive. The application of this concept revealed that the miniature lattices do possess a certain asymptotic region although it may be small.

7.2 CONCLUSIONS

Several conclusions can be drawn from the present work:

(a) The moments methods developed in this work have several advantages over the conventional curve-fitting method: better consistency, clearer physical meaning, and considerable saving in the computer time needed for data reduction. The advantages are particularly marked in the analysis of the axial buckling and the extrapolated height because of the uncertainties in the determination of the "best values" of these quantities by means of the curve-fitting method.

The moments method has the surprising property described in Chapter III of increasing the extent of the asymptotic region available for the analysis of the axial buckling. As a consequence, the moments method is applicable to a relatively small assembly such as the miniature lattices where the curve-fitting method fails completely.

(b) The moments methods do have an inherent disadvantage with respect to the curve-fitting method, namely, the truncation error incurred in the evaluation of the flux moments through a numerical integration. In the analysis of the axial buckling, the truncation error was found to be insignificant if the number of experimental data is greater than 11. For the analysis of the radial buckling, this inherent disadvantage can be troublesome because of the relatively small number of experimental data available. The difficulty is greatly reduced by the use of the iterative moments method, described in section 4.3. This method computes, for the experimental data, the correction to the theoretical value predicted by diffusion theory.

(c) Comparing the moments methods with the curve-fitting method on a general basis, we conclude that (i) for the analysis of the axial buckling and the extrapolated height, the moments method developed in Chapter III is preferable to the conventional curve-fitting method because the latter cannot determine the values of the axial buckling and extrapolated height independently even in full-size lattices; but (ii) for the analysis of the radial buckling, the curve-fitting method is probably preferable when experimental data are well representable by the asymptotic flux distribution and if the number of the experimental data is relatively small.

(d) With respect to the feasibility of making buckling measurements in miniature lattices, it is difficult to draw a firm general conclusion owing to the small number of experimental results available. However, the measurement of the material buckling for the total neutrons density (subcadmium and epicadmium) seems feasible with the moments method on the basis of single measurements which have been made in each of six miniature lattices. From the studies in Chapters II and VI, we suggest that the following improvements be made in the experimental arrangement at the M. I. T. Lattice Project:

(i) Make the source as nearly isotropic as possible by, say, placing some scattering medium such as D_2O between the source and the lattice.

(ii) Make the assembly bare to both subcadmium and epicadmium neutrons.

(iii) Make the radial flux traverse at an axial position which lies in the range 25 cm < z < 35 cm.

(iv) Increase the diameter of the assembly, if possible.

(e) The basic problems associated with the buckling measurements in the miniature lattices appear to be the source effect and the energy effect. The former can be reduced considerably by the use of the moments method developed in Chapter III. The transport effect alone does not seem to disturb the asymptotic fluxes seriously (Chapter VI). This implies the applicability of diffusion theory to the miniature lattices. As for the energy effect, an energy transient analysis by means of Laguerre polynomial expansion technique seems worth making and is recommended for further research.

(f) According to the First Fundamental Theorem of Reactor Theory expressed by Weinberg and Wigner, the material buckling is the same for all neutron energy groups, provided that the extrapolation distance is independent of energy. That this last assumption is not valid is evident from the energy dependence of transport cross sections and has also been observed in measurements of the material buckling, both in the full-size lattices (Chapters III and IV) and in the miniature lattices (Chapter V). Therefore, the First Fundamental Theorem is valid, to a good approximation, only in a large system where the variation of the extrapolation distance with energy is unimportant. When the variation of the extrapolation distance with energy cannot be neglected, a multigroup analysis would require a buckling that varies from group to group. The question then arises: can the energy-dependent values of the buckling be averaged to produce a value that would correspond to the actual critical size of the reactor? This question is especially important in fast reactors where it is usually difficult to show that the neutron flux can be separated in space and energy.

7.3 RECOMMENDATIONS FOR FUTURE WORK

7.3.1 The Analysis of Energy Transients

An analysis of energy transients due to spectral inequilibrium in a small subcritical assembly would supply valuable information as to how far the energy transients would penetrate into the assembly of interest. It might then be possible to locate the boundaries of the asymptotic region in a quantitative way. Such an analysis should be

useful in the choice of an appropriate position for measuring the various lattice parameters. Very little work has been done in this area. A possible approach would be the use of a Laguerre polynomial expansion technique (W2, T2) analogous to the spherical harmonics method for the analysis of the spatial transients (Chapter VI). The solution for the zeroth Laguerre moment, together with the use of geometric buckling as a parameter for testing the asymptotic conditions as suggested in Chapter II, would yield information about the energy transients. Another approach which combines the transport effect as well as the energy effect is the use of the multigroup spherical harmonics method as described in section 6.2.1.

7.3.2 An Optimization Study on the Design of a Subcritical Assembly

The ultimate aim of such a study is to determine the lower limit to the useful size of a subcritical assembly for a valid measurement of reactor parameters. Some work has been done by Peak (P2) in this area. However, his work which is based on age-diffusion theory is by no means complete.

A more rigorous approach would be to use the multigroup spherical harmonics method as described in section 6.2.1 to determine the total flux distribution and hence the dependence of the geometric buckling on position for assemblies of different size. An alternative approach would be to treat the energy effect and the transport effect separately: an analysis of the energy transients as recommended in section 7.3.1 should yield the asymptotic condition with respect to spectral equilibrium; and a spatial transient analysis as done in Chapter VI should provide the asymptotic condition with respect to the transport effect.

7.3.3 Further Experimental Work on Buckling Measurements

More measurements of the axial and radial flux distributions are needed to permit firmer conclusions with respect to the feasibility of the measurement of the material buckling in miniature lattices. Some improvements of the miniature lattice facility, as suggested in section 7.2, might help.

Appendix A

COMPUTER PROGRAMS

The computer codes developed in the present work for the analysis of the axial and radial bucklings by means of the moments methods are described in this appendix. A general description of each code is given first, followed by the input data required, an IBM-FORTRAN IV listing, and a sample input deck.

A.1 THE ABMOMENT CODE

A.1.1 General Description

The ABMOMENT code was programmed in FORTRAN IV language for the IBM Operating System 360 Model 65 computer at the M. I. T. Computation Center. The code is composed of a main program and two subroutine subprograms: HELENA and SAMSON.

The subprogram HELENA computes the axial flux moments from the activation data with the second-order Simpson's rule for equal intervals (Appendix B or Ref. L2) and also computes the values of the axial buckling and extrapolated height for various integral values of the moment index from Eqs. (3.14) and (3.18). The lowest value of the moment index is 3 and the highest value allowed by the code is 10. This was done to save computer time in evaluating higher flux moments but is not an intrinsic limitation; the procedure can be modified easily if necessary. Experience has shown that when the value of the moment index is greater than 8, the truncation error incurred in the numerical integration becomes so important that a moment index larger than 10 is useless.

The subprogram SAMSON calculates the experimental errors, the truncation errors, and the combined probable errors associated with the axial buckling and the extrapolated height, for a series of values of the moment index in accordance with the error analysis described in section 3.2.3. This provides a way of determining the best values of the axial buckling and the extrapolated height.

The amount of computer time required depends on the maximum value of the moment index used and the number of data points chosen. A typical run for a set of 15 experimental data points and a maximum moment index of 8 requires 10 seconds or less. This is considerably smaller than the amount of computer time required by the AXFIT code (P1) owing to the necessity of analyzing as many as 50 cases in one computer run.

A.1.2 Input Data for the ABMOMENT Code

Card 1 (Format (A5, I3, 2F10.4, F8.2, F11.4, I5)). The following quantities appear, in order, on this card:

RUN is the experimental run number for the set of data being analyzed;

N is the number of data points submitted and must be ODD;

ENRICH is the enrichment in percent of the fuel;

DELZ is the spacing in centimeters between any two successive data points equally spaced;

PITCH is the lattice spacing in inches;

ZB is the axial distance from the source, in centimeters, corresponding to the first data point chosen for the analysis;

NM is the maximum value of the moment index desired, the highest allowable value being 10.

Card 2 (Format (6F12.6)). The following quantities appear, in order, on this card:

A(I) are the relative experimental activation data. They are read in on successive cards according to the specified format until N data have been stored in the memory of the computer.

A.1.3 FORTRAN IV Listings of the ABMOMENT Code

```
//ABMOMENT  JOB  (M2940,5551,10,5000,200),'H.S.CHENG',MSGLEVEL=1
//STEP      EXEC  FORCLG,PARM.C=(EBCDIC,DECK,MAP)
//C.SYSIN   DD  *
C      AXIAL BUCKLING CODE 'ABMOMENT'       H.S.CHENG
C      THIS CODE IS BASED ON DIRECT MOMENTS METHOD FOR THE ANALYSIS OF
C      THE AXIAL BUCKLING AND THE EXTRAPOLATED HEIGHT. SIMPSON'S RULE FOR
C      EQUAL INTERVALS IS USED TO EVALUATE THE AXIAL FLUX MOMENTS.
       DIMENSION A(50), AM(50), FM(50,50), FMM(50,50), F(50,50), C(50,10)
      1, H(50,10), TRE(50,10), EXPE(50,10), EXPEH(50,10), GAMSQ(50), GAM(
      250), EXTH(50), CEXTH(50), VARG(50), VARGT(50), VARH(50), VARHT(50)
      3, DEVG(50), DEVGT(50), DEVH(50), DEVHT(50), AZERO(50), AZEROH(50),
      4 CNUM(50), DENO(50), SUMN(50), SUMD(50), SUMHN(50), SUMHD(50), X(5
      50), Z(50), R1(50), R2(50), D2(50), D4(50), CDD(50), HEA(50), ZSQDS
      6(50), SUM(50), ARGN(50), ARGD(50), ARG(50), Y(50), V1(50), V2(50),
      7 V3(50), CNUMG(50), DENOG(50), SUMF(50), HN(50), HD(50), GBSQ(50),
      8 SUMH(50), SUMHT(50), PQ1(50), PQ2(50), SUMFM(50,50), GSQTH(30),
      9HTH(30), GAMTH(30), CDEVA(50), CDEVR(50), CVARA(50), CVARR(50)
       COMMON A, AM, FM, FMM, F, C, H, TRE, EXPE, EXPEH, GAMSQ, GAM, EXTH
      1, CEXTH, VARG, VARGT, VARH, VARHT, DEVG, DEVGT, DEVH, DEVHT, AZERO
      2, AZEROH, N, K, DELZ, CNM1, CNM2, ZSQ, DZ4, ZB, C2, C4, B, V1, V2,
      3 V3, GBSQ, ZSQDS, D2, D4, R1, R2, X, Z, CNUM, DENO, CDD, HEA, ARGN
      4, ARGD, ARG, HN, HD, PQ1, PQ2, NM, CDEVA, CDEVR, CVARA, CVARR,
      5GSQTH, GAMTH, HTH
   10 FORMAT(1H1,20X19H PROGRAM 'ABMOMENT'//)
   20 FORMAT(1HO,114HDETERMINATION OF THE OPTIMAL VALUES OF MOMENTS INDE
      1X FOR THE CALCULATION OF AXIAL BUCKLING AND EXTRAPOLATED HEIGHT//)
   30 FORMAT(A5,I3,2F10.4,F8.2,F11.4,I5)
   35 FORMAT(6F12.6)
   40 FORMAT(5H RUN=A5,13H   ENRICH(I)=F7.4,13H   PITCH(IN)=F6.3,12H   D
      1ELZ(CM)=F7.4,4X,7HZB(CM)=F8.4)
   50 FORMAT(1HO,20H INPUT ACTIVITY DATA)
   52 FORMAT(1HO,5(I3,F10.6,2X)/(1HO,5(1X,I2,F10.6,2X)))
   56 FORMAT(1HO,34HCOMPUTED RESULTS OF MOMENTS METHOD)
   60 FORMAT(1HO,10X,6HMOMENT,7X,14HAXIAL BUCKLING,7X,19HEXTRAPOLATED HE
      1IGHT)
   70 FORMAT(10X,6H INDEX,12X,6H(CM-2),18X,4H(CM))
   71 FORMAT(1HO,12X,1HI,13X,8HGAMSQ(I),15X,8HCEXTH(I))
   80 FORMAT(1HO,11X,I2,10X,1PE13.6,12X,1PE13.6)
   90 FORMAT(1H1,39HCOMPUTED RESULTS OF EXPERIMENTAL ERRORS//)
   91 FORMAT(1HO,31H THE THEORETICAL AXIAL BUCKLING)
   94 FORMAT(1HO,36H THE THEORETICAL EXTRAPOLATED HEIGHT)
  110 FORMAT(1HO,2X,6HMOMENT,7X,18HSTANDARD DEVIATION,7X,21HSTANDARD DEV
```

```
   1LATION IN,7X,11HVARIANCE IN,7X,18HVARIANCE IN EXTRA-)
120 FORMAT(2X,6H INDEX,8X,17HIN AXIAL BUCKLING,8X,19HEXTRAPOLATED HEIG
   1HT,9X,14HAXIAL BUCKLING,4X,14HPOLATED HEIGHT)
130 FORMAT(1HO,4X,1HI,14X,7HDEVG(I),20X,7HDEVH(I),19X,7HVARG(I),10X,7H
   1VARH(I))
140 FORMAT(1HO,3X,I2,13X,1PE13.6,14X,1PE13.6,12X,1PE13.6,5X,1PE13.6)
180 FORMAT(1H1,37HCOMPUTED RESULTS OF TRUNCATION ERRORS//)
190 FORMAT(1HO,2X,6HMOMENT,7X,18HSTANDARD DEVIATION,7X,21HSTANDARD DEV
   1LATION IN,7X,11HVARIANCE IN,7X,18HVARIANCE IN EXTRA-)
210 FORMAT(2X,6H INDEX,8X,17HIN AXIAL BUCKLING,8X,19HEXTRAPOLATED HEIG
   1HT,9X,14HAXIAL BUCKLING,4X,14HPOLATED HEIGHT)
220 FORMAT(1HO,4X,1HI,14X,8HDEVGT(I),20X,8HDEVHT(I),19X,8HVARGT(I),10X
   1,8HVARHT(I))
270 FORMAT(1HO,3X,I2,13X,1PE13.6,14X,1PE13.6,12X,1PE13.6,5X,1PE13.6)
610 FORMAT(1H1,65HCOMPUTED RESULTS OF COMBINED ERRORS(EXPERIMENTAL PLU
   1S TRUNCATION)//)
620 FORMAT(1HO,2X,6HMOMENT,7X,18HSTANDARD DEVIATION,7X,21HSTANDARD DEV
   1LATION IN,7X,11HVARIANCE IN,9X,18HVARIANCE IN EXTRA-)
630 FORMAT(2X,6H INDEX,8X,17HIN AXIAL BUCKLING,7X,19HEXTRAPOLATED HEIG
   1HT,9X,14HAXIAL BUCKLING,6X,14HPOLATED HEIGHT)
640 FORMAT(1HO,4X,1HI,14X,8HCDEVA(I),18X,8HCDEVR(I),18X,8HCVARA(I),10X
   1,8HCVARR(I))
650 FORMAT(1HO,3X,I2,11X,1PE13.6,13X,1PE13.6,12X,1PE13.6,7X,1PE13.6)
    JOANNE = 101
  6 READ (5,30) RUN, N, ENRICH, DELZ, PITCH, ZB, NM
    READ (5,35) (A(I), I=1,N)
    WRITE (6,10)
    WRITE (6,20)
    WRITE (6,40) RUN, ENRICH, PITCH, DELZ, ZB
    WRITE (6,50)
    WRITE (6,52) (I,A(I),I=1,N)
    WRITE (6,56)
    CALL HELENA
    WRITE (6,60)
    WRITE (6,70)
    WRITE (6,71)
    WRITE (6,80) (I, GAMSQ(I), CEXTH(I), I=3,NM)
    WRITE (6,90)
    WRITE (6,40) RUN, ENRICH, PITCH, DELZ, ZB
    WRITE (6,110)
    WRITE (6,120)
    WRITE (6,130)
    CALL SAMSON
    WRITE (6,140) (I, DEVG(I), DEVH(I), VARG(I), VARH(I), I=3,NM)
    WRITE (6,180)
    WRITE (6,40) RUN, ENRICH, PITCH, DELZ, ZB
    WRITE (6,190)
    WRITE (6,210)
    WRITE (6,220)
    WRITE (6,270) (I, DEVGT(I), DEVHT(I), VARGT(I), VARHT(I), I=3,NM)
    WRITE (6,610)
    WRITE (6,40) RUN, ENRICH, PITCH, DELZ, ZB
    WRITE (6,620)
    WRITE (6,630)
    WRITE (6,640)
    WRITE (6,650) (I, CDEVA(I), CDEVR(I), CVARA(I), CVARR(I),I=3,NM)
    WRITE (6,91)
```

```
      WRITE (6,52) (J, GSQTH(J), J=3,NM)
      WRITE (6,94)
      WRITE (6,52) (J, HTH(J), J=3,NM)
      GO TO 6
      END
      SUBROUTINE HELENA
C     CALCULATION OF MOMENTS, AXIAL BUCKLING AND EXTRAPOLATED HEIGHT
      DIMENSION A(50), AM(50), FM(50,50), FMM(50,50), F(50,50), C(50,10)
     1, H(50,10), TRE(50,10), EXPE(50,10), EXPEH(50,10), GAMSQ(50), GAM(
     250), EXTH(50), CEXTH(50), VARG(50), VARGT(50), VARH(50), VARHT(50)
     3, DEVG(50), DEVGT(50), DEVH(50), DEVHT(50), AZERO(50), AZEROH(50),
     4 CNUM(50), DENO(50), SUMN(50), SUMD(50), SUMHN(50), SUMHD(50), X(5
     50), Z(50), R1(50), R2(50), D2(50), D4(50), CDD(50), HEA(50), ZSQDS
     6(50), SUM(50), ARGN(50), ARGD(50), ARG(50), Y(50), V1(50), V2(50),
     7 V3(50), CNUMG(50), DENOG(50), SUMF(50), HN(50), HD(50), GBSQ(50),
     8 SUMH(50), SUMHT(50), PQ1(50), PQ2(50), SUMFM(50,50), GSQTH(30),
     9HTH(30), GAMTH(30), CDEVA(50), CDEVR(50), CVARA(50), CVARR(50)
      COMMON A, AM, FM, FMM, F, C, H, TRE, EXPE, EXPEH, GAMSQ, GAM, EXTH
     1, CEXTH, VARG, VARGT, VARH, VARHT, DEVG, DEVGT, DEVH, DEVHT, AZERO
     2, AZEROH, N, K, DELZ, CNM1, CNM2, ZSQ, DZ4, ZB, C2, C4, B, V1, V2,
     3 V3, GBSQ, ZSQDS, D2, D4, R1, R2, X, Z, CNUM, DENO, CDD, HEA, ARGN
     4, ARGD, ARG, HN, HD, PQ1, PQ2, NM, CDEVA, CDEVR, CVARA, CVARR,
     5GSQTH, GAMTH, HTH
C     CALCULATION OF EXPERIMENTAL MOMENTS AM(I) BY SIMPSON'S RULE
      K = (N-3)/2
      CNM1 = N-1
      CNM2 = N-2
      ZSQ = DELZ*DELZ
      C2 = CNM1**2
      C4 = CNM1**4
      B = CNM1*DELZ
      DZ4 = 1./(DELZ**4)
      DO 17 J=1,12
      SUM(J)=0.0
      DO 18 I=1,K
   18 SUM(J)=SUM(J)+4.*A(2*I)*EXP((J-1)*ALOG(2.*I-1.))+2.*A(2*I+1)*EXP((
     1J-1)*ALOG(2.*I))
      IF(J .GT. 1) GO TO 19
      AM(1)=1./3.*(A(1)+SUM(1)+4.*A(N-1)+A(N))
      GO TO 17
   19 V1(J)=(J-1)*ALOG(CNM1)
      V2(J)=(J-1)*ALOG(CNM2)
      V3(J)=(J-2)*ALOG(CNM1)
      AM(J)=1./3.*(SUM(J)+4.*A(N-1)*EXP(V2(J))+A(N)*EXP(V1(J)))
   17 CONTINUE
      WRITE (6,290)
  290 FORMAT(1HO,20HEXPERIMENTAL MOMENTS)
      WRITE (6,310) (I,AM(I),I=1,12)
  310 FORMAT(1HO,5(I3,2X,1PE13.6,3X)/(1HO,5(1X,I2,2X,1PE13.6,3X)))
C     CALCULATION OF AXIAL BUCKLING, GAMSQ(I)
      DO 21 I=3,NM
      CNUMG(I)= I*(I+1)*AM(I)-2.*I*(I-1)*CNM1*AM(I-1)+(I-1)*(I-2)*C2*AM(
     1I-2)
      DENOG(I)= AM(I+2)-2.*CNM1*AM(I+1)+C2*AM(I)
      GAMSQ(I)= CNUMG(I)/(ZSQ*DENOG(I))
      GAM(I)= SQRT(GAMSQ(I))
C     CALCULATION OF EXTRAPOLATED HEIGHT, CEXTH(I)
```

```
      ARGN(I)=GAMSQ(I)*ZSQ*(CNM1*AM(I)-AM(I+1))+I*(I-1)*AM(I-1)-(I-1)*(I
     1-2)*CNM1*AM(I-2)
      ARGD(I)=GAMSQ(I)*ZSQ*((I-1)*AM(I+1)-I*CNM1*AM(I))-I*(I-1)**2*AM(I-
     11)+I*(I-1)*(I-2)*CNM1*AM(I-2)
      ARG(I)=GAM(I)*B*ARGN(I)/ARGD(I)
      Y(I)=(1.+ARG(I))/(1.-ARG(I))
C     CHECK THE ARGUMENT
      IF(Y(I) .LE. 0.) GO TO 3
      EXTH(I)= B+0.5*ALOG(Y(I))/GAM(I)
C     ZB IS THE DISTANCE FROM THE BOTTOM TO THE FIRST POINT OF INPUT
C     DATA CHOSEN IN THIS BUCKLING CALCULATION
      CEXTH(I)= ZB + EXTH(I)
   21 CONTINUE
      RETURN
    3 WRITE (6,9)
    9 FORMAT(1H0,20HTROUBLESOME ARGUMENT)
      RETURN
      END
      SUBROUTINE SAMSON
C     ESTIMATE OF EXPERIMENTAL AND TRUNCATION ERRORS IN AXIAL BUCKLING
C     AND EXTRAPOLATED HEIGHT
      DIMENSION A(50), AM(50), FM(50,50), FMM(50,50), F(50,50), C(50,10)
     1, H(50,10), TRE(50,10), EXPE(50,10), EXPEH(50,10), GAMSQ(50), GAM(
     250), EXTH(50), CEXTH(50), VARG(50), VARGT(50), VARH(50), VARHT(50)
     3, DEVG(50), DEVGT(50), DEVH(50), DEVHT(50), AZERO(50), AZEROH(50),
     4 CNUM(50), DENO(50), SUMN(50), SUMD(50), SUMHN(50), SUMHD(50), X(5
     50), Z(50), R1(50), R2(50), D2(50), D4(50), CDD(50), HEA(50), ZSQDS
     6(50), SUM(50), ARGN(50), ARGD(50), ARG(50), Y(50), V1(50), V2(50),
     7 V3(50), CNUMG(50), DENOG(50), SUMF(50), HN(50), HD(50), GBSQ(50),
     8 SUMH(50), SUMHT(50), PQ1(50), PQ2(50), SUMFM(50,50), GSQTH(30),
     9HTH(30), GAMTH(30), CDEVA(50), CDEVR(50), CVARA(50), CVARR(50)
      COMMON A, AM, FM, FMM, F, C, H, TRE, EXPE, EXPEH, GAMSQ, GAM, EXTH
     1, CEXTH, VARG, VARGT, VARH, VARHT, DEVG, DEVGT, DEVH, DEVHT, AZERO
     2, AZEROH, N, K, DELZ, CNM1, CNM2, ZSQ, DZ4, ZB, C2, C4, B, V1, V2,
     3 V3, GBSQ, ZSQDS, D2, D4, R1, R2, X, Z, CNUM, DENO, CDD, HEA, ARGN
     4, ARGD, ARG, HN, HD, PQ1, PQ2, NM, CDEVA, CDEVR, CVARA, CVARR,
     5GSQTH, GAMTH, HTH
      DO 23 J=3,NM
C     GENERATION OF THEORETICAL INPUT DATA F(J,I)
      DO 27 I=1,N
   27 F(J,I)=SINH(GAM(J)*EXTH(J)-(I-1)*GAM(J)*DELZ)
C     CALCULATION OF THEORETICAL MOMENTS BY SIMPSON'S RULE USING F(J,I)
      DO 28 L=1,12
      SUMFM(J,L)=0.0
      DO 29 M=1,K
   29 SUMFM(J,L)=SUMFM(J,L)+4.*F(J,2*M)*EXP((L-1)*ALOG(2.*M-1.))+2.*F(J,
     12*M+1)*EXP((L-1)*ALOG(2.*M))
      IF(L .GT. 1) GO TO 41
      FM(J,1)=1./3.*(F(J,1)+SUMFM(J,1)+4.*F(J,N-1)+F(J,N))
      GO TO 28
   41 FM(J,L)=1./3.*(SUMFM(J,L)+4.*F(J,N-1)*EXP(V2(L))+F(J,N)*EXP(V1(L))
     1)
   28 CONTINUE
C     CALCULATION OF ANALYTICAL MOMENTS FMM(J,I)
      X(J)=GAM(J)*(EXTH(J)-B)
      Z(J)=GAM(J)*EXTH(J)
      R1(J)=1./(GAM(J)*DELZ)
```

```
      R2(J)=1./(GAMSQ(J)*ZSQ)
      FMM(J,1)=R1(J)*(-COSH(X(J))+COSH(Z(J)))
      FMM(J,2)=-CNM1*R1(J)*COSH(X(J))-R2(J)*SINH(X(J))+R2(J)*SINH(Z(J))
      DO 42 I=3,12
   42 FMM(J,I)=-R1(J)*EXP(V1(I))*COSH(X(J))-(I-1)*R2(J)*EXP(V3(I))*SINH(
     1X(J))+(I-1)*(I-2)*R2(J)*FMM(J,I-2)
      ONUM(J)=J*(J+1)*FMM(J,J)-2.*J*(J-1)*CNM1*FMM(J,J-1)+(J-1)*(J-2)*C2
     1*FMM(J,J-2)
      DENO(J)=FMM(J,J+2)-2.*CNM1*FMM(J,J+1)+C2*FMM(J,J)
      GSQTH(J)=CNUM(J)/(ZSQ*DENO(J))
      GAMTH(J)=SQRT(GSQTH(J))
      D2(J)=DENO(J)**2
      D4(J)=DENO(J)**4
      CDD(J)=CNUM(J)**2/D4(J)
C     CALCULATION OF COEFFICIENTS C(J,I) FOR AXIAL BUCKLING
      C(J-2,1)=DZ4*((J-1)*(J-2))**2*C4/D2(J)
      C(J-1,2)=DZ4*4.*(J*(J-1))**2*C2/D2(J)
      C(J,3)=DZ4*(J*(J+1)*DENO(J)-C2*CNUM(J))**2/D4(J)
      C(J+1,4)=DZ4*4.*C2*CDD(J)
      C(J+2,5)=DZ4*CDD(J)
C     EVALUATION OF NORMALIZATION CONSTANT AZERO(J) FOR AXIAL BUCKLING
      SUMN(J)=0.0
      DO 43 I=1,5
   43 SUMN(J)=SUMN(J)+C(J+I-3,I)*AM(J+I-3)**2
      SUMD(J)=0.0
      DO 44 I=1,5
   44 SUMD(J)=SUMD(J)+C(J+I-3,I)*AM(J+I-3)*FM(J,J+I-3)
      AZERO(J)=SUMN(J)/SUMD(J)
C     ESTIMATE OF TRUNCATION ERRORS IN MOMENTS
      DO 46 I=1,5
   46 TRE(J+I-3,I)=FMM(J,J+I-3)-FM(J,J+I-3)
C     ESTIMATE OF EXPERIMENTAL ERRORS IN MOMENTS
      DO 47 I=1,5
   47 EXPE(J+I-3,I)=FM(J,J+I-3)-AM(J+I-3)/AZERO(J)
      VARGT(J)=0.0
      DO 48 I=1,5
   48 VARGT(J)=VARGT(J)+C(J+I-3,I)*TRE(J+I-3,I)**2
      DEVGT(J)=SQRT(VARGT(J))
      VARG(J)=0.0
      DO 49 I=1,5
   49 VARG(J)=VARG(J)+C(J+I-3,I)*EXPE(J+I-3,I)**2
      DEVG(J)=SQRT(VARG(J))
C     CALCULATION OF COEFFICIENTS H(J,I) FOR EXTRAPOLATED HEIGHT
      HN(J)=GAMSQ(J)*ZSQ*(CNM1*FMM(J,J)-FMM(J,J+1))+J*(J-1)*FMM(J,J-1)-
     1(J-1)*(J-2)*CNM1*FMM(J,J-2)
      HD(J)=GAMSQ(J)*ZSQ*((J-1)*FMM(J,J+1)-J*CNM1*FMM(J,J))-J*(J-1)**2*F
     1MM(J,J-1)+J*(J-1)*(J-2)*CNM1*FMM(J,J-2)
      GBSQ(J)=GAMSQ(J)*B*B
      HEA(J)=HD(J)*HD(J)-GBSQ(J)*HN(J)*HN(J)
      ZSQDS(J)=ZSQ/(HEA(J)*HEA(J))
      PQ1(J)=(HD(J)+J*HN(J))**2
      PQ2(J)=(HD(J)+(J-1)*HN(J))**2
      H(J-2,1)=((J-1)*(J-2))**2*C4*PQ1(J)*ZSQDS(J)
      H(J-1,2)=(J*(J-1))**2*C2*PQ2(J)*ZSQDS(J)
      H(J,3)=GBSQ(J)**2*PQ1(J)*ZSQDS(J)
      H(J+1,4)=GBSQ(J)*GAMSQ(J)*ZSQ*PQ2(J)*ZSQDS(J)
      H(J,5)=(-(EXTH(J)-B)/GAM(J)+B/(GAM(J)*HEA(J))*(HN(J)*HD(J)+2.*GAMS
```

```
     1Q(J)*ZSQ*HD(J)*(CNM1*FMM(J,J)-FMM(J,J+1))-2.*GAMSQ(J)*ZSQ*HN(J)*(
     2(J-1)*FMM(J,J+1)-J*CNM1*FMM(J,J))))**2
C      EVALUATION OF NORMALIZATION CONSTANT AZEROH(J)
       SUMHN(J)=0.0
       DO 61 I=1,4
   61  SUMHN(J)=SUMHN(J)+H(J+I-3,I)*AM(J+I-3)**2
       SUMHD(J)=0.0
       DO 62 I=1,4
   62  SUMHD(J)=SUMHD(J)+H(J+I-3,I)*AM(J+I-3)*FM(J,J+I-3)
       AZEROH(J)=SUMHN(J)/SUMHD(J)
C      ESTIMATE OF EXPERIMENTAL ERRORS IN MOMENTS
       DO 63 I=1,4
   63  EXPEH(J+I-3,I)=FM(J,J+I-3)-AM(J+I-3)/AZEROH(J)
       SUMHT(J)=0.0
       DO 64 I=1,4
   64  SUMHT(J)=SUMHT(J)+H(J+I-3,I)*TRE(J+I-3,I)**2
       VARHT(J)=SUMHT(J)+H(J,5)*VARGT(J)/(4.*GAMSQ(J))
       DEVHT(J)=SQRT(VARHT(J))
       SUMH(J)=0.0
       DO 66 I=1,4
   66  SUMH(J)=SUMH(J)+H(J+I-3,I)*EXPEH(J+I-3,I)**2
       VARH(J)=SUMH(J)+H(J,5)*VARG(J)/(4.*GAMSQ(J))
       DEVH(J)=SQRT(VARH(J))
C      CALCULATION OF COMBINED ERRORS IN AXIAL BUCKLING
C      AND EXTRAPOLATED HEIGHT
       CVARA(J)=VARG(J)+VARGT(J)
       CVARR(J)=VARH(J)+VARHT(J)
       CDEVA(J)=SQRT(CVARA(J))
       CDEVR(J)=SQRT(CVARR(J))
   23  CONTINUE
       RETURN
       END
/*
```

A.1.4 Sample Input Deck

```
ML5 13      1.0270      2.5400      2.50      8.8900      8
  0.465590      0.373470      0.286780      0.239050      0.181480      0.149180
  0.114120      0.093793      0.073366      0.058854      0.044442      0.033527
  0.022638
```

A.2 THE RAMBLER CODE

A.2.1 General Description

The RAMBLER code was programmed in FORTRAN IV for the same type of computer according to the iterative moments method described in section 4.3. The code computes the values of the radial buckling and the extrapolated radius as well as the probable errors in these quantities.

The code consists of a main program and four subroutine subprograms: MOMENT, CASE 1, CASE 2, and CASE 3. The subroutine MOMENT computes the radial flux moments by means of the second-order Simpson's rule for unequal intervals described in Appendix B. The subroutines CASE 1, CASE 2, and CASE 3 calculate the values of the radial buckling and the extrapolated radius as well as the probable errors in these quantities in accordance with the three cases considered in section 4.3.

A.2.2 Input Data for the RAMBLER Code

Card 1 (Format (A5, I3, 2F10.4, F8.2, F10.4)). The following quantities appear, in order, on this card:

RUN is the experimental run number for the set of data being analyzed;

N is the number of data points submitted and must be ODD;

ENRICH is the fuel enrichment in percent of the lattice being analyzed;

RODIA is the diameter of the fuel rod in inches;

PITCH is the lattice spacing in inches;

ALPH(1) is the initial guessed value in cm^{-1} of the square root of the radial buckling calculated by means of Eq. (4.1).

Card 2 (Format (6F12.6)). The following quantities appear, in order, on this card:

A(I) are the relative experimental activation data. They are read in on successive cards according to the specified format until N data have been stored in the memory of the computer.

Card 3 (Format (6F12.5)). The following quantities appear, in order, on this card:

R(I) are the radial positions, in centimeters, corresponding to the various experimental data points being analyzed. They are read in on successive cards according to the specified format until N values of the radial positions have been stored in the memory of the computer.

```
C      RADIAL BUCKLING CODE 'RAMBLER'        H.S.CHENG
C      THIS CODE IS BASED ON THE ITERATIVE MOMENTS METHOD FOR THE
C      EXTRACTION OF THE RADIAL BUCKLING AND THE EXTRAPOLATED RADIUS
C      FROM FOIL ACTIVATION DATA
       DIMENSION A(50),ALPH(20),ALPHSQ(20),R(30),H(30),W(30),SUMR(5),RMEX
      1P(5),RMTH(5),AJ0(20),AJ1(20),D1(20),D2(20),D3(20),G(20),HD(20),F(2
      20),U(20),V(20),D4(20),DELADA(20),DELASQ(20),DELRM(5)
       COMMON A, R, H, W, ALPH, ALPHSQ, RMEXP, RMTH, G, DELADA, DELRM,
      1DELASQ, AJ0, AJ1, D1, D2, D3, D4, HD, F, R4, ARGC, U, V, EXTR, M,
      2RATIO1, RATIO2, RATIO3, RSQ, N, B1, B2, B4, B6, AZERO, SIGASQ,SIGR
     1 FORMAT(1H1,20X18H PROGRAM 'RAMBLER'//)
     2 FORMAT(1H0,87H THE CALCULATION OF RADIAL BUCKLING AND EXTRAPOLATED
      1 RADIUS BY ITERATIVE MOMENTS METHOD//)
     3 FORMAT(A5,I3,2F10.4,F8.2,2F10.4)
     4 FORMAT(6F12.6)
     5 FORMAT(5H RUN=A5,19H   ENRICH(PERCENT)=F7.4,13H   PITCH(IN)=F6.3,
      113H   RODIA(IN)=F7.4//)
     6 FORMAT(1H0,27H INPUT RADIAL ACTIVITY DATA)
     7 FORMAT(1H0,5(I3,F10.6,2X)/(1H0,5(1X,I2,F10.6,2X)))
     8 FORMAT(1H1,21HTHE ITERATION RESULTS//)
     9 FORMAT(1H0,27H INPUT RADIAL POSITION DATA)
    10 FORMAT(10H ITERATION,4X,15HRADIAL BUCKLING,4X,13HCORRECTION IN)
    11 FORMAT(3X,5HINDEX,8X,9HALPHSQ(J),7X,15HRADIAL BUCKLING)
    12 FORMAT(5X,1HJ,11X,6H(CM-2),10X,12HDELALPHSQ(J))
    13 FORMAT(36X,6H(CM-2))
    14 FORMAT(1H0,37HTHE FINAL CONVERGENT RADIAL BUCKLING=1PE13.6,2X,25HI
      1NVERSE SQUARE CENTIMETER)
    15 FORMAT(1H0,38HTHE CORRESPONDING EXTRAPOLATED RADIUS=1PE13.6,2X,11H
      1CENTIMETERS)
    16 FORMAT(1H0,37HTHE DEGREE OF FIT IN RADIAL BUCKLING=1PE13.6,2X,25HI
      1NVERSE SQUARE CENTIMETER)
    17 FORMAT(1H0,41HTHE DEGREE OF FIT IN EXTRAPOLATED RADIUS=1PE13.6,2X,
      111HCENTIMETERS)
    20 FORMAT(1H0,27HTHE NORMALIZATION CONSTANT=1PE13.6)
    22 FORMAT(6F12.5)
    71 FORMAT(1H0,33HCASE1,THIRD TO FIRST MOMENT RATIO//)
    72 FORMAT(1H1,34HCASE2, FIFTH TO THIRD MOMENT RATIO//)
    73 FORMAT(1H1,34HCASE3, FIFTH TO FIRST MOMENT RATIO//)
C      THE FOLLOWING STATEMENT IS DUMMY
       HELEN=1.00
    21 READ (5,3) RUN, N, ENRICH, RODIA, PITCH, ALPH(1)
       READ (5,4) (A(I), I=1,N)
       READ (5,22) (R(I),I=1,N)
       WRITE (6,1)
       WRITE (6,2)
       WRITE (6,5) RUN, ENRICH, PITCH, RODIA
       WRITE (6,6)
       WRITE (6,7) (I,A(I),I=1,N)
       WRITE (6,9)
       WRITE (6,7) (I,R(I),I=1,N)
       CALL MOMENT
       WRITE (6,8)
       WRITE (6,71)
       WRITE (6,5) RUN, ENRICH, PITCH, RODIA
       WRITE (6,10)
       WRITE (6,11)
       WRITE (6,12)
```

```
      WRITE (6,13)
      CALL CASE1
      WRITE (6,14) ALPHSQ(M)
      WRITE (6,15) EXTR
      WRITE (6,16) SIGASQ
      WRITE (6,17) SIGR
      WRITE (6,20) AZERO
      WRITE (6,72)
      WRITE (6,5) RUN, ENRICH, PITCH, RODIA
      WRITE (6,10)
      WRITE (6,11)
      WRITE (6,12)
      WRITE (6,13)
      CALL CASE2
      WRITE (6,14) ALPHSQ(M)
      WRITE (6,15) EXTR
      WRITE (6,16) SIGASQ
      WRITE (6,17) SIGR
      WRITE (6,20) AZERO
      WRITE (6,73)
      WRITE (6,5) RUN, ENRICH, PITCH, RODIA
      WRITE (6,10)
      WRITE (6,11)
      WRITE (6,12)
      WRITE (6,13)
      CALL CASE3
      WRITE (6,14) ALPHSQ(M)
      WRITE (6,15) EXTR
      WRITE (6,16) SIGASQ
      WRITE (6,17) SIGR
      WRITE (6,20) AZERO
      GO TO 21
      END
      SUBROUTINE MOMENT
C     CALCULATION OF THE EXPERIMENTAL RADIAL FLUX MOMENTS
C     BY MEANS OF SIMPSON'S RULE FOR UNEQUAL INTERVALS
      DIMENSION A(50),ALPH(20),ALPHSQ(20),R(30),H(30),W(30),SUMR(5),RMEX
     1P(5),RMTH(5),AJ0(20),AJ1(20),D1(20),D2(20),D3(20),G(20),HD(20),F(2
     20),U(20),V(20),D4(20),DELADA(20),DELASQ(20),DELRM(5)
      COMMON A, R, H, W, ALPH, ALPHSQ, RMEXP, RMTH, G, DELADA, DELRM,
     1DELASQ, AJ0, AJ1, D1, D2, D3, D4, HD, F, R4, ARGC, U, V, EXTR, M,
     2RATIO1, RATIO2, RATIO3, RSQ, N, B1, B2, B4, B6, AZERO, SIGASQ,SIGR
      K = (N-1)/2
      H(1)=R(1)
      DO 26 I=2,N
   26 H(I)=R(I)-R(I-1)
      DO 23 I=1,K
      W(2*I)=(-H(2*I+1)**2+10.*H(2*I)*H(2*I+1)-H(2*I)**2)/(H(2*I+1)+H(2*
     1I))
      W(2*I+1)=(7.*H(2*I+1)**2-4.*H(2*I+1)*H(2*I)+H(2*I)**2)/(2.*(H(2*I+
     11)+H(2*I)))
   23 CONTINUE
      DO 24 J=1,5,2
      SUMR(J)=0.0
      DO 25 I=2,K
   25 SUMR(J)=SUMR(J)+W(2*I)*A(2*I)*EXP(J*ALOG(R(2*I)))+(W(2*I+1)+W(2*I-
     11))*A(2*I-1)*EXP(J*ALOG(R(2*I-1)))
```

```
      RMEXP(J)=0.3333333*(SUMR(J)+W(3)*A(1)*EXP(J*ALOG(R(1)))+W(2)*A(2)*
     1EXP(J*ALOG(R(2)))+W(N)*A(N)*EXP(J*ALOG(R(N)))+0.5*R(1)*A(1)*EXP(J*
     2ALOG(R(1))))
   24 CONTINUE
      RATIO1=RMEXP(3)/RMEXP(1)
      RATIO2=RMEXP(5)/RMEXP(3)
      RATIO3=RMEXP(5)/RMEXP(1)
      WRITE (6,27)
   27 FORMAT(1HO,42HEXPERIMENTAL RADIAL FLUX MOMENTS, RMEXP(I))
      WRITE (6,28) (I,RMEXP(I),I=1,5,2)
   28 FORMAT(1HO,5(I3,2X,1PE13.6,3X)/(1HO,5(1X,I2,2X,1PE13.6,3X)))
      WRITE (6,33)
   33 FORMAT(1HO,23HTHE FLUX MOMENTS RATIOS)
      WRITE (6,34) RATIO1, RATIO2, RATIO3
   34 FORMAT(1HO,18HRMEXP(3)/RMEXP(1)=1PE13.6,3X,18HRMEXP(5)/RMEXP(3)=1P
     1E13.6,3X,18HRMEXP(5)/RMEXP(1)=1PE13.6)
      RETURN
      END
      SUBROUTINE CASE1
C     CALCULATION OF THE RADIAL BUCKLING AND THE EXTRAPOLATED RADIUS
C     BY MEANS OF THE ITERATIVE MOMENTS METHOD WITH THE THIRD TO FIRST
C     MOMENT RATIO.
      DIMENSION A(50),ALPH(20),ALPHSQ(20),R(30),H(30),W(30),SUMR(5),RMEX
     1P(5),RMTH(5),AJ0(20),AJ1(20),D1(20),D2(20),D3(20),G(20),HD(20),F(2
     20),U(20),V(20),D4(20),DELADA(20),DELASQ(20),DELRM(5)
      COMMON A, R, H, W, ALPH, ALPHSQ, RMEXP, RMTH, G, DELADA, DELRM,
     1DELASQ, AJ0, AJ1, D1, D2, D3, D4, HD, F, R4, ARGO, U, V, EXTR, M,
     2RATIO1, RATIO2, RATIO3, RSQ, N, B1, B2, B4, B6, AZERO, SIGASQ,SIGR
      ALPHSQ(1)=ALPH(1)**2
      RSQ = R(N)**2
      DELASQ(1)=0.0
      DO 29 J=1,17
      ARGA=ALPH(J)*R(N)
      CALL BESJ(ARGA,0,BJ,1.0E-08,IER)
      AJ0(J)=BJ
      CALL BESJ(ARGA,1,BJ,1.0E-08,IER)
      AJ1(J)=BJ
      D1(J)=RSQ*AJ0(J)
      D2(J)=R(N)*AJ1(J)/ALPH(J)
      D3(J)=1./ALPHSQ(J)
      G(J)=2.*D3(J)*D1(J)+D2(J)*(RSQ-4.*D3(J))
      HD(J)=D1(J)*(8.*D3(J)-RSQ)+4.*D2(J)*(RSQ-4.*D3(J))
      F(J)= -D1(J) + 2.*D2(J)
      B1=G(J)-RATIO1*D2(J)
      B2=HD(J)-RATIO1*F(J)
      DELADA(J)=B1/B2
      ALPH(J+1)=ALPH(J)*(1+DELADA(J))
      ALPHSQ(J+1)=ALPH(J+1)**2
      DELASQ(J+1)=ALPHSQ(J)*DELADA(J)*(2.+DELADA(J))
      M= J+1
      IF(ABS(DELADA(J)) .LT. 1.0E-04) GO TO 200
   29 CONTINUE
  200 WRITE (6,30) (I, ALPHSQ(I), DELASQ(I), I=1,M)
   30 FORMAT(1HO,3X,I2,8X,1PE13.6,5X,1PE13.6)
      EXTR=2.4048/ALPH(M)
C     THE DEGREE OF FIT IS EVALUATED BY THE ESTIMATE OF ERRORS IN THE
C     EXPERIMENTAL RADIAL FLUX MOMENTS.
```

```
C       CALCULATION OF THE THEORETICAL RADIAL FLUX MOMENTS
        RMTH(1)=D2(M-1)-DELADA(M-1)*F(M-1)
        RMTH(3)=G(M-1)-DELADA(M-1)*HD(M-1)
        CCE=(-D2(M-1)*B2+F(M-1)*B1)/B2**2
        CC =ABS(CCE)
        AZERO=(RMTH(1)**2*RMEXP(3)**2+RMTH(3)**2*RMEXP(1)**2)/(RMTH(1)**2*
       1RMTH(3)*RMEXP(3)+RMTH(1)*RMEXP(1)*RMTH(3)**2)
        DELRM(1)=RMTH(1)-RMEXP(1)/AZERO
        DELRM(3)=RMTH(3)-RMEXP(3)/AZERO
        DELF = DELRM(3)**2/RMTH(1)**2 + RMTH(3)**2*DELRM(1)**2/RMTH(1)**4
        DELY =CC*SQRT(DELF)
C       SIGASQ IS THE DEGREE OF FIT FOR THE RADIAL BUCKLING
        SIGASQ = 2.*ALPHSQ(M)*(1.+DELADA(M-1))*DELY
        SIGR =1.2024*SIGASQ/ALPH(M)**3
        RETURN
        END
        SUBROUTINE CASE2
C       CALCULATION OF THE RADIAL BUCKLING AND THE EXTRAPOLATED RADIUS
C       BY MEANS OF THE ITERATIVE MOMENTS METHOD WITH THE FIFTH TO THIRD
C       MOMENT RATIO.
        DIMENSION A(50),ALPH(20),ALPHSQ(20),R(30),H(30),W(30),SUMR(5),RMEX
       1P(5),RMTH(5),AJO(20),AJ1(20),D1(20),D2(20),D3(20),G(20),HD(20),F(2
       20),U(20),V(20),D4(20),DELADA(20),DELASQ(20),DELRM(5)
        COMMON A, R, H, W, ALPH, ALPHSQ, RMEXP, RMTH, G, DELADA, DELRM,
       1DELASQ, AJO, AJ1, D1, D2, D3, D4, HD, F, R4, ARGO, U, V, EXTR, M,
       2RATIO1, RATIO2, RATIO3, RSQ, N, B1, B2, B4, B6, AZERO, SIGASQ,SIGR
        ALPHSQ(1)=ALPH(1)**2
        RSQ = R(N)**2
        R4=RSQ*RSQ
        DELASQ(1)=0.0
        DO 29 J=1,17
        ARGA=ALPH(J)*R(N)
        CALL BESJ(ARGA,0,BJ,1.0E-08,IER)
        AJO(J)=BJ
        CALL BESJ(ARGA,1,BJ,1.0E-08,IER)
        AJ1(J)=BJ
        D1(J)=RSQ*AJO(J)
        D2(J)=R(N)*AJ1(J)/ALPH(J)
        D3(J)=1./ALPHSQ(J)
        D4(J)=D3(J)**2
        G(J)=2.*D3(J)*D1(J)+D2(J)*(RSQ-4.*D3(J))
        HD(J)=D1(J)*(8.*D3(J)-RSQ)+4.*D2(J)*(RSQ-4.*D3(J))
        F(J)= -D1(J) + 2.*D2(J)
        U(J)=D2(J)*(64*D4(J)+R4-16*RSQ*D3(J))+4*D1(J)*D3(J)*(RSQ-8*D3(J))
        V(J)=6*D2(J)*(64*D4(J)+R4-16*RSQ*D3(J))-D1(J)*(R4+192*D4(J)-24*RSQ
       1*D3(J))
        B4=V(J)-RATIO2*HD(J)
        B6=U(J)-RATIO2*G(J)
        DELADA(J)=B6/B4
        ALPH(J+1)=ALPH(J)*(1.+DELADA(J))
        ALPHSQ(J+1)=ALPH(J+1)**2
        DELASQ(J+1)=ALPHSQ(J)*DELADA(J)*(2.+DELADA(J))
        M= J+1
        IF(ABS(DELADA(J)) .LT. 1.0E-04) GO TO 300
     29 CONTINUE
    300 WRITE (6,13) (I,ALPHSQ(I),DELASQ(I),I=1,M)
     13 FORMAT(1HO,2X,I2,8X,1PE13.6,5X,1PE13.6)
```

```
      EXTR=2.4048/ALPH(M)
C     THE DEGREE OF FIT IS EVALUATED BY THE ESTIMATE OF THE ERRORS IN
C     THE EXPERIMENTAL RADIAL FLUX MOMENTS.
C     CALCULATION OF THEORETICAL RADIAL FLUX MOMENTS
      RMTH(3)=G(M-1)-DELADA(M-1)*HD(M-1)
      RMTH(5)=U(M-1)-DELADA(M-1)*V(M-1)
      CCE=(-G(M-1)*B4+HD(M-1)*B6)/B4**2
      CC = ABS(CCE)
      AZERO=(RMTH(3)**2*RMEXP(5)**2+RMEXP(3)**2*RMTH(5)**2)/(RMTH(3)**2*
     1RMTH(5)*RMEXP(5)+RMTH(5)**2*RMTH(3)*RMEXP(3))
      DELRM(3)=RMTH(3)-RMEXP(3)/AZERO
      DELRM(5)=RMTH(5)-RMEXP(5)/AZERO
      DELF=DELRM(5)**2/RMTH(3)**2+RMTH(5)**2*DELRM(3)**2/RMTH(3)**4
      DELY=CC*SQRT(DELF)
C     SIGASQ IS THE DEGREE OF FIT FOR THE RADIAL BUCKLING
      SIGASQ = 2.*ALPHSQ(M)*(1.+DELADA(M-1))*DELY
      SIGR=1.2024*SIGASQ/ALPH(M)**3
      RETURN
      END
      SUBROUTINE CASE3
C     CALCULATION OF THE RADIAL BUCKLING AND THE EXTRAPOLATED RADIUS
C     BY MEANS OF THE ITERATIVE MOMENTS METHOD WITH THE FIFTH TO FIRST
C     MOMENT RATIO.
      DIMENSION A(50),ALPH(20),ALPHSQ(20),R(30),H(30),W(30),SUMR(5),RMEX
     1P(5),RMTH(5),AJ0(20),AJ1(20),D1(20),D2(20),D3(20),G(20),HD(20),F(2
     20),U(20),V(20),D4(20),DELADA(20),DELASQ(20),DELRM(5)
      COMMON A, R, H, W, ALPH, ALPHSQ, RMEXP, RMTH, G, DELADA, DELRM,
     1DELASQ, AJ0, AJ1, D1, D2, D3, D4, HD, F, R4, ARGO, U, V, EXTR, M,
     2RATIO1, RATIO2, RATIO3, RSQ, N, B1, B2, B4, B6, AZERO, SIGASQ,SIGR
      ALPHSQ(1)=ALPH(1)**2
      RSQ = R(N)**2
      R4=RSQ*RSQ
      DELASQ(1)=0.0
      DO 29 J=1,17
      ARGA=ALPH(J)*R(N)
      CALL BESJ(ARGA,0,BJ,1.0E-08,IER)
      AJ0(J)=BJ
      CALL BESJ(ARGA,1,BJ,1.0E-08,IER)
      AJ1(J)=BJ
      D1(J)=RSQ*AJ0(J)
      D2(J)=R(N)*AJ1(J)/ALPH(J)
      D3(J)=1./ALPHSQ(J)
      D4(J)=D3(J)**2
      G(J)=2.*D3(J)*D1(J)+D2(J)*(RSQ-4.*D3(J))
      HD(J)=D1(J)*(8.*D3(J)-RSQ)+4.*D2(J)*(RSQ-4.*D3(J))
      F(J)= -D1(J) + 2.*D2(J)
      U(J)=D2(J)*(64*D4(J)+R4-16*RSQ*D3(J))+4*D1(J)*D3(J)*(RSQ-8*D3(J))
      V(J)=6*D2(J)*(64*D4(J)+R4-16*RSQ*D3(J))-D1(J)*(R4+192*D4(J)-24*RSQ
     1*D3(J))
      B3=U(J)-RATIO3*D2(J)
      B5=V(J)-RATIO3*F(J)
      DELADA(J)=B3/B5
      ALPH(J+1)=ALPH(J)*(1+DELADA(J))
      ALPHSQ(J+1)=ALPH(J+1)**2
      DELASQ(J+1)=ALPHSQ(J)*DELADA(J)*(2.+DELADA(J))
      M= J+1
```

```
      IF(ABS(DELADA(J)) .LT. 1.0E-04) GO TO 200
   29 CONTINUE
  200 WRITE (6,30) (I, ALPHSQ(I), DELASQ(I), I=1,M)
   30 FORMAT(1HO,3X,I2,8X,1PE13.6,5X,1PE13.6)
      EXTR=2.4048/ALPH(M)
C     THE DEGREE OF FIT IS EVALUATED BY THE ESTIMATE OF ERRORS IN THE
C     EXPERIMENTAL RADIAL FLUX MOMENTS.
C     THE CALCULATION OF THEORETICAL RADIAL FLUX MOMENTS
      RMTH(1)=D2(M-1)-DELADA(M-1)*F(M-1)
      RMTH(5)=U(M-1)-DELADA(M-1)*V(M-1)
      CCE=(-D2(M-1)*B5+F(M-1)*B3)/B5**2
      CC=ABS(CCE)
      AZERO=(RMTH(1)**2*RMEXP(5)**2+RMTH(5)**2*RMEXP(1)**2)/(RMTH(1)**2*
     1RMTH(5)*RMEXP(5)+RMTH(1)*RMEXP(1)*RMTH(5)**2)
      DELRM(1)=RMTH(1)-RMEXP(1)/AZERO
      DELRM(5)=RMTH(5)-RMEXP(5)/AZERO
      DELF = DELRM(5)**2/RMTH(1)**2 + RMTH(5)**2*DELRM(1)**2/RMTH(1)**4
      DELY = CC*SQRT(DELF)
      SIGASQ = 2.*ALPHSQ(M)*(1.+DELADA(M-1))*DELY
      SIGR = 1.2024*SIGASQ/ALPH(M)**3
      RETURN
      END
/*
//G.SYSIN  DD  *
  ML6  5    1.0270    0.2500    1.75    0.0880
    1.108940    1.041130    0.925120    0.679740    0.459610
     2.31336     6.69833    11.13103    15.57074    20.01280
  MLJ 11    1.1430    0.2500    1.75    0.0882
    0.987640    0.951183    0.892010    0.811565    0.714850    0.600330
    0.480050    0.351612    0.223891    0.099272    0.000000
     2.54000     5.08000     7.62000    10.16000    12.70000    15.24000
    17.78000    20.32000    22.86000    25.40000    27.49600
/*
```

A.3 THE RADBUCK CODE

A.3.1 General Description

The RADBUCK code was programmed in FORTRAN IV for the same type of computer according to the direct moments method described in section 4.2. The code consists of a main program and two subroutine subprograms: JOANNE and ROCK. The subprogram JOANNE computes the radial flux moments with the second-order Simpson's rule for unequal intervals given in Appendix B and also computes the values of the radial buckling and the extrapolated radius for various values of the moment index. The lowest allowable value of the moment index is 3 and the largest permissible value is 9. The radial positions that correspond to the experimental data points are calculated with the formula

$$R(I) = \sqrt{D^2 + (I-1)^2(DELX)^2}, \quad I = 1, 2, 3, \ldots, N. \qquad (A.1)$$

where DELX is the equal spacing between any two successive data points that are positioned on an off-center line as shown in Figure A.1, and D is the distance from the central data point to the center of the cylinder. If the foils are not arranged in this manner, the program can be easily modified by treating R(I) as input data.

The subprogram ROCK calculates the probable errors in the radial buckling and the extrapolated height for various values of the moment index, and hence provides a way of determining the best values of the radial buckling and the extrapolated radius.

The amount of computer time is about 10 seconds or less per case.

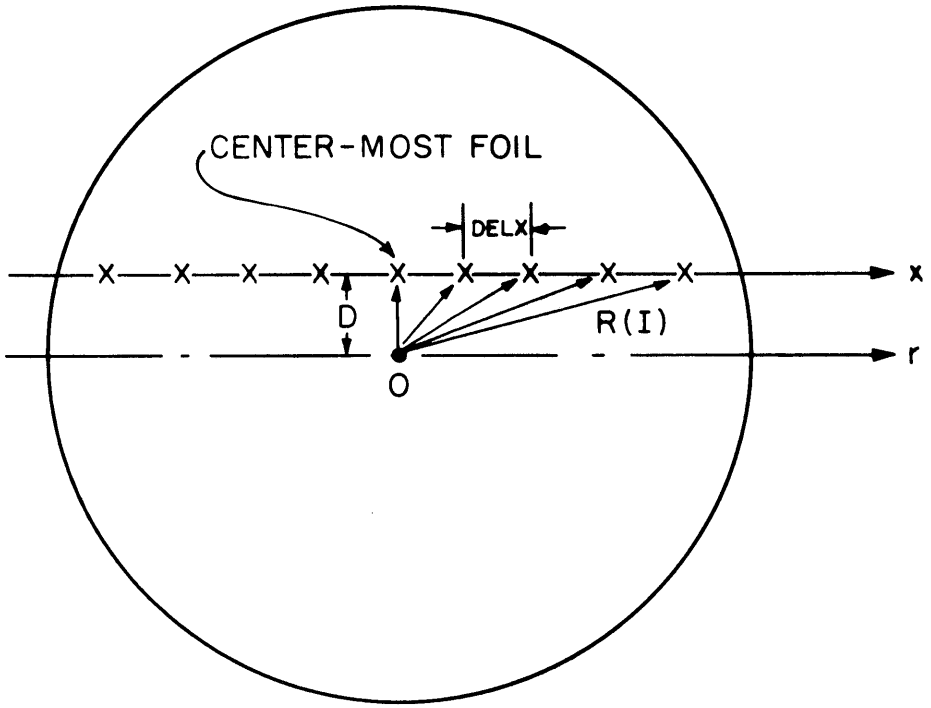

FIG. A.1 CONFIGURATION OF THE FOIL ARRANGEMENT FOR RADIAL FLUX TRAVERSES.

A.3.2 Input Data for the RADBUCK Code

Card 1 (Format (A5, I3, 2F10.4, F8.2, I4, F10.4)). The following quantities appear, in order, on this card:

RUN is the experimental run number for the set of data being analyzed;

N is the number of data points submitted and must be ODD;

ENRICH is the fuel enrichment in percent of the lattice being analyzed;

DELX is the spacing in centimeters between any two successive data points equally spaced;

PITCH is the lattice spacing in inches;

NM is the highest value of the moment index desired; the maximum value built in the code is 9 and the value of NM must be odd;

D is the distance in centimeters from the central data point to the center of the cylinder (see Figure A.1).

Card 2 (Format (6F12.6)). The following quantities appear, in order, on this card:

A(I) are the relative experimental activation data with the first data being the centermost data point. They are read in on successive cards according to the specified format until N data have been stored in the memory of the computer.

A .3.3 FORTRAN IV Listings of the RADBUCK Code

```
//RADBUCK  JOB  (M2940,5551,10,5000,200),'H.S.CHENG',MSGLEVEL=1
//STEP      EXEC  FORCLG,PARM.C=(EBCDIC,DECK,MAP)
//C.SYSIN  DD  *
C      RADIAL BUCKLING CODE 'RADBUCK'       H.S.CHENG
C      THIS CODE IS BASED ON DIRECT MOMENTS METHOD FOR THE ANALYSIS OF
C      THE RADIAL BUCKLING AND EXTRAPOLATED RADIUS. SIMPSON'S RULE FOR
C      UNEQUAL INTERVALS IS USED TO EVALUATE THE RADIAL FLUX MOMENTS.
       DIMENSION A(50), RM(50), FM(50,50), FMM(50,50), F(50,50), SUM(50),
      1 CNUMA(50), DENOA(50), ALPHSQ(50), ALPH(50), EXTR(50), Y(50,50), B
      2ESSO(50,50), SUMF(50,50), SUMFM(50), FMO(50), Z(50), BJO(50), BJ1(
      350), CNUM(50), DENO(50), D2(50), D4(50), C(50,10), SUMNA(50), SUMD
      4A(50), AZERO(50), TRE(50,10), EXPE(50,10), VARAT(50), VARAP(50), V
      5ARRT(50), VARRP(50), DEVAT(50), DEVAP(50), DEVRT(50), DEVRP(50), C
      6DEVA(50), CDEVR(50), CVARA(50), CVARR(50), SUMFO(50), V1(50), V2(5
      70), R(50), H(50), W(50), SUMR(50)
       COMMON A, RM, FM, FMM, F, N, K, CNM1, CNM2, XSQ, R, R2, R4, ALPHSQ
      1, ALPH, EXTR, AZERO, TRE, EXPE, VARAT, VARAP, VARRT, VARRP, DEVAT,
      2 DEVAP, DEVRT, DEVRP, DX4, CDEVA, CDEVR, CVARA, CVARR, DELX, NM, R
      3MO, H, W, C, BJO, BJ1, D
   10 FORMAT(1H1,20X18H PROGRAM 'RADBUCK'//)
   20 FORMAT(1HO,73H CALCULATION OF RADIAL BUCKLING AND EXTRAPOLATED RAD
      1IUS BY MOMENTS METHOD//)
```

```
 30 FORMAT(A5,I3,2F10.4,F8.2,I4,F10.4)
 40 FORMAT(6F12.6)
 50 FORMAT(5H RUN=A5,13H   ENRICH(I)=F7.4,13H   PITCH(IN)=F6.3,12H   D
   1ELX(CM)=F7.4)
  9 FORMAT(1HO,27H INPUT RADIAL POSITION DATA)
 60 FORMAT(1HO,27H INPUT RADIAL ACTIVITY DATA)
 70 FORMAT(1HO,5(I3,F10.6,2X)/(1HO,5(1X,I2,F10.6,2X)))
 80 FORMAT(1HO,37HCOMPUTED RESULTS OF SUBROUTINE JOANNE//)
 90 FORMAT(1HO,10X,6HMOMENT,7X,15HRADIAL BUCKLING,7X,19HEXTRAPOLATED R
   1ADIUS)
100 FORMAT(10X,6H INDEX,12X,6H(CM-2),18X,4H(CM))
110 FORMAT(1HO,12X,1HI,13X,9HALPHSQ(I),15X,7HEXTR(I))
120 FORMAT(1HO,11X,I2,10X,1PE13.6,12X,1PE13.6)
130 FORMAT(1H1,39HCOMPUTED RESULTS OF EXPERIMENTAL ERRORS//)
140 FORMAT(1HO,2X,6HMOMENT,7X,18HSTANDARD DEVIATION,7X,21HSTANDARD DEV
   1IATION IN,7X,11HVARIANCE IN,9X,18HVARIANCE IN EXTRA-)
150 FORMAT(2X,6H INDEX,8X,18HIN RADIAL BUCKLING,7X,19HEXTRAPOLATED RAD
   1IUS,9X,15HRADIAL BUCKLING,5X,14HPOLATED RADIUS)
160 FORMAT(1HO,4X,1HI,14X,8HDEVAP(I),19X,8HDEVRP(I),16X,8HVARAP(I),13X
   1,8HVARRP(I))
170 FORMAT(1HO,3X,I2,11X,1PE13.6,13X,1PE13.6,12X,1PE13.6,8X,1PE13.6)
180 FORMAT(1HO,37HCOMPUTED RESULTS OF TRUNCATION ERRORS)
190 FORMAT(1HO,2X,6HMOMENT,7X,18HSTANDARD DEVIATION,7X,21HSTANDARD DEV
   1IATION IN,7X,11HVARIANCE IN,9X,18HVARIANCE IN EXTRA-)
200 FORMAT(2X,6H INDEX,8X,18HIN RADIAL BUCKLING,7X,19HEXTRAPOLATED RAD
   1IUS,9X,15HRADIAL BUCKLING,5X,14HPOLATED RADIUS)
210 FORMAT(1HO,4X,1HI,14X,8HDEVAT(I),19X,8HDEVRT(I),16X,8HVARAT(I),13X
   1,8HVARRT(I))
220 FORMAT(1HO,3X,I2,11X,1PE13.6,13X,1PE13.6,12X,1PE13.6,8X,1PE13.6)
610 FORMAT(1HO,65HCOMPUTED RESULTS OF COMBINED ERRORS(EXPERIMENTAL PLU
   1S TRUNCATION))
620 FORMAT(1HO,2X,6HMOMENT,7X,18HSTANDARD DEVIATION,7X,21HSTANDARD DEV
   1IATION IN,7X,11HVARIANCE IN,9X,18HVARIANCE IN EXTRA-)
630 FORMAT(2X,6H INDEX,8X,18HIN RADIAL BUCKLING,7X,19HEXTRAPOLATED RAD
   1IUS,9X,15HRADIAL BUCKLING,6X,14HPOLATED RADIUS)
640 FORMAT(1HO,4X,1HI,14X,8HCDEVA(I),18X,8HCDEVR(I),18X,8HCVARA(I),13X
   1,8HCVARR(I))
650 FORMAT(1HO,3X,I2,11X,1PE13.6,13X,1PE13.6,12X,1PE13.6,7X,1PE13.6)
    NORMAN = 17
  6 READ (5,30) RUN, N, ENRICH, DELX, PITCH, NM, D
    READ (5,40) (A(I),I=1,N)
    WRITE (6,10)
    WRITE (6,20)
    WRITE (6,50) RUN, ENRICH, PITCH, DELX
    WRITE (6,60)
    WRITE (6,70) (I,A(I),I=1,N)
    WRITE (6,9)
    WRITE (6,70) (I,R(I),I=1,N)
    WRITE (6,80)
    CALL JOANNE
    WRITE (6,90)
    WRITE (6,100)
    WRITE (6,110)
    WRITE (6,120) (I, ALPHSQ(I), EXTR(I), I=3,NM,2)
    WRITE (6,130)
    WRITE (6,50) RUN, ENRICH, PITCH, DELX
    WRITE (6,140)
```

```
      WRITE (6,150)
      WRITE (6,160)
      CALL ROCK
      WRITE (6,170) (I, DEVAP(I), DEVRP(I), VARAP(I), VARRP(I),I=3,NM,2)
      WRITE (6,180)
      WRITE (6,190)
      WRITE (6,200)
      WRITE (6,210)
      WRITE (6,220) (I, DEVAT(I), DEVRT(I), VARAT(I), VARRT(I),I=3,NM,2)
      WRITE (6,610)
      WRITE (6,620)
      WRITE (6,630)
      WRITE (6,640)
      WRITE (6,650) (I, CDEVA(I), CDEVR(I), CVARA(I), CVARR(I),I=3,NM,2)
      GO TO 6
      END
      SUBROUTINE JOANNE
C     CALCULATION OF RADIAL MOMENTS, RADIAL BUCKLING AND EXTRAPOLATED
C     RADIUS BY MOMENTS METHOD
      DIMENSION A(50), RM(50), FM(50,50), FMM(50,50), F(50,50), SUM(50),
     1 CNUMA(50), DENOA(50), ALPHSQ(50), ALPH(50), EXTR(50), Y(50,50), B
     2ESSO(50,50), SUMF(50,50), SUMFM(50), FMO(50), Z(50), BJO(50), BJ1(
     350), CNUM(50), DENO(50), D2(50), D4(50), C(50,10), SUMNA(50), SUMD
     4A(50), AZERO(50), TRE(50,10), EXPE(50,10), VARAT(50), VARAP(50), V
     5ARRT(50), VARRP(50), DEVAT(50), DEVAP(50), DEVRT(50), DEVRP(50), C
     6DEVA(50), CDEVR(50), CVARA(50), CVARR(50), SUMFO(50), V1(50), V2(5
     70), R(50), H(50), W(50), SUMR(50)
      COMMON A, RM, FM, FMM, F, N, K, CNM1, CNM2, XSQ, R, R2, R4, ALPHSQ
     1, ALPH, EXTR, AZERO, TRE, EXPE, VARAT, VARAP, VARRT, VARRP, DEVAT,
     2 DEVAP, DEVRT, DEVRP, DX4, CDEVA, CDEVR, CVARA, CVARR, DELX, NM, R
     3MO, H, W, C, BJO, BJ1, D
      K = (N-1)/2
      XSQ=DELX*DELX
      DSQ=D*D
      DO 21 I=1,N
   21 R(I)=SQRT(DSQ+(I-1)**2*XSQ)
      R2=R(N)**2
      R4=R(N)**4
      H(1)=D
      DO 22 I=2,N
   22 H(I)=R(I)-R(I-1)
      DO 23 I=1,K
      W(2*I)=(-H(2*I+1)**2+10.*H(2*I)*H(2*I+1)-H(2*I)**2)/(H(2*I+1)+H(2*
     1I))
      W(2*I+1)=(7.*H(2*I+1)**2-4.*H(2*I+1)*H(2*I)+H(2*I)**2)/(2.*(H(2*I+
     11)+H(2*I)))
   23 CONTINUE
      DO 24 J=1,11,2
      SUMR(J)=0.0
      DO 25 I=2,K
   25 SUMR(J)=SUMR(J)+W(2*I)*A(2*I)*EXP(J*ALOG(R(2*I)))+(W(2*I+1)+W(2*I-
     11))*A(2*I-1)*EXP(J*ALOG(R(2*I-1)))
      RM(J)=1./3.*(SUMR(J)+W(3)*A(1)*EXP(J*ALOG(R(1)))+W(2)*A(2)*EXP(J*A
     1LOG(R(2)))+W(N)*A(N)*EXP(J*ALOG(R(N)))+0.5*R(1)*A(1)*EXP(J*ALOG(R(
     21))))
   24 CONTINUE
      WRITE (6,16)
```

```
   16 FORMAT(1HO,34HEXPERIMENTAL RADIAL MOMENTS, RM(I))
      WRITE (6,17) (I,RM(I),I=1,11,2)
   17 FORMAT(1HO,5(I3,2X,1PE13.6,3X)/(1HO,5(1X,I2,2X,1PE13.6,3X)))
C     CALCULATION OF RADIAL BUCKLING, ALPHSQ(I)
      ALPHSQ(3)=(16.*RM(3)-8.*R2*RM(1))/(-RM(5)+2.*R2*RM(3)-R4*RM(1))
      ALPH(3)=SQRT(ALPHSQ(3))
      EXTR(3)=2.4048/ALPH(3)
      DO 18 I=5,NM,2
      CNUMA(I)=(I+1)**2*RM(I)-2.*(I-1)**2*R2*RM(I-2)+(I-3)**2*R4*RM(I-4)
      DENOA(I)=-RM(I+2)+2.*R2*RM(I)-R4*RM(I-2)
      ALPHSQ(I)=CNUMA(I)/DENOA(I)
      ALPH(I)=SQRT(ALPHSQ(I))
C     CALCULATION OF EXTRAPOLATED RADIUS, EXTR(I)
      EXTR(I)=2.4048/ALPH(I)
   18 CONTINUE
      RETURN
      END
      SUBROUTINE ROCK
C     ESTIMATE OF EXPERIMENTAL AND TRUNCATION ERRORS IN RADIAL BUCKLING
C     AND EXTRAPOLATED RADIUS
      DIMENSION A(50), RM(50), FM(50,50), FMM(50,50), F(50,50), SUM(50),
     1 CNUMA(50), DENOA(50), ALPHSQ(50), ALPH(50), EXTR(50), Y(50,50), B
     2ESSO(50,50), SUMF(50,50), SUMFM(50), FMO(50), Z(50), BJO(50), BJ1(
     350), CNUM(50), DENO(50), D2(50), D4(50), C(50,10), SUMNA(50), SUMD
     4A(50), AZERO(50), TRE(50,10), EXPE(50,10), VARAT(50), VARAP(50), V
     5ARRT(50), VARRP(50), DEVAT(50), DEVAP(50), DEVRT(50), DEVRP(50), C
     6DEVA(50), CDEVR(50), CVARA(50), CVARR(50), SUMFO(50), V1(50), V2(5
     70), R(50), H(50), W(50), SUMR(50)
      COMMON A, RM, FM, FMM, F, N, K, CNM1, CNM2, XSQ, R, R2, R4, ALPHSQ
     1, ALPH, EXTR, AZERO, TRE, EXPE, VARAT, VARAP, VARRT, VARRP, DEVAT,
     2 DEVAP, DEVRT, DEVRP, DX4, CDEVA, CDEVR, CVARA, CVARR, DELX, NM, R
     3MO, H, W, C, BJO, BJ1, D
C     GENERATION OF THEORETICAL INPUT DATA F(I,J)
      DO 71 I=3,NM,2
      DO 72 J=1,N
      YY1=ALPH(I)*R(J)
      CALL BESJ(YY1,0,BJ,1.0E-08,IER)
      F(I,J)=BJ
   72 CONTINUE
C     CALCULATION OF THEORETICAL MOMENTS FM(I,J) BY SIMPSON'S RULE
      DO 73 L=1,11,2
      SUMF(I,L)=0.0
      DO 74 M=2,K
   74 SUMF(I,L)=SUMF(I,L)+W(2*M)*F(I,2*M)*EXP(L*ALOG(R(2*M)))+(W(2*M+1)+
     1W(2*M-1))*F(I,2*M-1)*EXP(L*ALOG(R(2*M-1)))
      FM(I,L)=1./3.*(SUMF(I,L)+W(3)*F(I,1)*EXP(L*ALOG(R(1)))+W(2)*F(I,2)
     1*EXP(L*ALOG(R(2)))+W(N)*F(I,N)*EXP(L*ALOG(R(N))))
   73 CONTINUE
C     CALCULATION OF ANALYTICAL MOMENTS FMM(I,J)
      Z1=ALPH(I)*R(N)
      CALL BESJ(Z1,0,BJ,1.0E-08,IER)
      BJO(I)=BJ
      CALL BESJ(Z1,1,BJ,1.0E-08,IER)
      BJ1(I)=BJ
      FMM(I,1)=R(N)*BJ1(I)/ALPH(I)
      DO 31 J=3,11,2
   31 FMM(I,J)=EXP(J*ALOG(R(N)))*BJ1(I)/ALPH(I)+(J-1)*EXP((J-1)*ALOG(R(N
```

```
     1)))*BJO(I)/ALPHSQ(I)-(J-1)**2*FMM(I,J-2)/ALPHSQ(I)
C      CALCULATION OF COEFFICIENTS C(I)
       IF(I .EQ. 3) GO TO 96
       CNUM(I)=(I+1)**2*FMM(I,I)-2.*(I-1)**2*R2*FMM(I,I-2)+(I-3)**2*R4*FM
      1M(I,I-4)
       GO TO 97
   96  CNUM(I)=16.*FMM(I,3)-8.*R2*FMM(I,1)
   97  DENO(I)=-FMM(I,I+2)+2.*R2*FMM(I,I)-R4*FMM(I,I-2)
       D2(I)=DENO(I)**2
       D4(I)=DENO(I)**4
       C(I-2,1)=(I-3)**4*EXP(8*ALOG(R(N)))/D2(I)
       C(I,2)=R4*(-2.*(I-1)**2*DENO(I)+R2*CNUM(I))**2/D4(I)
       C(I+2,3)=((I+1)**2*DENO(I)-2.*R2*CNUM(I))**2/D4(I)
       C(I+4,4)=CNUM(I)**2/D4(I)
C      EVALUATION OF NORMALIZATION CONSTANT AZERO(I)
       IF(I .EQ. 3) GO TO 51
       SUMNA(I)=0.0
       DO 32 J=1,4
   32  SUMNA(I)=SUMNA(I)+C(I+2*J-4,J)*RM(I+2*J-6)**2
       SUMDA(I)=0.0
       DO 33 J=1,4
   33  SUMDA(I)=SUMDA(I)+C(I+2*J-4,J)*RM(I+2*J-6)*FM(I,I+2*J-6)
       AZERO(I)=SUMNA(I)/SUMDA(I)
C      ESTIMATE OF TRUNCATION ERRORS IN MOMENTS
       DO 34 J=1,4
   34  TRE(I+2*J-4,J)=FMM(I,I+2*J-6)-FM(I,I+2*J-6)
C      ESTIMATE OF EXPERIMENTAL ERRORS IN MOMENTS
       DO 35 J=1,4
   35  EXPE(I+2*J-4,J)=FM(I,I+2*J-6)-RM(I+2*J-6)/AZERO(I)
C      CALCULATION OF VARIANCE AND STANDARD DEVIATION IN RADIAL BUCKLING
       VARAT(I)=0.0
       DO 36 J=1,4
   36  VARAT(I)=VARAT(I)+C(I+2*J-4,J)*TRE(I+2*J-4,J)**2
       VARAP(I)=0.0
       DO 37 J=1,4
   37  VARAP(I)=VARAP(I)+C(I+2*J-4,J)*EXPE(I+2*J-4,J)**2
       GO TO 57
   51  SUMNA(3)=C(3,2)*RM(1)**2+C(5,3)*RM(3)**2+C(7,4)*RM(5)**2
       SUMDA(3)=C(3,2)*RM(1)*FM(3,1)+C(5,3)*RM(3)*FM(3,3)+C(7,4)*RM(5)*FM
      1(3,5)
       AZERO(3)=SUMNA(3)/SUMDA(3)
       DO 52 J=2,4
   52  TRE(I+2*J-4,J)=FMM(I,I+2*J-6)-FM(I,I+2*J-6)
       DO 53 J=2,4
   53  EXPE(I+2*J-4,J)=FM(I,I+2*J-6)-RM(I+2*J-6)/AZERO(3)
       VARAT(3)=0.0
       DO 54 J=2,4
   54  VARAT(3)=VARAT(3)+C(I+2*J-4,J)*TRE(I+2*J-4,J)**2
       VARAP(3)=0.0
       DO 55 J=2,4
   55  VARAP(3)=VARAP(3)+C(I+2*J-4,J)*EXPE(I+2*J-4,J)**2
   57  DEVAT(I)=SQRT(VARAT(I))
       DEVAP(I)=SQRT(VARAP(I))
C      CALCULATION OF VARIANCE AND STANDARD DEVIATION IN
C      EXTRAPOLATED RADIUS
       DEVRT(I)=1.2024*DEVAT(I)/ALPH(I)**3
       DEVRP(I)=1.2024*DEVAP(I)/ALPH(I)**3
```

```
      VARRT(I)=DEVRT(I)**2
      VARRP(I)=DEVRP(I)**2
C     CALCULATION OF COMBINED ERRORS IN RADIAL BUCKLING
C     AND EXTRAPOLATED RADIUS
      CVARA(I)=VARAT(I)+VARAP(I)
      CVARR(I)=VARRT(I)+VARRP(I)
      CDEVA(I)=SQRT(CVARA(I))
      CDEVR(I)=SQRT(CVARR(I))
   71 CONTINUE
      RETURN
      END
/*
```

A.3.4 Sample Input Deck

```
N5 11    0.9470    3.8100    1.50    7    2.1996
 1.135600    1.121400    1.113100    1.046100    0.998070    0.909060
 0.820020    0.707990    0.606440    0.487050    0.366530
```

Appendix B

SIMPSON'S RULE FOR UNEQUAL INTERVALS

Suppose that we have an arbitrary function $y=y(x)$. If we expand the function around the point $x=x_i$ into a local power series, making use of the method of central differences according to Stirling's formula (L2, H10), we obtain

$$y(x_i+t) = y(x_i) + t\left.\frac{\delta y}{\delta x}\right|_{x_i} + \frac{t^2}{2}\left.\frac{\delta^2 y}{\delta x^2}\right|_{x_i} + \frac{t(t^2-1)}{6}\left.\frac{\delta^3 y}{\delta x^3}\right|_{x_i}$$

$$+ \frac{t^2(t^2-1)}{24}\left.\frac{\delta^4 y}{\delta x^4}\right|_{x_i} + \ldots, \qquad \text{(B.1)}$$

where the notation δ stands for the central difference. The local area under the curve $y=y(x)$ for the second-order Simpson's rule is obtained by truncating the higher order terms than the second in Eq. (B.1) (refer to Figure B.1):

$$A_i = \int_{x_{i-1}}^{x_{i+1}} y(x)\,dx = \int_{-h_i}^{h_{i+1}} y(x_i+t)\,dt \approx \int_{-h_i}^{h_{i+1}} \left\{ y(x_i) + t\left.\frac{\delta y}{\delta x}\right|_{x_i} + \frac{t^2}{2}\left.\frac{\delta^2 y}{\delta x^2}\right|_{x_i} \right\} dt$$

$$\approx y(x_i)(h_{i+1}+h_i) + \frac{1}{2}\left(h_{i+1}^2 - h_i^2\right)\left.\frac{\delta y}{\delta x}\right|_{x_i} + \frac{1}{6}\left(h_{i+1}^3 + h_i^3\right)\left.\frac{\delta^2 y}{\delta x^2}\right|_{x_i}, \qquad \text{(B.2)}$$

where

$$\left.\frac{\delta y}{\delta x}\right|_{x_i} \approx \frac{y\left(x_i + \frac{h_{i+1}}{2}\right) - y\left(x_i - \frac{h_i}{2}\right)}{\frac{1}{2}(h_{i+1}+h_i)} \approx \frac{\frac{1}{2}(y_{i+1} - y_{i-1})}{\frac{1}{2}(h_{i+1}+h_i)}, \qquad \text{(B.3)}$$

and

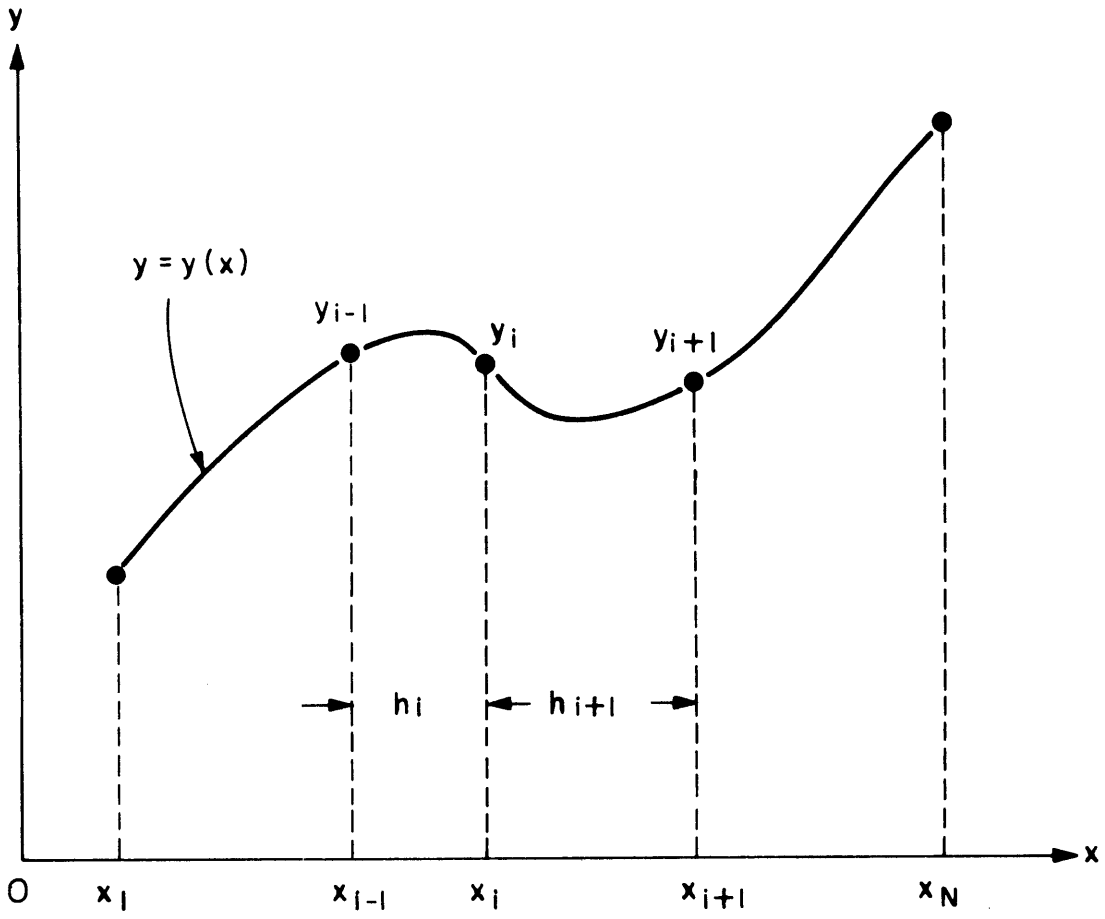

FIG. B.1 SCHEMATIC DIAGRAM OF THE CURVE $y = y(x)$

$$\left.\frac{\delta^2 y}{\delta x^2}\right|_{x_i} \approx \frac{y(x_i+h_{i+1}) - 2y(x_i) + y(x_i-h_{i-1})}{\frac{1}{4}(h_{i+1}+h_i)^2}$$

$$\approx \frac{y_{i+1} - 2y_i + y_{i-1}}{\frac{1}{4}(h_{i+1}+h_i)^2} . \tag{B.4}$$

Here, the notation $y_i \equiv y(x_i)$ has been used for ease of writing. Equation (B.2) then becomes

$$A_i \approx y_i(h_i+h_{i+1}) + \frac{1}{2}(y_{i+1}-y_{i-1})(h_{i+1}-h_i)$$

$$+ \frac{2}{3}(y_{i+1}-2y_i+y_{i-1}) \frac{h_{i+1}^2 - h_{i+1}h_i + h_i^2}{(h_i+h_{i+1})} . \tag{B.5}$$

As a check, let us consider the case of equal intervals; setting $h_{i+1} = h_i = h$, we obtain

$$A_i \approx h\left[\frac{1}{3} y_{i+1} + \frac{4}{3} y_i + \frac{1}{3} y_{i-1}\right] , \tag{B.6}$$

which is the familiar Simpson's rule for equal intervals. The total area under the given curve from x_1 to x_N is then

$$A = \int_{x_1}^{x_N} y(x)\, dx \approx \sum_{i=1}^{\left(\frac{N-1}{2}\right)} A_{2i}$$

$$\approx \sum_{i=1}^{\left(\frac{N-1}{2}\right)} \left\{ y_{2i}(h_{2i+1}+h_{2i}) + \frac{1}{2}(y_{2i+1}-y_{2i-1})(h_{2i+1}-h_{2i}) \right.$$

$$\left. + \frac{2}{3}(y_{2i+1}-2y_{2i}+y_{2i-1}) \frac{\left(h_{2i+1}^2 - h_{2i+1}h_{2i} + h_{2i}^2\right)}{(h_{2i+1}+h_{2i})} \right\}$$

$$\approx \frac{1}{3} \sum_{i=1}^{\left(\frac{N-1}{2}\right)} \{w_{2i+1}[y_{2i-1}+y_{2i+1}] + w_{2i}y_{2i}\} , \tag{B.7}$$

where

$$w_{2i+1} = \frac{7h_{2i+1}^2 - 4h_{2i}h_{2i+1} + h_{2i}^2}{2(h_{2i+1}+h_{2i})}, \tag{B.8}$$

and

$$w_{2i} = \frac{-h_{2i+1}^2 + 10h_{2i}h_{2i+1} - h_{2i}^2}{(h_{2i}+h_{2i+1})}. \tag{B.9}$$

We can rewrite Eq. (B.7) in the following form convenient for numerical calculation:

$$A \approx \frac{1}{3}[w_3y_1+w_2y_2+w_Ny_N] + \frac{1}{3}\sum_{i=2}^{(N-1)/2}[(w_{2i+1}+w_{2i-1})y_{2i-1}+w_{2i}y_{2i}]. \tag{B.10}$$

This is the second-order Simpson's rule for unequal intervals.

Appendix C

A MOMENTS METHOD FOR PARALLELEPIPED ASSEMBLIES

In a rectangular-parallelepiped critical or subcritical assembly, the flux distribution in one direction normal to the axis is given by a cosine function:

$$\phi(x) = A \cos (B_x x) , \tag{C.1}$$

where B_x^2 is the corresponding buckling.

Define the flux moments as

$$\phi_n \equiv \int_0^a x^n \phi(x)\, dx , \tag{C.2}$$

where a is the half width of the assembly. Substitution of Eq. (C.1) into Eq. (C.2) yields, after integration, the expression for the n^{th} flux moment:

$$\phi_n = \frac{a^n}{B_x} \sin (B_x a) + \frac{n a^{n-1}}{B_x^2} \cos (B_x a) - \frac{n(n-1)}{B_x^2} \phi_{n-2} . \tag{C.3}$$

The $(n-1)^{th}$ and $(n+1)^{th}$ flux moments are readily obtained:

$$\phi_{n-1} = \frac{a^{n-1}}{B_x} \sin (B_x a) + \frac{(n-1)a^{n-2}}{B_x^2} \cos (B_x a) - \frac{(n-1)(n-2)}{B_x^2} \phi_{n-3} , \tag{C.4}$$

and

$$\phi_{n+1} = \frac{a^{n+1}}{B_x} \sin (B_x a) + \frac{(n+1)a^n}{B_x^2} \cos (B_x a) - \frac{n(n+1)}{B_x^2} \phi_{n-1} . \tag{C.5}$$

Eliminating $\sin(B_x a)$ and $\cos(B_x a)$ from Eqs. (C.3), (C.4) and (C.5), we get

$$B_x^2 = \left\{ \frac{n(n+1)\ \phi_{n-1} - 2an(n-1)\ \phi_{n-2} + a^2(n-1)(n-2)\ \phi_{n-3}}{-\phi_{n+1} + 2a\phi_n - a^2\phi_{n-1}} \right\} ,$$

$$n = 3, 4, 5, \ldots, \infty . \qquad \text{(C.6)}$$

The extrapolated size length is then obtained from the formula

$$\tilde{a} = \frac{\pi}{\sqrt{B_x^2}} . \qquad \text{(C.7)}$$

The best value of B_x^2 is to be determined through an error analysis. To this end, define the variance of the transverse buckling as

$$\sigma^2_{B_x^2} \equiv |\delta B_x^2|^2 = \sum_{j=1}^{5} C_{n+j-4} \left(\delta\phi_{n+j-4}\right)^2 , \qquad \text{(C.8)}$$

where

$$C_{n+j-4} = \left(\frac{\partial B_x^2}{\partial \phi_{n+j-4}} \right)^2 , \qquad j = 1, 2, 3, 4, 5 . \qquad \text{(C.9)}$$

The calculation of $\delta\phi_{n+j-4}$ is the same as that described in section 3.2.3.

Appendix D

A FINITE DIFFERENCE METHOD FOR THE EVALUATION OF BUCKLING VALUES

We have shown in Chapter II that the geometric buckling is, in general, position-dependent but becomes independent of position when the neutron flux becomes asymptotic. This leads to a way of determining the asymptotic bucklings through the geometric bucklings:

$$B_z^2(z) \equiv \frac{\nabla^2\phi(z)}{\phi(z)} , \tag{D.1}$$

and

$$B_r^2(r) \equiv - \frac{\nabla^2\phi(r)}{\phi(r)} . \tag{D.2}$$

We refer here to a subcritical assembly.

The evaluation of the second derivative is the central problem of this method. There are several ways to do this: for example, the central difference method, the forward difference method, and the backward difference method (C1). Experience has shown, however, that values obtained by these methods are not quite accurate. We shall, therefore, investigate a different method based on the least-squares principle.

Suppose that a number of local experimental data can be represented by a theoretical curve of the form

$$A(x) = a + bx + cx^2 , \tag{D.3}$$

where the coefficients a, b, c are to be determined from the experimental data by means of a least-squares technique. To this end,

we form the difference

$$(\Delta A)^2 = \sum_{j=-N}^{+N} [A(x)-A_j]^2 . \tag{D.4}$$

Here we have chosen (2N+1) experimental data at equal spacings for the evaluation of the geometric buckling:

$$A_{-N}, A_{-(N-1)}, \cdots, A_{-1}, A_o, A_1, \cdots, A_{N-1}, A_N .$$

The notation A_j stands for A(x+jh) with h being the spacing between any two successive experimental data points. To determine the coefficients a, b, c, we substitute Eq. (D.3) in Eq. (D.4) and then minimize the difference $(\Delta A)^2$ with respect to a, b, and c:

$$\frac{\partial(\Delta A)^2}{\partial a} = \frac{\partial(\Delta A)^2}{\partial b} = \frac{\partial(\Delta A)^2}{\partial c} = 0 . \tag{D.5}$$

Solving the three equations simultaneously for the coefficient b, we obtain

$$b = \frac{\sum_{j=-N}^{j=N} jA_j}{2\sum_{j=1}^{N} j^2 h} \tag{D.6}$$

at the central point x=0. Now, differentiating Eq. (D.3) with respect to x, we obtain

$$\frac{dA(x)}{dx} = b + 2cx , \tag{D.7}$$

so that

$$\left.\frac{dA(x)}{dx}\right|_{x=0} = b . \tag{D.8}$$

The derivative at the central point x=0 is thus given by Eq. (D.6). To evaluate the second derivative at x=0, we apply the same procedure once more to the set of the first derivative. The following result is readily obtained:

$$\nabla^2 A(x)\Big|_{x=0} = \frac{\sum_{j=-N}^{+N} jb}{2\sum_{j=1}^{N} j^2 h}, \tag{D.9}$$

where b is given by Eq. (D.6). In the calculation of Eq. (D.9), the choice of N is important. Although it is desirable to have a large value of N from the standpoint of numerical calculation, we must also consider the possible contamination of the experimental data near the boundary by transient fluxes. An appropriate value of N is then N=2. In this case, we obtain the result:

$$B_x^2(x)_0 = \frac{1}{100h^2}\left[4A_{-4}+4A_{-3}+A_{-2}-4A_{-1}-10A_o-4A_1+A_2+4A_3+4A_4\right]. \tag{D.10}$$

Equation (D.10) has been used to calculate the values of the axial buckling for several U-D_2O lattices at the M.I.T. Lattice Project. The results are given in Table D.1 together with the values obtained by the moments method (Chapter III) and the curve-fitting method. The agreement among the three different methods is generally good.

Table D.1. Comparison of the calculation of axial bucklings from experimental data by means of various methods for slightly enriched uranium-D_2O lattices.

Fuel Enrichment (%)	Lattice Triangular Spacing (Inches)	Fuel Rod Diameter (Inch)	Run Number	AXIAL BUCKLING, γ^2 (μB)		
				Finite Difference Method	Moments Method	AXFIT Code
1.150	1.75	0.25	D2	1026	1006	1012
1.150	2.50	0.25	92	1385	1391	1390
1.150	1.25	0.25	81	1026	976	987
0.947	2.50	0.75	D8	1395	1389	1405
0.947	5.00	0.75	H9	225	254	260
0.947	5.00	0.75	J1	329	306	304

Appendix E

ERROR ANALYSIS FOR SECTION 4.6

Equation (4.121) gives the quantity

$$\frac{\alpha - \alpha_o}{\alpha_o} = \frac{B_1B_8 - B_6B_7}{B_4B_7 - B_2B_8}, \tag{E.1}$$

where the B_i are given by Eqs. (4.93) through (4.100). The radial buckling α^2 is given by

$$\alpha^2 = \alpha_o^2(1+x)^2 , \tag{E.2}$$

where

$$x = \frac{B_1B_8 - B_6B_7}{B_4B_7 - B_2B_8}. \tag{E.3}$$

By differentiation, we obtain

$$\delta\alpha^2 = (1+x)^2\,\delta\alpha_o^2 + 2\alpha_o^2(1+x)\,\delta x \simeq 2\alpha_o^2(1+x)\,\delta x , \tag{E.4}$$

where $\delta\alpha_o^2 \approx 0$ when the iteration converges. The deviation δx is readily obtained as

$$\delta x = \frac{B_8}{D}\,\delta B_1 + \frac{NB_8}{D^2}\,\delta B_2 - \frac{NB_7}{D^2}\,\delta B_4 - \frac{B_7}{D}\,\delta B_6$$

$$- \left(\frac{B_6}{D} + \frac{NB_4}{D^2}\right)\delta B_7 + \left(\frac{B_1}{D} + \frac{NB_2}{D^2}\right)\delta B_8 , \tag{E.5}$$

where

$$N \equiv (B_1B_8 - B_6B_7) , \tag{E.6}$$

and

$$D \equiv (B_4B_7 - B_2B_8) . \tag{E.7}$$

The δB_i are obtained from Eqs. (4.93) through (4.100) and are:

$$\delta B_1 = - \frac{R}{\alpha_o} J_1(\alpha_o R)\, \delta\left(\frac{\psi_3}{\psi_1}\right) ,$$

$$\delta B_2 = - F\, \delta\left(\frac{\psi_3}{\psi_1}\right) ,$$

$$\delta B_4 = - H\, \delta\left(\frac{\psi_5}{\psi_3}\right) ,$$

$$\delta B_6 = G\, \delta\left(\frac{\psi_5}{\psi_3}\right) ,$$

$$\delta B_7 = - \frac{R}{\beta_o} I_1(\beta_o R)\, \delta\left(\frac{\psi_3}{\psi_1}\right) ,$$

and

$$\delta B_8 = g\, \delta\left(\frac{\psi_5}{\psi_3}\right) . \tag{E.8}$$

Here the deviations in the flux moments ratios are to be calculated by means of Eqs. (4.64) and (4.65).

The probable error in the radial buckling is defined as

$$\sigma_{\alpha^2} \equiv |\delta\alpha^2| = \alpha_o^2 |(1+x)| \cdot |\delta x| . \tag{E.9}$$

To compute the $\delta\psi_i$, we need to know the normalization constant A_r. It can be determined by setting

$$\frac{d\sigma_{\alpha^2}}{dA_r} = 0 \tag{E.10}$$

to minimize the probable error. This leads to the following results:

$$A_r = \frac{\left\{ \frac{(a_1+a_2+a_5)}{\left(\psi_1^{th}\right)^4}\left[\left(\psi_1^{th}\right)^2\left(\psi_3^{exp}\right)^2+\left(\psi_3^{th}\right)^2\left(\psi_1^{exp}\right)^2\right] + \frac{(a_3+a_4+a_6)}{\left(\psi_3^{th}\right)^4}\left[\left(\psi_3^{th}\right)^2\left(\psi_5^{exp}\right)^2+\left(\psi_5^{th}\right)^2\left(\psi_3^{exp}\right)^2\right]\right\}}{\left\{ \frac{(a_1+a_2+a_5)}{\left(\psi_1^{th}\right)^4}\left[\left(\psi_1^{th}\right)^2\left(\psi_3^{th}\psi_3^{exp}\right)+\left(\psi_3^{th}\right)^2\left(\psi_1^{th}\psi_1^{exp}\right)\right] + \frac{(a_3+a_4+a_6)}{\left(\psi_3^{th}\right)^4}\left[\left(\psi_3^{th}\right)^2\left(\psi_5^{th}\psi_5^{exp}\right)+\left(\psi_5^{th}\right)^2\left(\psi_3^{th}\psi_3^{exp}\right)\right]\right\}} \qquad \text{(E.11)}$$

where

$$a_1 = \left(\frac{B_8}{D}\right)^2 \frac{R^2}{\alpha_o^2} J_o^2(\alpha_o R) ,$$

$$a_2 = \left(\frac{NB_8}{D^2}\right)^2 F^2 ,$$

$$a_3 = \left(\frac{NB_7}{D^2}\right)^2 H^2 ,$$

$$a_4 = \left(\frac{B_7}{D}\right)^2 G^2 ,$$

$$a_5 = \left(\frac{B_6}{D} + \frac{NB_4}{D^2}\right)^2 \frac{R^2}{\beta_o^2} I_1^2(\beta_o R) ,$$

$$a_6 = \left(\frac{B_1}{D} + \frac{NB_2}{D^2}\right)^2 g^2 . \qquad \text{(E.12)}$$

Appendix F

AN ESTIMATE OF THE COEFFICIENT C BY MEANS OF A LEAST-SQUARES TECHNIQUE

Suppose that the radial flux distribution is describable by the function

$$\phi(r) = A[J_o(\alpha r) + c\, I_o(\beta r)]. \tag{F.1}$$

We wish to estimate the coefficient c from experimental activation data. A formal way would be to fit the data to the curve (F.1) with respect to the four parameters A, α, c, and β independently by means of a least-squares technique. This is difficult and inconsistent as we have mentioned in section 4.6. We, therefore, assume that both α and β are known from the two-group criticality equation and estimate the coefficient c from a set of flux ratios to avoid the determination of the normalization constant A. This is sufficient for the purpose of estimating the initial value of c to begin the kind of iteration suggested in section 4.6. The set of flux ratios is formed with the flux at or near the center ϕ_o as the basis: ϕ_j/ϕ_o, $j = 1, 2, 3, \ldots, N$. To apply the least-squares principle, we form the residual of the flux ratios:

$$\Delta x = \sum_{j=1}^{N} \left\{ \left[\frac{\phi_j}{\phi_o}\right]_{exp.} - \left[\frac{\phi_j}{\phi_o}\right]_{th.} \right\}^2, \tag{F.2}$$

where the subscript exp denotes the experimental flux ratios and th stands for the theoretical values. To determine c, set $\frac{d(\Delta x)}{dc} = 0$ to minimize the residual. This leads to the following result:

$$c = \frac{J_o(\alpha r_o)}{I_o(\beta r_o)} \frac{\sum_{j=1}^{N} \left\{ \left[\frac{I_o(\beta r_j)}{I_o(\beta r_o)} - \frac{J_o(\alpha r_j)}{J_o(\alpha r_o)} \right] \left[\left(\frac{\phi_j}{\phi_o} \right)_{exp} - \frac{J_o(\alpha r_j)}{J_o(\alpha r_o)} \right] \right\}}{\sum_{j=1}^{N} \left\{ \left[\frac{I_o(\beta r_j)}{I_o(\beta r_o)} - \frac{J_o(\alpha r_j)}{J_o(\alpha r_o)} \right] \left[\frac{I_o(\beta r_j)}{I_o(\beta r_o)} - \left(\frac{\phi_j}{\phi_o} \right)_{exp} \right] \right\}} , \qquad \text{(F.3)}$$

where r_o is the radial position corresponding to the base flux ϕ_o, and r_j corresponds to the flux ϕ_j.

Appendix G

A NOTE ON THE MEASURE OF THE DEGREE OF FIT OF THE ASYMPTOTIC FLUX DISTRIBUTIONS DERIVED FROM EXPERIMENTAL DATA BY MEANS OF THE MOMENTS METHOD

In this appendix we shall compare the moments method and the curve-fitting method in terms of the flux residual defined as

$$(\Delta\phi)^2 \equiv \sum_{i=1}^{N} w_i \left(\phi_i^{th} - \frac{\phi_i^{exp}}{A} \right)^2 , \tag{G.1}$$

where the ϕ_i^{th} are the theoretical flux values, the ϕ_i^{exp} are the experimental activation data, A is a normalization constant to be determined, and the w_i are a set of appropriate weighting factors. The value of the flux residual, as defined in Eq. (G.1), is often used by experimenters as a measure of "goodness of fit."

To determine the normalization constant A, we minimize the flux residual with respect to A by setting

$$\frac{d}{dA} (\Delta\phi)^2 = 0 . \tag{G.2}$$

If we choose unity as the weighting factors, Eq. (G.2) leads to the expression for A:

$$A = \frac{\sum_{i=1}^{N} \left(\phi_i^{exp} \right)^2}{\sum_{i=1}^{N} \phi_i^{th} \phi_i^{exp}} . \tag{G.3}$$

In the case of the axial flux distribution, the asymptotic theoretical flux values are given by

$$\phi_i^{th} = \sinh \gamma(\tilde{H}-z_i) , \quad i = 1, 2, 3, \ldots, N , \tag{G.4}$$

where γ^2 is the axial buckling and $\tilde{H}$ is the extrapolated height. For the radial flux distribution, the corresponding theoretical flux values are:

$$\phi_i^{th} = J_o(\alpha r_i) , \quad i = 1, 2, 3, \ldots, N , \tag{G.5}$$

where α^2 is the radial buckling.

To compare the moments method and the curve-fitting method in terms of the flux residual defined above, we chose from Chapters III and IV a number of experimental runs for which the two methods yielded significant differences in the values of the buckling. The results obtained for the flux residuals in nineteen experimental measurements of the axial buckling are given in Table G.1; those for seventeen measurements of the radial buckling are given in Table G.2. It is evident that in the case of the axial buckling the moments method yields smaller values of the flux residual than does the curve-fitting method for all the runs except J3 and 83. In the case of the radial buckling, the moments method yields either comparable or larger values of the flux residual than the curve-fitting method. This may be due to the small number of data points available for the analysis for radial flux traverses.

It may be advisable in the future to incorporate the calculation of the flux residual into the ABMOMENT, RAMBLER, and RADBUCK codes as an additional criterion for the choice of the moment index.

Table G.1. Comparison of the moments method and the curve-fitting method for the analysis of the axial buckling and the extrapolated height in terms of the flux residual.

Run* Number	MOMENTS METHOD			CURVE-FITTING METHOD		
	γ^2 (μB)	$\tilde{H}$ (cm)	Flux Residual	γ^2 (μB)	$\tilde{H}$ (cm)	Flux Residual
P9	1370	131.05	0.1310	1382	135.30	0.2210
R4	1360	125.98	0.2180	1387	127.30	0.2250
Q1	1380	128.26	0.0896	1332	131.60	0.1420
J 3	285	122.71	0.0026	310	121.90	0.0024
H8	269	123.68	0.0007	288	125.80	0.0012
K4	282	123.76	0.0015	250	123.60	0.0017
K6	279	124.41	0.0031	300	126.20	0.0035
K1	259	124.34	0.0016	298	125.40	0.0041
92	1391	125.64	0.1072	1390	127.90	0.1278
M1	34	123.92	0.0009	65	126.30	0.0031
M2	21	124.94	0.0001	35	126.60	0.0003
M4	18	125.01	0.0001	45	126.50	0.0009
83	954	136.29	0.0767	947	134.70	0.0682
62	916	132.34	0.0069	925	133.50	0.0100
35	1603	130.32	0.0864	1623	139.30	0.2460
27	1622	135.52	0.3493	1640	138.50	0.5590
58	1627	136.91	0.2010	1633	141.90	0.3210
47	1622	139.67	0.0789	1629	142.40	0.1184
44	1624	135.39	0.1892	1639	138.00	0.2601

* For the lattice specifications of these runs, refer to Tables 3.3 through 3.7.

Table G.2. Comparison of the moments method and the curve-fitting method for the analysis of the radial buckling in terms of the flux residual.

Run* Number	Moments Method		Curve-Fitting Method	
	α^2 (μB)	Flux Residual	α^2 (μB)	Flux Residual
N7	2426	0.00071	2382	0.00050
P6	2425	0.00092	2374	0.00051
N3	2415	0.00017	2364	0.00015
P0	2389	0.00017	2335	0.00035
K9	1467	0.00255	1399	0.00150
L8	1426	0.00061	1388	0.00041
L5	1436	0.00033	1412	0.00031
I 1	1437	0.00038	1394	0.00017
J 2	1432	0.00046	1387	0.00013
H7	1435	0.00073	1396	0.00032
Q9	2605	0.00095	2446	0.00011
R6	2606	0.00070	2473	0.00015
11	2324	0.00131	2255	0.00180
86	2562	0.00029	2531	0.00034
82	2528	0.00300	2504	0.00323
69	2439	0.00075	2342	0.00026
31	2365	0.00033	2305	0.00032

* For the lattice specifications of these runs, refer to Tables 4.1 through 4.11.

Appendix H

REFERENCES

A1 Andrews, W. M., "Measurement of the Temperature Dependence of Neutron Diffusion Properties in Beryllium Using a Pulsed Neutron Technique," UCRL 6083 (August, 1960).

A2 Abramowitz, M., and I. A. Stegun, "Handbook of Mathematical Functions with Formulas, Graphs, and Mathematical Tables," National Bureau of Standards, Applied Mathematics Series - 55 (1964).

A3 Amaldi, E., "The Production and Slowing Down of Neutrons," Encyclopedia of Physics, Vol. 38/2 (Berlin: Springer-Verlag, 1959).

A4 Argonne National Laboratory, "Reactor Physics Constants," ANL-5800, Second Edition (July, 1963).

B1 Beckurts, K. H., and K. Wirtz, Neutron Physics (New York: Springer-Verlag, 1964).

B2 Beers, Y., Introduction to the Theory of Error (Reading: Addison-Wesley Publishing Company, 1957).

B3 Bliss, H. E., I. Kaplan, and T. J. Thompson, "Use of a Pulsed Neutron Source to Determine Nuclear Parameters of Lattices of Partially Enriched Uranium Rods in Heavy Water," MIT-2344-7, MITNE-73 (September, 1966).

B4 Beckurts, K. H., "Transient Effects in Space, Time, and Energy," Proceedings of the Brookhaven Conference on Neutron Thermalization, Volume III, BNL-719 (C-32) (1962).

C1 Clark, M., and K. F. Hansen, Numerical Methods of Reactor Analysis (New York and London: Academic Press, 1964).

C2 Corngold, N., "The Interpretation of Pulsed Neutron Experiments," Reactor Physics in the Resonance and Thermal Regions, Volume I (Cambridge: The M.I.T. Press, 1966).

D1 Dresner, L., "On the Validity of the Second Fundamental Theorem in a Medium with Anisotropic Scattering," Nuclear Sci. and Eng., 7, 419 (1960).

D2 Davison, B., Neutron Transport Theory (Oxford: The Clarendon Press, 1958).

D3 Daitch, P. B., and D. B. Ebeoglu, "Transients in Pulsed Moderators," Proceedings of the Brookhaven Conference on Neutron Thermalization, Vol. IV, 1132, BNL-719 (C-32) (1962).

E1 Evans, R. D., The Atomic Nucleus (New York: McGraw-Hill Book Company, 1955).

F1 Ferziger, J. H., and P. F. Zweifel, The Theory of Neutron Slowing Down in Nuclear Reactors (Cambridge: The M.I.T. Press, 1966).

F2 Fermi, E., Ricerca Scientifica, 7 (2), 13 (1936).

F3 Fano, U., and L. V. Spencer, "Penetration and Diffusion of X-Rays," Encyclopedia of Physics 38, Part 2 (Berlin: Springer-Verlag).

G1 Gelbard, E. M., and J. A. Davis, "The Behavior of Extrapolation Distances in Die-Away Experiments," Nuclear Sci. and Eng., 13, 237 (1962).

G2 Glasstone, S., and M. C. Edlund, The Elements of Nuclear Reactor Theory (Princeton: D. Van Nostrand Company, Inc., 1952).

H1 Thompson, T. J., I. Kaplan, and A. E. Profio, "Heavy Water Lattice Project Annual Report," NYO-9658 (September, 1961).

H2 Kaplan, I., A. E. Profio, and T. J. Thompson, "Heavy Water Lattice Project Annual Report," NYO-12208, MITNE-26 (September, 1962).

H3 Kaplan, I., D. D. Lanning, and T. J. Thompson, "Heavy Water Lattice Project Annual Report," NYO-10212, MITNE-46 (September, 1963).

H4 Lanning, D. D., I. Kaplan, and F. M. Clikeman, "Heavy Water Lattice Project Annual Report," MIT-2344-3, MITNE-60 (September, 1964).

H5 Thompson, T. J., I. Kaplan, F. M. Clikeman, and M. J. Driscoll, "Heavy Water Lattice Project Annual Report," MIT-2344-4, MITNE-65 (September, 1965).

H6 Thompson, T. J., I. Kaplan, and M. J. Driscoll, "Heavy Water Lattice Project Annual Report," MIT-2344-9, MITNE-79 (September, 1966).

H7 Hellens, R. L., and E. Andersen, "Some Problems in the Interpretation of Exponential Experiments," Proceedings of the Symposium on Exponential and Critical Experiments, Vol. II, p. 21 (Vienna: IAEA, 1964).

H8 Harrington, J., "Measurement of the Material Buckling of a Lattice of Slightly Enriched Uranium Rods in Heavy Water," M.S. Thesis, M.I.T. Nuclear Eng. Dept. (July, 1963).

H9 Harrington, J., D. D. Lanning, I. Kaplan, and T. J. Thompson, "Use of Neutron Absorbers for the Experimental Determination of Lattice Parameters in Subcritical Assemblies," MIT-2344-6, MITNE-69 (February, 1966)

H10 Hildebrand, F. B., Introduction to Numerical Analysis (New York: McGraw-Hill Book Company, Inc., 1956).

H11 Hellens, R. L., and E. Andersen, BNL-7293.

H12 Hellens, R. L., and G. A. Price, "Reactor Physics Data for H_2O Moderated Lattices of Slightly Enriched Uranium," Selected Reviews on Reactor Technology, p. 529 (1964).

H13 Halpern, O., R. Lueneburg, and O. Clark, Phys. Rev., 51, 1020 (1937).

I1 Inönü, E., "On the Validity of the Second Fundamental Theorem for Small Reactors," Nuclear Sci. and Eng., 5, 248 (1959).

I2 Inönü, E., "The Effect of the Boundary Region in the Determination of the Extrapolation Length from Experiments with Critical Cylinders," ORNL-3016, p. 188 (1960).

K1 Kouts, H., G. Price, K. Downes, R. Sher, and V. Walsh, "Exponential Experiments with Slightly Enriched Uranium Rods in Ordinary Water," Proceedings of the First International Conference on the Peaceful Uses of Atomic Energy, 5, 183 (1956).

K2 Kaplan, I., "Measurements of Reactor Parameters in Subcritical and Critical Assemblies: A Review," NYO-10207, MITNE-25 (August, 1962).

K3 Kleijn, H. R., A. W. Van Der Heijden, and H. Van Dam, "Theory of Material Buckling in Subcritical Assemblies," Proceedings of the Symposium on Exponential and Critical Experiments, Vol. III, p. 113 (Vienna: IAEA, 1964).

K4 Kladnik, R., "Milne's Problem for Thermal Neutrons," Proceedings of the Brookhaven Conference on Neutron Thermalization, Vol. IV, 1211, BNL-719 (1962).

K5 Kaplan, S., "Properties of the Relaxation Lengths in P_L, Double-P_L, and Angle-Space Synthesis-Type Approximations," Nuclear Sci. and Eng., 28, 456 (1967).

K6 Kaplan, I., and A. Travalli, "Nuclear Reactor Theory," Notes of Course 22.21, Dept. of Nuclear Eng., M.I.T. (1965).

K7 Kaplan, I., "The Analysis of Critical and Subcritical Experiments, a Comparison," Kjeller Report KR-117 (1966).

K8 Kouts, H., "The Buckling Concept in Reactor Theory and Experiment," KR-117 (1966).

K9 Kouts, H., et al., "Physics of Slightly Enriched, Normal Water Lattices (Theory and Experiment)," Proceedings of the Second International Conference on the Peaceful Uses of Atomic Energy, 12, 446 (1958).

K10 Kouts, H., and R. Sher, "Experimental Studies of Slightly Enriched 0.6-Inch-Diameter Metallic Uranium, Water Moderated Lattices," Progress in Nuclear Energy, Series II, Reactors, Vol. 2, p. 285 (London: Pergamon Press, 1958).

K11 Kofink, W., "Complete Spherical Harmonics Solution of the Boltzmann Equation for Neutron Transport in Homogeneous Media with Cylindrical Geometry," Nuclear Sci. and Eng., 6, 475 (1959).

L1 Lamarsh, J. R., Introduction to Nuclear Reactor Theory (Reading: Addison-Wesley Publishing Company, Inc., 1966).

L2 Lanczos, C., Applied Analysis (Englewood Cliffs: Prentice-Hall, Inc., 1956).

L3 Lutz, H. R., T. Auerbach, W. Heer, and R. W. Meier, "Two-Region, Heavy Water, Natural Uranium Lattice Studies in the Subcritical Assembly MINOR," Proceedings of the Symposium on Exponential and Critical Experiments, Vol. II (Vienna: IAEA, 1964).

M1 Meghreblian, R. V., and D. K. Holmes, Reactor Analysis (New York: McGraw-Hill Book Company, 1960).

M2 Morse, P. M., and H. Feshbach, Methods of Theoretical Physics, Vol. I (New York: McGraw-Hill Book Company, 1953).

M3 Maĭorov, L. V., "Asymptotic Distribution of Thermal Neutrons Far from a Planar Source," Proceedings of the Brookhaven Conference on Neutron Thermalization, Vol. IV, 1375, BNL-719 (1962).

M4 Murray, R. L., Nuclear Reactor Physics, p. 124 (Englewood Cliffs: Prentice-Hall, Inc., 1957).

N1 Nikolaev, M. N., "Analysis and Utilization of Cell Parameter Measurements," KR-117 (1966).

N2 Noble, L. D., and J. O. Mingle, "Boundary Conditions for the Unsymmetrical Spherical-Harmonics Method in Cylindrical Geometry," Nuclear Sci. and Eng., 21, 240 (1965).

O1 Okrent, D., R. Avery, and H. H. Hummel, "A Survey of the Theoretical and Experimental Aspects of Fast Reactor Physics," Proceedings of the First International Conference on the Peaceful Uses of Atomic Energy, Vol. 5, p. 347 (1956).

P1 Palmedo, P. F., I. Kaplan, and T. J. Thompson, "Measurements of the Material Bucklings of Lattices of Natural Uranium Rods in D_2O," NYO-9660, MITNE-13 (January, 1962).

P2 Peak, J. C., I. Kaplan, and T. J. Thompson, "Theory and Use of Small Subcritical Assemblies for the Measurement of Reactor Parameters," NYO-10204, MITNE-16 (April, 1962).

P3 Perrson, R., M. Bustraan, and E. Blomsjö, "Some Experiences from Measurements on an Exponential Pile of Uranium and Heavy Water," Proceedings of the First International Conference on the Peaceful Uses of Atomic Energy, 5, 239 (1956).

P4 Perrson, R., et al., "Exponential Experiments on Heavy Water Natural Uranium Metal and Oxide Lattices," Proceedings of the Second International Conference on the Peaceful Uses of Atomic Energy, 12, 364 (1958).

P5 Price, W. J., Nuclear Radiation Detection, Second Edition (New York: McGraw-Hill Book Company, Inc., 1964).

P6 Pomraning, G. C., "Transport Methods for the Calculation of Spatially Dependent Thermal Spectra," Reactor Physics in the Resonance and Thermal Regions, Vol. I (Cambridge: The M. I. T. Press, 1966).

P7 Persson, R., "The Evaluation of Buckling and Diffusion Coefficients from Two-Region Experiments," Proceedings of the Symposium on Exponential and Critical Experiments, Vol. III, p. 289 (Vienna: IAEA, 1964).

R1 Rodeback, G. W., "Least-Squares Analyses of Axial Neutron Flux Distribution in Exponential Assemblies," NAA-SR-MEMO-4189 (July, 1959).

R2 Raišić, N., S. Takać, H. Marković, and T. Bošević, "Determination of D_2O-2% Enriched Uranium Lattice Parameters by Means of a Critical System," Proceedings of the Symposium on Exponential and Critical Experiments, Vol. II, p. 509 (Vienna: IAEA, 1964).

S1 Sefchovich, E., I. Kaplan, and T. J. Thompson, "The Measurement of Reactor Parameters in Slightly Enriched Uranium, Heavy Water Moderated Miniature Lattices," MIT-2344-8, MITNE-76 (October, 1966).

S2 Serdula, K., "Determination of Radial Buckling in Reflected Systems," Nuclear Sci. and Eng., 26, 1 (1966).

T1 Tralli, N., and J. Agresta, "Spherical Harmonic Calculations for a Cylindrical Cell of Finite Height," Nuclear Sci. and Eng., 10, 132 (1961).

T2 Takahashi, H., "Space and Time Dependent Eigenvalue Problem in Neutron Thermalization," Proceedings of the Brookhaven Conference on Neutron Thermalization, Vol. IV, 1299, BNL-719 (C-32) (1962).

W1 Weinberg, A. E. and E. P. Wigner, The Physical Theory of Neutron Chain Reactors (Chicago: University of Chicago Press, 1958).

W2 Williams, M. M. R., "Space-Energy Separability in Pulsed Neutron Systems," Proceedings of the Brookhaven Conference on Neutron Thermalization, Vol. IV, 1331, BNL-719 (C-32) (1962).

W3 Watson, G. N., A Treatise on the Theory of Bessel Functions, Second Edition (Cambridge: The University Press, 1958).

W4 Windsor, H., "The Effect of Radial-Energy Transients on Experimental Material-Buckling Measurements," Trans. Am. Nucl. Soc., 9, No. 1, 130 (1966).

W5 Wikdahl, C. E., and F. Akerhielm, "Measurements of Disadvantage Factors in a Small Mockup," Proceedings of the Second International Conference on the Peaceful Uses of Atomic Energy, Vol. 12, 162 (1958).

W6 Weast, R. C., and S. M. Selby, Handbook of Tables for Mathematics, Third Edition, p. 714 (Cleveland: Chemical Rubber Publishing Company, 1964).

W7 Wick, G. C., Rend. Linc., 23, 774 (1936).

Y1 Yip, S., and P. F. Zweifel, "Escape-Probabilities in Asymptotic Reactor Theory," Nuclear Sci. and Eng., 10, 362 (1961).

ERRATA

Page	Correction
90	In Eq. (3.46) change n+j-r to n+j-4
127	In Eq. (4.20) change $\alpha^2(z)$ to $\alpha^2(2)$
136	Line 6: Change ϕ_{α^2} to σ_{α^2}
144	Abscissa title of Fig. 4.4: change $\tilde{R}$ to $r/\tilde{R}$
153	In Eq. (4.114) change β to B on right-hand side of equation (twice)
213	In the denominator of Eq. (5.17) enclose all terms following R^2 in brackets
246	In the last term of Eq. (6.9) replace ϕ by ϕ^{uc}
256	In Eq. (6.46) enclose the last three terms, beginning with $-\frac{4}{5}$ ..., in brackets
264	In Eq. (6.84) precede the term on the second line by +
284	In Eq. (6.137) replace C by c (three times)
286	In the last line on the page, replace $\|\alpha_1\|^2$ by α^2
289	On line 9 enclose all terms following A_1 in brackets